IL
NUOVO CIMENTO
ORGANO DELLA SOCIETÀ ITALIANA DI FISICA
SOTTO GLI AUSPICI DEL CONSIGLIO NAZIONALE DELLE RICERCHE

VOL. IX, N. 4 *Serie decima* 16 Agosto 1958

Phenomenological Theory of the S-Matrix and T, C and P Invariance.

J. WERLE

Institute for Nuclear Research and University of Warsaw

(ricevuto il 21 Febbraio 1958)

Summary. — General expressions for the transition matrix are given for reactions between four particles of arbitrary spins. Restrictions imposed by T, C or P invariance requirements are expressed in terms of simple equations between some phenomenological scalar coefficients which occur in the general expression for the transition matrix. For any given type of reaction one can find in this way definite physical relations which have the advantage of being free of any special assumptions and approximations.

1. – Introduction.

Recent discovery of the non-conservation of parity [1] urged the physicists to a thorough revision of some other conservation laws as well. It seems to be certain that the invariance under charge conjugation (C) cannot be an exact law either. However, it has been suggested [2] that all the interactions may be still invariant under the product (CP) of charge conjugation and space

(1) T. D. LEE and C. N. YANG: *Phys. Rev.*, **104**, 254 (1956); C. S. WU *et al.*: *Phys. Rev.*, **105**, 1413 (1957); **106**, 1361 (1957); L. GARVIN, L. M. LEDERMAN and M. WEINRICH: *Phys. Rev.*, **105**, 1415 (1957); J. FRIEDMAN and V. L. TELEGDI: *Phys. Rev.*, **105**, 1681 (1957); and others. See also *Reports on the VII-th Rochester Conference* and *Reports on the Padua-Venice Conference* (1957).

(2) T. D. LEE and C. N. YANG: *Phys. Rev.*, **105**, 1671 (1957); L. D. LANDAU: *Nuclear Phys.*, **3**, 127 (1957).

inversion. Because of the so-called TCP theorem ([3]) the invariance under (CP) is rather completely equivalent to the invariance under time reversal transformation T. The problem whether all the physical processes are in fact invariant or not invariant under time reversal is still open. Solution of this problem seems to be much more difficult than in the case of space inversion. There the mere presence of a spatial pseudoscalar in the cross-section was an unequivocal proof of the non-conservation of parity. On the other hand time reversal invariance does not exclude the occurrence of time pseudoscalars in the cross-sections. Thus, one cannot prove violation of time reversal invariance without a more detailed theory. Several authors have been investigating this problem ([4,5]) but most of their results have only a limited value as they are based on a whole series of simplyifying assumptions and approximations. Most authors investigate just the primary interactions and not their final results, *i.e.* the reaction itself. In order to obtain definite results they usually assume that all the interactions are local, do not contain any derivatives etc.; sometimes they even assume a particular type of coupling. Furthermore, most calculations are based on the perturbation expansion or other approximative methods and it is often not clear which results are generally valid and which are not. With respect to the β-transitions there are also some doubts whether the usual treatment of these processes is correct ([6]).

It seems, therefore, advisable to investigate the problem on the basis of the general phenomenological S-matrix formalism which can be made free of most of the simplifying assumptions and other disadvantages mentioned above. The aim of this paper is first to construct a general theory of the transition matrix with the least possible number of assumptions and then to investigate what restrictions are to be imposed due to P, C, or T invariance requirements. In the present paper we shall discuss only the general and rather formal relations. A discussion of physical implications and some examples will be given in another paper.

In order to be able to discuss not only reactions between so-called elementary particles but also those which involve some composed particles (*e.g.* nuclei) we shall consider in this paper reactions between four particles of arbitrary spins.

([3]) G. Lüders: *Kgl. Danske Videns. Sels. Mat.-Fys. Medd.*, **28**, No. 5 (1954); *Annals of Phys.*, **2**, 1 (1957).; W. Pauli: in *Niels Bohr and the Development of Physics* (New York, 1955).

([4]) T. D. Lee, R. Oehme and C. N. Yang: *Phys. Rev.*, **106**, 340 (1957); G. Lüders and B. Zumino: *Phys. Rev.*, **106**, 385 (1957).

([5]) Jackson, Treiman and Wyld: *Phys. Rev.*, **106**, 517 (1957). F. Coester: *Phys. Rev.*, **107**, 298 (1957); R. B. Curtis and R. R. Lewis: *Phys. Rev.*, **107**, 543 (1957); M. Morita and R. Saito Morita: *Phys. Rev.*, **107**, 139, 1316 (1957).

([6]) M. A. Markov: private communication.

2392

Notation. – Small Greek indices (*e.g.* α, β, γ, δ) are used as ordinary four-dimensional tensor indices which run from 1 to 4. Small Latin indices (*e.g.* r, s, u, v) are used as abbreviations for whole groups of tensor indices of some fixed but unspecified rank and order. Capital indices are reserved for other purpose. With respect to all tensor indices we adopt the usual summation convention: repetition of a tensor index in an upper and a lower position means a summation over this index. Lowering or raising of tensor indices is performed by means of the metric tensor $g^{\alpha\beta} = g_{\alpha\beta}$ ($g_{11} = g_{22} = g_{33} = -1$, $g_{44} = +1$). Thus we have for the position vector x^μ and the momentum vector p^μ

$$x^\mu = (\boldsymbol{r}, t), \quad x_\mu = (-\boldsymbol{r}, t), \quad p^\mu = (\boldsymbol{p}, \omega), \quad p_\mu = (-\boldsymbol{p}, \omega), \quad p_\mu p^\mu = p^2 = \omega^2 - \boldsymbol{p}^2 .$$

A tensor function $G^{\mu\nu\ldots}(\boldsymbol{p}, \omega)$ can be, therefore, denoted by $G^r(p^\alpha)$. We shall have often to do with the transformation

$$G^{\mu\nu\ldots}(\boldsymbol{p}, \omega) \to g_{\mu\alpha} g_{\nu\beta} \ldots G^{\alpha\beta\ldots}(\boldsymbol{p}, \omega) = G_{\mu\nu\ldots}(\boldsymbol{p}, \omega)$$

followed by the transformation

$$G_{\mu\nu\ldots}(\boldsymbol{p}, \omega) \to G_{\mu\nu\ldots}(-\boldsymbol{p}, \omega) .$$

Using our conventions we can write the result of these two transformations in the following more compact form

$$G^r(p^\alpha) \to G_r(p_\alpha) .$$

The symbol $\gamma^\mu = (\boldsymbol{\gamma}, \gamma_4)$ denotes four 4×4 Dirac matrices which satisfy the following relations

$$\gamma^\mu \gamma^\nu + \gamma^\nu \gamma^\mu = 2 g^{\mu\nu}, \qquad \boldsymbol{\gamma}^+ = -\boldsymbol{\gamma}, \qquad \gamma_4^+ = \gamma_4, \qquad \gamma_\mu = \gamma^{\mu +} = \gamma_4 \gamma^\mu \gamma_4 = (-\boldsymbol{\gamma}, \gamma_4) .$$

It follows that the matrix $\gamma_5 = i\gamma_1\gamma_2\gamma_3\gamma_4$ is Hermitian and anticommutes with γ_μ:

$$\gamma_5 \gamma^\mu = -\gamma^\mu \gamma_5, \qquad \gamma_5^+ = \gamma_5, \qquad \gamma_5^2 = +1 .$$

The symbol $(+)$, $(*)$ and $(\sim)$ denote the operations of Hermitian conjugation, complex conjugation and transposition respectively.

Natural units are used in which $c = h = 1$.

2. – Definition of P, C and T operations.

Since we are interested in transitions between asymptotic states in which only free (*i.e.* non-interacting) particles are present, we shall use the interaction picture. In the interaction picture all the field operators satisfy free

field equations of motion and free field commutation relations. Bosons of any particular spin value can be described by a tensor field $\varphi^{r}(x^{\varkappa})$ which satisfies the Klein-Gordon equation

$$(\partial_{\mu}\partial^{\mu} + m^{2})\varphi^{r}(x^{\varkappa}) = 0\,, \qquad (\partial_{\mu} = \partial/\partial x^{\mu}) \tag{1}$$

and some other additional equations whose form depends on the spin and mass of the particles. Fermions of any particular spin value can be described in Rarita-Schwinger formalism by a « spinor-tensor » field $\psi^{u}(x^{\varkappa})$ which satisfies the Dirac equation

$$(-i\gamma^{\mu}\partial_{\mu} + m)\psi^{u}(x^{\varkappa}) = 0 \tag{2}$$

and some other equations whose form depends on the spin and mass of the particles. It is understood that besides the tensor index (u) the function ψ^{u} has also a four-spinor index which will be not denoted explicitly. Both φ^{r} and ψ^{u} are q-numbers.

P, C, and T operations will be now defined as follows:

a) Space inversion operator P is a linear, unitary operator defined by the following transformation laws for the fields φ^{r} and ψ^{u}:

$$\begin{cases} P\varphi^{r}(x^{\varkappa})P^{-1} = \eta_{P}\varphi_{r}(x_{\varkappa}), & P\varphi^{r+}(x^{\varkappa})P^{-1} = \eta_{P}^{*}\varphi_{r}^{+}(x_{\varkappa})\,, \\ P\psi^{u}(x^{\varkappa})P^{-1} = \eta'_{P}\gamma_{4}\psi_{u}(x_{\varkappa}), & P\overline{\psi}^{u}(x^{\varkappa})P^{-1} = \eta'^{*}_{P}\overline{\psi}_{u}(x_{\varkappa})\gamma_{4}\,, \end{cases} \tag{3}$$

where $\overline{\psi}^{u} = \psi^{u+}\gamma_{4}$. The phase factors η_{P}, η'_{P} are ordinary c-numbers of modulus 1.

b) Charge conjugation operator C is a linear, unitary operator defined by the following transformation laws

$$\begin{cases} C\varphi^{r}(x^{\varkappa})\,C^{-1} = (-1)^{\tau_{r}}\eta_{C}\varphi^{r+}(x^{\varkappa}), & C\varphi^{r+}(x^{\varkappa})\,C^{-1} = (-1)^{\tau_{r}}\eta_{C}^{*}\varphi^{r}(x^{\varkappa})\,, \\ C\psi^{u}(x^{\varkappa})\,C^{-1} = (-1)^{\tau_{u}}\eta'_{C}\mathcal{C}\overline{\psi}^{u}(x^{\varkappa}), & C\overline{\psi}^{u}(x^{\varkappa})\,C^{-1} = -(-1)^{\tau_{u}}\eta'^{*}_{C}\psi^{u}(x^{\varkappa})\mathcal{C}^{-1} \end{cases} \tag{4}$$

where the 4×4 matrix $\mathcal{C}$ is defined by

$$\mathcal{C}^{+} = \mathcal{C}^{-1}\,, \qquad \mathcal{C}^{\sim} = -\mathcal{C}\,, \qquad \mathcal{C}\gamma_{\mu}^{\sim}\mathcal{C}^{-1} = -\gamma_{\mu}\,. \tag{5}$$

For the sake of simplicity we do not consider isotopic spin in this work The symbols τ_{r} and τ_{u} denote the ranks of the tensor indices (r) and (u) respectively. *E.g.* $\tau_{r} = \tau_{u} = 0$ for 0 and $\frac{1}{2}$ spins, $\tau_{r} = \tau_{u} = 1$ for 1 and $\frac{3}{2}$ spins etc. The phase factors η_{C}, η'_{C} are ordinary c-numbers of modulus 1.

2394

c) Time reversal operator T is an antiunitary (*i.e.* anti-linear-unitary) operator defined by the following transformation laws (7)

$$(6)\quad \begin{cases} T\varphi^{r}(x^{\varkappa})\,T^{-1} = \eta_T \varphi_r(-x_\varkappa), & T\varphi^{r+}(x^{\varkappa})\,T^{-1} = \eta_T^{*}\,\varphi_r^{+}(-x_\varkappa)\,, \\ T\psi^{u}(x^{\varkappa})\,T^{-1} = \eta'_T \mathcal{C}^{-1}\gamma_5 \psi_u(-x_\varkappa)\,, & T\bar{\psi}^{u}(x^{\varkappa})\,T^{-1} = \eta'^{*}_T\,\bar{\psi}_u(-x_\varkappa)\gamma_5\mathcal{C}\,. \end{cases}$$

The phase factors η_T and η'_T are again ordinary c-numbers of modulus 1.

As P, C are linear and T antilinear we have for any c-number

$$(7)\qquad P\,c\,P^{-1} = c\,, \qquad C\,c\,C^{-1} = c\,, \qquad T\,c\,T^{-1} = c^{*}\,.$$

Furthermore we require that under any one of the transformations P, C and T the vacuum be transformed into vacuum.

In the following we shall use mainly momentum representation. Since all the $\varphi^{r}(x^{\varkappa})$ and $\psi^{u}(x^{\varkappa})$ satisfy Klein-Gordon equation we define their Fourier transforms as follows:

$$(8)\quad \begin{cases} \{\varphi^{r}(x^{\varkappa});\,\psi^{u}(x^{\varkappa})\} = \int \{\varphi^{r}(p^{\varkappa});\,\psi^{u}(p^{\varkappa})\}\,\delta(p^2 - m^2)\exp[-ip_\varkappa x^{\varkappa})\,\mathrm{d}p, \\ \{\varphi^{r+}(x^{\varkappa});\,\bar{\psi}^{u}(x^{\varkappa})\} = \int \{\varphi^{r+}(p^{\varkappa});\,\bar{\psi}^{u}(p^{\varkappa})\}\,\delta(p^2 - m^2)\exp[+ip_\varkappa x^{\varkappa})\,\mathrm{d}p\,, \end{cases}$$

where $\mathrm{d}p = \mathrm{d}_{(3)}\boldsymbol{p}\,\mathrm{d}\omega$; δ is Dirac delta function. Inserting (8) into (3), (4) and (6) we find the transformation laws for the momentum representation:

$$(9)\quad \begin{cases} P\varphi^{r}(p^{\varkappa})\,P^{-1} = \eta_P \varphi_r(p_\varkappa)\,, & P\varphi^{r+}(p^{\varkappa})P^{-1} = \eta_P^{*}\varphi_r^{+}(p^{\varkappa})\,, \\ P\psi^{u}(p^{\varkappa})\,P^{-1} = \eta'_P\gamma_4\psi_u(p_\varkappa)\,, & P\bar{\psi}^{u}(p^{\varkappa})\,P^{-1} = \eta'^{*}_P\,\bar{\psi}_u(p_\alpha)\gamma_4\,, \end{cases}$$

$$(9')\quad \begin{cases} C\varphi^{r}(p^{\alpha})C^{-1} = (-1)^{\tau_r}\eta_C\varphi^{r+}(-p^{\varkappa})\,, & C\varphi^{r+}(p^{\alpha})C^{-1} = (-1)^{\tau_r}\eta_C^{*}\varphi^{r}(-p^{\varkappa})\,, \\ C\psi^{u}(p^{\varkappa})C^{-1} = (-1)^{\tau_u}\eta'_C\mathcal{C}\bar{\psi}^{u}(-p^{\alpha})\,, & C\bar{\psi}^{u}(p^{\varkappa})C^{-1} = -(-1)^{\tau_u}\eta'^{*}_C\psi^{u}(-p^{\varkappa})\mathcal{C}^{-1}, \end{cases}$$

$$(9'')\quad \begin{cases} T\varphi^{r}(p^{\varkappa})\,T^{-1} = \eta_T\varphi_r(p_\varkappa)\,, & T\varphi^{r+}(p^{\alpha})T^{-1} = \eta_T^{*}\varphi_r^{+}(p_\varkappa)\,, \\ T\psi^{u}(p^{\varkappa})\,T^{-1} = \eta'_T\mathcal{C}^{-1}\gamma_5\psi_u(p_\varkappa)\,, & T\bar{\psi}^{u}(p^{\varkappa})\,T^{-1} = \eta'^{*}_T\,\bar{\psi}_u(p_\varkappa)\gamma_5\mathcal{C}\,. \end{cases}$$

Lowering (or raising) of external (r, u) as well as of internal (α) indices at P and T transformations is to be noted.

(7) This definition of time reversal is just a simple extension of that used *e.g.* by G. LÜDERS (*Ann. of Phys.*, **2**, 1 (1957)) and others. S. WATANABE (*Rev. Mod. Phys.*, **27**, 40 (1957)) uses another definition of time reversal which differs from T by the operation of complex conjugation.

Let us define charge conjugate (antiparticle) fields

$$\varphi_C^r(p^\varkappa) = \varphi^{r+}(-p^\varkappa)\,, \qquad \psi_C^u(p^\varkappa) = C\overline{\psi}^u(-p^\varkappa)\,. \tag{10}$$

Under proper Lorentz transformations φ_C^r and ψ_C^u transform exactly in the same way as φ^r and ψ^u respectively. Under P, C or T transformations φ_C^r and ψ_C^u transform essentially in the same way as φ^r and ψ^u respectively but the phase factors can be different in this case.

From (3), (4) and (6) one can easily find the transformation laws under any product of P, C and T. For triple products

$$\begin{cases} W_1 = TCP, & W_2 = PTC, \quad W_3 = CTP, \\ W_4 = PCT, & W_5 = CPT, \quad W_6 = TPC, \end{cases} \tag{11}$$

we find

$$\begin{cases} W_L\varphi^r(p^\varkappa)\,W_L^{-1} = (-1)^{\tau_r}\eta_L\varphi^{r+}(-p^\varkappa)\,, \\ W_L\varphi^{r+}(p^\alpha)W_L^{-1} = (-1)^{\tau_r}\eta_L^*\varphi^r(-p^\alpha)\,, \\ W_L\psi^u(p^\varkappa)\,W_L^{-1} = (-1)^{\tau_u}\eta_L'\tilde{\gamma}_5\tilde{\gamma}_4\overline{\psi}^u(-p^\alpha)\,, \\ W_L\overline{\psi}^u(p^\varkappa)\,W_L^{-1} = -(-1)^{\tau_u}\eta_L'^*\psi^u(-p^\varkappa)\,\tilde{\gamma}_4\tilde{\gamma}_5\,, \end{cases} \tag{12}$$

with

$$\begin{cases} \eta_1 = \eta_T^*\eta_C^*\eta_P^*\,, & \eta_2 = \eta_T^*\eta_C^*\eta_P^*\,, & \eta_3 = \eta_T\eta_C\eta_P^*\,, \\ \eta_4 = \eta_T\eta_C\eta_P^*\,, & \eta_5 = \eta_T\eta_C\eta_P\,, & \eta_6 = \eta_T^*\eta_C^*\eta_P\,, \\ \eta_1' = -\eta_T'^*\eta_C'^*\eta_P'^*\,, & \eta_2' = \eta_T'^*\eta_C'^*\eta_P'^*\,, & \eta_3' = -\eta_T'\eta_C'\eta_P'^*\,, \\ \eta_4' = \eta_T'\eta_C'\eta_P'^*\,, & \eta_5' = -\eta_T'\eta_C'\eta_P'\,, & \eta_6' = \eta_T'^*\eta_C'^*\eta_P'\,. \end{cases} \tag{12'}$$

From now on we shall forget about the co-ordinate space regarding (7), (9), (9′), (9″) as basic relations that define the P, C and T operations in the momentum representation. In the following we shall ascribe quantised Boson ($\varphi^r(p)^\varkappa$) or Fermion ($\psi^u(p^\varkappa)$) fields not only to the so-called elementary particles but also to nuclei that are composed particles. This is surely not allowed in the Lagrangian or Hamiltonian formalism since the primary interactions can depend on the structure of the particles, *i.e.* on some internal co-ordinates. However, in the S-matrix formalism we are interested in the final results of these interactions and we have to do with free particles whose internal degrees of freedom do not change any more. Thus it seems possible to describe a freely moving (non-interacting) nucleus just in the same way as we describe free elementary particles. The structure of a particle manifests itself only in the interaction and this can be accounted for by taking the most general form of the transition matrix.

2396

3. – Conditions imposed on the S-matrix by P, C and T invariance requirements.

In this section we shall study the conditions imposed on the S-matrix by P, C, T and W_L invariance requirements. The S-matrix is given by the formula

$$S = \lim_{t\to\infty} U(t, 0)\, U(0, -t)\,, \tag{13}$$

with $U(t, 0)$ and $U(0, -t)$ defined as solutions of

$$\frac{\mathrm{d}}{\mathrm{d}t}U(t, 0) = -iH(t)\, U(t, 0)\,, \qquad \frac{\mathrm{d}}{\mathrm{d}t}U(0,-t) = -iU(0,-t)H(-t)\,, \qquad U(0,0) = 1\,. \tag{14}$$

$H(t) = H^{+}(t)$ is the interaction Hamiltonian.

The theory is invariant under P, C or T transformation if

$$PH(t)P^{-1} = H(t)\,, \qquad CH(t)C^{-1} = H(t)\,, \qquad TH(t)T^{-1} = H(-t) \tag{15}$$

respectively. It follows from (13), (14) and (15) that, when applied to the S-matrix, the P, C or T invariance conditions have the forms

$$P\,S\,P^{-1} = S\,, \qquad C\,S\,C^{-1} = S\,, \qquad T\,S\,T^{-1} = S^{+}\,. \tag{16}$$

Consequently we find the following invariance condition under triple products W_L

$$W_L S W_L^{-1} = S^{+}\,. \tag{17}$$

Conditions (16) and (17) are quite general but they have no practical value unless we know the form of the matrix S. However, we can write our invariance conditions in another equivalent form which will enable us to draw definite physical conclusions for any given type of reaction without any detailed knowledge of S.

Let us consider processes of some fixed type specified by the spins, charges and masses of all the interacting particles

$$A + B + \ldots \rightleftarrows A' + B' + \ldots\,. \tag{18}$$

A process obtained from (18) by changing one or more of the particles occurring in the initial (final) state into antiparticles occuring in the final (initial) state belongs by definition to the same type as (18). If we consider processes of

some fixed type we can split the S-matrix into two parts

$$S = 1 + iM + iR \,, \tag{19}$$

where R is defined as that part of the S-matrix which does not give any contribution to any process $i \to f$ belonging to the type under consideration:

$$\langle f | R | i \rangle = 0 \,. \tag{20}$$

The part M will be called transition matrix for this type of processes. Now we can write our invariance conditions in terms of M instead of S:

a) P invariance:

$$P M P^{-1} = M \,, \tag{21}$$

b) C invariance:

$$C M C^{-1} = M \,, \tag{22}$$

c) T invariance:

$$T M T^{-1} = M^{+} \,, \tag{23}$$

d) W_L invariance:

$$W_L M W_L^{-1} = M^{+} \,, \tag{24}$$

We shall now forget the fact that we have deduced relations (21)–(24) from some symmetry assumptions about the interaction Hamiltonian. We shall regard the invariance conditions (21)–(24) as relations which are to have the same form even for theories which are non-local in the interaction or have no Hamiltonian. Relations (21)–(24) have the advantage of giving a possibility for drawing definite physical conclusions which are independent of any particular approximation method and of any particular choice of the form of coupling. In fact for any given type of reaction we can construct a general form of the transition matrix which:

a) conserves energy and momentum,

b) conserves electric and nucleonic charges,

c) is invariant under homogeneous proper Lorentz transformations.

These are just invariance properties which are still believed to be « absolute ».

In the next three sections we shall construct general forms of M satisfying these « absolute » invariance conditions for all reactions between four particles of arbitrary spins. Consequently we shall be able to express our invariance

2398

conditions in a more transparent form which can be then interpreted in terms of definite relations between physical observables.

In order to avoid repetitions and detailed discussions of many particular cases differing only with respect to the values of charges let us first make some general remarks about electric and nucleonic charge conservation. For any given type of reaction between n particles the matrix M contains products of n (and only n) field operators chosen suitably from the set φ^r_A, ψ^u_A, φ^{r+}_A, $\overline{\psi}^u_A$, where $A = 1 \ldots n$. Instead of φ^{r+}_A and $\overline{\psi}^u_A$ we can also take charge conjugates of φ^r_A and ψ^u_A given by (10). Electric charge conservation requires that M be invariant under the following transformation:

$$\varphi^r_A \to \exp\,[iq_A\varepsilon]\varphi^r_A\,, \qquad \varphi^{r+}_A \to \exp\,[-iq_A\varepsilon]\varphi^{r+}_A\,, \tag{25}$$

$$\psi^u_A \to \exp\,[iq_A\varepsilon]\psi^u_A\,, \qquad \overline{\psi}^u_A \to \exp\,[-iq_A\varepsilon]\overline{\psi}^u_A\,, \tag{26}$$

whe $q_A (= 0, 1, 2, \ldots.)$ is the electric charge of the particle A and ε is an arbitrary real constant. Similar condition but with different values of q_A is to be imposed on M by nucleonic charge conservation. Both charge conservation requirements restrict the number of possible combinations of φ^r_A, ψ^u_A, φ^{r+}_A, $\overline{\psi}^u_A$ which are allowed to occur in M. However, apart from a difference in the constant phase factors, the results to be obtained below are independent of any particular combination of the fields and their Hermitian (or charge) adjoints. Therefore, for the sake of convenience we introduce two new symbols $\Phi^r(p^\varkappa)$ and $\Psi^u(p^\varkappa)$ defined as follows:

$$\Phi^r(p^\varkappa) = \varphi^r(p^\varkappa) \quad \text{or} \quad \Phi^r(p^\varkappa) = \varphi^r_c(p^\varkappa) = \varphi^{r+}(-p^\varkappa)\,, \tag{27}$$

$$\Psi^u(p^\varkappa) = \psi^u(p^\varkappa) \quad \text{or} \quad \Psi^u(p^\varkappa) = \psi^u_c(p^\varkappa) = \mathcal{C}\overline{\psi}^u(-p^\varkappa)\,, \tag{28}$$

according to the type of reaction. We shall assume in the following that all the M's contain such combinations of particle and antiparticle fields which satisfy both electric and nucleonic charge conservation. Of course in more detailed considerations one must state explicitly what fields occur in the actual expression for M.

4. – Processes between four Bosons.

In this Section we shall discuss reactions between four Bosons of arbitrary spins, The particles will be described by four tensor fields $\Phi^r_1(p^\mu_1)$, $\Phi^s_2(p^\mu_2)$, $\Phi^u_3(p^\mu_3)$, $\Phi^v_4(p^\mu_4)$ and their Hermitian adjoints. Let us discuss first the case when all four Bosons are different. We find for this case the following general

expression for M which satisfies all the « absolute » requirements listed at the end of the preceding section:

$$M = \int \delta_4\Big(\sum_{A=1}^{4} p_A\Big) \prod_{A=1}^{4} \{\delta(p_A^2 - m_A^2)\,\mathrm{d}p_A\} \cdot \{\Phi_{1r}\Phi_{2s}\Phi_{3u}\Phi_{4v} I^{r\,uv} + \Phi_{4v}^{+}\Phi_{3u}^{+}\Phi_{2s}^{+}\Phi_{1r}^{+}\hat{I}^{r\,uv}\}\,,$$

where the tensors $I^{r\,uv}$ and $\hat{I}^{r\,uv}$ are c-numbers of the following structure

$$(30) \qquad \begin{cases} I^{rsuv} = \sum_{K=1}^{N} a_K G_K^{rsuv} + \sum_{R=1}^{N'} a'_R\, \varepsilon^{\alpha\beta\gamma\delta} G_{R:\alpha\beta\gamma\delta}^{rsuv}\,, \\ \hat{I}^{rsuv} = \sum_{K=1}^{N} b_K G_K^{rsuv} + \sum_{R=1}^{N'} b'_R\, \varepsilon^{\alpha\beta\gamma\delta} G_{R:\alpha\beta\gamma\delta}^{r\,uv}\,. \end{cases}$$

The coefficients a_K, a'_R, b_K, b'_R are, in general unknown, scalar functions of two scalar products of the four-momenta p_A^μ (since because of the energy-momentum conservation only two of the scalar products are independent). $\varepsilon^{\alpha\beta\gamma\delta}$ is the well known antisymmetric pseudotensor satisfying the relation

$$(31) \qquad \varepsilon_{\alpha\beta\gamma\delta} = -\,\varepsilon^{\alpha\beta\gamma\delta}\,.$$

The G_K^{rsuv} and $G_{R:\alpha\beta\gamma\delta}^{rsuv}$ are known tensors constructed from the three independent momenta and from the metric tensor $g^{\mu\nu}$; they do not contain the pseudotensor $\varepsilon^{\alpha\beta\gamma\delta}$ and any complex numbers. The numbers of N and N' of linearly independent (*) tensors of each kind and their actual form depend of course on the type of reaction, *i.e.* essentially on the spins and masses of the interacting particles. We have to note some important identities which follow from the definition of the G's:

$$(32) \qquad \begin{cases} G_K^{rsuv*} = G_K^{rsuv}\,, & G_{R:\alpha\beta\gamma\delta}^{rsuv*} = G_{R:\alpha\beta\gamma\delta}^{rsuv}\,, \\ G_{K:rsuv}(p_{A\mu}) = G_K^{rsuv}(p_A^\mu)\,, & G_{R:rsuv}^{\alpha\beta\gamma\delta}(p_{A\mu}) = G_{R:\alpha\beta\gamma\delta}^{rsuv}(p_A^\mu)\,, \\ (-1)^\tau G_K^{rsuv}(-p_A^\mu) = G_K^{rsuv}(p_A^\mu)\,, & (-1)^\tau G_{R:\alpha\beta\gamma\delta}^{rsuv}(-p_A^\mu) = G_{R:\alpha\beta\gamma\delta}^{rsuv}(p_A^\mu)\,, \end{cases}$$

where τ is the rank of the tensor $(rsuv)$.

Let us now investigate what conditions are to be imposed on (29) due to each of the conditions (21)–(24).

a) *TCP invariance.* – Transformation of the φ's under any of the triple products W_L is given by (11). Apart from some constant phase factors of

(*) This means that any other tensor $Q^{r\,uv}$ constructed from p_A^μ and $g^{\mu\nu}$ can be written as a linear superposition of N linearly independent tensors G_K^{rsuv} with scalar coefficients, provided that we take both equations of motion and energy-momentum conservation into account. The same is true for the tensors $G_{R:\alpha\beta\gamma\delta}^{rsuv}$.

modulus 1 all the Φ's are transformed into their Hermitian adjoints with a simultaneous change of sign of the arguments $p_A^\mu \to -p_A^\mu$. Introducing new integration variables $p_A'^\mu = -p_A^\mu$ we can transfer this change of sign of internal arguments from the Φ's upon the Γ's. Now, in order to be able to compare right and left hand sides of (24) we assume that kinematically different Boson fields commute. On the other hand in the presence of two or more non-commuting Boson fields the matrix M must be symmetrized in the corresponding field operators (8). Under these two assumptions it is now always possible to arrange the operators occuring on both sides of (24) in the same order and to compare the coefficients. Remembering that under W_L the Γ's transform into Γ^*'s we find that the W_L invariance condition $W_L M W_L^{-1} = M^+$ reduces to

$$(33) \qquad \begin{cases} (-1)^\tau \varrho_L^* \Gamma^{rsuv}(-p_A^\mu) = \Gamma^{rsuv}(p_A^\mu) , \\ (-1)^\tau \varrho_L \hat{\Gamma}^{rsuv}(-p_A^\mu) = \hat{\Gamma}^{rsuv}(p_A^\mu) , \end{cases}$$

where ϱ_L is the product of four phase factors η_{AL} or η_{AL}^* corresponding to four fields Φ_A^μ. It can easily be seen from (30), (32) that relation (33) will always be satisfied provided that we take $\varrho_L = +1$.

Just the same assumptions about commutation properties of the Boson fields and similar arguments with suitable new integration variables are to be used in the subsequent analysis of P, C and T invariance. For the sake of brevity we shall state only the main results.

b) *P invariance* condition (21) reduces to

$$(34) \qquad \begin{cases} \varrho_P \Gamma_{rsuv}(p_{A\mu}) = \Gamma^{rsuv}(p_A^\mu) , \\ \varrho_P^* \hat{\Gamma}_{rsuv}(p_{A\mu}) = \hat{\Gamma}^{rsuv}(p_A^\mu) , \end{cases}$$

where ϱ_P is the product of four phase factors corresponding to four fields Φ_A^μ. Because of (30), (31) and (32) the relations (34) are equivalent to the following set of equations

$$(35) \qquad \varrho_P a_K = a_K , \qquad \varrho_P a'_R = -a'_R , \qquad \varrho_P^* b_K = b_K , \qquad \varrho_P^* b'_R = -b'_R .$$

(8) The assumptions about the commutation relations used in this paper are sufficient but not necessary for the validity of the *TCP* theorem. *E.g.* we can assume that kinematically different Fermion fields commute with each other and with all Boson fields and the *TCP* theorem will remain valid with slightly changed definitions of the constant phase factors ϱ_L. It is to be noted that in the case when the commutator (or anticommutator) of two field operators is a c-number different from zero the matrix M must be symmetrized (or antisymmetrized) in the corresponding field operators. Compare: G. LÜDERS: *Vertauschungsrelationen zwischen verschiedenen Feldern* (to be published).

There are two possible sets of solutions of (35):

$$\begin{cases} a'_R = b'_R = 0 & \text{if} \quad \varrho_P = +1\,, \\ a_K = b_K = 0 & \text{if} \quad \varrho_P = -1\,. \end{cases} \tag{36}$$

c) *C invariance* condition (22) reduces to

$$(-1)^{\tau}\varrho_C \Gamma^{rsuv}(-p_A^{\mu}) = \hat{\Gamma}^{rsuv}(p_A^{\mu})\,. \tag{37}$$

Because of (30) and (32) the relations (37) are equivalent to

$$\varrho_C a_K = b_K\,, \qquad \varrho_C a'_R = b'_R\,. \tag{38}$$

d) *T invariance* condition (23) reduces to

$$\varrho_T \Gamma_{r.uv}(p_A^{\mu}) = \hat{\Gamma}^{r.uv}(p_A^{\mu})\,. \tag{39}$$

Because of (30), (32) and (31) this is equivalent to

$$\varrho_T^* a_K = b_K\,, \qquad \varrho_T^* a'_R = -b'_R\,. \tag{40}$$

ϱ_T and ϱ_C denote again the products of the four phase factors corresponding to the fields Φ_A^n which occur in (29).

e) *M is Hermitian* if

$$\Gamma^{rsuv*} = \hat{\Gamma}^{rsuv}\,. \tag{41}$$

This is equivalent to

$$b_K = a_K^*\,, \qquad b'_R = a'^*_R\,. \tag{42}$$

5. – Processes between two Bosons and two Fermions.

In this Section we shall investigate the matrix M for reactions between two Bosons and two Fermions of arbitrary spins. It can be shown that in the present case the general expression for M which satisfies all the absolute invariance requirements has the following form

$$M = \int \delta_{(4)}(p_1 + p_2 - p_3 + p_4) \prod_{A=1}^{4} \{\delta(p_A^2 - m_A^2)\,\mathrm{d}p_A\} \cdot \\ \cdot \{\Phi_{1r}\Phi_{2s}\overline{\Psi}_{3u}\Gamma^{rsuv}\Psi_{4v} + \overline{\Psi}_{4v}\hat{\Gamma}^{r.uv}\Psi_{3u}\Phi^{+}_{2s}\Phi^{+}_{1r}\}\,, \tag{43}$$

where the Γ's are given by

$$(44)\qquad \begin{cases} \Gamma^{rsuv} = \sum_{K=1}^{N} (a_K + \gamma_5 a'_K)\, G_K^{rsuv}\,, \\ \hat{\Gamma}^{rsuv} = \sum_{K=1}^{N} \gamma_4\, G_K^{rsuv}\gamma_4 (b_K - \gamma_5 b'_K)\,. \end{cases}$$

The coefficients a_K, a'_K, b_K, b'_K are, in general unknown, scalar functions depending on two scalar products of the four momenta p_A^μ. The G_K^{rsuv} are known covariant forms constructed from the three independent momenta p_A^μ, Dirac matrices γ^μ and the metric tensor $g^{\mu\nu}$; they do not contain the pseudotensor $\varepsilon^{\alpha\beta\gamma\delta}$ or any complex numbers. We have to note three important identities which follow from the definition of the G's:

$$(45)\qquad \begin{cases} \gamma_4 G_{K:rsuv}(p_{A\mu}, \gamma^\nu)\gamma_4 = G_{K:rsuv}(p_{A\mu}, \gamma_\nu) = G_K^{rsuv}(p_A^\mu, \gamma^\nu)\,, \\ (-1)^\tau \gamma_5 G_K^{rsuv}(-p_A^\mu, \gamma^\nu)\gamma_5 = G_K^{rsuv}(p_A^\mu, \gamma^\nu)\,, \\ (-1)^\tau \mathcal{C}\{G_K^{rsuv}(-p_A^\mu, \gamma^\nu)\}^{\sim} \mathcal{C}^{-1} = \gamma_4 \{G_K^{rsuv}(p_A^\mu, \gamma^\nu)\}^{+} \gamma_4\,. \end{cases}$$

Let us now investigate what conditions are to be imposed on (43) due to W_L, P, C or T invariance requirements. In order to be able to arrange the field operators occuring on both sides of (21)–(24) in the same order and then to compare the coefficients we must make some further assumptions about the commutation relations between the field operators. We assume that different Fermion fields anticommute but all the Boson fields commute with all the Fermion fields. In the presence of two or more non-commuting Fermion fields the matrix M should be antisymmetrized in the corresponding field operators ([8]).

a) *TCP invariance* condition (24) can be now reduced to

$$(46)\qquad \begin{cases} \varrho_L^*(-1)^\tau \gamma_5 \Gamma^{rsuv}(-p_A^\mu, \gamma^\nu)\gamma_5 = \Gamma^{rsuv}(p_A^\mu, \gamma^\nu)\,, \\ \varrho_L(-1)^\tau \gamma_5\, \hat{\Gamma}^{rsuv}(-p_A^\mu, \gamma^\nu)\gamma_5 = \hat{\Gamma}^{rsuv}(p_A^\mu, \gamma^\nu)\,. \end{cases}$$

It can easily be seen from (44) and (45) that (46) will be always satisfied provided that we can take $\varrho_L = +1$.

b) *P invariance condition* (21) reduces to

$$(47)\qquad \begin{cases} \varrho_P \gamma_4 \Gamma_{rsuv}(p_{A\mu}, \gamma^\nu)\gamma_4 = \Gamma^{rsuv}(p_A^\mu, \gamma^\nu)\,, \\ \varrho_P^* \gamma_4\, \hat{\Gamma}_{rsuv}(p_{A\mu}, \gamma^\nu)\gamma_4 = \hat{\Gamma}^{rsuv}(p_A^\mu, \gamma^\nu)\,. \end{cases}$$

Because of (44) and (45) this is equivalent to the following set of equations

$$\varrho_P a_K = a_K\,, \qquad \varrho_P a'_K = -a'_K\,, \qquad \varrho_P^* b_K = b_K\,, \qquad \varrho_P^* b'_K = -b'_K\,. \tag{48}$$

There are again two possible solutions of (48):

$$\begin{cases} a'_K = b'_K = 0 & \text{if} \quad \varrho_P = +1\,, \\ a_K = b_K = 0 & \text{if} \quad \varrho_P = -1\,. \end{cases} \tag{49}$$

c) *C invariance* condition (22) reduces to

$$\varrho_C(-1)^\tau \mathcal{C}\{\Gamma^{\tau s u v}(-p_A^\mu, \gamma^\nu)\}^\sim \mathcal{C}^{-1} = \hat{\Gamma}^{\tau s u v}(p_A^\mu, \gamma^\nu)\,. \tag{50}$$

Because of (44) and (45) this is equivalent to the following set of equations

$$\varrho_C a_K = b_K\,, \qquad \varrho_C a'_K = -b'_K\,. \tag{51}$$

d) *T invariance* condition (23) reduces to

$$\varrho_T \gamma_5 \mathcal{C}\{\Gamma_{\tau s u v}(p_{A\mu}, \gamma^\nu)\}^* \mathcal{C}^{-1}\gamma_5 = \gamma_4\{\hat{\Gamma}^{\tau s u v}(p_A^\mu, \gamma^\nu)\}^+ \gamma_4\,. \tag{52}$$

Because of (44) and (45) this is equivalent to the following set of equations

$$\varrho_T^* a_K = b_K\,, \qquad \varrho_T^* a'_K = b'_K\,. \tag{53}$$

e) *M is Hermitian if*

$$\hat{\Gamma}^{\tau s u v} = \gamma_4 \Gamma^{\tau s u v +} \gamma_4\,. \tag{54}$$

This is equivalent to

$$b_K = a_K^*\,, \qquad b'^*_K = a'^*_K\,. \tag{55}$$

6. – Reactions between four Fermions.

Now we shall investigate the form of the transition matrix M for reactions between four Fermions of arbitrary spins. It can easily be seen that the most general expression for the transition matrix that satisfies all the « absolute » invariance requirements has now the following form:

$$M = \int \delta_{(4)}(p_1 - p_2 + p_3 - p_4) \prod_{A=1}^{4} (\delta(p_A^2 - m_A^2)\,\mathrm{d}p_A\} \cdot \\ \cdot \{\overline{\Psi}_{1r} \cdot \overline{\Psi}_{3u} \cdot \Gamma^{\tau s u v} \cdot \Psi_{2s} \cdot \Psi_{4v} + \overline{\Psi}_{4v} \cdot \overline{\Psi}_{2s} \cdot \hat{\Gamma}^{\tau s u v} \cdot \Psi_{3u} \cdot \Psi_{1r}\}\,, \tag{56}$$

where the Γ's have the following structure

$$(57)\qquad \begin{cases} \Gamma^{rsuv} = \sum_{K=1}^{N} (a_K \gamma_5 + a'_K)\, G_K^{rsuv}\,, \\ \Gamma'^{rsuv} = \sum_{K=1}^{N} \gamma'_4\, \gamma_4 G_K^{rsuv} + \gamma_4\, \gamma'_4 (b_K - \gamma_5 b'_K)\,. \end{cases}$$

If two or more Fermion fields that occur in the reaction do not commute the matrix M should be antisymmetrized in the corresponding field operators ([8]).

In order to be able to write M in a more compact form we have introduced two sets of Dirac matrices γ'^{μ} and γ^{μ} with the convention that γ'^{μ} acts only on Ψ_{1r} and Ψ_{2s} or their Hermitian adjoints; on the other hand γ^{ν} act on Ψ_{3u} and Ψ_{4v} or their Hermitian adjoints only. All the γ'^{μ} commute with all the γ^{ν}.

The coefficients a_K, a'_K, b_K, b'_K are again, in general unknown, scalar functions of two independent scalar products of the four-momenta p_A^{μ}. The G's are known covariant forms constructed from p_A^{μ}, γ'^{ν}, γ^{λ}, γ'_5, γ_5 and $g^{\mu\nu}$ only; they do not contain any other complex numbers. The matrices γ'_5 and γ_5 can occur in the G's only in the form of a factor $\gamma'_5\gamma_5$. We have to note the following three identities which follow from the definition of the G's:

$$(58)\qquad \begin{cases} \gamma'_4\gamma_4 G_{K\,rsuv}(p_{A\mu}, \gamma'^{\nu}, \gamma^{\lambda})\gamma_4\gamma'_4 = G_{K\,rsuv}(p_{A\mu}, \gamma'_{\nu}, \gamma_{\lambda}) = G_K^{rsuv}(p_A^{\mu}, \gamma^{\nu}, \gamma^{\lambda})\,, \\ (-1)^r \gamma'_5\gamma_5 G_K^{rsuv}(-p_A^{\mu}, \gamma'^{\nu}, \gamma^{\lambda})\gamma_5\gamma'_5 = G_K^{rsuv}(p_A^{\mu}, \gamma'^{\nu}, \gamma^{\lambda})\,, \\ (-1)^r \acute{e}\acute{e} \{G_K^{rsuv}(-p_A^{\mu}, \gamma'^{\nu}, \gamma^{\lambda})\}^{\sim} e^{-1}\acute{e}^{-1} = \gamma'_4\gamma_4 \{G_K^{rsuv}(p_A^{\mu}, \gamma'^{\nu}, \gamma^{\lambda})\}^{+}\gamma_4\gamma'_4\,. \end{cases}$$

Using just the same assumptions and the same procedure as in the preceding section we can again reduce the general invariance conditions (21)–(24) to some relations between the Γ's. Because of the identities (58) we can express these relations in terms of some simple equations between the scalar coefficients a_K, a'_K, b_K, b'_K. The results obtained in this way are formally the same as those of the preceding section. Thus:

a) *TCP invariance* condition (24) will be always satisfied provided that we take $\varrho_L = +1$.

b) *P invariance* condition (21) reduces to

$$(59)\qquad \begin{cases} a'_K = b'_K = 0 \qquad \text{if} \qquad \varrho_P = +1\,, \\ a_K = b_K = 0 \qquad \text{if} \qquad \varrho_P = -1\,. \end{cases}$$

c) *C invariance* condition (22) reduces to

$$\varrho_C a_K = b_K\,, \qquad \varrho_C a'_K = -\,b'_K\,. \tag{60}$$

d) *T invariance* condition (23) reduces to

$$\varrho_T^* a_K = b_K\,, \qquad \varrho_T^* a'_K = b'_K\,. \tag{61}$$

e) *M is Hermitian* if

$$a_K^* = b_K\,, \qquad a'^*_K = b'_K\,. \tag{62}$$

7. – Summary and outlook.

In Sect. **4-6** we have constructed the most general expression for the transition matrix M describing all the possible processes involving four particles of arbitrary spins. Just the same procedure can be applied to the general case of a reaction between n particles of arbitrary spins. We always find that the structure of the transition matrix M is determined first by the product of n field operators, second by some covariant forms denoted here by the symbols Γ, $\hat{\Gamma}$. The Γ's are c-numbers and can always be written as sums of products of unknown scalar coefficients multiplied by known covariant forms G_{A}^{rsuv} which can be chosen to satisfy some simple identities. The word « known » means that the G's can always be found without any essential difficulties for any given type of reaction ([9,10]). For higher spins, however, the task of finding the set of basic independent G's can be quite laborious.

It turns out that the assumption of invariance of the theory under proper Lorentz transformations together with some assumptions about the commutation relations between the fields are just sufficient to secure the invariance under triple products TCP etc. Strictly speaking the TCP invariance requirement imposes some restriction upon the constant phase factors ϱ_L only, but does not lead to any other physical relations unless supplemented by some additional restrictive assumptions. On the other hand the P, C and T invariance requirements or Hermiticity condition impose much more serious restrictions upon the general form of M. Because of the identities satisfied by the G's these restrictions can be always expressed in terms of some simple

([9]) Compare M. KAWAGUCHI: *Prog. Theor. Phys.*, **12**, 760 (1954), where some reactions between particles of spins 0, $\frac{1}{2}$ and 1 are discussed.

([10]) Some more detailed considerations about the form of basic independent tensors G_K^{rsuv} are given in another paper: J. WERLE: *Bull. Pol. Ac. Sc.* (to be published).

equations between the phenomenological scalar coefficients that occur in the general expression for the transition matrix.

The problem which stands now before us in that of physical interpretation of our formal relations. However, it seems that this cannot be done in such a generality as that obtained in this paper and that we must study every reaction separately. Some examples and a discussion of physical implications will be given in another paper.

* * *

The author would like to express his thanks to Prof. L. INFELD and Dr. W. KRÓLIKOWSKI and to the members of the Theoretical Division of CERN, expecially to Dr. J. PRENTKI and Dr. R. OMNES for many helpful discussions.

RIASSUNTO (*)

Si danno espressioni generali per la matrice di transizione delle reazioni fra quattro particelle di spin arbitrari. Le restrizioni imposte dall'esigenza dell'invarianza di T, C o P si esprimono in termini di semplici equazioni tra alcuni coefficienti scalari fenomenologici che compaiono nell'espressione generale della matrice di transizione. Per ogni dato tipo di reazione si possono così trovare relazioni fisiche definite che offrono il vantaggio di essere esenti da qualsiasi ipotesi e approssimazione generali.

(*) *Traduzione a cura della Redazione.*

On the Symmetry Law and the Pion Decay.

H. Umezawa and H. Miyazawa

Department of Physics, University of Tokyo - Tokyo

(ricevuto il 15 Marzo 1958)

Summary. — Assuming the global symmetry of the strong pion-interactions, a simple combination of the V- and A-types the β-interaction is introduced to explain the problem of the β- and radiative β-decays of the pion. This combination is in good accordance with the rule saying that the weak interactions are invariant under the transformation, under which the nucleon and the Ξ are interchanged and γ_5 appearing in the baryon changes its sign.

It has long been known that the π-nucleon interaction together with the interaction for β-disintegration of the nucleon leads us to the β- and radiative β-decays of the pion. So far no events of these decay processes, have appeared in experiments. This means that

$$[\sigma(\pi \to \mathrm{e} + \nu) \quad \text{or} \quad \sigma(\pi \to \mathrm{e} + \nu + \gamma)]/\sigma(\pi \to \mu + \nu) \lesssim 10^{-5} .$$

Since the life time for the π-μ decay is known to be $2.5 \cdot 10^{-8}$ s, the life times for the β- and radiative β-decays of the pion are longer than 10^{-3} s.

Only the P- and A-types of the β-interaction contribute to the non-radiative β-decay of the pion as far as we disregard the radiative corrections due to the electromagnetic and weak interactions. The β-interaction of the P-type gives us the life time shorter than 10^{-8} s. As for the A-type, the lowest order approximation in the perturbation theory leads to the life time $\tau_\beta = 2 \cdot 10^{-4}$ s with the choice of the cut-off momentum equal to the nucleon mass [1]. This life time is shorter than the experimental value.

As for the radiative β-decay ($\pi \to \mathrm{e} + \nu + \gamma$), the life time τ_γ in the case of

[1] S. B. Treiman and H. W. Wyld, jr.: *Phys. Rev.*, **101**, 1552 (1956).

the V- or A-type for the β-interactions is quite large, τ_γ being 3 s for the A-type and 0.4 s for the V-type. The β-interaction of the T-type gives a somewhat longer life time of $\sim 10^{-3}$ s (1).

The recent trend in the theory of β-decay indicates the combination of V-A for the β-interaction. The presence of A-type interaction, however, causes difficulties since it gives a too short life time for $\pi \to e+\nu$ as we have seen. It has been known that the difficulties concerned with the β- and radiative β-decays of the pion are hard to be settled by means of a linear combination of the interactions (2). KAWAGUCHI and NISHIJIMA (3) discussed the situation by taking into account the effect due to the Ξ-particle, and showed that the rate of the radiative β-decay is much reduced in the case of the T- and V-couplings when all the interactions concerned are assumed to be invariant under the transformation exchanging the Ξ and nucleon. The problem concerned with the A-type, however, has been left open. In this note we shall give a theory, where both the β- and radiative β-decays are forbidden or much reduced even when the A-type exists.

Let us discuss the pion decay processes due to the β-interaction of the V- and A-types:

$$H_\beta = f(\psi\tau_-\cdot\gamma_\mu(a+b\gamma_5)\psi)L_\mu\,, \tag{1}$$

where

$$L_\mu = \bar{\varphi}_e\gamma_\mu(\alpha+\beta\gamma_5)\varphi_\nu\,.$$

Here ψ is the field operator of the sixteen components describing the Ξ-particle and nucleons. It is assumed that a and b can depend only on the matrix u, whose eigenvalue is 1 for the nucleon and -1 for the Ξ. We shall further assume the global symmetry for the strong π-interactions (4). We shall first discuss the process $\pi \to e+\nu$. A cancellation occurs between the nucleon loop and the Ξ loop when $b = u$ is assumed. In this case the transition matrix element is roughly proportional to $(\Delta M/M)$, the mass difference between the nucleon and Ξ. One then obtains $\tau_\beta = 2\cdot 10^{-4}(M/\Delta M)^2 \approx 10^{-3}$ s which is not inconsistent with the experiment.

In a same way the transition probability for the radiative β-decay is also proportional to $(\Delta M/M)^2$, when $b = u$ and a is independent of u. It should be noted that the situation does not much change even when a depends on u. This is because the transition probability of the radiative β-decay due to the A- and V-types is quite small whatever the constants a and b are.

---

(2) See, however, F. LOW and K. HUANG: *Phys. Rev.*, **109**, 1400 (1958).

(3) S. KAWAGUCHI and K. NISHIJIMA: *Phys. Rev.*, **108**, 907 (1957).

(4) J. SCHWINGER: *Phys. Rev.*, **104**, 1164 (1956); M. GELL-MANN: *Phys. Rev.*, **106**, 1296 (1957).

2109

One can prove that both the β- and radiative β-decays are completely forbidden, when $b - a$, a is independent of u and the global symmetry holds (*i.e.*, ΔM and the radiative corrections are neglected). Let us call the charge conjugation, T-transformation ($\psi \to \tau_1 \psi$, $\varphi_1^{(\pi)} \to \varphi_1^{(\pi)}$, $\varphi_2^{(\pi)} \to -\varphi_2^{(\pi)}$, $\varphi_3^{(\pi)} \to -\varphi_3^{(\pi)}$) and the exchange of the nucleon and Ξ-particle the C, T and G transformations respectively. In the theory of global symmetry the strong π-interactions are invariant under the CTG-transformation. Under this transformation τ_-, a, and b in (1) change as follows,

$$\tau_- \to \tau_- , \qquad a \to -a , \qquad b \to -b .$$

Thus the process $\pi \to \mathrm{e} + \nu$ is forbidden in the approximation under consideration. The current of the nucleon and the Ξ-particle is of the form

$$\frac{ie}{2} \bar{\psi} \gamma_\mu (u + \tau_3) \psi$$

and one has

$$\gamma_\mu \to -\gamma_\mu , \qquad u \to -u , \qquad \tau_3 \to -\tau_3$$

under the CTG-transformation. The current is thus invariant under this transformation. Same is true for the current of the pion. In this way one can prove that the process $\pi \to \mathrm{e} + \nu + \gamma$ is also forbidden in the approximation under consideration.

However, the decay probabilities are not exactly zero because of the mass difference ΔM. It should be noted, however, that ΔM would not be necessarily equal to the observed value; it could be smaller than the observed value because *high energy* baryons are involved in the virtual states. However, there is a reason to imagine that ΔM could not be much different from its observed value. Indeed, assuming the observed value for ΔM, the theory of global symmetry gives the life time $5 \cdot 10^{-15}$ s of the neutral pion ([5]), which is not much different from the maximum value of the experimental life time.

The type of the interaction (1) suggests us a possible way of extending the law of global symmetry into weak interactions. This is to assume that the latter interactions are invariant under the transformation, under which the nucleon and the Ξ are interchanged and γ_5 appearing in the baryon parts of the weak interactions changes its sign. An experimental proof for this symmetry law may be given by the cascade decay of the Ξ-particle:

$$\Xi^- \to \Lambda + \pi^- , \qquad \Lambda \to \mathrm{p} + \pi^- .$$

([5]) J. Tiomno: *Nuovo Cimento*, **6**, 255 (1957).

Indeed, the Λ produced in the first step should be polarized in the direction of its momentum, and therefore, the distribution $\Phi(\theta)$ of the pion due to the subsequent Λ-decay would show forward-backward asymmetry ([6]):

$$\Phi(\theta) \propto (1 + \alpha \cos\theta) .$$

Here θ is the angle between the momentum of the produced Λ-particle and that of the pion in the rest system of the Λ-particle. The global symmetry law for the weak interactions says that the asymmetry factor α should be positive.

Let us now come to the problem of the process $\pi \to \mu + \nu$. We are forced to introduce the direct interaction for this process as far as we assume the interaction (3) (with $\varphi_e \to \varphi_\mu$: the μ-meson field) with $b = u$, because the latter interaction leads us to a too long life time ($\gg 10^{-8}$ s) for the process under consideration. We can omit the direct interaction when we assume the following interaction:

$$f\bar{\psi}\tau_- \gamma_\mu(a + \gamma_5)\psi \cdot (\varphi_\mu \gamma_\mu(\alpha + \beta\gamma_5)\varphi_\nu) .$$

In other words, we can explain both of the $(\pi \to \mu)$ decay and $(\pi \to e)$ decay by means of the weak fermion-fermion interactions, when $b = u$ and $b = 1$ are assumed for the β-interaction and for the baryon-μ-meson interaction, respectively. In this way, however, the universality of the weak interaction is lost.

* * *

We are grateful to Prof. S. Nakamura and Professor S. Machida for their inspiring discussions. We are also indebted to Dr. M. Konuma, and K. Nakagawa for their excellent cooperation.

([6]) H. Umezawa, M. Konuma and K, Nakagawa: *Nuclear Physics*, Vol. 7, No. 2.

— —

RIASSUNTO (*)

Assumendo la simmetria globale delle interazioni forti dei pioni, si introduce una semplice combinazione dei tipi V ed A dell'interazione β, onde spiegare il problema dei decadimenti β e β-radiativi del pione. Tale combinazione è in buon accordo con la regola che stabilisce che le interazioni deboli sono invarianti rispetto alla trasformazione che scambia nucleone e Ξ e muta il segno del γ_5 che compare nel barione.

(*) *Traduzione a cura della Redazione.*

Slow Mesons Accompanying High Energy Interactions (*).

B. Chamany (+) and A. G. Barkow

Marquette University - Milwaukee, Wisconsin

(ricevuto il 5 Aprile 1958)

Summary. — Four nuclear events were found in G-5 emulsions, exposed in Texas at an altitude of 104 000 feet, where the breakup of the primary or the resulting interaction was accompanied by the emission of slow pions. Two of the events could be analysed as nucleon-nucleon interactions, and the energies of the slow pion produced were $(8.06 \pm .09)$ and (8.6 ± 0.1) MeV respectively. On the basis of existing theories on multiple meson production an attempt was made to calculate the probability of observing the production of a 10 MeV pion or less. Computations for two energies of the incident nucleon were made. When the incident nucleon in the laboratory system of co-ordinates was 1.38 GeV, one meson was produced and the probability that it had an energy of 10 MeV or less was found to be 6 in 100. If the incident nucleon is 11.1 GeV ($N=2$), the probability that one meson had an energy of 10 MeV or less was found to be 2 in 1000.

1. – Introduction.

In the systematic scanning of a stack of G-5 Ilford emulsions, four high energy interactions accompanied by slow mesons were observed. The stack was exposed at San Angelos, Texas, at a magnetic latitude of 31° N for a period of better than 10 hours at an altitude of 104 000 feet. In a total of 40 000 stars, 37 events were observed involving heavy nuclear collisions or breakups. The charged distribution of 37 events is given in Table I. The energy of the fragments was obtained from grain count and scattering measu-

(*) Work supported by the National Science Foundation.

(+) Present address: Purdue University, West LaFayette, Indiana.

rements while the energy of the heavy primary was obtained by the opening angle measurement of the α-particles ([1]). The identification of charge was made by δ-ray count and gap count.

TABLE I. – *Charge-energy distribution of the 37 events.*

Z	Number	Energy (GeV/nucleon)
2	12	$1.2 \div 1.6$
6	4	$0.8 \div 2.2$
7	2	$0.8 \div 2.0$
8	2	$1.1 \div 1.9$
10	4	$1.4 \div 2.6$
12	3	$1.0 \div 2.4$
> 12	10	$1.0 \div 1.8$

The four interactions that were accmpanied by the emission of slow mesons are pictured in Fig. 1-4.

2. – Description of events and measurements.

Event 1, Fig. 1. A heavy cosmic ray particle identified as a nitrogen nucleus enters the stack at an angle of 29° with the vertical. The nitrogen nucleus traveled a distance of 6.5 cm in the emulsion and then broke up into three α-particles and a proton. One of the α-particles traveled an added distance of 2.2 cm and made a nuclear interaction, while the other particles and proton left the plate. Their ranges in the emulsion were approximately 5 cm. The nuclear breakup is accompanied by the emission of a slow positive pion. The pion is produced at an angle of 60° with the initial direction of the primary particles. The pion had a total range of 1576 μm in the emulsion at the end of which it underwent a μ-e decay in the plane of the emulsion. The energy of the pion was $(8.06 \pm .09)$ MeV. The basic reactions that participated in the production of the π^+ can be written as

$$\mathrm{P} + \mathrm{P} \rightarrow \mathrm{P} + \mathrm{n} + \pi^+$$

$$\mathrm{n} + \mathrm{P} \rightarrow \mathrm{n} + \mathrm{n} + \pi^+$$

with the first one preferred for the balance of charge in the event.

([1]) M. F. KAPLON, B. PETERS, G. T. REYNOLDS and D. M. RITSON: *Phys. Rev.* **85**, 295 (1952); J. H. NOON and M. F. KAPLON: *Phys. Rev.*, **97**, 769 (1955).

Event 2, Fig. 2. A primary cosmic ray which was identified as that of a carbon nucleus enters the stack at an angle of 30° with the zenith and after traveling a distance of 8 cm broke up into two α tracks and three protons. All of the particles left the emulsion without making any further nuclear interactions. The interaction was accompanied by the emission of a low energy negative pion at angle of 59° to the initial direction of the primary particle It traveled a distance of 1765 μm, after which it was absorbed by a nucleus of the emulsion producing a one prong σ-star. The energy of the pion was (8.6 ± 0.1) MeV. The basic reactions that participated in the production of the π^- can be written as

$$P + n \rightarrow P + P + \pi^-$$

$$n + n \rightarrow n + P + \pi^-$$

with the latter reaction preferred for the balance of charge in the event.

Event 3, Fig. 3. This event was produced by a carbon nucleus and resulted in a jet of 17 minimum tracks, two slow protons, and a slow π^- meson. The slow π^- was emitted at an angle of 63° to the original direction of the primary, has a range of 6700 μm which was followed by the characteristic μ-e decay. The energy of the pion was (18.3 ± 0.2) MeV.

Event 4, Fig. 4. A high energy nuclear interaction of a primary α-particle with one of the nuclei in the emulsion. The interaction was accompanied by a cone of lightly ionizing tracks, two gray tracks and three pions, two negative ones which are identified by the σ-stars they produced, and a positive pion which undergoes a π-μ-e decay. In the cone of lightly ionizing particles are two electron pairs produced by neutral π-meson.

The first two events were observed under very ideal conditions for measurements, being practically in the plane of the emulsion.

The identification of charge of the primary particle producing events 1 2 and 3 was done by δ-ray counting on the primaries and also on the α-particles emitted in the breakups. Let Z_1, Z_2 and Z_3 be the charge of the particle producing event (1), (2) and (3) and N_1, N_2 and N_3 the number of δ-rays per 100 μm along their respective tracks, and N_α the δ-ray density for an α-particle. The δ-ray density has been shown to be proportional to the square of the charge and is constant at relativistic energies The number of δ's associated with the particles in question will be given by

$$N_i = KZ_i^2 + A \qquad \text{where } i = 1, 2, 3, \alpha$$

The values of N_i for the three particles are $N_1 = 6.3 \pm 32$, $N_2 = 4.8 \pm .62$, $N_3 = 4.46 \pm .49$ and $N_\alpha = 0.65 \pm .05$. The error due to background is .1.

PHYS

Fig. 1. – Breakup of a nitrogen nucleus into three alphas, one proton and one π^+ meson of energy (8.06 $\pm$ .09) MeV. The suggested reaction is ${}^{4}_{7}\mathrm{N} + \mathrm{p} \rightarrow 3\alpha + \mathrm{p} + \mathrm{xn} + \pi^+$ and can be considered as a nucleon-nucleon interaction.

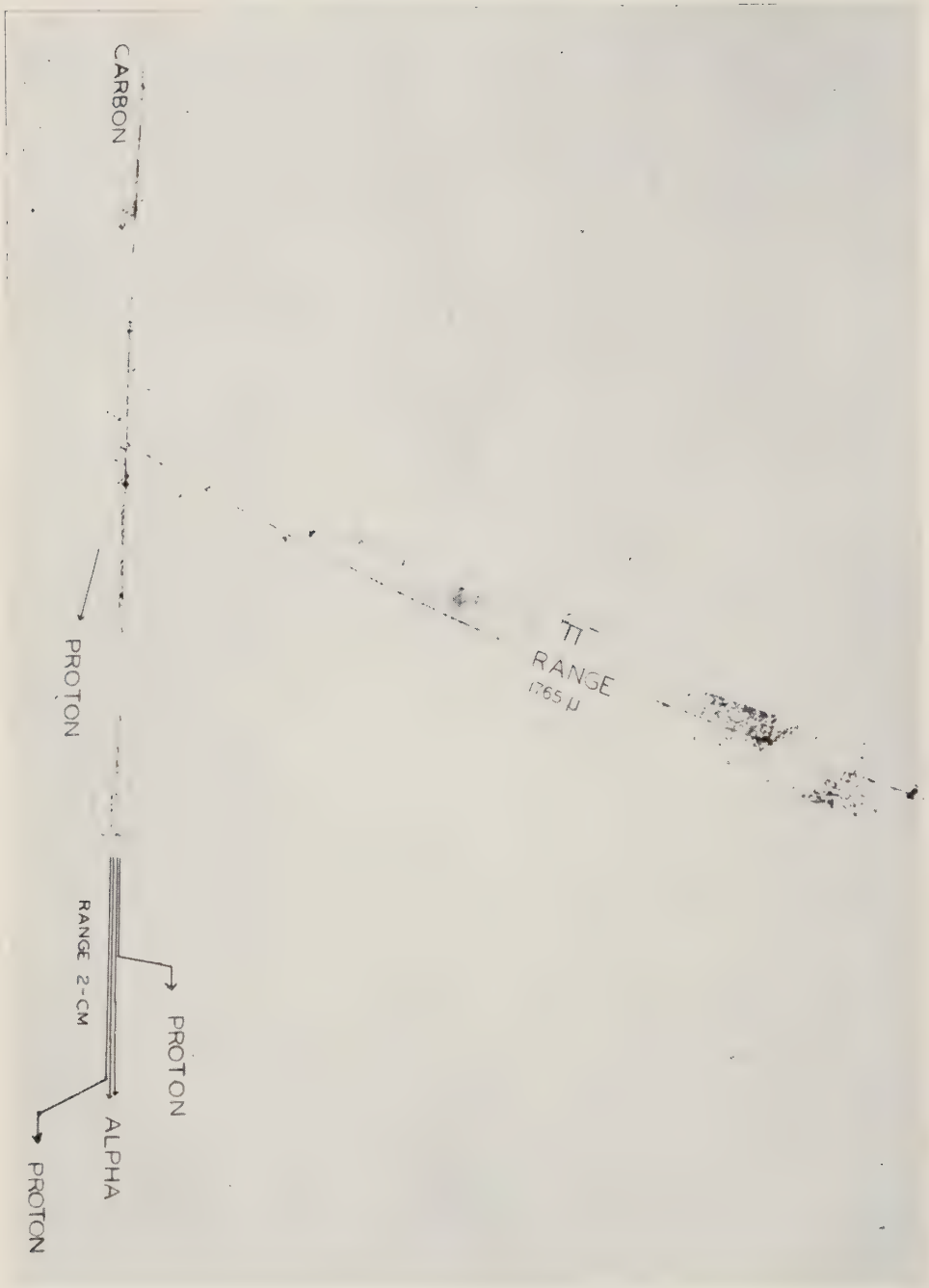

Fig. 2. – Breakup of a carbon nucleus into three protons and two alphas with a π^- meson of energy (8.6 $\pm$ 0.1) MeV. The suggested reaction is ${}^{4}_{6}\mathrm{C}+\mathrm{n}\rightarrow 2\alpha+3\mathrm{p}+\mathrm{xn}+\pi^-$ and can be considered as a nucleon-nucleon, interaction.

Fig. 3. – Collision of a carbon nucleus with a heavy nucleus and the emission of a slow π^+ meson of energy $(18.3 \pm .5)$ MeV together with a jet of high energy pions and nucleons. This reaction cannot be considered as a simple nucleon-nucleon interaction.

Fig. 4. – A collision of an α-particle with a heavy nucleus resulting in the emission of two slow π^- and one slow π^+. The associated jet consisted of seven high energy mesons, four high energy protons, and two sets of electron pairs originating from two π^0.

TABLE II. – *Measurements on fragment particles in events no. 1 and 2. All energies are in* MeV/*nucleon with the exception of the pion.*

EVENT NO. 1

Particle	Range	Ionization (× minimum)	Energy (MeV)/nucleon	Energy (*) (MeV)/nucleon	p (MeV/c)	p^* (MeV/c)
Alpha	2.2 cm	1.04 ±.02	920 ± 86	$1.27\ ^{+45.7}_{-11.7}$	1603 ± 99	$48.7^{+240}_{-3.5}$
Alpha	5 cm	1.06 ±.02	835 ± 77	$.203^{+\ 35}_{-\ .07}$	1504 ± 90	$28.5^{+244}_{-12.4}$
Alpha	5 cm	1.06 ±.02	820 ± 75	$.435^{+38.1}_{-\ .23}$	1486 ± 89	24.4^{+308}_{-190}
Proton	5 cm	0.9655±.02	1295 ±194	$30.8\ ^{+129.2}_{-\ 29.3}$	2026 ±213	51.9^{+232}_{-283}
Pion	1576±31 μm	—	8.06± .09	103±18	48.3± .40	195±33

$\beta = .8486 \pm .0371$ $\gamma = 1.890 \pm .225$ Energy of proton in rest system = (837±246) MeV

EVENT NO. 2

Alpha	2 cm	1.049 ±.027	880 ± 70	$1.34\ ^{+31.1}_{-1.34}$	1557 ± 81	$49.8^{+212}_{-48.4}$
Alpha	2 cm	1.062 ±.129	840 ± 70	$0.385^{+\ 25}_{-\ .38}$	1510 ± 82	$26.8^{+194}_{-\ 25}$
Proton	2 cm	1.083 ±.033	810 ± 90	$1.56\ ^{+39.5}_{-1.56}$	1479 ±102	$53.9^{+227}_{-52.4}$
Proton	2 cm	1.108 ±.030	760 ± 90	$1.93\ ^{+\ 43}_{-\ .70}$	1415 ±111	$60.1^{+232}_{-\ 13}$
Proton	2 cm	1.169 ±.024	625 ± 90	$70\ ^{+120}_{-\ 17}$	1250 ±110	$70\ ^{+257}_{-\ 71}$
Pion	1765±35 μm	—	8.6 ± 0.1	108.9±23.5	49.7± 0.3	196±31.7

$\beta = .8423 \pm .0393$ $\gamma = 1.856 \pm .224$ Energy of neutron in rest system = (803±198) MeV

If one takes the ratio of successive differences, we obtain the expressions

$$(2) \qquad \begin{cases} \dfrac{Z_1^2-4}{Z_2^2-4} = \dfrac{N_1-N_\alpha}{N_2-N_\alpha} = 1.36 \pm 0.02 \,, \\ \dfrac{Z_1^2-4}{Z_3^2-4} = \dfrac{N_1-N_\alpha}{N_3-N_\alpha} = 1.52 \pm 0.2 \quad . \end{cases}$$

Assuming various values of Z_1, Z_2 and Z_3 the best fit is found four $Z_1 = 7$ and $Z_2 = Z_3 = 6$.

The complete data for events No. 1 and 2 are given in Table II.

Energy and momenta in the rest system of the primary are indicated by the asterisks. The values of β and γ were obtained from the relationship

$$\beta = \frac{\sum P_{ix}}{\sum U_i} \,,$$

where P_{ix} and U are the components of momentum and total energy of the α's involved in the breakup.

3. – Theory. Production of mesons.

HEISENBERG ([3]), FERMI ([4]), LANDAU ([5]), and others ([6-10]) have designed various theories to explain the multiple emission of pions in nucleon-nucleon collision. When nucleon-nucleon encounters take place at very high energies, *i.e.*, 100 GeV or more, many mesons are produced. Up to the present time three somewhat different theories have been proposed by HEISENBERG, FERMI and LANDAU. Of these the thermodynamic theory of Fermi and the hydrodynamic theory of Landau appear to have the greatest potentialities. The theory proposed by FERMI has certain limitations, but up to the present time has met with some experimental verification.

When two fast nucleons collide the energy is released in a very small volume V given by the common volume of two very thin Lorentz contracted discs.

([3]) W. HEISENBERG: *Zeits. f. Phys.*, **101**, 533 (1936); **113**, 61 (1939); **126**, 569 (1959).
([4]) E. FERMI: *Prog. Theor. Phys.*, **5**, 570 (1950); *Phys. Rev.*, **81**, 683 (1951).
([5]) L. D. LANDAU: *Izv. Akad. Nauk USSR, Ser. Fiz.*, **17**, 51 (1953).
([6]) H. W. LEWIS J. R. OPPENHEIMER and S. A. WOUTHUYSEN: *Phys. Rev.*, **73**, 127 (1948).
([7]) H. FUKUDA and G. TAKEDA: *Prog. Theor. Phys.*, **5**, 957 (1950).
([8]) H. UMEZAWA, Y. TAKAHASHI and S. KAMEFUCHI: *Phys. Rev.*, **85**, 505 (1952).
([9]) E. CLEMENTEL and N. DALLAPORTA: *Nuovo Cimento*, **5**, 234 (1948); **5**, 298 (1948).
([10]) R. GLAUBER: *Phys. Rev.*, **84**, 395 (1951).

Where the discs collide we have a region of very high energy density and extremely strong interaction and, therefore, one can assume that a large proportion of the proton energy goes into the mesonic field. The volume V in which the energy is released is determined by the dimensions of the nucleon cloud, whose radius is of the order h/mc, where m is the mass of the π-meson ($\Delta p \Delta x \sim h$). Since the nucleons move at high velocity the cloud will undergo Lorentz contraction in the direction of the nucleon's motion. Hence, the volume will be of the order

$$V = V_0 \cdot \gamma = \frac{4\pi}{3}\left(\frac{h}{mc}\right)^3 \cdot \frac{2Mc^2}{E} , \tag{1}$$

where M is the nucleon mass and E is the total energy of two colliding nucleons in the center of the mass system. The particles are created in the volume V at the initial moment of collision according to the laws of statistical equilibrium, and assuming that they no longer interact with each other escape from the volume in a frozen state. The states involved in the equilibrium are the ordinary free particle states of the mesons and nucleons not the states of free particles confined to the spheroid. In this way, dropping constant factors we have

$$\mathrm{erg/cm^3} = \frac{E}{V} \sim T^4 ,$$

and since temperature is energy per particle

$$T \sim E/N$$

so that

$$\frac{E}{V} \sim \frac{E^4}{N^4}; \quad N \sim V^{\frac{1}{4}} \cdot E^{\frac{3}{4}} .$$

If E is the available energy in the center of mass system, we can make the further assumption (Eq. (1))

$$V \sim \frac{1}{E} \qquad \text{or} \qquad N \sim E^{\frac{1}{2}} . \tag{2}$$

Lewis, Oppenheimer and Wouthuysen [6], and others have modified Eq. (2) by introducing the existing field theory with the result

$$N \approx 0.9\, E_0^{\frac{1}{4}} \ (\mathrm{GeV}) , \tag{3}$$

where E_0 is the energy of the primary in the laboratory system.

Numerous attempts have been made to crystallize existing theories into some workable form. The two best review papers are those by MILBURN ([11]) and LEWIS ([12]).

4. – Computations and results.

If we assume a nucleon-nucleon collision to be responsible for the events No. 1 and 2, we can apply the theory of multiple meson production and try to calculate the probability of observing a meson of some energy E in the laboratory system. Since both observed mesons were about 9 MeV we asked ourselves the question, « What is the probability of observing a pion of energy 10 MeV or less in the laboratory system when the incident nucleon energy is sufficient to produce one pion and two pions? » Calculations for any other energy pion and for any incident nucleon can be made in the same way.

In transforming an event to the center of the mass system of the two nucleons it is more applicable to transform total energy U and momenta P_x, P_y and P_z than velocities. By a systematic application of the Lorentz transformation it can be shown that

$$U^* = \gamma(U - \beta c P_x)$$

$$cP_x^* = \gamma(cP_x - \beta U)$$

$$P_y^* = P_y$$

$$P_z^* = P_z .$$

U^* and P^* are the total energy and momentum of the particle in units of MeV and MeV/c respectively in the moving system, U and P being the

TABLE III. – *Data for transformation of* 10 MeV *pion to the laboratory system.* (For 10 MeV pion, $pc = 53.75$ MeV).

No. of pions	E_0 (GeV)	β_c	γ_c	β_U	E^* (CM)	Area of Fig. 5 and 6	Area of Fig. 7*a* and 7*b*	Probability
1	1.38	.652	1.32	98 MeV	600 MeV	.2775 units	.0168	6/100
2	11.1	.923	2.65	138 MeV	3 MeV	2.28 units	.00384	2/1000

U = total energy of the particle to be transformed.

([11]) R. H. MILBURN: *Rev. Mod. Phys.*, **27**, 1 (1955).
([12]) H. W. LEWIS: *Rev. Mod. Phys.*, **24**, 241 (1952).

respective quantities in the laboratory system. Where γ is the ratio of the total energy of the collision to the rest energy of the center of mass.

On the basis of a nucleon-nucleon collision LEWIS ([6]) has developed an expression

$$(4) \qquad P(\theta, \varepsilon, p) = \exp\left\{-\frac{N(M+k)}{2kE_0}\left[\varepsilon - p\,\frac{M-k}{M-k}\cos\theta\right]\right\}\frac{\mathrm{d}p}{\varepsilon},$$

where $P(\theta, \varepsilon, p)$ is the probability of finding a pion of energy ε and $\varepsilon+\mathrm{d}\varepsilon$, momentum p and $p+\mathrm{d}p$ at an angle θ with the initial direction of motion of the parent nucleon. If we integrate Eq. (4) over all angles, we get

$$(5) \qquad P(\varepsilon, \mathrm{d}\varepsilon) = \exp\left[-\frac{N(M+k)\varepsilon}{2kE_0}\right]\cdot\sinh\left[\frac{N(M-k)p}{2kE_0}\right]\cdot\mathrm{d}\varepsilon\,,$$

where $P(\varepsilon, \mathrm{d}\varepsilon)$ is the probability of finding a pion between ε and $\varepsilon+\mathrm{d}\varepsilon$ (or p and $p+\mathrm{d}p$) anywhere in space. E_0 is the energy of the incident nucleon in the center of the mass system of co-ordinates, N is the multiplicity, M the mass of the nucleon and k the mass of the pion in electronic masses.

Fig. 5 and 6 are plots of Eq. (5) for incident nucleon energy of 1.38 and 11.1 GeV respectively.

To determine the probability of observing a pion of 10 MeV or less emitted in any direction in the laboratory system of co-ordinates, we transform the pion into the center of the mass system of the colliding nucleon. This was done for both the 1.38 and 11.1 GeV nucleons and the results are shown in Fig. 7.

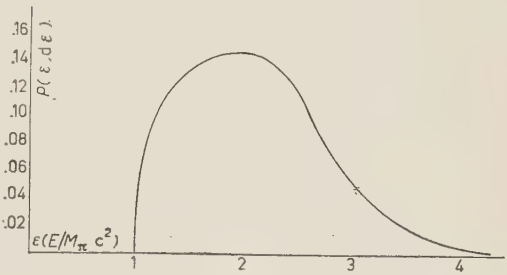

$P(\varepsilon, \mathrm{d}\varepsilon) = e^{-1.79\varepsilon}\sinh(1.33\,p)\,\mathrm{d}\varepsilon$; $N=1$, $E_0(LS)=1.38$ GeV
$E_0(cM)=300$ MeV/nucleon; $E_0/M_\pi c^2=2.15$
Area $=.278$ units; Area $=0.25\,\Sigma$ (ordinates)

Fig. 5. – Energy distribution of all pions formed in a 1.38 GeV nucleon-nucleon collision.

All pions of 10 MeV or less in the laboratory system will have their momentum vector in the center of the mass system terminate in the area shown. If we graphically integrate these areas with the aid of Eq. (4) and compare them with the areas of Fig. 5 and 6, we can calculate the probability of observing a pion of any energy produced in a nucleon-nucleon collision. It must be remembered that Fig. 5 and 6 give the probability of finding a meson of total energy ε anywhere in space regardless of direction in the center of mass system. In our problem the meson occupies a volume given by particular limits of angle and momentum in the center of mass space. For this reason we

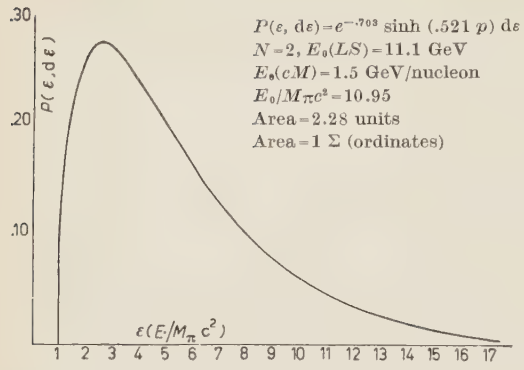

Fig. 6. – Energy distribution of all pions formed in an 11.1 GeV nucleon-nucleon collision.

cannot use Fig. 5 and 6 directly in finding the probability of observing a meson of total energy between the values ε and $\varepsilon + d\varepsilon$. The probabilities were found to be 6 in 100 for nucleons of 1.38 GeV and 2 in 1 000 for 11.1 GeV.

In a total of 40 000 stars there were observed 42 events that involved heavy nuclei, endings of which 4 were thindowns, 1 was thindown associated with breakup ([13]), 4 were breakups associated with the emission of slow mesons and 33 were ordinary breakups. The distribution of the events was given in Table I.

It must be realized that the statistical data are not sufficient to warrant the drawing of definite conclusions. If we are permitted to assume that Events No. 1 and 2 can be considered as a nucleon-nucleon interaction, the probability that a meson of energy of 10 MeV or less be formed is found to be 2 in 37, or about

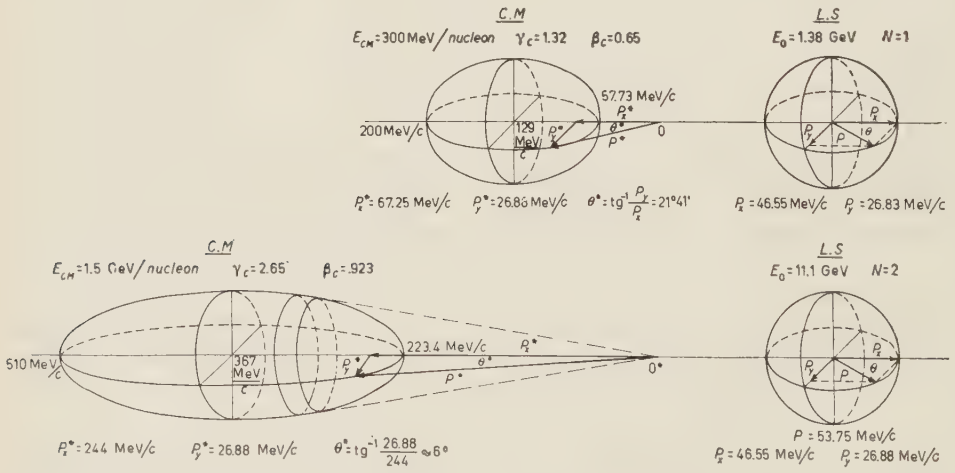

Fig. 7. – Transformation of all π-mesons of energy 10 MeV or less from momentum space in the laboratory system of co-ordinates (L.S.) to momentum space in the center of mass system of co-ordinates (C.M.). The transformation was made for two energies of the incident nucleon. The top diagram for $E_0 = 1{,}38$ GeV, multiplicity of 1; the bottom diagram for $E_0 = 11.1$ GeV and multiplicity of 2.

([13]) A. G. BARKOW, B. CHAMANY and R. E. MCDANIEL: *Nuovo Cimento*, **6**, 125 (1957).

2120

5 in 100, which agrees favorably with theory. The study is being continued and it is hoped that added events will contribute much to the data.

To date two events have been found in a stack of plates exposed for 8 hours at 110 000 feet at the magnetic equator (Guam). Preliminary results indicate nuclei of $Z = 7$ and $Z = 8$, with plus pions being formed at angles 55° and 61° with respective energies of (7.06 $\pm$ 0.3) MeV and (9.3 $\pm$ 0.2) MeV.

* * *

The authors are very grateful to Professor MARCEL SCHEIN of the University of Chicago for his generous assistance in regard to this problem.

RIASSUNTO (*)

In emulsioni G-5 esposte nel Texas ad un'altezza di 104 000 piedi furono trovati 4 eventi nucleari in cui la frammentazione del primario o l'interazione risultante erano accompagnate dall'emissione di pioni lenti. Due degli eventi hanno potuto essere identificati come interazioni nucleone-nucleone e le energie dei pioni lenti prodotti risultarono di (8.06 $\pm$ 0.9) e (8.6 $\pm$ 0.1) MeV, rispettivamente. Sulla scorta delle teorie esistenti sulla produzione multipla dei mesoni, si è tentato di calcolare la probabilità di osservare la produzione di un pione di 10 MeV o meno. I calcoli sono stati eseguiti per due energie del nucleone incidente. Se il nucleone incidente era di 1.38 GeV nel sistema del laboratorio si produceva un mesone e la probabilità che questo avesse energia di 10 MeV o meno si trovò essere del 6%. Se il nucleone incidente è di 11.1 GeV ($N = 2$), la probabilità che uno dei mesoni prodotti abbia energia 10 MeV o meno fu trovata del 0.2%.

(*) *Traduzione a cura della Redazione.*

$M1$ Transitions in ^{141}Pr and ^{191}Ir.

M. C. Joshi, B. N. Subba Rao and B. V. Thosar
Tata Institute of Fundamental Research, Bombay, India

(ricevuto l'11 Aprile 1958)

Summary. — K-conversion coefficients of the 145 keV transition in ^{141}Pr and the 129 keV transition in ^{191}Ir have been determined to be $0.34 \pm .035$ and $2.1 \pm .3$ respectively. These values are found to be in better agreement with the finite nuclear size corrected values rather than with the point nucleus values.

1. – Introduction.

Following the theoretical investigations of Sliv and Listengarten [1] regarding the finite nuclear size effect on K-conversion coeffcients, a few experimental investigations [3-7] have been made. The results of these investigations indicate that for $M1$ transitions, the experimental K-conversion coefficients are in better agreement with those calculated by Sliv and Band [8], rather than with those calculated by Rose *et al.* [2]. More recent theoretical work [9,10] indicates that the conversion coefficients may depend on the finer

[1] L. Sliv and M. A. Listengarten: *Žu. Èksp. Theor. Fiz.*, **22**, 29 (1952).
[2] M. E. Rose *et al.*: *Beta- and Gamma-ray Spectroscopy*, Ed. K. Siegbahn (1955) and *ORNL*-1023.
[3] A. H. Waspstra and G. J. Nijgh: *Nucl. Phys.*, **1**, 245 (1956).
[4] C. Nordling *et al. Nucl. Phys.*, **1**, 326 (1956).
[5] F. K. McGowan and P. H. Stelson: *Phys. Rev.*, **103**, 1133 (1956).
[6] K. O. Nielson *et al.*: *Nucl. Phys.*, **2**, 476 (1957).
[7] G. T. Ewan *et al.*: *Phys. Rev.*, **108**, 1308 (1957).
[8] L. A. Sliv and I. M. Band: *AEC/Tr* 2888.
[9] E. L. Church and J. Weneser: *Phys. Rev.*, **104**, 1328 (1956).
[10] S. G. Nilsson: *UCRL*-3803

2422

features of the nuclear structure. So, it was felt that more experimental investigations in this field would be helpful.

In the case of the 145 keV transition in ^{141}Pr and the 129 keV transition in ^{191}Ir, there was considerable disagreement about the conversion coefficients and conversion ratios among the previous authors. So, we have re-investigated these transitions.

2. – Experimental methods and results.

By studying the internal conversion spectrum and the photoelectron spectrum of γ-rays in the intermediate image β-ray spectrometer, we have determined the values of conversion coefficients and conversion ratios. The spectrometer has been used with 8% transmission and 4% resolution. In one method, the area under the conversion peak is compared with the area under the β-continuum as computed from the experimentally determined Kurie plot. When the decay scheme is simple and well-established this method yields satisfactory values of conversion coefficients. In the other method, described in detail elsewhere ([18]), from the areas under the photo-electron peaks from a radiator, the intensities of γ-rays and X-rays are compared.

3. – ^{141}Pr.

The 145 keV transition in ^{141}Pr arises due to the β^--decay of ^{141}Ce ($T\frac{1}{2} = 33$ days) to the 145 keV excited state of ^{141}Pr. Though the decay scheme seems to be well established, the conversion coefficients determined by various workers ([11-16]) indicate considerable disagreement (Table II).

^{141}Ce was obtained by irradiating a « spec-pure » sample of Ce_2O_3 in the Harwell pile. ^{143}Ce ($T\frac{1}{2} = 33$ hours) which decays into ^{143}Pr which further decays with a half life of 13.7 days to stable ^{143}Nd, was also found with ^{141}Ce These short-lived activities were allowed to decay for about four months. Then, using a source of about 0.2 mg/cm^2 surface density, deposited on an aluminum backing (0.15 mg/cm^2), the internal conversion spectrum, shown in Fig. 1, was observed. The counter window had a cut-off energy at about

([11]) M. S. FREEDMAN *et al.*: *Phys. Rev.*, **79**, 897 (1950).
([12]) R. L. HEATH: *Phys. Rev.*, **87**, 1132 (1952).
([13]) S. A. E. JOHANSSON: *Arkiv f. Fysik*, **3**, 536 (1952).
([14]) E. KONDAIAH: *Arkiv f. Fysik*, **4**, 122 (1952).
([15]) J. T. JONES *et al.*: *Phys. Rev.*, **97**, 1031 (1955).
([16]) G. B. ZORZOLI: *Nuovo Cimento*, **5**, 289 (1957).

4 keV. The results of the analysis of the β-spectrum by the Fermi-Kurie plot (Fig. 2) are summarized in Table I. These results are in agreement with those of earlier workers ([14-16]).

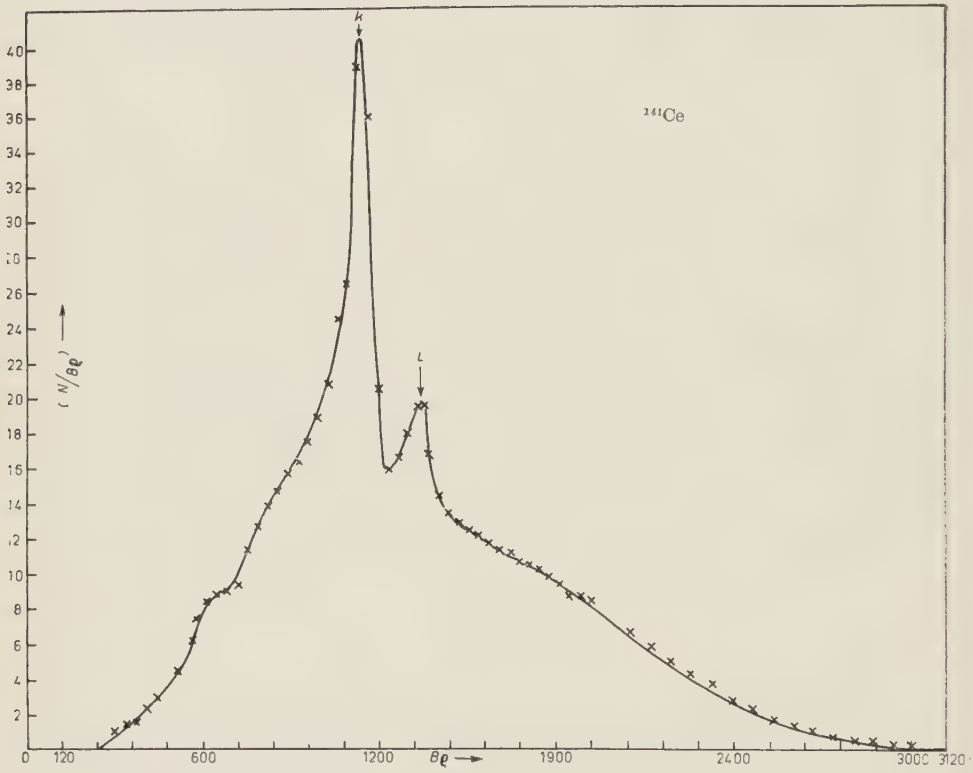

Fig. 1. – Internal conversion spectrum of ^{141}Ce.

Fig. 1 shows that K and $L+M$ conversion lines of the 145 keV transition, along with a weak broad line at about 32 keV which can be identified as the Auger lines of ^{141}Pr following the internal conversion of the 145 keV transition. Using the intensities of the partial β-groups from Table I and the intensities

TABLE I. – *Analysis of* β*-spectra* of ^{141}Ce.

Energy of the β groups (keV)	Relative intensity (%)	log *ft*
β_1 580 ± 5	22 ± 2	7.9
β_2 440 ± 9	78 ± 2	6.8

24241

of conversions lines, the K-conversion coefficient, α^K, was found to be $0.36 \pm .03$. The $K/(L+M)$ ratio was found to be 5.6 ± 0.4 from which K/L was calculated, in an approximation ([17]), to be 6.6 ± 0.8.

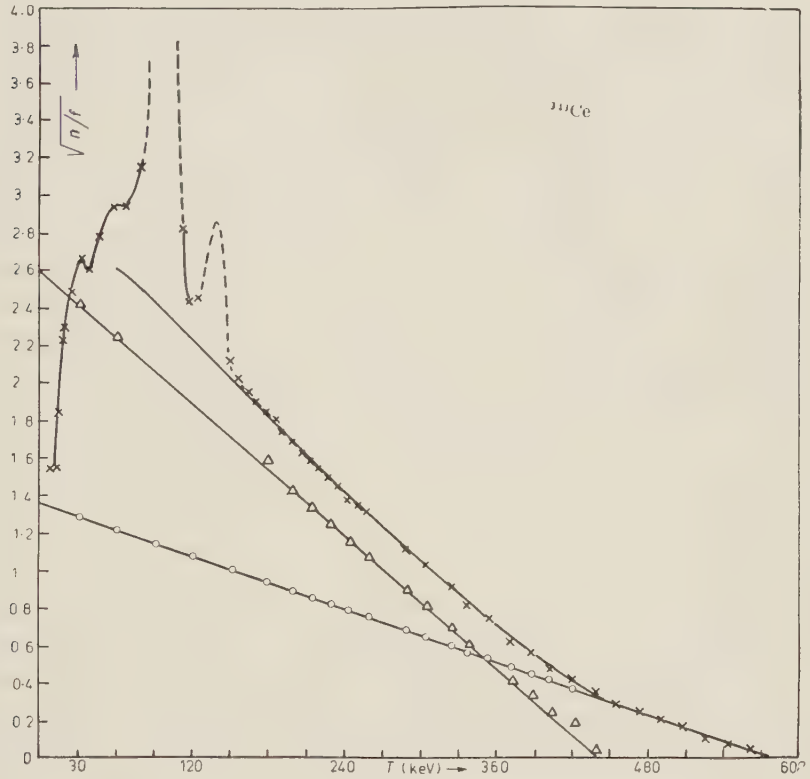

Fig. 2. – Kurie plot for ^{141}Ce.

The photoelectron spectrum of the X-rays and γ-rays of ^{141}Pr was studied. For this purpose, β-rays and internal conversion electrons were absorbed in 350 mg/cm² thick perspex absorber. In view of the low energy of Pr X-rays, a copper converter of about 0.25 mg/cm² thickness deposited by vacuum evaporation on to a perspex disc, was used. The photoelectron spectrum observed in this way, is shown in Fig. 3. In this figure X_{α_K} and X_{γ_L} represent the K and L photoelectrons of K_α X-rays respectively, X_{β_K} and γ_K represent the K-photoelectrons of K_β–X-rays and the 145 keV γ-rays, respectively. Adopting a method similar to our earlier one ([18]), the K-conversion coefficient

([17]) D. E. ALBURGER: *Handbuch der Physik*, **42**, 26 (1957).

([18]) M. C. JOSHI, B. N. SUBBA RAO and B. V. THOSAR: *Proc. Ind. Acad. Sci.*, **45**, 390 (1957).

2425

was calculated by comparing the areas under the photoelectron peaks of X-rays and γ-rays after correcting for the variation in photoelectric cross-section with energy ([19]), for the absorption of X- and γ-rays in the source material and perspex absorber, and for the fluorescence yield ([20]) in Pr (ω_K=0.88). Thus α^K was found to be 0.32 ± 0.04. Average of α^K from these two methods gave $0.34 \pm .035$.

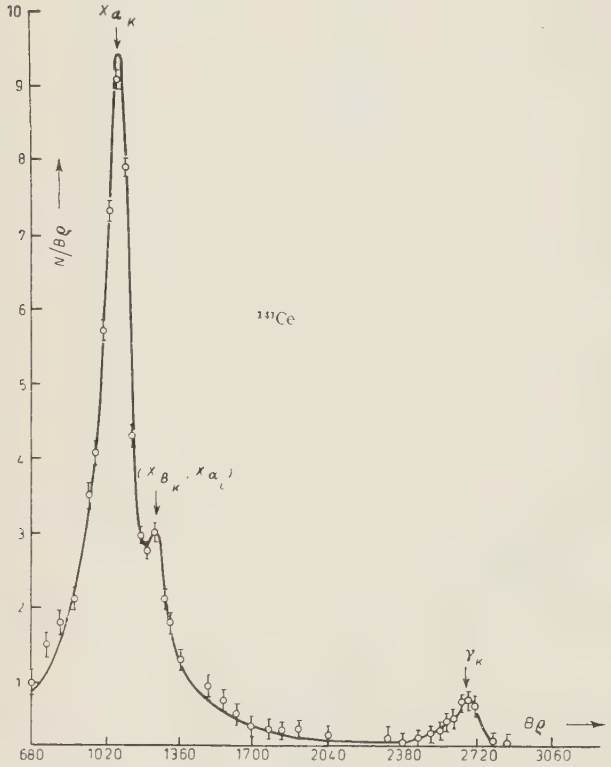

Fig. 3. – Photo-electron spectrum of ^{141}Ce.

Our experimental values are compared with those of earlier workers and with the theoretical ones in Table II. The theoretical values of ROSE were obtained from the K, L_{I}, L_{II}, and L_{III} conversion coefficients from the tables of ROSE *et al.* ([2]) by linear interpolation on log α against z plot.

From Table II, by comparing the experimental values of K/L with

TABLE II. – 145 keV *transition in* ^{141}Pr.

Quantity	References						Present work	Theoretical			
	(11)	(12)	(13)	(14)	(15)	(16)		ROSE *et al.* (2)		SLIV *et al.* (8)	
								*M*1	*E*1	*M*1	*E*2
K/L	5.5	5±1	—	6.5	6.35	6.2	6.6±0.8	7.5	2.6	—	—
α^K	0.25	0.46	0.48	0.33	0.22	0.37	0.34±.035	0.43	0.42	0.39	0.37

([19]) C. M. DAVISSON: *Beta and Gamma-ray Spectroscopy*, Ed. K. SIEGBAHN (1955), p. 869.

([20]) I. BERGSTROM: *Beta and Gamma-ray Spectroscopy*, Ed. K. SIEGBAHN, (1955), p. 630.

the theoretical ones of ROSE, it is seen that this transition should be predominantly $M1$ ($93 \pm 10\%$) with a small admixture of $E2$. AMBLER *et al.* ([21]) from their experiments with aligned nuclei have shown that the transition is mostly $M1$ with only about 4% $E2$ component. From similar experiments CACHO *et al.* ([22]) have found that $E2/M1 = 0.007$. HEYDENBERG and TEMMER ([23]) did not observe any 145 keV γ-ray in Coulomb excitation experiments on ^{141}Pr thereby indicating the almost complete absence of the $E2$ component. Life-time determinations led H. DE WAARD *et al.* ([24]) to conclude that the 145 keV transition in ^{141}Pr is a l-forbidden $M1$ transition. From all this evidence, it may be inferred that the $E2$ admixture to this transition is negligible so that this should be an almost pure $M1$ transition.

Our observed value of α^K may be compared with theoretical values. It is clearly seen from Table II, that the observed value is in better agreement with the value of SLIV *et al.* rather than with that of ROSE *et al.* The observed values of α_K of 0.34 is slightly less than the value for a pure $M1$ transition given by SLIV *et al.* ([8]). It is possible that the nuclear model dependence predicted by CHURCH and WENESER ([9]) is operative.

4. – ^{191}Ir.

It is known that ^{191}Os decays by β^--emission with a half-life of 15 days to the 170 keV isomeric level (life-time = 5 s) of ^{191}Ir. This level decays by the emission of a 42 keV transition followed by a 129 keV transition leading to the ground state. The decay scheme ([30]) seems to be established. Still, the conversion coefficients, and conversion ratios of the 129 keV transition, determined by previous workers ([25-29]), indicate wide differences.

Osmium powder was irradiated in the Harwell pile and the resulting activity consisted of ^{185}Os ($T\frac{1}{2}$=97 days), ^{191}Os ($T\frac{1}{2}$=15 days) and ^{193}Os ($T\frac{1}{2}$= 33 h). ^{193}Os was allowed to decay sufficiently before the present observations were started. Activity of the electron capture isotope, ^{185}Os, was very weak.

([21]) E. AMBLER *et al.*: *Phys. Rev.*, **101**, 196 (1955); **97**, 1212 (1955).
([22]) C. F. M. CACHO *et al.*: *Phil. Mag.*, **46**, 1287 (1955).
([23]) N. P. HEYDENBERG and G. M. TEMMER: *Phys. Rev.*, **100**, 150 (1955).
([24]) H. DE WAARD and T. R. GERHOLM: *Nucl. Phys.*, **1**, 281 (1956).
([25]) E. KONDAIAH: *Arkiv f. Fysik*, **3**, 47 (1951).
([26]) J. B. SWAN and R. D. HILL: *Phys. Rev.*, **88**, 831 (1952).
([27]) R. D. HILL and J. W. MIHELICH: *Phys. Rev.*, **89**, 323 (1953).
([28]) (*a*) F. K. MCGOWAN: *Phys. Rev.*, **93**, 163 (1954); (*b*) F. K. MCGOWAN and P. H. STELSON: *Phys. Rev.*, **107**, 1674 (1956).
([29]) E. M. BERNSTEIN and H. W. LEWIS: *Phys. Rev.*, **105**, 1524 (1957).
([30]) J. W. MIHELICH *et al.*: *Phys. Rev.*, **96**, 1450 (1954).

2427

Using a source of about 0.25 mg/cm² thickness deposited on a plastic film (0.6 mg/cm²) coated with a thin coating of aquadag to make it conducting, the internal conversion spectrum (shown in Fig. 4) was observed.

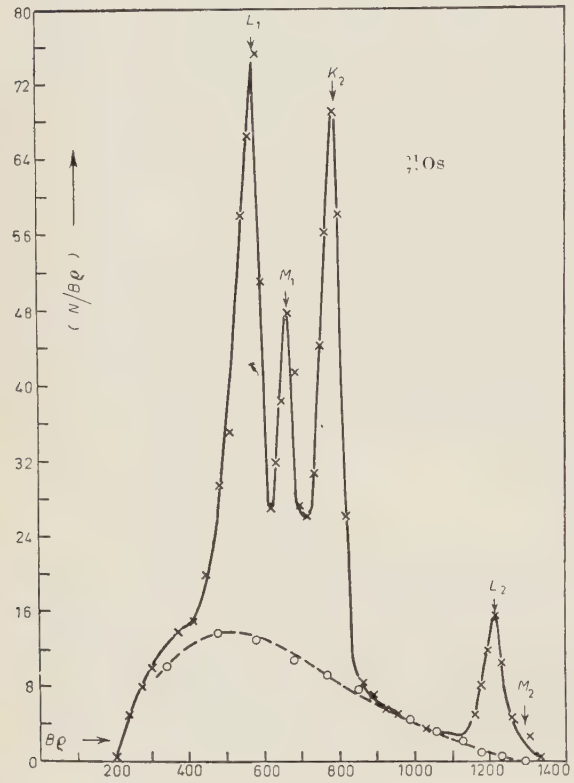

Fig. 4. – Internal conversion spectrum of ^{191}Os.

In this figure, L_1 and M_1 represent the L and M conversion lines of the 41 keV transition, K_2 and L_2 represent the K and L conversion lines of the 129 keV transition. Fermi-Kurie plot was constructed with the points between the K and L conversion lines of the 129 keV transition. The maximum energy was found to be (135 ± 5) keV. This corresponds to a log ft of 5.2, indicating that this transition is of the allowed type. Using the Fermi-Kurie plot to reconstruct the β-spectrum, relative intensities of the β-spectrum and the conversion lines were determined. The L/M ratio of the 41 keV transition was found to be 2.6 ± 0.1. The $K/(L+M)$ and K/L ratios of the 129 keV transitions were found to be 3.7 ± 0.15 and 4.2 ± 0.2, respectively. Using the intensity of the β-spectrum as a measure of the total number of disintegrations leading to the 129 keV level, α^K was found to be 2.10 ± 0.25. All the values quoted above are the mean values of two runs.

Using a thin tin converter (0.15 mg/cm²) evaporated on to a perspex disc, the photoelectron spectrum was observed. β-rays and conversion electrons from the source were absorbed in perspex discs (150 mg/cm²). The photoelectron spectrum, shown in Fig. 5, indicates the K photoelectron peaks of the K_α X-rays, K_β X-rays and the 129 keV γ-ray denoted respectively by X_{α_K}, X_{β_K}, γ_K and the L photoelectron peaks of the three radiations denoted by X_{α_L}, X_{β_L}, γ_L, respectively. Adopting the procedure described in the case of ^{141}Pr, the K conversion coefficient of the 129 keV transition in ^{191}Ir was found

to be $\alpha_K = 2.1 \pm 0.35$, as the mean of two runs. In the evaluation of this quantity, the contribution of Rhenium X-rays due to the capture isotope ^{185}Os to the Iridium X-rays due to internal conversion, was estimated. For this purpose when ^{191}Os had spent nearly 15 half lives, the ^{185}Os radiations were studied under similar conditions and the required intensity computed. This contribution, however, was found to be very small.

The mean value from these two methods is $\alpha^K = 2.10 \pm 0.30$. Our observed values of α^K and K/L are compared with those of earlier authors and with the theoretical values in Table III.

It is seen from Table III that the K/L ratio from the present work is higher than that reported by some authors. Absorption in the counter window can affect these low energy conversion lines. We have used a window with a cut-off energy at about 4 keV, so that the relative intensity

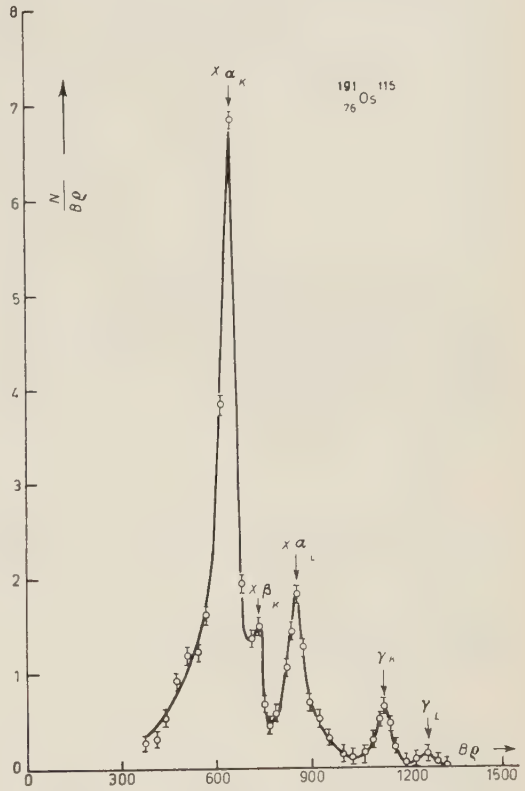

Fig. 5. – Photo-electron spectrum of ^{191}Os.

TABLE III. – *Conversion coefficients and conversion ratios of the* 129 keV *transition in* ^{191}Ir.

Quantity	References					Present work	Theoretical			
	(25)	(26)	(27)	(28)	(29)		Rose *et al.* (2)		Sliv *et al.* (8)	
							$M1$	$E2$	$M1$	$E2$
K/L	2.1	2.2	—	—	3.9	4.2 ± 0.2	6.2	0.5	—	—
α^K	—	1.36	2	2.07 ± 0.1 (*a*) 2.90 ± 0.58 (*b*)	—	2.1 ± 0.3	2.95	0.46	2.45	0.44

of these conversion lines should not be affected to any appreciable extent.

The K/L ratio or α^K alone compared with theoretical values indicates that the transition has a strong $M1$ component. In order to get a better idea of the transition, we may compare the K/L and α^K values with theoretical values graphically, following the method of WAPSTRA *et al.* ([3]).

Let $\beta_1^i (i=K, L_1, L_{11}, L_{111})$ and $\alpha_2^j (j=K, L_1, L_{11}, L_{111})$ denote theoretical conversion coefficients of $M1$ and $E2$ transitions, respectively. Let a represent the fraction of the $M1$ component in a $M1+E2$ transition. For such a transition, the K and L conversion coefficients, α^K and α^L respectively, may be written as,

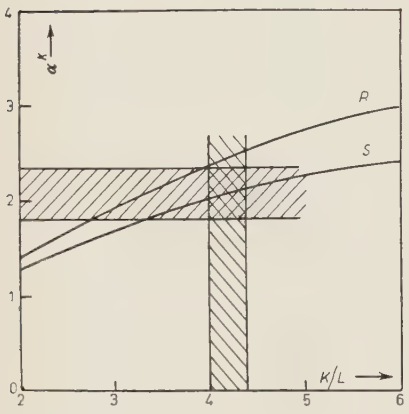

Fig. 6. – α^K-(K/L) plot on point-nucleus (R) and finite size nucleus (S) basis.

$$\alpha^K = a\beta_1^K + (1-a)\alpha_2^K , \tag{1}$$

and

$$\alpha^L = a\beta_1^L + (1-a)\alpha_2^L . \tag{2}$$

Eliminating between these equations, it is seen that

$$\alpha^K = \frac{(\beta_1^K\alpha_2^L - \alpha_2^K\beta_1^L)K/L}{(\beta_1^K - \alpha_2^K) - (\beta_1^L - \alpha_2^L)K/L} . \tag{3}$$

Fig. 6 indicates α^K as a function of K/L. The shaded region being the experimental one. Using the conversion coefficients $\beta_1^i (i=K, L)$ and $\alpha_2^j (j=K, L)$ of ROSE ([2]), the curve R is drawn. The other curve S is drawn, using β_1^K and α_2^K of SLIV and BAND ([8]), and the finite nuclear size corrected values ([32]) of β_1^L and α_2^L. The experimental values are seen, from this figure, to be in better agreement with Sliv's values than with those of ROSE.

Using Sliv's values of β_1^K and α_2^K and our value of α^K, the $M1$ component is found to be $a = 0.82 \pm 0.10$, so that the transition is predominantly $M1$. This is in agreement with the value of $M1/E2 = 5$ given by SUNYAR ([31]), in his summary of lifetimes of $M1+E2$ type of transitions.

([31]) A. W. SUNYAR: *Phys. Rev.*, **98**, 653 (1955).
([32]) Privately circulated tables of M. E. ROSE.

* * *

Our thanks are due to Mr. BHAGWAT and Mr. PANAT for their help during the experiments.

RIASSUNTO (*)

I coefficienti della transizione a 145 keV nel ^{141}Pr e di quella a 129 keV nel ^{191}Ir sono stati determinati, risultando, rispettivamente $0.34 \pm .035$ e $2.1 \pm .3$. Si trova che questi valori si accordano meglio coi valori per il nucleo di dimensioni finite che con quelli per il nucleo puntiforme.

(*) *Traduzione a cura della Redazione.*

Dispersion Relations for Form Factors (*).

Y. Nambu

The Enrico Fermi Institute for Nuclear Studies
The University of Chicago - Chicago, Ill.

(ricevuto il 22 Aprile 1958)

Summary. — The dispersion relations for form factors are studied in perturbation theory. In particular, the relations are proved for a realistic nucleon in the form usually assumed in literature. It is demonstrated, however, that in more general cases the mass spectrum in the dispersion relations depends on the masses of the contributing particles in a peculiar way, which is different from the simple relation hitherto believed. Such a situation arises, for example, in the case of some hyperon models and bound systems such as the deuteron. A formula concerning the final state interaction to be used in conjunction with the dispersion relations is also derived from the invariance of the theory under space-time reversal.

1. – Introduction.

In this paper we are concerned with the properties of the form factor F of a particle

$$\langle q^0 | F(p-q) | p^0 \rangle = \langle q | j(x) | p \rangle \exp [-i(p-q)\cdot x] . \tag{1.1}$$

Here $j(x)$ is a local Heisenberg operator such as the charge-current density; $|p\rangle$ and $|q\rangle$ are true eigenstates of a particle characterized by four-momenta p and q, and other quantum numbers which are suppressed; $|p^0\rangle$ and $|q^0\rangle$ are the corresponding eigenfunctions for an interaction-free particle.

It has been generally believed that $F(p-q) = F(k)$ should be representable in a form analogous to the dispersion relations for scattering matrices. For

(*) This work was supported by the United States Atomic Energy Commission.

example, if the particle has no spin, $j(x)$ is a scalar density, and $F(k) \to 0$ sufficiently rapidly as $k^2 \to \infty$, we should have [1]

$$F(k) = \int_{m_0^2}^{\infty} \frac{\varrho(m^2)}{k^2 + m^2} \, \mathrm{d}(m^2) \,. \tag{1.2}$$

$\pi\varrho(-k^2)$ is the so-called absorptive part of $F(k)$, which should exist only above a threshold $-k^2 \geqslant m_0^2$ for material creation out of vacuum by the external probing field of frequency k_0 and wave number $\boldsymbol{k}$.

In fact, such « dispersion relations » for form factors have been proved under some restrictive conditions from the general properties of field theory, including notably the local commutativity of field operators [2]. For the form factors of a nucleon (mass M) interacting with pion field (mass μ), for example, equations of the type Eq. (1.2) are valid with

$$m_0 = 2\mu \tag{1.3}$$

provided that

$$\mu > (\sqrt{2} - 1) M \,. \tag{1.3'}$$

On the other hand, the relation was proved by the author in every order of perturbation in an example of quantum electrodynamics where $m_0 = 0$ [3]. The present paper will deal with an extension of the proof in perturbation theory so as to include the case of nucleon form factors. In particular, it will be shown that the relation (1.3) is valid for actual nucleons without the restriction (1.3'), which is not satisfied by the real pion.

For practical applications, it is also important to relate the absorptive part of F to other observable quantities, thereby making the dispersion relations, at least in principle, equations to be solved for F. The main idea behind this is very similar to the so-called final state interaction in nuclear reactions formulated by WATSON [4].

These problems will be treated in the following sections, specifically with the nucleon form factors in mind. In the course of the development, it will also become clear that some modifications are necessary with regard to the

[1] G. F. CHEW, R. KARPLUS, S. GASIOROWICZ and F. ZACHARIASEN: *Phys. Rev.* **110** 265 (1958); M. GOLDBERGER and S. TREIMAN: preprints on form factors for weak interactions. Also a lecture by GOLDBERGER on nucleon form factors at Stanford Conference, 1957.

[2] H. J. BREMERMANN, R. OEHME and J. G. TAYLOR: *Phys. Rev.* **109** 2178 (1958).

[3] Y. NAMBU: *Nuovo Cimento*, **6**, 1064 (1957). This paper will be quoted as I.

[4] K. WATSON: *Phys. Rev.*, **95**, 228 (1954).

usually held statement about the lower limit m_0 of the dispersion integral when more general classes of problems are considered. The discussion of this situation will be made in the last two sections.

2. – Representoation of the nucleon form factors.

We consider here the realistic case of the baryon (nucleon and hyperon) field interacting with π and K meson fields (spin zero). The interaction is to be renormalizable. Among the particles, the nucleon and the pion are characterized by the fact that they are respectively the lowest states of the baryon and the meson families, which will turn out to be an important point in the following. Other details are not essential.

We are interested in the electromagnetic form factor of a nucleon

$$\langle q^0 | F_\mu(k) | p^0 \rangle = \langle q | j_\mu(x) | p \rangle \exp [-i(p-q)\cdot x] , \tag{2.1}$$

$j_\mu(x)$ is the total charge-current density of the participating fields. From Lorentz and gauge invariance it follows immediately that

$$F_\mu^{\mathrm{p,n}} = eF_1^{\mathrm{p,n}}(k^2) i\gamma_\mu + \frac{e}{2M} F_2^{\mathrm{p,N}}(k^2) i\sigma_{\mu\nu}k_\nu , \tag{2.2}$$

$$(\mathrm{n} = \text{proton}, \quad \mathrm{p} = \text{neutron}) .$$

The above decomposition can be carried out in perturbation theory for each Feynman diagram. Let such a contribution from a single diagram $\mathcal{G}$ be simply called F_μ. Then we want to show that

$$\begin{cases} F_1^{\mathrm{p,n}}(k^2) = \left(\dfrac{1+\tau_3}{2}\right)^{\mathrm{p\,n}} - k^2 \displaystyle\int_{(2\mu)^2}^{\infty} \frac{\varrho_1^{\mathrm{p,n}}(m^2)}{k^2 + m^2 - i\varepsilon} \, \mathrm{d}m^2 , \\ F_2^{\mathrm{p,n}}(k^2) = \displaystyle\int_{(2\mu)^2}^{\infty} \frac{\varrho_2^{\mathrm{p,n}}(m^2)}{k^2 + m^2 - i\varepsilon} \, \mathrm{d}m^2 . \end{cases} \tag{2.3}$$

The different forms of the representation for F_1 and F_2 are due to their different behavior for large k^2. It is also a reflection of the fact that F_1 requires an infinite charge renormalization whereas F_2, the anomalous moment part, converges without a corresponding renormalization. This is well known, and will not be discussed here. Another point to make is that the same function F_μ can represent creation or annihilation of a nucleon pair by an external

2434

electromagnetic field. In such cases k^2 will be $\leqslant -4M^2$, whereas for a form factor $k^2 \geqslant 0$.

2·1. – According to the results of I, F_1 and F_2 should have a representation

$$\text{(2.4)} \qquad \begin{cases} F_1(k^2) = F_1(0) - k^2 \sum_{n=1}^{N_1} \int\int\int_0^\infty \frac{f_1^{(n)}(\alpha\beta\gamma)}{(J + M^2 - i\varepsilon)^n} \, \mathrm{d}\alpha \, \mathrm{d}\beta \, \mathrm{d}\gamma \, , \\ F_2(k^2) = \sum_{n=1}^{N_2} \int\int\int_0^\infty \frac{f_2^{(n)}(\alpha\beta\gamma)}{(J + M^2 - i\varepsilon)^n} \, \mathrm{d}\alpha \, \mathrm{d}\beta \, \mathrm{d}\gamma \, , \\ J = \alpha p^2 + \beta q^2 + \gamma k^2 = -(\alpha + \beta) M^2 + \gamma k^2 \, . \end{cases}$$

These equations establish the analyticity of $F(k^2)$ for $\mathrm{Im}\,(-k^2) > 0$. In general, there will be a singularity where

$$J + M^2 = 0 \qquad \text{or} \qquad -k^2 = (1 - \alpha - \beta) M^2/\gamma \, .$$

In comparing Eq. (2.4) with Eq. (2.3), the different powers of the denominator will not matter since they do not affect the region of singularity.

2·2. – In order to determine the singularities of Eq. (2.4), we must use Theorem (5) of I, which says that under certain conditions one can find a reduced (lower order) diagram $\mathcal{G}_0$ and a corresponding $F_0(k^2)$ with $J_0(p, q, k) = \alpha_0 p^2 + \beta_0 q^2 + \gamma_0 k^2$ such that

$$\text{(2.5)} \qquad J_0(x, y, z) \geqslant J(x, y, z) \, ,$$

if x, y, z are real and $x + y + z = 0$. and if the « mass term » M^2 is always normalized to the same value.

Let us consider $J(p, q, k)$ as a function of two independent vectors $k = p - q$ and $l = p + q$. Write

$$J(p, q, k) = J(k, l) = J_{11} k^2 + 2 J_{12} k \cdot l + J_{22} l^2 \, .$$

In our case $k \cdot l = p^2 - q^2 = 0$, and Eq. (2.5) means

$$\text{(2.6)} \qquad 0 \leqslant J_{11} \leqslant J_{11}^0 \, , \qquad 0 \leqslant J_{22} \leqslant J_{22}^0 \, .$$

Now both k and l are time-like if $0 < -k^2 < 4M^2$, so that with $|k| \equiv \sqrt{-k^2}$, $|l| \equiv \sqrt{-l^2}$ we get

$$\text{(2.7)} \qquad \begin{cases} J(k, l) = -J_{11} |k|^2 - J_{22} |l|^2 \, , \\ \qquad\quad \geqslant -J_{11}^0 |k|^2 - J_{22}^0 |l|^2 = J_0(k, l) \, . \end{cases}$$

Suppose $J_0 + M^2 > 0$ at the same time for $0 < -k^2 < m_0^2 \leqslant 4M^2$. Then *a fortiori*

$$J + M^2 > 0 .$$

Once this is satisfied, $J + M^2$ and $J_0 + M^2$ will have no zeros for $-k^2 < m_3^2$ since they are increasing functions of k^2, and Eq. (2.3) will have been proven.

2·3. – Let us classify the Feynman diagrams in the following way. Since the nucleon number is conserved, a diagram consists of

a) a baryon line starting with the initial nucleon line and ending with the final nucleon line, carrying a mass $m \geqslant M$;

b) any number of baryon closed loops;

b') meson (π or K) lines connecting the baryon lines, carrying a mass $m \geqslant \mu$.

The external field (« γ ray ») may act on any of the charge carrying lines. So classify F into F_a and F_b according as the γ-ray acts on the baryon line *a*) or the others. Then we carry out the following operations:

1) Reduce the masses appearing in the Δ_F functions on the baryon line *a*) from their original values to M. (We may leave untouched the factor $\gamma \cdot \partial - m$ of S_F).

2) Reduce the masses appearing in the Δ_F functions in *b*) and *b'*) to the pion mass $\mu < M$. We will now refer to all these lines simply as « meson » lines.

Under these operations, the mass term called M^2 in I obviously decreases (or at least does not increase).

3) If the γ-acts on the baryon line (case F_a), remove all the « meson » lines except one, so that we get a typical lowest order diagram Fig. 1*a*.

4) If the γ-ray acts on one of the meson lines (case F_b), remove as many « meson » lines as possible. We will end up with another typical diagram Fig. 1*b* (*).

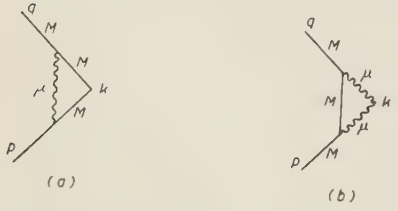

Fig. 1. – Comparison diagrams for the nucleon form factors.

The final diagrams thus obtained we now call $\mathcal{G}_0$. According to Lemma (4)

(*) In case there exists a vector meson, the situation should be different because of different selection rules.

of I, J will increase (or at least not decrease) to J^0 during the operation 3 or 4. Thus after all the operations 1 to 4, the inequality (28) of I; $J/M^2 \leqslant J_0/M_0$ or

$$J \leqslant J_0 ,$$

for our choice of normalization, is certainly valid.

For the diagrams 1*a* and 1*b*, we can easily verify the dispersion relations. We find (*)

$$\left\{ \begin{array}{ll} m_0 = 2M(> 2\mu) & \text{for} \quad F_a , \\ = 2\mu & \text{for} \quad F_b . \end{array} \right. \tag{2.8}$$

This is a more precise statement than is indicated in Eq. (2.3).

In the problem of nucleon form factors, a most puzzling point is the apparent big difference of proton and neutron charge radii, which implies near equality of isotopic vector and scalar parts of the charge form factor. Using a similar technique as above, we can prove that the scalar part has, as has been usually claimed, $m_0 = 3\mu$ in contrast to $m_0 = 2\mu$ for the vector part.

3. – A theorem about the final state interaction (5).

The results of the previous sections show that the absorptive part of F exists only if k is time-like and $-k^2 \geqslant 4\mu^2$. As was noticed before, the function F for $-k^2 > 0$ does not correspond to a form factor, but rather to a matrix element for the transformation of a virtual γ-ray into a nucleon pair if $-k^2 \geqslant 4M^2$. In this region the absorptive part can be interpreted as arising from the interaction of the produced pair. Below the threshold, $F(k^2)$ must be considered as an analytic continuation, which can still have an absorptive part because real mesons may be produced in the intermediate states.

The exact mathematical statement about the final state interaction will be derived as follows: Let us assume that the dispersion formulas obtained in perturbation theory are valid for the entire form factors, and consider the matrix element

$$\langle -p, q^{\text{out}} | j_\mu(k) | 0 \rangle , \qquad -k^2 \geqslant 4M^2 ,$$

(*) In deriving the result (2.8), it may seem that a difficulty arises from vanishing of the denominators corresponding to the initial and final nucleon lines in Fig. 1 when we set $p^2 = q^2 = -M^2$. This can be avoided by first setting $p^2 = q^2 > -M^2$ and taking the limit.

(5) This is an adaptation of a theorem formulated for the case of scattering dispersion relations by S. Fubini, Y. Nambu and V. Wataghin; to be published.

where $\langle -p, q^{\text{out}}|$ is an outgoing state of a nucleon pair. Because of the invariance under time reversal and space reflection, we have

$$\langle -\tilde{p}, \tilde{q}^{\text{out}}|Uj_\mu U^{-1}|0\rangle^* = \langle 0|Uj_\mu U^{-1}|-\tilde{p}, \tilde{q}^{\text{out}}\rangle = \tag{3.1}$$
$$= \langle -p, q^{\text{in}}|j_\mu|0\rangle = \sum_n \langle -p, q^{\text{in}}|n^{\text{out}}\rangle\langle n^{\text{out}}|j_\mu|0\rangle ,$$

$\langle -\tilde{p}, \tilde{q}^{\text{out}}|$ here is the space-time reversed state ($p, q \to p, q,\ \sigma \to -\sigma$), and U the associated transformation operator. n runs over a complete set of states, which includes the nucleon pair state. $\langle -p, q^{\text{in}}|n^{\text{out}}\rangle$ is an element of the S-matrix $S^+ = S^{-1}$. By the nature of the operator j_μ, n will consist of states of nucleon number zero, angular momentum one, and odd spatial and charge parities. For a nucleon pair, in particular, it involves ${}^3S_1$ and ${}^3D_1$ states, reflecting the fact that there are two invariants $i\gamma_\mu$ and $i\sigma_{\mu\nu}k_\nu$.

Let us now introduce the generalized form factor $\mathcal{F}_\mu$ by

$$\langle n^0|\mathcal{F}_\mu|0\rangle = \langle n^{\text{out}}|j_\mu|0\rangle , \tag{3.2}$$

for an arbitrary $|n\rangle$. As in the case of F_μ, $\mathcal{F}_\mu$ may be decomposed into a sum of different invariants

$$\mathcal{F}_\mu = \sum_i O_\mu^{(i)} \mathcal{F}_i(k^2, \alpha_r) , \tag{3.3}$$

where O_μ is a hermitian operator. α_r are scalar numbers, other than k^2, which are necessary to fix the state. For a given k^2 there will be only a finite number of invariants since only a finite number of particles can be present in $|n\rangle$.

The relation (3.1) then becomes in this case.

$$\begin{cases} \langle n^0|U\mathcal{F}_\mu U^{-1}|0\rangle^* = \sum_m \langle n^0|S^+|m^0\rangle\langle m^0|\mathcal{F}_\mu|0\rangle \\ \text{or} \\ \sum_i \langle n^0|O_\mu^{(i)}\mathcal{F}_i^*(k^2, \alpha_r)|0\rangle = \sum_i \sum_{m,\alpha_r'} \langle n^0|S^+|m^0\rangle\langle m^0|O_\mu^{(i)}\mathcal{F}_i(k^2, \alpha_r'|0\rangle . \end{cases} \tag{3.4}$$

We may write it symbolically

$$\sum_i O_\mu^{(i)}\mathcal{F}_i^* = \sum_i S^+ O_\mu^{(i)}\mathcal{F}_i . \tag{3.5}$$

Alternatively, with $S \equiv 1 + iR$,

$$i\sum_i O_\mu^{(i)}(\mathcal{F}_i^* - \mathcal{F}_i) = \sum_i R^+ O_\mu^{(i)}\mathcal{F}_i . \tag{3.5'}$$

On the left-hand side, $i(\mathcal{F}_i^* - \mathcal{F}_i)$ is twice the absorptive part of $\mathcal{F}$. Assuming S to be given, this expresses a set of linear homogeneous equations to be satisfied by the absorptive and dispersive parts of $\mathcal{F}_i$. It must be understood

2438

that they are meaningful even below reaction thresholds through analytic continuation.

Eq. (3.5) or (3.5′) and the dispersion relation (2.3) together constitute coupled integral equations for the absorptive and dispersive parts of F_1 and F_2 as functions of k^2. Since other generalized form factors also appear in Eqs. (3.5) and (3.5′), it may be suggested that all $\mathcal{F}_i$ should have their own dispersion relations like

$$\mathcal{F}_i(k^2, \alpha_r) = \mathcal{F}_i(0, \alpha_r) - \frac{k^2}{\pi} \int_{m_i^2}^{\infty} \frac{\operatorname{Im} \mathcal{F}_i(m^2, \alpha_r)}{k^2 + m^2 - i\varepsilon} \frac{\mathrm{d}m^2}{m^2} , \tag{3.6}$$

with an appropriate choice of the parameters α_r. Then we would have a set of integral equations for all $\mathcal{F}_i$. In fact, Eq. (3.6), may be easily derived from the representations of general Green's functions. This will be shown in the Appendix I.

We will not attempt to solve the integral equations for $\mathcal{F}_i$. Except for the single channel case where only one $\mathcal{F}_i$ has an absorptive part, the only practical way seems to be perturbation expansion starting from $\operatorname{Re} \mathcal{F}_i = \mathcal{F}_i(0)$. But the solution may not be unique. If there is more than one solution, the difference of two such solutions must satisfy homogeneous dispersion relations.

4. – Form factors in a more general case [6].

As is clear from the proof in Sect. 2, the derivation of the mass limit Eq. (2.8) depends critically on the fact that nucleon and pion are respectively the lightest particles of baryon and meson families. In case, for example, the form factor of a hyperon is considered, the proof will not go through since a hyperon can change to a lighter particle, and destroys the necessary inequalities in the proof.

Such a situation can be handled as follows: Since a hyperon form factor is not of immediate practical interest, we will adopt a simplified model, consisting of a hyperon, a nucleon, and a K-meson field, with the respective masses $M_1 > M > \varkappa$. Then a form factor diagram will contain:

a) A baryon line (or baryonic charge carrying line) connecting the initial and final hyperon lines.

b) A strangeness carrying line, which may overlap with *a*), also connecting the initial and final lines.

[6] A very similar observation to the one in this section was recently done by KARPLUS, SOMMERFELD and WICHMANN: preprint.

c) Baryonic charge loops and strangeness loops.

These lines will overlap each other to form a connected diagram. The external γ-ray may act on any of the lines.

In order to facilitate the comparison with standard diagrams, we will first observe the following theorem.

Theorem. In order that the inequalities (27) of I

$$\left\{\begin{array}{l} I(z_i, \alpha_r)\, M^2(\alpha_r) \geqslant I_0(z_i, \alpha_r^0)\, M_0^2(\alpha_r^0)\,, \\ J(q_i, \beta_r)/M^2(\beta_r) \leqslant J_0(q_i, \beta_r^0)/M_0^2(\beta_r^0)\,, \end{array}\right. \tag{4.1}$$

be realized for two diagrams $\mathcal{G}$ and $\mathcal{G}_0$, and for any particular sets z, α or q, β, it is necessary and sufficient that the following inequality be satisfied:

$$\mathcal{J}(z_i) \geqslant \mathcal{J}_0(z_i)\,. \tag{4.2}$$

The function $\mathcal{J}(z_i)$ is defined for a diagram by

$$\mathcal{J}(z_i) = \mathrm{Min}\,\left(\tfrac{1}{2}\sum_i m_s r_s\right)^2\,, \tag{4.2'}$$

$r_s \geqslant 0$ is the length of a propagation line, m_s the mass of the propagating particle, and the summation is over all the lines that occur in the diagram. The minimum is taken with respect to the co-ordinates of the internal vertex points. The proof of the theorem rests on the property

$$I(z_i, \alpha_r)\, M^2(\alpha_r) \geqslant \mathcal{J}(z_i)\,,$$

which will be derived in the Appendix.

Now proceeding more or less in the same way as before, and making use of the above theorem, we find the following comparison diagrams (with the corresponding I_0)

1) If the γ-ray acts on the baryon line *a*), take Fig. 2*a*.

2) If the γ-ray acts on the strangeness line *b*), take Fig. 2*b*.

3) If the γ-ray acts on a (baryon or strangeness) loop, take either Fig. 2*c* or 2*c'*, according as it is connected to the baryon line *a*) or the strangeness line *b*). The masses on the connecting lines have all been reduced to $\varkappa$.

It is not difficult to see that Fig. 2*c* and 2*c'* may further be replaced by Fig. 2*d* and 2*d'* respectively, which are combinations of the vertex diagram 2*a* or 2*b*, and a self-energy diagram.

The main interest is in the vertex diagrams. They are essentially the same

as Fig. 1, except that we now put $-p^2 = -q^2 = M_1^2 > M^2$. By direct calculation, the lower limit m_0^2 of the dispersion relation (2.3) now turns out to be different for the following three cases.

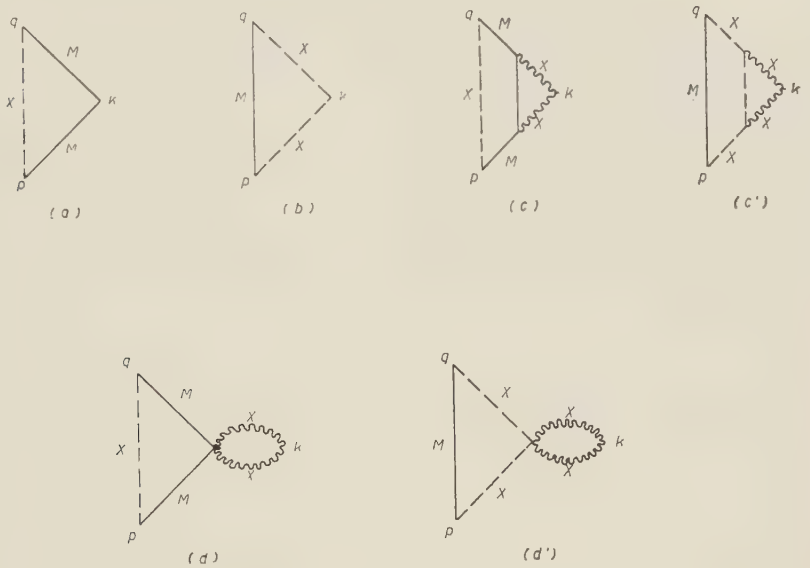

Fig. 2. – Comparison diagrams for the hyperon form factors in our model. Solid line: baryonic charge line. Broken line: strangeness line. These are not necessarily actual diagrams.

Case 1. If $M_1^2 \leqslant M^2 + \varkappa^2$, then

$$m_0 = 2M \qquad \text{Fig. } 2a\,, \tag{4.3}$$

$$= 2\varkappa \qquad \text{Fig. } 2b \text{ and } 2d.$$

The overall lower limit is thus $m_0 = 2\varkappa$.

Case 2. If $M^2 + \varkappa^2 \leqslant M_1^2 < (M+\varkappa)^2$, then

$$m_0^2 = (2M)^2 - \frac{\Delta^2}{\varkappa^2} \quad (\geqslant 0) \qquad \text{Fig. } 2a\,, \tag{4.3'}$$

$$= (2\varkappa)^2 - \frac{\Delta^2}{M^2} \quad (\geqslant 0) \qquad \text{Fig. } 2b \text{ and } 2c,$$

$$= \text{Min}\left(2\varkappa,\ (2m)^2 - \frac{\Delta^2}{\varkappa^2}\right) \qquad \text{Fig. } 2d'.$$

$$\Delta = M_1^2 - M^2 - \varkappa^2\,.$$

The overall lower limit is $m_0^2 = (2\varkappa)^2 - \Delta^2/M^2$.

Case 3. If $M_1 > M + \varkappa$ (the hyperon unstable), then

$$m_0^2 = -\infty \quad (*). \tag{4.3''}$$

This result indicates that the usual argument for the lower limit m_0 as given in Sect. 2 does not necessarily hold for each Feynman diagram, nor for each order of perturbation expansion.

In the general derivation of the dispersion relations from properties of local field operators, the spectrum of the total energy-momentum of intermediate states is specified, but not the masses of individual particles. Thus in the present example we would regard $M_2 = M + \varkappa$ and $2\varkappa$ (or $2M$) as the lowest total masses of the intermediate states. In order to have the Case 1 above, it is then necessary that

$$M_1^2 \leqslant M^2 + \varkappa^2 ,$$

for fixed M_2 and any $\varkappa \leqslant M_2$. Since the right-hand side takes a minimum value $M_2^2/2$ for $\varkappa = M = M_2/2$, that means

$$M_2^2 \geqslant 2M_1^2 \quad \text{or} \quad M_2 - M_1 \geqslant (\sqrt{2} - 1)M_1 . \tag{4.4}$$

This coincides with the condition (1.3′) obtained by BREMERMANN, OEHME and TAYLOR [2] for the derivability of the dispersion relations on the basis of local field theory. It would seem, therefore, that their condition (1.3) is, at least partly, caused by their inability to specify the detailed nature of the intermediate states, rather than their inability to take account of the unitarity condition in general.

5. – Concluding remarks.

We have examined in some generality the validity of the « dispersion relations » for form factors in perturbation theory. In particular, it has been shown that the nucleon form factors should satisfy the usually assumed relations. Thus the large difference of the observed proton and neutron charge radii still remains to be understood. On the other hand, it has become clear that the mass spectrum in the dispersion integral does depend on the masses of the individual particles in a peculiar way.

The last point is of practical significance since any qualitative as well as quantitative appreciation of dispersion relations depends on the mass spectrum. It would be necessary to understand the mass spectrum conditions from a

(*) The actual values of M_1, M, $\varkappa$ correspond to the case 2.

more general point of view. The relation between causality and the validity of the dispersion relations with the modified spectral conditions is not yet clear.

Another interesting point turns up when we consider bound states. It has been shown recently [7] that one can describe bound systems in field theory in much the same way as the so-called elementary particles. One may expect then that the form factors of a deuteron, for example, should satisfy the same kind of dispersion relations as the nucleon. On the other hand, we know that the deuteron form factor should be determined largely by the binding energy according to the uncertainty principle.

It would be absurd if in this case the mass spectrum of the dispersion relation started from $m_0 = 2\mu$, as would be expected if the original argument about m_0 was correct. As a matter of fact, if we calculate the deuteron form factor from the virtual process ($M_p = M_n = M$ assumed for simplicity)

$$\mathrm{D} \rightleftarrows \mathrm{n} + \mathrm{p} ,$$

with *local* interaction, we do fall in the Case 2 of Sect. **4**, with

$$m_0^2 = 4M_D^2(1 - M_D^2/4M^2) ,$$

$$\sim 16\varepsilon M ,$$

where ε is the binding energy. Thus the radius of the deuteron should be $\sim 4\sqrt{\varepsilon M}$. This is just what one gets from the deuteron wave function which falls off as $\exp[-\sqrt{\varepsilon M}r]/r$. ($r$ is the proton-neutron distance, whereas the radius is measured from the center of gravity).

Appendix I

Representation for generalized form factors.

A generalized form factor $\mathcal{F}$, as defined in Eq. (3.2), is essentially a certain n-point Green's function $G_n(k, p_2, \ldots, p_n)$ ($n \geqslant 2$), considered as a function of one momentum k, the other $n-1$ momenta p_i being those of free particles. In other words

$$\mathcal{F}(k, p_i) = L_1(k) \prod_{i=2}^{n} L_i(p_i)\, G_n(k, p_i) , \tag{A.1}$$

where the L_i's are the free-field differential operators, and $p_i^2 = -m_i^2$.

According to the results of I, each invariant $\mathcal{F}_i$, Eq. (3.3), will therefore

[7] K. Nishijima: preprint; W. Zimmermann: preprint.

have a typical representation like

$$\mathcal{F}_i(k, p_i) = C_i - k^2 \sum_{m=1}^{N_i} \int \cdots \int \frac{g_m(\beta_r)}{(J + M^2 - i\varepsilon)^m} \Pi \, \mathrm{d}\beta_r \,,$$

$$J = \beta_1 k^2 + \sum_{i=2}^{n} \beta_i p_i^2 + \sum_{i>j}^{2n} \beta_{ij} (p_i + p_j)^2 + \sum_{i>j>k}^{2n} \beta_{ijk} (p_i + p_j + p_k)^2 + \cdots \tag{A.2}$$

The summation continues until all combinations of $n-1$ momenta p_i. Note that we have deliberately avoided the explicit appearance of combinations like $k+p_i$, $k+p_i+p_j$, ..., by replacing them by the complementary sums. Thus

$$J = \beta_1 k^2 + \sum_{i,j}^{2n} \gamma_{ij} p_i \cdot p_j = \beta_1 k^2 - \sum_i \gamma_{ii} m_i^2 + 2 \sum_{i>j} \gamma_{ij} p_i \cdot p_j \,, \tag{A.3}$$

where $\beta_1 \geqslant 0$, $\gamma_{ij} \geqslant 0$ and the matrix γ_{ij} forms a non-negative quadratic form.

Eq. (A.3) contains $n + (n-1)(n-2)/2 = 1 + n(n-1)/2$ scalar products, whereas only $n(n-1)/2$ of them should be lineraly independent since

$$k^2 = (-\sum p_i)^2 = \sum_{i,j} p_i \cdot p_j \,. \tag{A.4}$$

So eliminate, for example, $p_2 \cdot p_3$ by the above relation, or

$$2 p_2 \cdot p_3 = k^2 - \sum_{i,j}{}' p_i \cdot p_j \,. \tag{A.4'}$$

Then J takes the form

$$\left\{ \begin{array}{ll} J = ck^2 + J'(\alpha_r) \,, & \\ c = \beta_1 + \gamma_{23} \geqslant 0 \,, & \\ \alpha_r = p_i \cdot p_j \,, & i \geqslant 2,\ j \geqslant 4,\ i < j. \end{array} \right. \tag{A.5}$$

Thus for fixed parameters α_r, $\mathcal{F}_i(k^2, \alpha_r)$ is analytic for $\mathrm{Im}\,(-k^2) > 0$ as was expected. The problem remains as to the lower limit m_0 of the mass spectrum in this case. We will not try to determine it since at any rate such generalized form factors will be of little pratical significance.

Appendix II

Proof of the Theorem in Sect. 4.

By the results of I, the quantities $I(z)$ and M^2 are

$$\left\{ \begin{array}{l} I(z_i) = \mathrm{Min}\, \frac{1}{2} \sum_s a_s z_s^2 \,, \\ M^2 = \frac{1}{2} \sum \frac{m_s^2}{a_s} \,, \end{array} \right. \tag{A.6}$$

$a_s > 0$ is the parameter attached to a propagation line z_s in the diagram. The minimum is taken with respect to the variation of the internal vertex co-ordinates.

Now we want to find the double minimum $\mathcal{J}(z_i)$ of $I(z_i, a)M^2(a_s)$ with respect to both the co-ordinates and the parameters a_s. By taking variation with respect to a_s, we immediately find

$$a_s = \frac{m_s}{r_s}\sqrt{\frac{I}{M^2}}\,, \qquad (r_s = \sqrt{z_s^2}) \tag{A.7}$$

and

$$IM^2 = (\tfrac{1}{2}\sum m_s r_s)^2\,. \tag{A.7'}$$

Thus

$$\mathcal{J}(z_i) = \mathrm{Min}\,(\tfrac{1}{2}\sum m_s r_s)^2\,, \tag{A.8}$$

the minimum now being with respect to the internal co-ordinates in the diagram.

For any two diagrams, for which one can realize

$$I(z, a)\,M^2(a) \geqslant I_0(z, a_0)\,M_0^2(a_0)\,, \tag{A.9}$$

for ony given set of parameters a, it follows that

$$\begin{cases} IM^2 \geqslant I_0 M_0^2 \geqslant \mathrm{Min}_{a_0}\, I_0 M_0^2 = \mathcal{J}_0(z)\,, \\ \mathrm{Min}_a\, IM^2 = \mathcal{J}(z) \geqslant \mathcal{L}_0(z)\,. \end{cases} \tag{A.10}$$

Conversely, if $\mathcal{J}(z) \leqslant \mathcal{J}_0(z)$, this does not necessarily mean the inequality (A.9), to be valid for fixed a, a_0 and all z. However, for any fixed a and z, there must be some set $a_0(a, z)$ such that (A.9) is satisfied since otherwise $\mathcal{J}(z) \geqslant \mathcal{J}_0(z)$ would not hold. This means in turn that for any fixed a_r and q_i there is some set $a_0(a, q)$ such that

$$J(a, q)/M^2(a) \geqslant J_0(a_0, q)/M_0^2(a_0)\,,$$

is satisfied. For our present purposes in Sect. **4**, this should be sufficient.

RIASSUNTO (*)

Colla teoria delle perturbazioni si studiano le relazioni di dispersione pei fattori di forma. Si dimostrano in particolare tali relazioni per un nucleone reale nella forma usualmente assunta in letteratura. Si dimostra, tuttavia, che nei casi più generali lo spettro di massa comparente nelle relazioni di dispersione dipende dalle masse delle particelle che danno contributo in un modo particolare, differente dalla semplice relazione finora ritenuta esatta. Tale situazione si presenta, per esempio, nel caso di qualche modello d'iperone e di sistemi legati quali il deuterone. Dall'invarianza della teoria rispetto all'inversione dello spazio-tempo si deriva anche una formula riguardante l'interazione degli stati finali da usare in unione alle relazioni di dispersione.

(*) *Traduzione a cura della Redazione.*

Λ^0- and θ^0-Particles Produced in Iron.

G. Alexander (*), C. Ballario (+), R. Bizzarri (×), B. Brunelli, E. Di Capua, A. Michelini, G. C. Moneti and A. Zichichi (+)

Istituto di Fisica dell'Università - Roma
Istituto Nazionale di Fisica Nucleare - Sezione di Roma

(ricevuto il 23 Aprile 1958)

Summary. — The results of an experiment on some properties of Λ^0- and θ^0-particles produced in the plates of a cloud chamber are discussed. 115 V^0-events are analysed by means of angle measurements and ionization estimates. The frequency of production of Λ^0, θ^0-pairs is found to be small. For neither type of particle is any evidence found for anisotropy in the decays. The V^0 production cross-section appears larger for a pion primary than for a nucleon, and increases with the energy released in the shower.

1. – Introduction.

For some years the masses and the decay schemes of Λ^0 and θ^0 particles have been well-known mostly from measurements in magnetic cloud chambers (1). Although some decisive results have been recently obtained for Λ^0 particles (2), much room for improvement remains regarding the knowledge of their other properties, such as spin, mean lifetimes, behaviour with respect to inversion operators, and the details of their processes of production.

(*) Now at Dublin Institute for Advanced Studies, Dublin.
(+) Now at CERN, Geneva.
(×) Now at « Enrico Fermi » Institute for Nuclear Studies, University of Chicago.
(1) See, *e.g.* the paper by C. Franzinetti and G. Morpurgo: *Suppl. Nuovo Cimento*, **6**, 469 (1957), chap. 3 and 4.
(2) Ibid., chap. 15. F. S. Crawford *et al.*: *Phys. Rev.*, **108**, 1102 (1957); F. Eisler *et al.*: *Phys. Rev.*, **108**, 1353 (1957); F. Eisler *et al.*: *Nuovo Cimento*, **7**, 222 (1958).

This paper gives the results of a study of some of these latter properties. The investigation was carried out on 107 Λ^0 and θ^0 particles produced in the iron plates of a multiplate cloud chamber exposed to cosmic radiation at an altitude of 3 500 m above sea level.

The dominant decay modes of Λ^0 and θ^0 particles are well known to be:

(1) $$\Lambda^0 \rightarrow p + \pi^- + 37 \text{ MeV}$$

and

(2) $$\theta^0 \rightarrow \pi^+ + \pi^- + 214 \text{ MeV}.$$

If other neutral particles exist which disintegrate into two charged bodies, these latter particles are rare (1). It is therefore possible to make use of decay events that are not completely measurable. A V^0 decay into two secondaries that is definitely not a Λ^0 decay (1) can reasonably be assumed to be a θ^0 decay (2) and viceversa. Events selected in this way are of value for statistical studies giving information about relative frequencies of production, angular and energy distribution and mean lifetimes.

In our experiment we considered only V^0 decays for which an evident origin existed in the plane of the V^0 secondaries and we measured the angles θ_1 and θ_2 which the decay products of the V^0 particles formed with its line of flight. From these angles it is possible to calculate the ionization of the two prongs for the possible decay schemes Λ^0 and θ^0. If, as often happens, these ionizations are sufficiently different in the two cases, the nature of the V^0-particle can be established by simple visual estimation of the ionizations. The method of analysis and the selection criteria, as well as the bias introduced by them into our sample of V^0-events are discussed in Sect. 3.

Sect. 4 presents the results obtained concerning the relative production frequency of Λ^0 and θ^0-particles, Sect. 6 those relating to angular distributions, and Sect. 7 those relating to the parent showers.

Our estimate of the lifetimes of Λ^0 and θ^0-particles has already been published (3) and is referred to in Sect. 5. Sect. 2, which follows, describes some features of the cloud chamber and of the reprojection system; they have been described in detail elsewhere (4).

(3) C. Ballario, R. Bizzarri, B. Brunelli, A. De Marco, E. Di Capua, A. Michelini, G. C. Moneti, E. Zavattini and A. Zichichi: *Nuovo Cimento*, **6**, 994 (1957).

(4) C. Ballario, B. Brunelli, A. De Marco and E. Zavattini: to be published in *Nuovo Cimento*.

2. – Experimental apparatus and measurements.

The useful volume of the cloud chamber is $(30 \times 35 \times 20)$ cm^3. As Fig. 1 shows, there are four iron plates, each of thickness 12 mm. The figure also shows the arrangement of the triggering counters and of the lead transition layer.

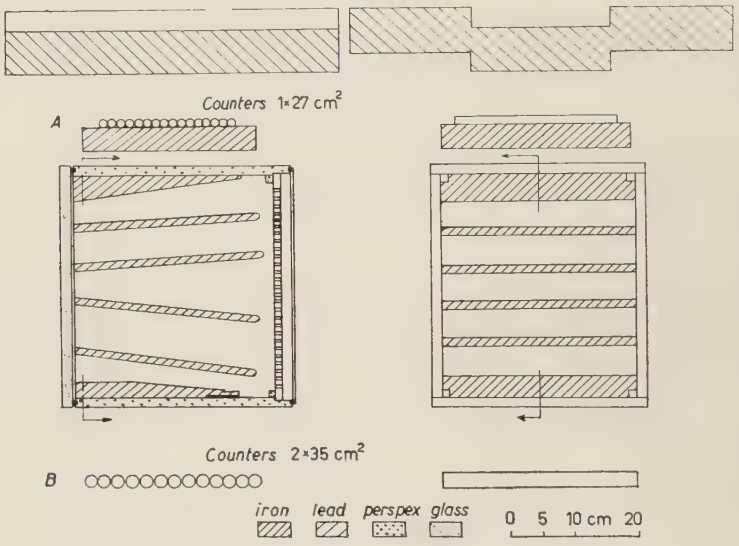

Fig. 1. – Cloud chamber and trigger system.

The chamber was triggered by either of the following two coincidences:

a) between at least 2 counters of tray A and at least 3 counters of tray B;

b) between at least 4 counters of tray A and at least 2 counters of tray B.

With a chamber dead time of about 3 minutes, the rate of expansions was 15 per hour.

The chamber was photographed by two cameras. Stereoscopic photographs were reprojected by a system similar to that used for photography.

There are various possible methods for the spatial reconstruction of the events [4]. In most cases the angles θ_1 and θ_2 were traced directly onto a screen on which the two stereoscopic pictures had been superimposed. A correction was always made for gas motion during expansion.

For the purpose of estimating the errors in reprojection and calculation, we chose four typical events, and for each of them made ten calculations of the value of θ $(=\theta_1 + \theta_2)$. We found that the half-breadth of the distribution of

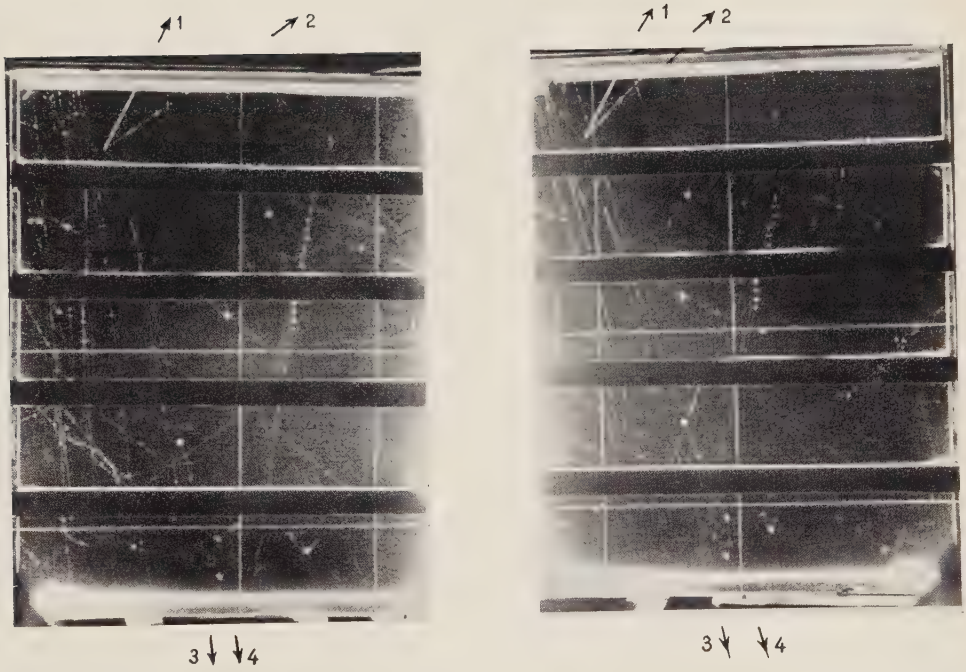

Typical photograph with two indipendent V^0-events.

values was always less than 1 degree. So we generally assumed an error of 1°; for some events in awkward positions we increased the error to 1.5°. The errors in the partial angles were mainly due to the indeterminacy of the origin of the star.

3. – Selection and analysis.

3·1. *General procedure.* – With the equipment described we took about 30 000 photographs, which were scanned for V^0-events.

It was decided to regard as neutral hyperon or heavy meson decays all those V^0-events which were associated with a nuclear interaction in iron, coplanar within 3°, and satisfying the following conditions:

a) 1) At least one of the two tracks showed an ionization exceeding twice the minimum; *or*

2) At least one of the two tracks penetrated a plate without multiplying and without being deviated by more than 20°; *or*

3) The angle θ between the two tracks was bigger than 20°; *and*

b) The two secondary particles displayed no perceptible multiple scattering in the gas; *and*

c) Both branches had at least 12 mm of measurable track;

d) The vertex was in a position where the scanning efficiency could be assumed to be constant and there was only a negligible chance that a fortuitous coincidence of two tracks might simulate a V^0-event ([5]).

Conditions *a*) and *b*) were designed to eliminate electron pairs; condition *d*) made it possible to calculate the probability of every V^0-event being observed ([6]) With our chamber this probability varies considerably from event to event and this had to be allowed for.

Concerning condition *a* 2) it should be noted that the thickness of each plate is 0.7 radiation lengths. It may be objected that this is not thick enough; however, in the case of 8 out of 11 V^0-events admitted on this criterion (see Table I), one or both secondary particles traversed at least two plates. The critical angle for the deviation of the secondary particles in their passage through

([5]) Cf. C. Ballario, R. Bizzarri, B. Brunelli, A. De Marco, E. Di Capua A. Michelini, G. C. Moneti, E. Zavattini and A. Zichichi: *Nuovo Cimento*, **6**, 994 (1957).

([6]) D. B. Gaythier and C. Butler: *Phil. Mag.*, **46**, 467 (1955).

the plate was taken to equal twice the mean square deviation angle of a pion leaving the plate with double the minimum ionization.

TABLE I. – *Distribution of the events admitted by virtue of the various alternatives of condition a).*

Alternative	Number of events
1	1
2	11
3	15
1 and 2	2
1 and 3	14
2 and 3	50
1, 2 and 3	22

A total of 115 V⁰-events were selected according to these criteria. All the photographs were examined twice, and each scanning for events satisfying the selection conditions had a 95% efficiency. In these circumstances the possibility that any event may have escaped detection in both scannings may be neglected.

The photographs were stereoscopically projected, as described, and each event was geometrically analysed. We measured:

1) The angle θ between the two secondary tracks;

2) The angles θ_1 and θ_2 between the line of flight of the V⁰-particle and each of the two secondary tracks. In the following we shall assume that $\theta_1 \leqslant \theta_2$;

3) The path length of the secondary particles within the iron plates;

4) When the primary particle of the star which generated the V⁰-particle was charged and visible, we measured the angle Φ between the line of flight of the V⁰-particle and the track of the primary particle, the angle between the production plane, *i.e.* the plane defined by the primary track and the line of flight, and the decay plane.

Finally we estimated visually the ionization of the two secondary tracks.

The V⁰-events were classified according to the following method. From the angles θ and θ_1 the ionization of the two branches of the V⁰-event can be calculated for each of the two types of decay. The visual estimate of ionization enables us to choose between the two interpretations Λ^0 and 0^0, when

$$\frac{I_{1\Lambda^0}}{I_{1\theta^0}} \frac{I_{2\theta^0}}{I_{2\Lambda^0}} > 2 \qquad \left(\text{or } < \frac{1}{2}\right), \tag{3}$$

where $I_{1\Lambda^0}$, $I_{1\theta^0}$, $I_{2\Lambda^0}$, $I_{2\theta^0}$, are the ionizations of the two tracks according to the two interpretations.

Equation (3) is the quantitative expression of the assumption that the ratio of the ionization of one track to the known ionization of another track can be visually estimated only within a factor of 2. The equation is in a form which will facilitate the discussion of the bias introduced by our method of classification, and will also enable us to calculate, by statistical methods, how many of the unidentified particles were Λ^0 or θ^0-particles.

When equation (3) is not satisfied both interpretations are possible, unless information about the range or the ionization change in the passage through the plates enables the two types of decay to be distinguished.

For a first rapid analysis the curves in Fig. 2, 3 and 4 are very useful. These curves represent θ as a function of θ_+ for Λ^0-particles, and of θ_1, for

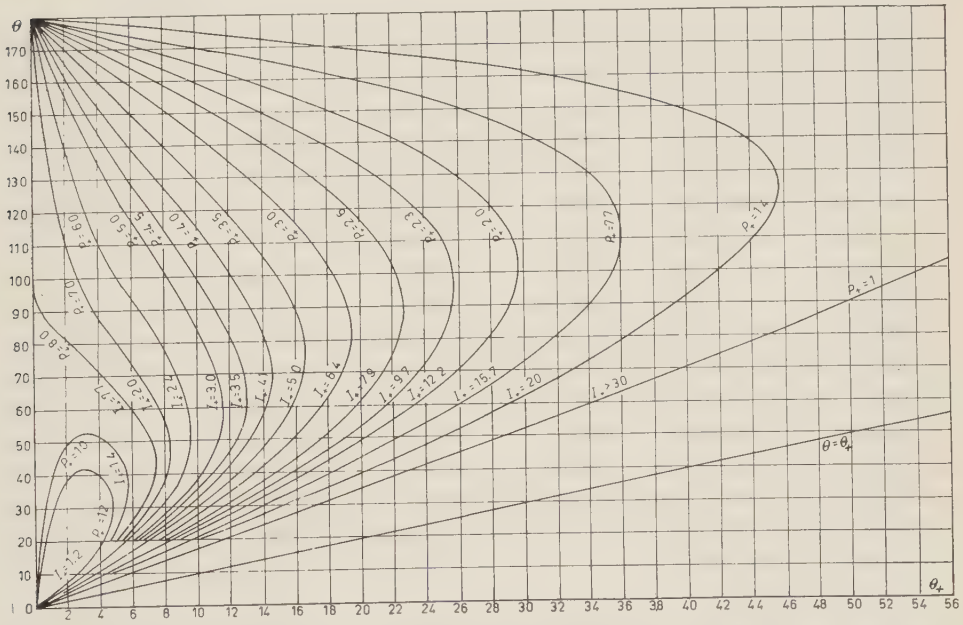

Fig. 2. – Λ^0 decay. θ *vs.* θ_+ (*i.e.* the angle between the proton track and the line of flight of the V^0-particle) for various values of the proton's momentum p_+. Angles are in degrees, p_+ in 10^8 eV; ionization is expressed as a ratio to minimum ionization.

θ^0-particles, the momentum (and hence the ionization) of one secondary particle being assumed constant.

In a more detailed graphical analysis the experimental point defined by the angles θ and θ_1, for each V^0-event was marked in the plane (α, ε) (7).

(7) J. PODOLANSKI and R. ARMENTEROS: *Phil. Mag.* **45**, 13 (1954).

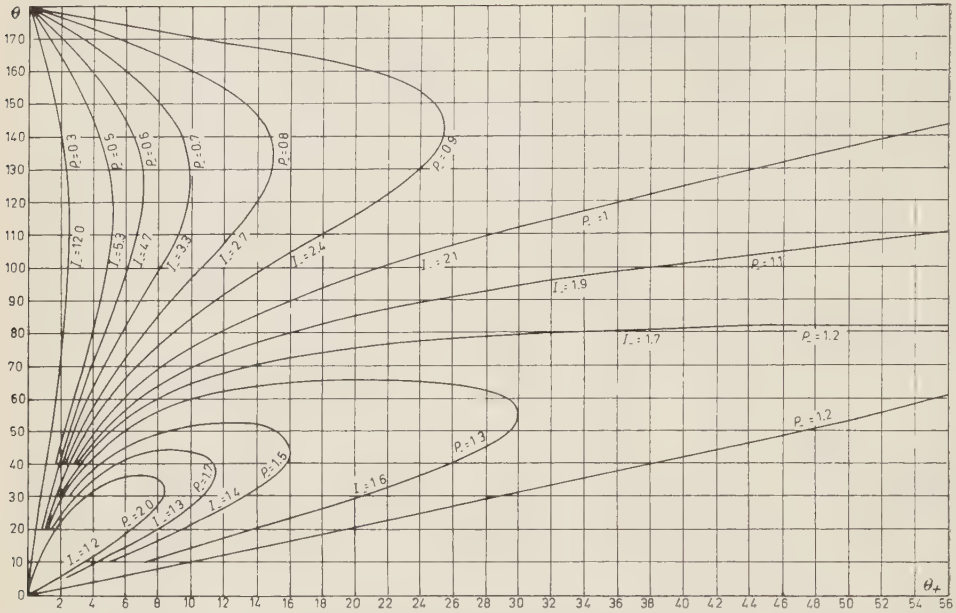

Fig. 3. Λ^0 decay. θ *vs.* θ_+ for various values of the momentum p of the π^- secondary.

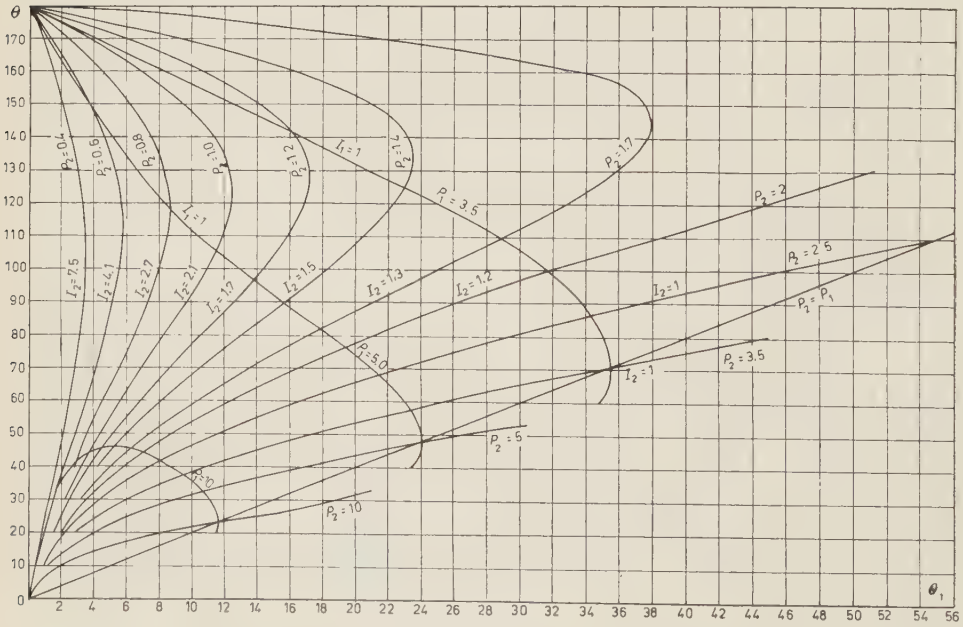

Fig. 4. – θ^0 decay. θ *vs.* θ_1 for various values of the momenta p_1 and p_2 of the secondaries.

This makes it possible to calculate rapidly, for each interpretation, the mean values and the corresponding maximum errors of the momentum p of the V^0-particle, of momenta p_1 and p_2 of the secondary particles, and of the cosine of the emission angle θ^* of the positive secondary particle in the centre of mass system (*).

The following values were assigned to the constants of the two decay schemes:

	Q	α^*	ε^*
Λ^0	37 MeV	0.693	0.180
θ^0	214 MeV	0.000	0.83

By the method described we obtained the following classification of the 115 V^0-events:

Identification	Total number of events	Number of events for which range information was needed for identification
Λ^0	27	5
θ^0	42	2
Λ^0 or θ^0	38	—
Neither Λ^0 nor θ^0	8	—

3·2. *Apparently « anomalous » events.* – In most cloud chamber experiments V^0-events have been observed that are incompatible with the decay schemes (1) and (2). It is now well established that 3-body decays of mesons occur and many « anomalous » V^0-events are probably of this type. In our experiment the size of the chamber and the selection requirement that an origin for the V^0-particle should lie in the plane defined by two charged secondary particles makes it improbable that our « neither Λ^0 nor θ^0 » events should be due to 3-body decay processes. Unfortunately, we have insufficient measurements of the individual events to enable us to draw any conclusions regarding their nature.

There remains the possibility of a statistical explanation of the presence of such events without recourse to the hypothesis of anomalous decay. There may be a number of reasons:

1) The shower in which the V^0-particle is generated may not be the one with which the analysis associates the event. The origin of the latter shower

(*) For a θ^0-decay it is actually not possible to distinguish the positive secondary track from the negative one; hence we can only get the absolute value of $\cos\theta^*$.

may have been in the decay plane by accident, while the former was not visible in the chamber.

2) The margin of error allowed for ionization estimates and angle measurements may be insufficient, because in exceptional cases the error exceeds the maximum values found from a number of standard events.

A simple calculation based on the frequency of the showers found in the photographs which show a V^0-event leads to the conclusion that about one spurious event is expected in our sample due to the first cause.

The second cause seems even more plausible. All the events classified as «neither Λ^0 nor θ^0» have some geometrical peculiarities, generally tracks with a steep inclination towards the window of the chamber, which raise special difficulties both for ionization estimates and for stereoscopic projection. It seems reasonable, therefore, to assume that at least some of the « neither Λ^0 nor θ^0» events are produced by abnormally large errors of measurement.

Other causes, such as two-pronged stars produced by neutral primary particles are less plausible.

3·3. *Bias in selection and analysis.* – At this point it will be well to examine and discuss the bias introduced by our criteria of selection and analysis.

Given the decay scheme, each selection condition defines a region of the plane ($\cos\theta^*$, p) which comprises all the points, and only the points, corresponding to the events meeting the condition.

Moreover, if we neglect the few events that could not be identified without range information, equation (3) defines a region of the plane ($\cos\theta^*$, p) corresponding to the identifiable events.

Fig. 5 and 6 show the curves delimiting these regions. We have drawn curves corresponding to two different values of ionization, range and total

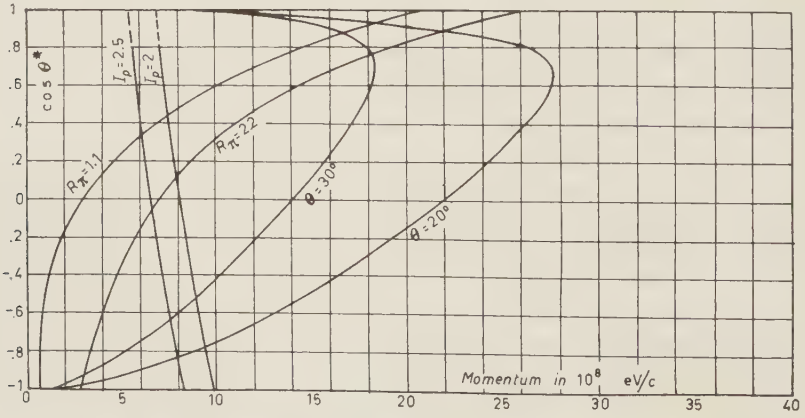

Fig. 5. – ($\cos\theta^*$, p) diagram for Λ^0 decay (see text).

angle, so as to see to what extent these criteria are critical. Note that for the Λ^0-particle the curves $I_p = 2$ and $I_p = 2.5$ nearly coincide with the curves

$$\frac{I_{1\Lambda^0}}{I_{1\theta^0}} \frac{I_{2\theta^0}}{I_{2\Lambda^0}} = 2 \text{ and } = 2.5 \,. \tag{3}$$

(The curve $(I_{1\Lambda^0}/I_{1\theta^0})(I_{2\theta^0}/I_{2\Lambda^0}) = \frac{1}{2}$ is of no practical interest).

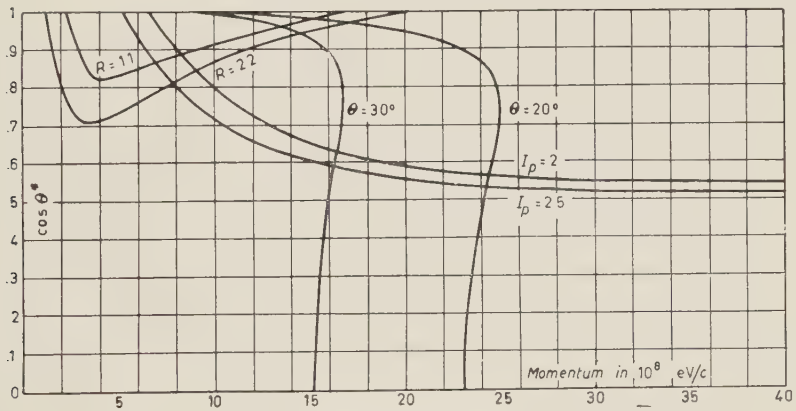

Fig. 6. – $(\cos\theta^*, p)$ diagram for θ^0 decay (see text).

An examination of Fig. 5, shows at once that for the Λ^0-particles the selection criteria introduce no bias with respect either to the momenta or to $\cos\theta^*$, while the impossibility of distinguishing θ^0-particles cuts off the spectrum between 0.7 and 1.0 GeV/c and introduces a slight bias against small values of θ^*.

Fig. 6 shows that for the θ^0-particles the selection condition $\theta > 20°$ introduces a fairly definite bias with respect to the momentum, by excluding momenta exceeding 2.4 GeV/c. However, this bias applies only to events the position of which in the chamber is such that it is not possible to establish whether the secondary particles do or do not penetrate through the plates. On the other hand, the identification equation (3) introduces a bias against small values of θ^* and high momenta.

As regards the scanning, we can say that, looking at the few V^0-events first detected in the second scanning, the scanning does not seem to introduce any noticeable bias against any particular category of events.

Finally, as regards the number of events analysed on the assumption of a line of flight mistakenly associated with the event by reason of chance coplanarity, we estimate that this number is about unity.

Before going on to present the results of our experiment, we must attempt at least a statistical determination of the nature of the V⁰-events classified as « Λ^0 or θ^0 ».

The curve $I_{1\Lambda^0} I_{2\theta^0} / I_{1\theta^0} I_{2\Lambda^0} = 2$, which we shall call the « identification curve », never has zero ordinate (see Fig. 6). This fact enables us to estimate the percentages of Λ^0 and θ^0-particles in the category in question. If we introduce the hypothesis of isotropy of the θ^0-decay in the centre of mass system, the ordinate of the identification curve for any given momentum represents the probability that our method should lead to identification, without range information, of a θ^0-particle with that momentum.

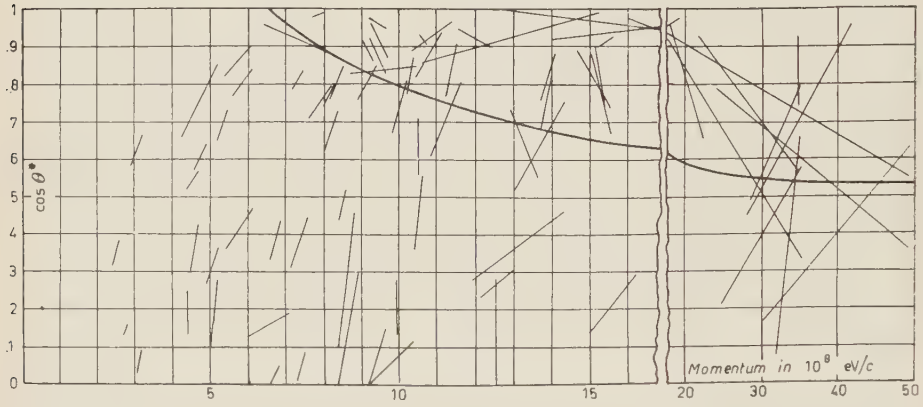

Fig. 6-*bis*. – Distribution of θ^0 events and of « Λ^0 or θ^0 » events, analysed as θ^0, in the plane (p, $\cos\theta^*$). The represented errors are due to the errors of the angle measurements. All the events that, within the errors, are represented by points above the curve, are classified as « Λ^0 or θ^0 » events.

Let $n(p)\,\Delta p$ be the number of V⁰-events identified as θ^0 without range information, with a momentum in the interval Δp around p (*) and $h(p)$ be the corresponding (average) ordinate of the identification curve. The corrected number of θ^0 in the interval Δp is $n'(p)\,\Delta p = (n(p)/h^*(p))\,\Delta p$, where $h^*(p) = h(p) + \frac{1}{2}\,\Delta\cos\theta^*$, $\Delta\cos\theta^*$ being the average value of the errors with respect to $\cos\theta^*$ for θ^0-events represented in the plane (p, $\cos\theta^*$) by points lying on the identification curve in the interval Δp (+).

(*) The θ^0 events identified by means of range information are in this context included with the « Λ^0 or θ^0 » V⁰-events.

(+) Since the errors with respect to $\cos\theta^*$ are due to almost constant errors of angle measurement, the former errors are fully determined by the co-ordinates of the decay in the plane (p, $\cos\theta^*$).

The number of θ^0 among the events which were classified as «Λ^0 or θ^0» would then be

$$N(\theta^0) = \sum_i \left[\frac{n(p_i)}{h^*(p_i)} - n(p_i) \right] \Delta p_i ,$$

and the number of Λ^0 would be

$$N(\Lambda^0) = N(\Lambda^0 \text{ or } \theta^0) - N(\theta^0) .$$

Setting apart the two θ^0 identified by range information, we find that our 38 «Λ^0 or θ^0» include only 4 to 8 θ^0, all with a momentum exceeding $7 \cdot 10^8$ eV/c and with $\cos\theta^*$ between 0.8 and 1.0. This means that if we regard all «Λ^0 or θ^0» V^0-events as Λ^0 and add them to the 27 certain Λ^0-events, we should expect the resulting 65 Λ^0-events to have something like 8 per cent θ^0 contamination. This is insignificant for the shape of the histograms which we shall presently examine.

Note that this result rests in the assumption of isotropy of the θ^0-decays. We shall, in Sect. **6**, discuss to what extent this hypothesis is consistent with the experimental results so far obtained; here, it may merely be stated that unless the deviations from isotropy of our θ^0-decays (see Fig. 11) are due merely to statistical fluctuations, they would tend to diminish the percentage of θ^0 in the V^0-events classified as «Λ^0 or θ^0».

4. – Relative production frequencies.

The frequencies discussed so far are the frequencies of observation of Λ^0 and θ^0 events with our apparatus. As we have stated at the outset, we limited ourselves to V^0-decays generated by coplanar showers and we subdivided those events into decays of the type (1) and (2).

Now, while it is highly probable that these are the only two-body decays with charged secondaries, it is also known that Λ^0 and θ^0 particles can disintegrate in a different manner, that is into two neutral bodies, two charged bodies and one neutral one, and probably into three neutral ones. Moreover, the θ^0-particle almost certainly has no determinate mean lifetime but is a superimposition with equal amplitude of θ_1^0 and θ_2^0. Since only θ_1^0 particles could disintegrate into two charged or neutral pions and θ_2^0 would have a mean life at least 500 times as long as θ_1^0 ([8,9]) and almost all of them would

([8]) F. Eisler, R. Plano, N. Samios, M. Schwartz and J. Steinberger: *Nuovo Cimento*, **5**, 1700 (1957).

([9]) M. Bordon, W. Chinowsky, M. Fuchs, K. Landé, L. M. Lederman and J. Tinlot: *Nevis* 61.

thus escape from the chamber, we can assume that our θ^0 particles are all θ_1^0. The probability that contamination may simulate a two-body decay compatible with the decay schemes (1) and (2) is negligible in the light of our discussion in Sect. 3.

To calculate the probability of a Λ^0 decay (1) and of a θ^0 decay (2), we can use the experimental results of EISLER *et al.* (8). We obtain

$$P_{\Lambda^0}(p, \pi^-) = 0.68 \pm 0.05 , \tag{4}$$

and

$$P_{\theta_1^0}(\pi^+, \pi^-) = 0.86 \pm 0.06 . \tag{5}$$

The probability of a θ^0 decay (1) is found by halving this last value, to take account of the probability of a θ^0 particle being θ_2^0:

$$P_{\theta^0}(\pi^+, \pi^-) = 0.43 \pm 0.03 . \tag{6}$$

Now, it should be noted that owing to the size of our chamber and the spectrum of momenta of the V^0-events observed, the probability of observation varies considerably as between various events. To arrive at the corrected ratios of production frequencies, each event has to be weighted with a statistical factor w equal to the inverse of its observation probability (6).

For the 27 «certain Λ^0» we get:

$$\sum w_i = 82 , \qquad \sum w_i^2 = 524$$

and for 42 «certain θ^0»:

$$\sum w_i = 99 , \qquad \sum w_i^2 = 274 .$$

The weighted numbers of V^0-events are

$$N_{\Lambda^0} = 82 \pm 23 ,$$

$$N_{\theta^0} = 99 \pm 17 .$$

These figures still have to be corrected to take account of the Λ^0 and θ^0 decays included in the V^0-events classified as «Λ^0 or θ^0». To this end we can repeat the calculation of the preceding section, applying it this time to the *weighted* spectrum of momenta of our «certain θ^0» decays. We find that the total weight corresponding to the number of θ^0 among the «Λ^0 or θ^0» has the value 20 ± 6.

Now we can attribute to the approximately 32 Λ^0 included in the «Λ^0 or θ^0» group the average weight of the 38 «Λ^0 or θ^0» events analysed as Λ^0. This

weight can obviously not be appreciably affected by the small contamination. In this manner we get for the weighted number of Λ^0 among the « Λ^0 or θ^0 » 93 ± 22. The error allows also for the (not statistical) errors in momentum measurement, which are altogether negligible for the « certain Λ^0 » and « certain θ^0 » categories.

Let us now consider the distribution of the angles Φ (see Fig. 7). To allow for the events which remained unobserved because $\Phi \simeq 90°$, we must increase the weighted number of Λ^0 by about 20% and that of θ^0 by about 10%.

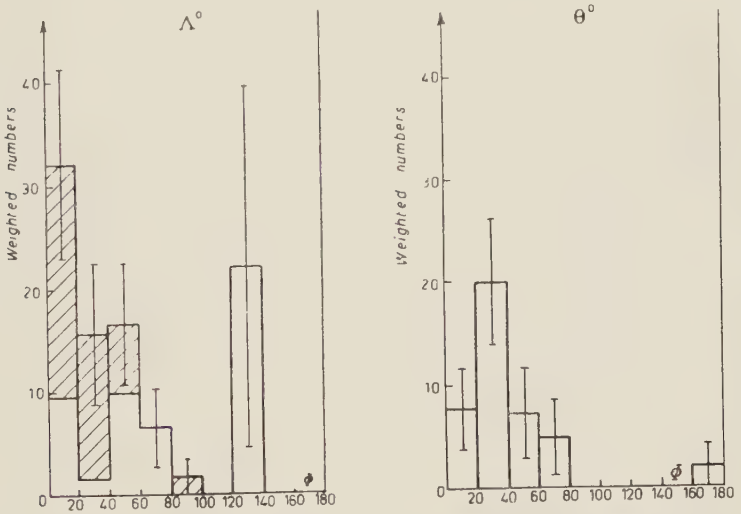

Fig. 7. – Distribution of the angle Φ for Λ^0 and θ^0 events. The shaded area represents the contribution of 19 unclassified events. The errors shown are calculated as $(\sum_i w_i^2)^{\frac{1}{2}}$.

Another bias tending to reduce the frequency of V^0-events is due to our selection criterion *a*) 3), which requires a total angle of more than 20° between the two tracks of a V^0-event, in the absence of secondary tracks seen to penetrate the plates or having $I > 2I$ min. Consider the spectra of momenta of the 65 Λ^0 and the 42 θ^0 events and compare them with the curves in Fig. 5 and 6 which delimit, in the respective planes ($\cos\theta^*$, p), the region in which the points satisfying the above-mentioned selection criterion are located. It will be seen that the bias has practically no effect at all for θ^0, and a negligible one, in relation to the other bias effects previously considered, for Λ^0.

To determine the true production frequencies, those corrected figures finally have to be weighted with the inverse of the probabilities (4) and (6) of charged decays; we find

$$N'_{\Lambda^0} = 309 \pm 79 ,$$

$$N'_{\theta^0} = 305 \pm 67 .$$

Hence the ratio of production frequencies is

$$\frac{N'_{\Lambda^0}}{N'_{\theta^0}} = 1.0 \pm 0.4 .$$

This figure should be compared with various cosmic ray and machine results, which have been fully discussed by COOPER *et al.* [10].

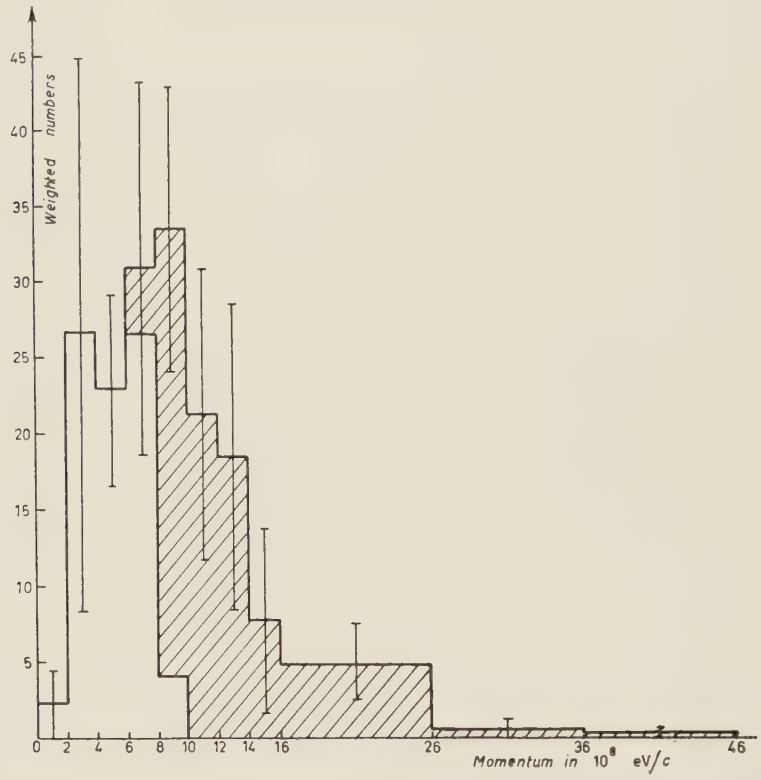

Fig. 8. Distribution of momenta for 65 Λ^0-events. The shaded area represents the contribution of 36 « Λ^0 or θ^0 » V^0-events. Errors as in Fig. 7.

The cases of associated V^0 production which we observed had best be treated separately. There were three showers associated with a pair of V^0-events that satisfied our selection conditions. In only one of the three cases we were able to identify both V^0-events, one as Λ^0 and one as θ^0. In each of the other two cases only one V-^{0}event was identified, and it was 0^0.

([10]) W. A. COOPER, H. FILTHUTH, L. MONTANET, J. A. NEWTH, G. PETRUCCI, R. A. SALMERON and A. ZICHICHI: to be published in the *Nuovo Cimento*.

2460

We can proceed as for the identification of the events classified as « Λ^0 or θ^0 », and conclude that the two incompletely identified pairs are almost certainly made up of one Λ^0 and one θ^0. Assuming then that they are (Λ^0, θ^0) pairs, we get

$$N(\Lambda^0, \theta^0) = 3 .$$

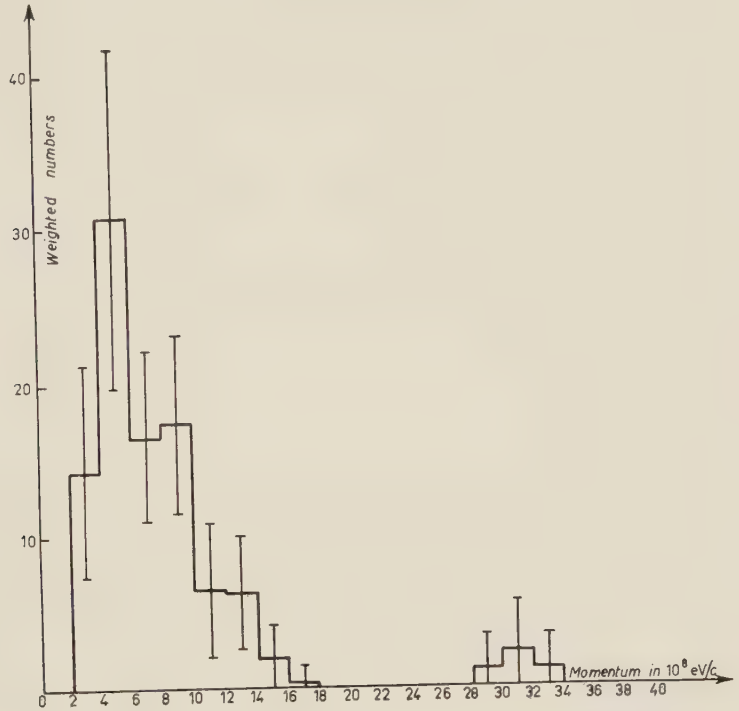

Fig. 9. – Distribution of momenta for 42 θ^0-events. Errors as in Fig. 7.

This figure has to be weighted and corrected as above leading to the result

$$N'(\Lambda^0, \theta^0) = 79 \pm 65 .$$

In speaking of Λ^0 production, we have so far included Λ^0 particles produced directly or by Σ^0 decay. The ratio between the frequency of Λ^0 particles produced without being paired with a θ^0 (Λ^0 sing) and of those produced together with a θ^0 particle (Λ^0 ass) is

$$\frac{N(\Lambda^0 \text{ sing})}{N(\Lambda^0 \text{ ass})} = 2.9^{+4.5}_{-1.4} .$$

If we assume that all the observed Λ^0 particles are produced by π or n and that each final state has the same frequency as its charge symmetric state, the value of the ratio should be unity.

The deviation may of course be due simply to statistical fluctuation. However, it is interesting to consider its significance if it were real. One possible cause of charge asymmetry in the final states may be asymmetry in the incident flux of the π-mesons and nucleons. It will readily be appreciated, however, that a marked effect of this kind is hardly probable; another possible cause is the presence of $\Sigma^{\pm}$ and $\overline{\mathrm{K}}$-particles in the incident flux.

It should be noted, finally, that in the calculation of the ratio under discussion the effect of θ^0 absorption in the iron plates has been neglected. If we assume that the absorption length coincides with the geometrical one, the value of the ratio would be diminished by only about 10%, that is, by much less than would be required to reduce it to unity.

If the observed charge asymmetry were to be attributed entirely to absorption, then we must assume that the absorption length is about $\frac{1}{2}$ the geometrical one, but the available data on the interaction of K and $\overline{\mathrm{K}}$ particles ([11]) give cross-sections never exceeding the geometrical.

5. – Mean lifetimes ([12]).

We estimated the mean lifetimes of 25 of the 27 «certain Λ^0» and of 38 of the 42 «certain θ^0» particles. The particles excluded from the estimation sample were analysed on the assumption that one of the secondary particles stops in the iron plate. This kind of information is not always reliable, because of possible interactions in iron with emission of neutral products only.

A discussion of these estimates, and particularly of the errors involved, has been published ([3]). Here we merely repeat the results, namely

$$\tau_{\Lambda^0} = (2.14^{+0.80}_{-0.47}) \cdot 10^{-10} \text{ s} ,$$

$$\tau_{\theta^0} = (0.92^{+0.30}_{-0.18}) \cdot 10^{-10} \text{ s} .$$

6. – Angular distributions.

The angular distributions $I(\varphi)$ of the angle φ between production plane and decay plane, and $I(\theta^*)$ of the angle θ^* formed by the tracks of the decay products and the line of flight of the V^0-particle in the latter's center of mass

([11]) W. K. H. Panofsky, V. L. Fitch, R. W. Motley and W. G. Chesnut: *BNL* 3410.

([12]) For a summary of earlier results and literature see: C. Franzinetti and G. Morpurgo: *Suppl. Nuovo Cimento*, **6**, 469 (1957); more recent estimates are given by Cooper *et al.* and by C. Graves and D. Glaser, circulating preprints.

system, have been studied by various authors in connection with the properties of V^0-particles ([13]).

The angle φ is described by the vector $\boldsymbol{k}(\pi^-) \times \boldsymbol{k}(V^0)$, perpendicular to the decay plane, when, by counter-clockwise rotation from the direction $\boldsymbol{k}(V^0)$, it is moved to the position occupied by the vector $\boldsymbol{k}(\text{prim}) \times \boldsymbol{k}(V^0)$ where, $\boldsymbol{k}(\text{prim})$, $\boldsymbol{k}(V^0)$, $\boldsymbol{k}(\pi^-)$ are the momenta of the primary particle, the V^0-particle and the π^- secondary, respectively.

In this manner we get $0 \leqslant \varphi < 2\pi$ for the Λ^0 particles, and $0 \leqslant \varphi < \pi$ for θ^0 particles, for which π^+ cannot be distinguished from π^-.

Similarly, we get $0 \leqslant \theta^* \leqslant \pi$ for Λ^0 particles (taking the proton trajectory as positive direction) and $0 \leqslant \theta^* \leqslant \pi/2$ for θ^0.

The distribution of other angles would also be of interest, but in our experiment we were unable to measure them.

The presence of anisotropy in one or both distributions indicates first of all that the particles emerge at least partly polarized from the production event. Any asymmetries of $I(\varphi)$ with respect to 90° and 180°, and of $I(\theta^*)$ with respect to 90° would be very interesting, in that they would indicate that one of the following assumptions is not correct: 1) that the particles have a determinate parity; 2) that there are no parity doublets; 3) that parity is conserved in the decay. Other forms of anisotropy can be studied better in distributions of φ folded over with respect to 180° and 90° and of θ^* folded over with respect to 90°.

In the conditions of our experiment a number of circumstances might have attenuated or destroyed such anisotropy:

1) The V^0-events may have been produced either by pions or by nucleons and the primary energies may have varied over a wide range.

2) V^0-particles may have been generated by a secondary collision inside the nucleus and hence the primary track was not relevant to the elementary reaction producing the V^0 particle.

3) We could not calculate the V^0 emission angle in the center of mass system of the colliding particle which produce the V^0-event. It is not known how the polarization depends on this angle.

4) Before leaving the nucleus in which it is produced, a V^0-particle may experience nuclear collisions ([14]) and change its polarization.

([13]) See, *e.g.* G. MORPURGO: *Nuovo Cimento*, **3**, 1069 and **4**, 1222 (1956); **5**, 1785 (1957); S. B. TREIMAN and H. W. WYLD: *Phys. Rev.*, **100**, 879 (1955); S. B. TREIMAN, G. T. REYNOLDS and A. L. HODSON: *Phys. Rev.*, **97**, 244 (1955); R. K. ADAIR: *Phys. Rev.*, **100**, 1540 (1955).

([14]) G. D. JAMES and R. A. SALMERON: *Phil. Mag.*, **46**, 571 (1955).

In our conditions, observation of anisotropy is therefore rather difficult, but, provided it were significant, it would all the same yield useful information ([15]).

Let us consider the distributions $I(\varphi)$ and $I(\cos\theta^*)$ for Λ^0 and θ^0 in Fig. 10, 11, 12 and 13. The category Λ^0 here again includes not only those individually identified, but also the « Λ^0 or θ^0 » events analysed as if they were all Λ^0 decays.

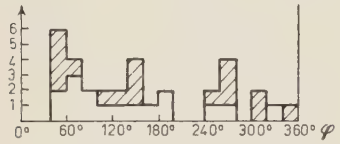

Fig. 10. – Distribution of the angle φ for 33 Λ^0-events. The shaded area corresponds to « Λ^0 or θ^0 » V^0-events.

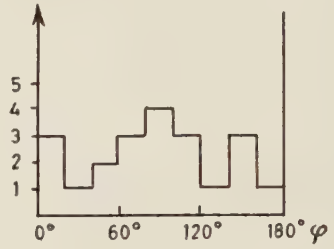

Fig. 12. – Distribution of the angle φ for 21 θ^0-events.

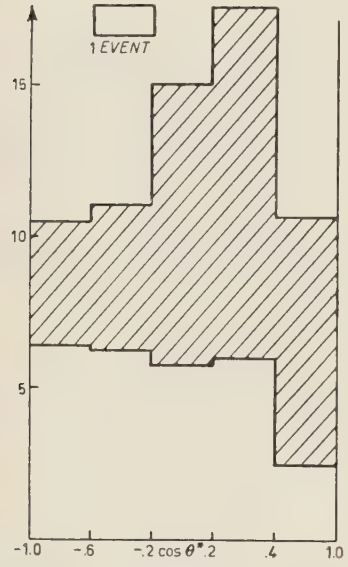

Fig. 11. – Distribution of $\cos\theta^*$ for 65 Λ^0-events. The shaded area corresponds to « Λ^0 or θ^0 » V^0-events.

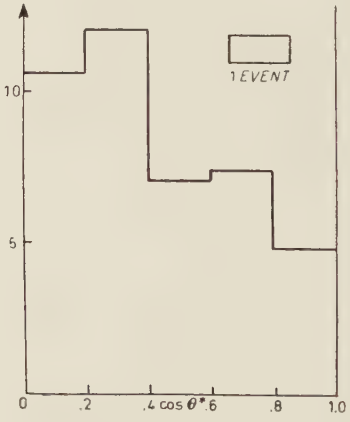

Fig. 13. – Distribution of $\cos\theta^*$ for 42 θ^0-events.

([15]) J. Ballam *et al.*: *Phys. Rev.*, **97**, 245 (1955); D. B. Gaythe *Phil. Mag.*, **45**, 570 (1954); **46**, 467, 1362 (1955); F. Eisler, R. Plano, A. Prodell, N. Samios, M. Schwartz, J. Steinberger, P. Bassi, V. Borelli, G. Puppi, H. Tanaka, P. Waloscheck, V. Zoboli, M. Conversi, P. Franzini, I. Mannelli, R. Santangelo, V. Silvestrini, G. L. Brown, D. A. Glaser and C. Graves: *Nuovo Cimento*, **7**, 222 (1958); C. Graves and D. Glaser: circulating preprint.

1) $I(\varphi)$ for Λ^0: this distribution suggests some slight anisotropy; we find

$$\frac{N(\varphi<180°)}{N(\varphi>180°)}=\frac{21}{12}=1.75^{+1.25}_{-0.70}.$$

The folded distribution ($0<\varphi<90°$) shows no other anisotropies.

2) $I(\cos\theta^*)$ for Λ^0: this distribution shows a crowding of events around $\theta^*=90°$. However, it is not a true crowding, since it is due:

(i) to the presence of a considerable number of V^0-events with very indeterminate $\cos\theta^*$ and hence always comprising the central part of the distribution, and

(ii) to the contamination of θ^0-events present among the « Λ^0 or θ^0 », since one can see that, when analysed as Λ^0, they give a contribution to small positive values of $\cos\theta^*$. We may draw the conclusion that $I(\cos\theta^*)$ is consistent with isotropy.

It may be of interest to consider separately the low momentum Λ^0 which should be emitted backwards in the center of mass system of the production reaction ([10]). We have selected 11 Λ^0-events, with momentum less than 500 MeV/c; 8 of them have $\cos\theta^*<0$, 3 have $\cos\theta^*>0$. If we add these numbers to the previous results given by the CERN Jungfraujoch group ([10]) we get a total backward/forward ratio $=69/39$. The probability that such a distribution is due to statistical fluctuation is 3%.

3) $I(\varphi)$ for θ^0: this histogram shows no indication of anisotropy.

4) $I(\cos\theta^*)$ for θ^0: this histogram apparently deviates from isotropy. If, however, we keep in mind that approximately 6 θ^0 events have to be added in the interval $0.4<\cos\theta^*<1.0$ in order to allow for doubtful identification, it will be seen that the deviation from isotropy is quite insignificant.

7. – Analysis of the parent interactions.

While scanning the photographs we have collected information on nuclear interactions with a view to learning something about the production of V^0-particles.

In the scanning we considered as useful nuclear interactions all those associated with V^0-events and those without V^0 which satisfied the condition that at least two particles were capable of traversing a plate and that it was possible to establish whether the primary particle was charged or neutral (the uncertain cases were less than 8%. Showers without V^0 and with less than

two penetrating prongs were excluded because, in comparing them with V^0 showers, we must somehow allow for the fact that there can be no V^0-particles in showers with an energy below the production threshold. We also excluded showers with more than 8 penetrating particles, because there is a great likelihood, in these cases, of not seeing any V^0-particles which may be present.

Since the error in our results is mainly due to the small number of V^0-events available, we did not think that there was any point in extending the laborious scanning for non-V^0 showers to all the 30 000 photographs. We limited ourselves to a group of photographs chosen at random. The number N_{π} of showers generated by pions was calculated from the number N_c of charged primaries ($\pi^{\pm}$ and protons) and from the number N_0 of neutral primaries (neutrons), taking into account: (i) that equal numbers of protons and neutrons impinge on the shower-producing lead above the chamber; (ii) that consequently we have to expect below the lead an excess of neutrons over protons roughly equal to the excess in lead-nuclei, (iii) that the triggering system introduces bias against neutrons entering the chamber; this bias has been evaluated looking at the interactions with charged primaries and gives a loss of $\sim 15\%$ for neutral primaries.

The following results of this scanning may be of interest:

1) The ratio between the number of Λ^0-showers with a primary $\pi^{\pm}$ and the number of all showers, whether or not accompanied by V^0-events, with a primary $\pi^{\pm}$, was found to be

$$\frac{N^{\pi}_{\Lambda^0}}{N^{\pi}_{S}} = 0.08 \ (1 \pm 0.5) ,$$

similarly for θ^0 we have $N^{\pi}_{\theta^0}/N^{\pi}_{S} = 0.06 \ (1 \pm 0.4)$.

2) The ratio between the number of Λ^0-showers with nucleon primary and the number of all showers with nucleon primary, was found to be

$$\frac{N^{n}_{\Lambda^0}}{N^{n}_{S}} = 0.03 \ (1 \pm 0.6) ,$$

similarly for θ^0 we have

$$\frac{N^{n}_{\theta^0}}{N^{n}_{S}} = 0.04 \ (1 \pm 0.6) .$$

These production frequencies are corrected for unobservable decays and geometrical biases.

These results indicate once more ([16]) that the V^0-particles belonging to showers triggering our chamber (see the histograms of Fig. 14, 15), are more often than not generated by $\pi^{\pm}$.

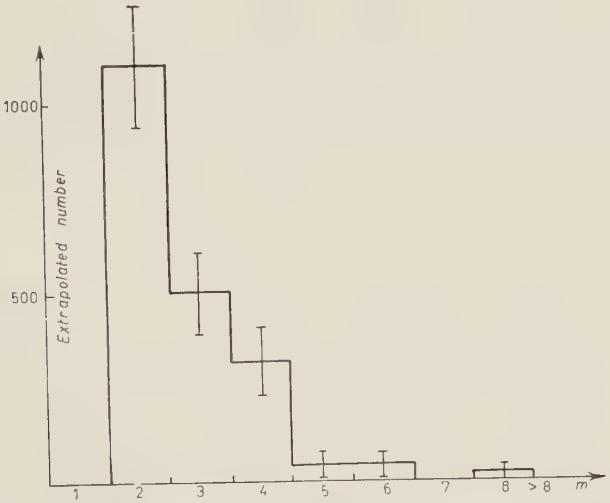

Fig. 14. - Distribution of showers without V^0-events *vs.* multiplicity m (1355 showers scanned).

3) The two histograms of Fig. 14, 15: The histogram of Fig. 14 represents the number of showers of multiplicity m, defined as the number of particles penetrating at least one plate, that of Fig. 15 represents the number

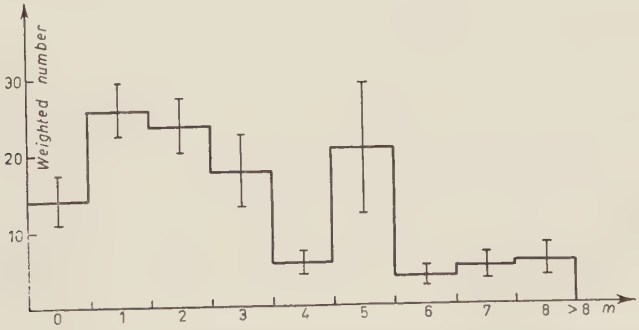

Fig. 15. – Distribution of showers with V^0-events *vs.* multiplicity m (number of showers considered: 48).

([16]) R. B. Leighton, S. D. Wanlass and C. D. Anderson: *Phys. Rev.*, **89**, 148 (1953); W. B. Fretter, M. M. May and M. P. Nakada: *Phys. Rev.*, **89**, 168 (1953); H. S. Bridge, C. Peyrou, B. Rossi and S. Safford: *Phys. Rev.*, **91**, 362 (1953).

of V^0-particles produced in showers of multiplicity m. These two histograms are normalized to the same number of pictures. Since many V^0-particles belonging to zero-multiplicity showers and having a neutral primary could not be included in this sample, the ordinate for $m = 0$ is open to doubt. We have not distinguished between Λ^0 and θ^0 because from the analysis of the associated interactions no significant differences have arisen.

A comparison of the two histograms agrees with the observation of other authors ([17]) namely that V^0-production increases with the energy released in the shower.

* * *

We are very grateful to Dr. J. P. Astbury, Dr. J. A. Newth and the theoretical group in Rome for helpful discussions; to Dr. A. De Marco for help in running the experimental apparatus and in the analysis of the events; to Prof. E. Amaldi for his interest and encouragement. One of us (G.A.) expresses his gratitude to Prof. E. Amaldi for the facilities extended to him in the Institute and to Ing. A. Mayer for a financial grant.

([17]) H. S. Bridge *et al.*: loc. cit.

RIASSUNTO (*)

Si discutono i risultati di un'esperienza su alcune proprietà delle particelle Λ^0 e θ^0 prodotte nei tetti di una camera a nebbia. Per mezzo di misure angolari e stime della ionizzazione si analizzano 115 eventi V^0. Si trova che la frequenza di produzione di coppie Λ^0, θ^0 è bassa. Per nessun tipo di particella si trova alcuna prova di anisotropia nei decadimenti. La sezione d'urto per la produzione di V^0 risulta maggiore per un pione primario che per un nucleone e aumenta con l'energia liberata nello sciame.

(*) *Traduzione a cura della Redazione.*

IL NUOVO CIMENTO Vol. IX, N. 4 16 Agosto 1958

Comparaison des deux méthodes d'obtention des équations du mouvement en relativité générale.

T. H. Pham

Institut Henri Poincaré - Paris

(ricevuto il 28 Aprile 1958)

Sommaire. — Il existe en relativité générale deux méthodes d'approximation pour déduire les équations du mouvement d'un système de corps à partir des équations du champ. L'une utilise une représentation de la matière par les singularités du champ extérieur; l'autre fait jouer un rôle au tenseur d'impulsion-énergie. La liaison entre ces deux points de vue peut être établie en observant que les discontinuités du tenseur d'Einstein sont représentées par le tenseur d'impulsion-énergie. Utilisant alors le théorème de Stokes, nous montrons que les deux méthodes sont équivalentes.

I. - Rappels géométriques.

1. – La variété espace-temps.

Dans la théorie de la relativité générale, l'élément primitif est constitué par la variété espace-temps. C'est une variété différentiable V_4 à quatre dimensions, de classe de différentiabilité (c^2, c^4 par morceaux) sur laquelle est définie une métrique riemannienne partout de type hyperbolique normal, à un carré positif et trois carré négatifs:

$$ds^2 = g_{\alpha\beta}(x^\lambda)\,dx^\alpha\,dx^\beta \qquad (\alpha, \beta \text{ et tout indice grec} = 0, 1, 2, 3).$$

Les dix coefficient $g_{\alpha\beta}(x^\lambda)$ sont appelés potentiels de gravitation pour le système de coordonnées locales (x^λ).

L'équation $ds^2 = 0$ définit en chaque point x de V_4 un cône réel C_x, le cône élémentaire en x. Une direction est dite orientée dans le temps ou orientée

dans l'espace selon qu'elle est intérieure ou extérieure au cône C_x. Pour qu'une hypersurface à trois dimensions, définie localement par l'équation $f(x^\lambda) = 0$, soit orientée dans l'espace, il faut et il suffit que:

$$\Delta_1 f = g^{\alpha\beta}\partial_\alpha f \partial_\beta f > 0\,, \qquad \left(\partial_\alpha = \frac{\partial}{\partial x^\alpha}\right).$$

Un système de coordonnées sera dit physiquement admissible ou interprétable dans l'espace et dans le temps si:

1) les hypersurfaces W_3 définies par $x^0 = \text{const.}$ sont orientées dans l'espace (ce qui entraine $g^{00} > 0$);

2) les lignes L sur lesquelles la variable x^0 varie seule sont orientées dans le temps (alors $g_{00} > 0$).

Dans un tel système de coordonnées nous dirons que x^0 est une variable temporelle, x^1, x^2, x^3 définissant les variables spatiales correspondantes. Les variétés W_3 seront appelées sections d'espace et les lignes L, lignes de temps.

Nous supposerons dans la suite que l'espace-temps V_4 a été rapporté à un système de coordonnées physiquement admissible, caractérisé par l'ensemble des deux propriétés $g_{00} > 0$ et $g^{00} > 0$, et nous adopterons sur les sections d'espace W_3 la métrique ds^{*2} intrinsèquement définie, c'est-à-dire invariante par tout changement de système de sections d'espace:

$$ds^{*2} = \left(g_{ij} - \frac{g_{0i}g_{0j}}{g_{00}}\right) dx^i\, dx^j \quad (i,\ j \text{ et tout indice latin} = 1, 2, 3).$$

2. – Le système des équations d'Einstein.

Les propriétés géométriques de l'espace-temps introduisent uniquement les phénomènes de gravitation. Le tenseur métrique $g_{\alpha\beta}$ est astreint à vérifier le système des dix équations d'Einstein:

$$S_{\alpha\beta} = \chi T_{\alpha\beta}$$

qui généralisent les équations de Laplace-Poisson qui sont à la base de la théorie du potentiel. $S_{\alpha\beta}$ et $T_{\alpha\beta}$ sont deux tenseurs symétriques, χ désigne un facteur constant lié à la constante d'attraction universelle.

Le tenseur $T_{\alpha\beta}$ dont l'interprétation est purement physique doit décrire au mieux, en chaque point de l'espace-temps V_4, l'état de la distribution énergétique (cas intérieur). Dans les régions de V_4 non balayées par l'énergie $T_{\alpha\beta}$ doit être identiquement nul (cas extérieur).

Le tenseur $S_{\alpha\beta}$, d'origine géométrique, qui ne dépend que des $g_{\alpha\beta}$ et de leurs dérivées des deux premiers ordres, est linéaire par rapport aux dérivées du second ordre et satisfait aux *identités de conservation*:

$$\nabla_\beta S_\alpha^\beta = 0 \qquad (\nabla_\beta \text{ opérateur de dérivation covariante}).$$

Ce tenseur s'exprime en fonction du tenseur de Ricci $R_{\alpha\beta}$ de la variété riemannienne par la formule:

$$S_{\alpha\beta} = R_{\alpha\beta} - \tfrac{1}{2} g_{\alpha\beta}(R + 2\lambda) \qquad (\lambda, \text{ constante cosmologique}).$$

II. - La déduction des équations du mouvement à partir des équations du champ.

3. – Généralités et hypothèses.

La théorie de la relativité générale est une théorie du champ pur en ce sens que l'on peut déduire les équations du mouvement à partir des équations du champ seules. Cette déduction est basée sur l'approximation des équations du champ. Ayant calculé une solution approchée de celles-ci, on définit les équations du mouvement comme des conditions que cette solution doit satisfaire en raison même des équations du champ. Nous verrons dans les deux paragraphes suivants quelles conditions il conviendra de prendre suivant que l'on veut utiliser les équations d'Einstein du cas extérieur ou celles du cas intérieur. Il existe en effet deux techniques différentes pour traiter par approximations le problème du mouvement de N masses gravitantes. L'une utilise une représentation des masses par de pures singularités du champ extérieur, l'autre fait jouer un rôle au tenseur d'impulsion-énergie $T_{\alpha\beta}$. Elles sont connues respectivement sous les noms de *méthode des singularités* [1,2,3,9] et de *méthode du tenseur d'impulsion-énergie* [4,5,7,8].

---

(1) A. Einstein, L. Infeld et B. Hoffmann: *Ann. Math.*, **39**, 65 (1938).

(2) A. Einstein et L. Infeld: *Ann. Math.*, **41**, 455 (1940); *Can Journ. Math.*, **1**, 209 (1949).

(3) L. Infeld: *Acta Phys. Pol.*, **16**, 177 (1957).

(4) V. A. Fock: *Journ. Phys. Acad. Sci. URSS*, **1**, 81 (1939).

(5) M.me F. Hennequin: *Etude mathématique des approximations en relativité générale et en théorie unitaire de Jordan-Thiry*, « Bull. scient. Com. Trav. hist. et scient.», **1** (1956). 2a partie: *Mathématiques* (Paris, 1957). p. 73-154 (Thèse Sc. math. Paris, 1956).

(6) A. Lichnerowicz: *Les théories relativistes de la gravitation et de l'électromagnetisme* (Paris, 1955).

(7) A. Papapetrou: I: *Proc. Phys. Soc.*, A **64**, 57 (1951); II: *Proc. Phys. Soc.*, A **64**, 302 (1951).

(8) N. M. Petrova: *Akad. Nauk SSSR, Žu. Éksper. Teoret. Fiz.*, **19**, 989 (1949) (en russe).

La méthode des singularités peut être présentée d'une manière autonome car il n'est pas nécessaire, du moins théoriquement, de préciser la nature des singularités du champ. Mais une comparaison entre les deux méthodes n'a évidemment de sens que si les divers champs intérieurs et le champ extérieur sont créés par le même ensemble de distributions énergétiques dans l'espace-temps. On doit donc envisager des métriques globalement régulières: la notion de modèle d'univers (6) que nous allons rappeler nous en donnera une idée précise.

Un *modèle d'univers* est une variété V_4 munie d'une métrique partout régulière satisfaisant aux conditions:

1) Dans les domaines de V_4 balayés par une distribution énergétique et limités par des hypersurfaces frontières S, la métrique est régulière et satisfait aux équations d'Einstein du cas intérieur.

2) Dans les domaines de V_4 qui ne sont pas balayés par aucune distribution énergétique, la métrique est régulière et satisfait aux équation d'Einstein du cas extérieur.

3) A la traversée d'une hypersurface S, les potentiels et leurs dérivées premières sont continus conformément aux conditions de raccordement.

Quand il est possible de construire un tel modèle d'univers, le champ extérieur peut être considéré comme effectivement produit par les différentes masses ou distributions énergétiques en mouvement et c'est le raccordement des champs intérieurs des différentes distributions avec un même champ qui assure l'interdépendence des mouvements (6).

Les hypothèses que nous faisons dans le problème du mouvement sont les suivantes:

a) Nous considérons un modèle d'univers à N tubes massiques représentés dans chaque section d'expace W_3 par N domaines à trois dimensions $\overset{s}{B}{}^3$ $(s=1,...,N)$ connexes et bornés, sans point commun, qui correspondent à des corps.

b) La métrique est quasi-euclidienne et à comportement asymptotique euclidien. Les potentiels admettent des développements limités selon les puissances de c^{-2} (c, vitesse de la lumière), dont les premiers termes sont les potentiels euclidiens $(+1, -1, -1, -1)$ de Minkowski.

c) Nous supposons également que les vitesses des corps sont faibles par rapport à celle de la lumière. La dérivée partielle ∂_0 est alors d'un ordre infinitésimal supérieur aux dérivées partielles ∂_i:

$$\partial_0 = 0(1/c) .$$

4. – Identités de conservation et équations du mouvement (*).

4'1. *Identités de conservation.* – La représentation de la matière peut s'effectuer en relativité générale par des schémas du type hydrodynamique. Un fluide relativiste est alors considéré comme un milieu matériel continu, déformable, doué des propriétés suivantes:

1) il possède une densité propre ϱ;

2) il est possible de définir un vecteur vitesse unitaire $\boldsymbol{u}$ pour chaque point du milieu.

Le tenseur d'impulsion-énergie $T_{\alpha\beta}$ est destiné à assurer une représentation aussi complète que possible d'une distribution énergétique déterminée. Ce tenseur contiendra ainsi différents termes correspondant aux différentes sortes d'énergie de la distribution et à leur interaction. La description de ces différents termes, leur importance relative, sont fournies par l'expérience.

Soit $T_{\alpha\beta}$ le tenseur d'énergie du schéma matériel considéré. Le tenseur $S_{\alpha\beta}$ étant conservatif, il en est de même du tenseur $T_{\alpha\beta}$ qui est astreint, d'après les équations d'Einstein, à n'en différer que par un facteur constant:

$$\nabla_\beta T^\beta_\alpha = 0 \,. \tag{4.1}$$

Ces relations sont appelées identités de conservation du schéma considéré.

On déduit de (4.1) un certain nombre de propriétés de « conservation » pour les éléments physiques qui figurent dans l'expression du tenseur d'énergie considéré (masses, pressions, vitesses, champ électromagnétique, champ des températures propres). Examinons les relations (4.1) pour les tenseurs associés aux schémas usuels.

1) *Schéma matière pure.* – Le terme le plus important dans $T_{\alpha\beta}$ lorsqu'il existe correspond toujours à l'énergie pondérale. Si l'on néglige toutes les autres formes d'énergie, on aura alors le schéma matière pure avec:

$$T_{\alpha\beta} = \varrho u_\alpha u_\beta \,. \tag{4.2}$$

Les identités de conservation s'écrivent:

$$\nabla_\beta T^\beta_\alpha = \nabla_\beta(\varrho u^\beta)\cdot u_\alpha + \varrho u^\beta \nabla_\beta u_\alpha = 0 \,. \tag{4.3}$$

(*) Cf. M.me F. HENNEQUIN [5]

Formons la combinaison linéaire $u^\nu(\nabla_\beta T^\beta_\nu)$ et tenant compte de $u^\nu u_\alpha = 1$, il vient :

$$u^\nu(\nabla_\beta T^\beta_\nu) = \nabla_\nu(\varrho\, u^\nu) = 0\,. \tag{4.4}$$

C'est l'équation de continuité du milieu. Les équations (4.3) se réduisent alors à :

$$u^\beta \nabla_\beta u_\nu = 0\,. \tag{4.5}$$

Le système (4.5) exprime que les lignes de courant, définies comme trajectoires du champ de vecteurs $\boldsymbol{u}$, sont géodésiques de la variété riemannienne.

Ce qu'on nomme le principe des géodésiques apparait comme une conséquence de (4.1) et des conditions de raccordement de Schwarzschild. Si l'on considère une masse d'épreuve dans un champ de gravitation extérieur donné, la nécessité d'un raccordement entre champ intérieur et champ extérieur fait que la masse d'épreuve doit décrire une géodésique du ds^2 extérieur.

2) *Schéma fluide parfait.* – On appelle ainsi un état de la matière dont la description peut être faite à l'aide des grandeurs $\boldsymbol{u}$, ϱ, p, les deux grandeurs scalaires étant supposées liées par une relation fonctionnelle dite équation d'état $\varrho = \varphi(p)$. Le tenseur d'énergie associé est de la forme :

$$T_{\alpha\beta} = \left(\varrho + \frac{p}{c^2}\right) u_\alpha u_\beta - \frac{p}{c^2}\, g_{\alpha\beta}\,. \tag{4.6}$$

Ecrivons les identités de conservation pour ce tenseur :

$$\nabla_\beta T^\beta_\nu = \nabla_\beta\left[\left(\varrho + \frac{p}{c^2}\right) u^\beta\right] \cdot u_\alpha + \left(\varrho + \frac{p}{c^2}\right) u^\beta \nabla_\beta u_\alpha - \partial_\alpha \frac{p}{c^2} = 0\,. \tag{4.7}$$

Alors

$$u^\alpha(\nabla_\beta T^\beta_\alpha) = \nabla_\alpha\left[\left(\varrho + \frac{p}{c^2}\right) u^\alpha\right] - u^\alpha \partial_\alpha \frac{p}{c^2} = 0\,, \tag{4.8}$$

et les conditions de conservation (4.7) deviennent

$$u^\beta\, \nabla_\beta u_\nu = \frac{\partial_\beta(p/c^2)}{\varrho + (p/c^2)}\,(g^\beta_\nu - u^\beta u_\nu)\,. \tag{4'9}$$

Ces équations définissent les géodésiques d'une métrique conforme à la métrique

riemannienne $ds^2 = F^2 ds^2$ où la fonction F, appelée indice du fluide, est définie par

$$F = \exp \int_{p_1}^{p} \frac{dp}{\varrho c^2 + p} \quad (6) .$$

4'2. *Equations spatio-temporelles du mouvement.* – Nous voyons par ce qui précède que les identités de conservation ont un contenu physique important. En particulier elles fournissent le système différentiel aux lignes de courant.

Nous donnerons donc la définition suivante:

Les équations spatio-temporelles du mouvement d'une masse d'épreuve placée dans un champ sont fournies par les identités de conservation du tenseur d'impulsion-énergie représentant les distributions énergétiques du champ.

Il revient évidemment au même de considérer des combinaison linéaires indépendantes de ces relations. Les quatres identités de conservation du tenseur d'impulsion-énergie correspondent à trois équations du mouvement au sens classique ($\nabla_\beta T_i^\beta = 0$) et à une équation de continuité $u^\nu(\nabla_\beta T_\nu^j) = 0$.

1) *Equations du mouvement au sens classique.* – L'introduction des densités tensorielles permet de mettre les identités de conservation sous une forme intéressante, notamment du point de vue des calculs d'approximation. Nous serons amenés alors à multiplier ces identités par $\sqrt{-g}$, et nous écrirons les trois équations spatio-temporelles, généralisant les équations classiques du mouvement sous la forme:

$$\sqrt{-g}\nabla_\beta T_i^\beta \equiv \partial_\beta(T_i^\beta \sqrt{-g}) - \tfrac{1}{2}(T^{\alpha\beta}\sqrt{-g})\partial_i g_{\alpha\beta} = 0 . \tag{4.10}$$

Les équations spatio-temporelles du mouvement d'un corps seront obtenues en intégrant les équations spatio-temporelles d'une masse d'épreuve sur le volume d'espace occupé par le corps. En mettant en évidence l'élément de volume de W_3 ($\sqrt{-g^*}\, dx^1 \wedge dx^2 \wedge dx^3$) les équations du mouvement d'un corps B^3 sont donc:

$$\int_{B^3} \sqrt{\frac{g}{g^*}}\, \nabla_\beta T_i^\beta \cdot \sqrt{-g^*}\, dx^1 \wedge dx^2 \wedge dx^3 = 0 . \tag{E.1}$$

Nous poserons dans la suite $w = \sqrt{g}/g^*$.

2) *Equation de continuité.* – Multiplions l'équation (4.4) par $\sqrt{-g}$ et écrivons le premier membre de l'équation obtenue sous la forme d'une divergence ordinaire. Posons d'autre part

$$u^\nu = u^0 v^\nu , \tag{4.10}$$

ou $v^i = \mathrm{d}x^i/\mathrm{d}t$ est la vitesse d'espace et $v^0 = 1$. Il vient

$$\sqrt{-g}\nabla_\alpha(\varrho u^\alpha) \equiv \partial_\alpha(\varrho u^0\sqrt{-g}v^\alpha) = 0\,. \tag{4.11}$$

La comparaison avec l'écriture classique des conditions de continuité nous conduit à choisir comme densité de masse la quantité

$$m = \varrho u^0\sqrt{-g}\,. \tag{4.12}$$

Intégrons l'équations $u^\lambda(\nabla_\beta T^\beta_\lambda)\sqrt{-g} = 0$ sur un domaine D_4 à quatre dimensions limité par un tube de courant T^3 et deux sections d'expace $B^3(x^0 = ct)$ et $B'^3(x^0 = ct')$. Il vient

$$\int_{D_4} u^\alpha(\nabla_\beta T^\beta_\alpha)\sqrt{-g}\,\mathrm{d}x^0\wedge\mathrm{d}x^1\wedge\mathrm{d}x^2\wedge\mathrm{d}x^3 = 0\,. \tag{4.13}$$

En transformant (4.13) en une intégrale étendue à la frontière de D_4, on déduit les propriétés suivantes relatives aux schémas usuels:

Dans le cas d'un schéma matière pure, la masse $M = \int_{B^3} m\,\mathrm{d}x^1\wedge\mathrm{d}x^2\wedge\mathrm{d}x^3$ est constante au cours du temps.

Dans le cas d'un schéma fluide parfait, la variation de la masse M au cours du temps est uniquement liée aux termes de pression p. Le choix de m nous donne donc la masse la plus conservative associée au schéma fluide parfait (5).

4·3. *Rôle des conditions d'isothermie.* – Nous avons à rechercher une solution approchée des équations du champ et à la substituer dans les équations du mouvement. Les dix équations du champ ne sont pas indépendantes, leurs premiers membres satisfont à quatre identités de conservation. On peut donc fixer localement quatre potentiels, ou plus généralement se donner quatre relations de coordonnées. Pour avoir des résultats qui puissent être interprétables physiquement, il nous faut choisir parmi l'ensemble des systèmes de coordonnées un système qui soit adapté le mieux possible à la réalité physique. A ce point de vue, les coordonnées qui s'imposent sont les coordonnées isothermes (G. Darmois).

Dans un système isotherme, $S^{\lambda\beta}$ se réduit à une expression que nous désignons par $S^{\lambda\beta}_{(\mathcal{J})}$. Dans chaque équation $S^{\lambda\beta}_{(\mathcal{J})} = \chi T^{\lambda\beta}$ ne figurent que les dérivées secondes de $g^{\lambda\beta}\sqrt{-g}$. Cette propriété nous permet de faire usage d'un procédé en cascade d'approximations. Quand nous aurons à notre disposition une solution approchée, nous appellerons équations approchées du mouvement ce que l'on obtient en substituant la solution approchée dans les équations du mouvement.

Cependant, notre but initial était la résolution de:

$$S^{\alpha\beta} = \chi T^{\alpha\beta} .$$

En choisissant un système de coordonnées isothermes, nous nous sommes ramenés au système plus simple

$$S^{\alpha\beta}_{(\mathcal{J})} = \chi T^{\alpha\beta} ,$$

pour lesquelles nous avons écrit les équations du mouvement sous la forme habituelle $\nabla_\beta T^\beta_\alpha = 0$; on peut se demander si les conditions d'isothermie sont vérifiées pour la solution trouvée, c'est-à-dire si le problème premier a bien été traité dans sa généralité.

La réponse à cette question a été apportée par Mme F. HENNEQUIN. L'auteur a étudié le rôle des conditions d'isothermie et démontré que les équations du mouvement approchée d'ordre p entrainent les conditions d'isotermie approchées d'ordre p (5).

Il y a ainsi équivalence des conditions d'isothermie et des équations du mouvement relatives à une solution approchée. Certains auteurs (N. M. PETROVA, V. A. FOCK) ont utilisé effectivement les conditions d'isothermie pour former les équations du mouvement; A. PAPAPETROU et Mme F. HENNEQUIN ont utilisé les conditions de conservation (*).

5. – Flux et équations du mouvement.

La déduction des équations du mouvement pour un système de corps à partir des équations du champ extérieur:

$$S_{\alpha\beta} = 0 , \tag{5.1}$$

repose essentiellement sur les propriétés que possède le flux du vecteur $\hat{\boldsymbol{S}}_{(\alpha)} = w\boldsymbol{S}_{(\alpha)}$ de composantes $wS^k_{(\alpha)}$ (α, indice fixé quelconque) défini sur une section d'espace W_3.

$w = \sqrt{g/g^*}$ définit un scalaire sur W_3. Ce facteur est mis dans $\hat{\boldsymbol{S}}_{(\alpha)} = w\boldsymbol{S}_{(\alpha)}$ simplement pour faciliter la comparaison des équations (E.1) (p. 653) et (E.2)

(*) La dépendance entre les équations du mouvement et les conditions d'isothermie subsiste pour le champ extérieur, d'après la continuité des $g_{\alpha\beta}$ et $\partial_\lambda g_{\alpha\beta}$ (les conditions d'isothermie sont définies par $-g^{\alpha\beta}\Gamma^\lambda_{\alpha\beta} = 0$) et d'après les résultats obtenus dans la comparaison des deux méthodes (voir plus loin).

(p. 659). Son emploi n'est pas indispensable dans l'étude des équations du mouvement par la méthode des singularités (9). Naturellement, on aurait pu aussi définir les équations (E.1) sans le facteur w et utiliser alors le flux du vecteur $\boldsymbol{S}_{(\alpha)}$.

Considérons dans W_3 un champ d'intégration à trois dimensions *contenant un corps B^3 déterminé*. Soit C^3 ce champ d'intégration et soit ∂C^3 sa frontière Désignons par $\Omega_{(\alpha)}$ la forme différentielle extérieure d'ordre 2 associée au vecteur $\boldsymbol{S}_{(\alpha)}$:

$$\Omega_{(\alpha)} = \tfrac{1}{2}\eta^*_{ijk}(wS^k_\alpha)\,\mathrm{d}x^i \wedge \mathrm{d}x^j\,, \tag{5.2}$$

η^*_{ijk} est le tenseur complètement antisymétrique attaché à la forme élément de volume de W_3. Par définition le flux du vecteur $\hat{\boldsymbol{S}}_{(\alpha)}$ à travers la frontière de C^3 est l'intégrale de la 2-forme $\Omega_{(\alpha)}$ sur le 2-champ ∂C^3:

$$\mathrm{flux}^*_{\partial C^3}\hat{\boldsymbol{S}}_{(\alpha)} = \int_{\partial C^3}\Omega_{(\alpha)}\,. \tag{5.3}$$

1) Soit $\mathrm{d}\Omega_{(\alpha)}$ la différentielle extérieure de la forme $\Omega_{(\alpha)}$:

$$\mathrm{d}\Omega_{(\alpha)} = \tfrac{1}{2}\varepsilon_{ijk}\mathrm{d}(S^k_\alpha\sqrt{-g})\wedge\mathrm{d}x^i\wedge\mathrm{d}x^j = \partial_k(S^k_\alpha\sqrt{-g})\,\mathrm{d}x^1\wedge\mathrm{d}x^2\wedge\mathrm{d}x^3\,. \tag{5.4}$$

Etudions la condition $\mathrm{d}\Omega_{(\alpha)} = 0$ à l'aide des identités de conservation

$$\nabla_\beta S^\beta_\alpha = \frac{1}{\sqrt{-g}}\,\partial_\beta(S^\beta_\alpha\sqrt{-g}) - \tfrac{1}{2}S^{\lambda\mu}\partial_\alpha g_{\lambda\mu} = 0\,. \tag{5.5}$$

Ces identités peuvent s'écrire encore, après multiplication par $\sqrt{-g}$:

$$\partial_k(S^k_\alpha\sqrt{-g}) + \partial_0(S^0_\alpha\sqrt{-g}) - \tfrac{1}{2}\sqrt{-g}\;S^{\lambda\mu}\partial_\alpha g_{\lambda\mu} = 0\,. \tag{5.6}$$

Par conséquent la condition $\partial_k(S^k_\alpha\sqrt{-g}) = 0$, c'est-à-dire $\mathrm{d}\Omega_{(\alpha)} = 0$, ne peut pas être satisfaite identiquement. Cependant la dérivée partielle ∂_0 est d'ordre $1/c$, de même que les $\partial_\gamma g_{\lambda\mu}$ (*). On en déduit que la quantité $\mathrm{d}\Omega_{(\alpha)}$ d'ordre l est nulle si les équations du champ d'ordre $(l-1)$ sont vérifiées, ce que nous traduirons par

$$\mathrm{d}\Omega_{(\alpha)} \overset{l}{=} 0\,, \tag{5.7}$$

(9) T. H. Pham: *La méthode des singularités pour les équations du mouvement en relativité générale et en théorie du champ unifié* (Thèse Sc. math., Paris, 1957) (multigraphiée); *Compt. Rend. Ac. Sci. Paris*, **246**, 61 (1958); voir aussi dans: Réunion d'études et de mises au point tenue sous la présidence de L. de Broglie, Paris, 1958: *Problèmes actuels en théorie de la relativité* (à paraître).

(*) Avec les développements habituels des potentiels en coordonnées isothermes les $\partial_\alpha g_{\lambda\mu}$ son d'ordre $1/c^2$ au moins.

la notation $\overset{l}{=}$ signifiant que l'égalité a lieu à chaque ordre l en vertu des approximations antérieures.

Considérons deux champs d'intégration C'^3 et C''^3 dont l'un est intérieur à l'autre. La forme $\Omega_{(\alpha)}$ étant régulière dans le domaine $(C'^3 - C''^3)$ compris entre les frontières $\partial C'^3$ et $\partial C''^3$, il vient par application du théorème de Stokes:

$$\int_{\partial C'^3} \Omega_{(\alpha)} - \int_{\partial C''^3} \Omega_{(\alpha)} = \int_{\partial(C'^3 - C''^3)} \Omega_{(\alpha)} = \int_{C'^3 - C''^3} \mathrm{d}\Omega_{(\alpha)} . \tag{5.8}$$

Les relations (5.7) et (5.8) entrainent que *le flux du vecteur* $\mathbf{S}_{(\alpha)}$ *ne dépend pas du choix de* C^3. En particulier on peut évaluer ce flux en déterminant sa valeur sur la frontière du corps contenu dans C^3:

$$\int_{\partial C^3} \Omega_{(\alpha)} \overset{l}{=} \int_{\partial B^3} \Omega_{(\alpha)} . \tag{5.9}$$

2) Examinons maintenant la manière dont les potentiels des divers ordres interviennent dans l'intégrale (5.3).

Pour calculer cette intégrale nous utiliserons un espace euclidien de représentation $\mathcal{E}_3$ à trois dimensions. Désignons par Δ le domaine représentatif de C^3, et par $\partial\Delta$ sa frontière que nous rapportons à des paramètres (t^1, t^2). Sur ∂C^3 la forme $\Omega_{(\alpha)}$ admet une forme induite $\Omega_{(\alpha)}$ qui peut s'exprimer à l'aide des variables (t^1, t^2) par la formule

$$\Omega_{(\alpha)} = f_{(\alpha)} \mathrm{d}t^1 \wedge \mathrm{d}t^2 , \tag{5.10}$$

où

$$f_{(\alpha)} = \tfrac{1}{2} \eta^*_{ijk} (w S^k_\alpha) \frac{D(x^i, x^j)}{D(t^1, t^2)} . \tag{5.11}$$

L'intégrale de la forme $\Omega_{(\alpha)}$ sur le champ ∂C^3 n'est autre que l'intégrale de la fonction $f_{(\alpha)}$ sur le champ $\partial\Delta$. On sait qu'elle peut se mettre sous la forme

$$\int_{\partial C^3} \Omega_{(\alpha)} = \int_{\partial\Delta} w S^k_\alpha \nu_k \sqrt{|g'|}\, \mathrm{d}t^1 \wedge \mathrm{d}t^2 , \tag{5.12}$$

où: (ν_k) = normale unitaire à ∂C^3,

g' = déterminant de la forme quadratique fondamentale de ∂C^3 rapporté aux variables (t^1, t^2) (*).

(*) Voir A. LICHNEROWICZ: *Algèbre et analyse linéaires* (Paris, 1947), p. 192-194.

Explicitons maintenant l'expression S_α^k qui figure sous le signe d'intégration. Posons:

$$F^\lambda \equiv -g^{\alpha\beta}\Gamma^\lambda_{\alpha\beta} = \frac{1}{\sqrt{-g}}\partial_\varrho \mathfrak{g}^{\varrho\lambda}. \qquad (\mathfrak{g}^{\alpha\beta} = g^{\alpha\beta}\sqrt{-g}) \ (*). \tag{5.13}$$

Par un calcul classique on obtient la formule

$$S^{\alpha\beta} = \frac{1}{2\sqrt{-g}}(g^{\lambda\mu}\partial_{\lambda\mu}\mathfrak{g}^{\alpha\beta} - \mathfrak{g}^{\alpha\varrho}\partial_\varrho F^\beta - \mathfrak{g}^{\beta\varrho}\partial_\varrho F^\alpha + \mathfrak{g}^{\alpha\beta}\partial_\varrho F^\varrho) + H^{\alpha\beta}, \tag{5.14}$$

$H^{\alpha\beta}$ désignant une fonction des potentiels et de leurs dérivées premières. De (5.14) on tire:

$$S_\alpha^k = \Phi_\alpha^k + \Lambda_\alpha^k, \tag{5.15}$$

où

$$\Phi_\alpha^k = \tfrac{1}{2}\,\delta_{\alpha\beta}\partial_l(-\partial_l\mathfrak{g}^{\beta k} + \partial_l\mathfrak{g}^{\beta k} + \delta_l^\beta\partial_s\mathfrak{g}^{sk} - \delta_k^\beta\partial_s\mathfrak{g}^{sl}) \tag{5.16}$$

est l'ensemble des *termes linéaires qui ne comportent aucune dérivation par rapport à la variable* x^0; Λ_α^k comprend les autres termes linéaires ainsi que les termes non linéaires de S_α^k.

Nous avons séparé les terms de S_α^k en deux groupes. La raison en est la suivante: si l'on considère l'expression S_α^k d'ordre l quelconque, seul Φ_α^k contient les potentiels d'ordre l tandis que Λ_α^k ne fait intervenir que les potentiels d'ordre au plus égal à $(l-1)$. Ceci est une conséquence de l'hypothèse *c*).

On constate que Φ_α^k est de la forme $\partial_l F^{kl}_{(\alpha)}$ où $F^{kl}_{(\alpha)}$ est antisymétrique par rapport aux indices k, l. On peut alors montrer que dans l'espace euclidien de répresentation $\mathfrak{E}_3$ rapporté à des coordonnées rectilignes, la partie de l'intégrale (5.12) qui porte sur Φ_α^k peut se ramener à l'intégrale sur $\partial\Delta$ d'une 2-forme homologue à zèro. Le champ d'intégration $\partial\Delta$ ayant une frontière nulle, une telle intégrale est toujours identiquement nulle (+). Ainsi, seul Λ_α^k contribue à l'intégrale (5.12), ce qui montre que *le flux de* $\hat{\boldsymbol{S}}_{(\alpha)}$ *d'ordre* l *ne dépend effectivement que des potentiels d'ordre* $(l-1)$. Il résulte que le calcul du flux d'ordre l n'est lié qu'à la solution des équations du champ d'ordre $(l-1)$. Cette propriété importante signifie que si l'on substitue aux $\mathfrak{g}^{\alpha\beta}$ une solution des équations $S_{\alpha\beta} = 0$ *le flux de* $\hat{\boldsymbol{S}}_{(\alpha)}$ *ne sera pas identiquement nul.*

(*) Sur l'emploi de la densité tensorielle $\mathfrak{g}^{\alpha\beta}$ comme variable de champ, cf. (9), 2e référence.

(+) Cf. (1,2) (cas de la variété V_4) et (9) (cas d'une variété V_n à n dimensions).

2480

Or les équations du champ $S_{\alpha\beta} = 0$ impliquent nécessairement

$$\int_{\partial C^3} \Omega_{(\alpha)} = 0 . \tag{5.17}$$

En raison des propriétés du flux de $\hat{\mathbf{S}}_{(\alpha)}$, ces conditions ne sont pas vides. Elles constituent des relations que doit vérifier toute solution approchée des équations du champ, relations qui ne dépendent que de la frontière du corps contenu dans C^3. Nous pouvons donc les prendre comme définition des équation spatio-temporelles du mouvement.

De façon plus précise, les équations du mouvement au sens classique s'obtiennent à partir de

$$\int_{\partial C^3} \Omega_{(i)} = \int_{\partial B^3} \Omega_{(i)} = 0 . \tag{E.2}$$

La condition (5.17) pour $\alpha = 0$, ou plutôt une combinaison analogue à (4.13)

$$\int_{\partial D_4} \Omega = 0 , \qquad \Omega = \frac{1}{3!} \eta_{\lambda\mu\nu\varrho} (u^\alpha S^\varrho_\alpha) \, \mathrm{d}x^\lambda \wedge \mathrm{d}x^\mu \wedge \mathrm{d}x^\nu , \tag{5.18}$$

renseignera sur la variation de la masse (*). L'intégrale (5.18) est étendue à la frontière d'un domaine D_4 à quatre dimensions limité par un tube de courant et deux sections d'espace, $\eta_{\lambda\mu\nu\varrho}$ désigne le tenseur complètement antisymétrique attaché à la forme élément de volume V_4.

III. - Comparaison des deux méthodes d'obtention des équations du mouvement.

6. – Généralisation de la méthode utilisant le flux.

Nous nous proposons dans cette section d'établir le rapport entre la méthode du tenseur d'impulsion-énergie et la méthode des singularités. Nous utili-

(*) Dans les applications, la méthode des singularités a toujours été envisagée comme un procédé autonome. La condition:

$$\int_{\partial C^3} \Omega_{(\alpha)} = 0$$

joue de ce fait un rôle tout autre. Elle intervient alors dans l'approximation des équations du champ; associée avec les conditions de coordonnées elle permet de déterminer les fonctions harmoniques qui s'introduisent dans la solution des équations du champ extérieur.

serons principalement les relations entre le tenseur d'impulsion-énergie et les discontinuités du tenseur d'Einstein. Ces discontinuités se produisent pendant la traversée d'une hypersurface frontière S limitant une domaine de V_4 balayé par une distribution énergétique. D'autre part, pour la clarté de l'exposé nous considérerons des équations intermédiaires qui se prêtent bien à la comparaison avec les équations du mouvement (E1) et (E2). Nous obtiendrons ces équations en généralisant la méthode utilisant le flux au cas des équations du champ intérieur.

Ecrivons en effet les équations d'Einstein du cas intérieur sous la forme:

$$s_{\alpha\beta} \equiv S_{\alpha\beta} - \chi T_{\alpha\beta} = 0 \,. \tag{6.1}$$

Introduisons le vecteur d'espace $\hat{\boldsymbol{s}}_{(\alpha)}$ qui admet les composantes contravariantes $ws^k_{(\alpha)}$, et soit

$$\omega_{(\alpha)} = \tfrac{1}{2}\eta^*_{ijk}(ws^k_\alpha)\,\mathrm{d}x^i \wedge \mathrm{d}x^j \,, \tag{6.2}$$

la forme différentielle extérieure d'ordre 2 associée à ce vecteur. Considérons les équations suivantes

$$\int_{\hat{c}B^3} \omega_{(\alpha)} = 0 \,, \tag{6.3}$$

qui expriment que le flux du vecteur $\hat{\boldsymbol{s}}_{(\alpha)}$ à travers la frontière du corps B^3 est nul pour toute solution des équations (6.1).

Nous raisonnerons sur les équations (6.3) en vue de montrer l'équivalence complète des deux méthodes. Les résultats obtenus s'appliqueront *a fortiori* aux équations

$$\int_{\hat{c}B^3} \omega_{(i)} = 0 \,, \tag{E.3}$$

qui correspondent aux équations du mouvement au sens classique.

7. – Relation entre les équations (E.1) et (E.3).

La métrique satisfaisant aux équations (6.1) est regulière dans B^3. Nous pouvons appliquer le théorème de Stokes à l'intégrale de surface (6.3) et la transformer en une intégrale de volume étendue au domaine B^3:

$$\int_{\hat{c}B^3} \omega_{(\alpha)} = \int_{B^3} \mathrm{d}\omega_{(\alpha)} \,, \tag{7.1}$$

où $\mathrm{d}\omega_{(\alpha)}$ désigne la différentielle extérieure de la forme $\omega_{(\alpha)}$:

$$\mathrm{d}\omega_{(\alpha)} = \tfrac{1}{2}\varepsilon_{ijk}\,\mathrm{d}(s^k_\alpha\sqrt{-g})\wedge\mathrm{d}x^i\wedge\mathrm{d}x^j = \partial_k(s^k_\alpha\sqrt{-g})\,\mathrm{d}x^1\wedge\mathrm{d}x^2\wedge\mathrm{d}x^3. \tag{7.2}$$

D'autre part, le tenseur $s_{\alpha\beta}$ qui est symétrique vérifie la formule

$$\sqrt{-g}\,\nabla_\beta s^\beta_\alpha = \partial_\beta(s^\beta_\alpha\sqrt{-g}) - \tfrac{1}{2}\sqrt{-g}\,s^{\varrho\sigma}\partial_\alpha g_{\varrho\sigma}\,, \tag{7.3}$$

que l'on peut écrire encore

$$\partial_k(s^k_\alpha\sqrt{-g}) = \sqrt{-g}\,\nabla_\beta s^\beta_\alpha - [\partial_0(s^0_\alpha\sqrt{-g}) - \tfrac{1}{2}\sqrt{-g}\,s^{\varrho\sigma}\partial_\alpha g_{\varrho\sigma}]\,. \tag{7.4}$$

Il vient donc

$$\int_{\partial B^3}\omega_{(\alpha)} = \int_{B^3}\sqrt{-g}\,\nabla_\beta s^\beta_\alpha\,\mathrm{d}x^1\wedge\mathrm{d}x^2\wedge\mathrm{d}x^3 - \int_{B^3}[\partial_0(s^0_\alpha\sqrt{-g}) - \tfrac{1}{2}\sqrt{-g}\,s^{\varrho\sigma}\partial_\alpha g_{\varrho\sigma}]\mathrm{d}x^1\wedge\mathrm{d}x^2\wedge\mathrm{d}x^3. \tag{7.5}$$

Examinons l'intégrale (7.5) d'ordre l. Le deuxième terme du second membre qui ne fait intervenir que les $s_{\alpha\beta}$ d'ordre $(l-1)$ est nul parce que les équations du champ d'ordre $(l-1)$ sont vérifiées. Il en résulte que cette intégrale se réduit au premier terme du second membre qui est égal à

$$\int_{\partial B^3}\omega_{(\alpha)} \overset{l}{=} \int_{B^3}\sqrt{-g}\,\nabla_\beta(S^\beta_\alpha - \chi T^\beta_\alpha)\,\mathrm{d}x^1\wedge\mathrm{d}x^2\wedge\mathrm{d}x^3 = -\chi\int_{B^3}\sqrt{-g}\,\nabla_\beta T^\beta_\alpha\,\mathrm{d}x^1\wedge\mathrm{d}x^2\wedge\mathrm{d}x^3\,, \tag{7.6}$$

puisque le tenseur d'Einstein est conservatif. Rappelons que $\overset{l}{=}$ signifie: égalité à chaque ordre l en vertu des approximations antérieures.

Ainsi, on voit que les équations du mouvement (E.1) peuvent être remplacées par les équations (E.3) qui en constituent une autre formulation.

Nous noterons que le tenseur $S_{\alpha\beta}$ a disparu des équations (7.6) grâce aux identités de conservation. Dans les équations du mouvement ne figure donc plus que le tenseur $T_{\alpha\beta}$. De là vient la simplicité relative des calculs d'approximation auxquels conduit l'emploi du champ intérieur.

8. – Relation entre les équations (E.2) et (E.3).

La comparaison de ces équations est immédiate. Affectons respectivement du signe + et du signe — les expressions de $S_{\alpha\beta}$ à l'intérieur et à l'exté-

rieur de B^3 et désignons par

$$[S_{\alpha\beta}] = S^+_{\alpha\beta} - S^-_{\alpha\beta}$$

la discontinuité subie par le tenseur d'Einstein à la traversée de ∂B^3. *Sur* ∂B^3 on a l'égalité

$$s_{\alpha\beta} \equiv S^+_{\alpha\beta} - \chi T_{\alpha\beta} = S^-_{\alpha\beta} + [S_{\alpha\beta}] - \chi T_{\alpha\beta} . \tag{8.1}$$

En portant (8.1) dans l'expression de $\omega_{(\alpha)}$ on voit que l'intégrale (6.3) se met sous la forme

$$\int_{\partial B^3} \omega_{(\alpha)} = \int_{\partial B^3} \Omega_{(\alpha)} + \int_{\partial B^3} \tfrac{1}{2} \eta^*_{ijk}\, w([S^k_\alpha] - \chi T^k_\alpha)\, \mathrm{d}x^i \wedge \mathrm{d}x^j . \tag{8.2}$$

Mais la discontinuité du tenseur d'Einstein est précisément représentée par $\chi T_{\alpha\beta}$:

$$[S_{\alpha\beta}] = \chi T_{\alpha\beta} ,$$

et la deuxième intégrale de (8.2) est nulle. Donc

$$\int_{\partial B^3} \omega_{(\alpha)} = \int_{\partial B^3} \Omega_{(\alpha)} ,$$

ce qui montre en particulier que les équations (E.3) sont équivalentes aux équations du mouvement (E.2).

9. – Equivalence des deux méthodes.

En raisonnant sur les équations (6.3) nous obtenons non seulement l'équivalence de (E.1) et (E.2) mais aussi celle de (4.13) et (5.18). Par un calcul analogue et en tenant compte de l'ordre de grandeur des $\partial_\beta u^\alpha$, nous pouvons d'ailleurs démontrer directement que les équations (4.13) et (5.18) se ramènent l'une à l'autre. Ainsi se trouve établie l'équivalence entre la méthode du tenseur d'impulsion-énergie et la méthode des singularités.

Nous pouvons énoncer:

THÉORÈME. – *Dans la théorie de la relativité générale les équations spatio-temporelles du mouvement de N masses gravitantes peuvent être définies par les*

4N conditions (6.3):

$$\int_{\partial B^3} \omega_{(\alpha)} = 0\,, \qquad \omega_{(\alpha)} = \frac{1}{2!}\,\eta^*_{ijk} w s^k_{\alpha}\, \mathrm{d}x^i \wedge \mathrm{d}x^j\,,$$

où $s_{\alpha\beta}$ *désigne indifféremment l'une ou l'autre des expressions*:

$$s_{\alpha\beta} = S^+_{\alpha\beta} - \chi T_{\alpha\beta} \quad et \quad s_{\alpha\beta} = S^-_{\alpha\beta}$$

suivant que l'on considère le champ intérieur ou le champ extérieur.

Les conditions

$$\int_{\partial B^3} \omega_{(i)} = 0$$

correspondent aux équations du mouvement au sens classique tandis que la combinaison linéaire

$$\int_{\partial D_4} \omega = 0\,, \qquad \omega = \frac{1}{3!}\,\eta_{\alpha\beta\gamma\delta} S^{\delta}_{\lambda} u^{\lambda}\, \mathrm{d}x^{\alpha} \wedge \mathrm{d}x^{\beta} \wedge \mathrm{d}x^{\gamma}\,,$$

joue le rôle d'une équation de continuité généralisée.

RIASSUNTO (*)

Esistono in relatività generale due metodi d'approssimazione per dedurre le equazioni del moto d'un sistema di corpi partendo dalle equazioni del campo. Uno utilizza una rappresentazione della materia per mezzo delle singolarità del campo esterno; l'altro fa intervenire il tensore energia-quantità di moto. Si può stabilire il legame tra questi due punti di vista osservando che le discontinuità del tensore di Einstein sono rappresentate dal tensore energia-quantità di moto. Allora, utilizzando il teorema di Stokes, si dimostra che i due metodi sono equivalenti.

(*) *Traduzione a cura della Redazione.*

IL NUOVO CIMENTO VOL. IX, N. 4 16 Agosto 1958

On the Mechanism of the (n, 2n) Reaction at 14 MeV Neutron Energy.

E. REMY (*) and K. WINTER (+)

Laboratoire de Physique Atomique et Moléculaire du Collège de France - Paris

(ricevuto il 28 Aprile 1958)

Summary. — Neutron spectra emitted by ^{9}Be, ^{55}Mn, Fe, ^{127}I and ^{181}Ta under bombardment of 14 MeV neutrons have been measured by using time-of-flight techniques. Continua of the first neutrons are separated from low energy groups due to the second neutrons. Successive emission is predominant for medium weight and heavy nuclei. A possible contribution of simultaneous emission by light nuclei cannot be decided. The conclusion is used to interprete inelastic scattering data from the interaction of 14 MeV neutrons.

1. – Introduction.

There now exist some investigations of the process of the (n, 2n) reaction on ^{9}Be ([1,2]). However, no experiments on the mechanism of this reaction are known for heavier elements. The knowledge of this mechanism and of the subsequent energy spectrum of the emitted neutrons is important for the interpretation of inelastic scattering data from the interaction of 14 MeV neutrons in the aspects of the statistical model.

HUBER and WAGNER ([1]) investigated the energy spectrum of neutrons emitted by ^{9}Be under bombardment of 3.7 MeV neutrons. Using photographic emulsion techniques, they found discrete neutron groups at energies corres-

(*) Now at Max-Planck-Institut für Physik, Göttingen, Germany.
(+) Now at CERN, SC-Division, Geneva 23, Switzerland.
([1]) P. HUBER and R. WAGNER: *Helv. Phys. Acta*, **30**, 257 (1957).
([2]) N. S. ANSEROVA *et al.*: *Rec. Trav. Inst. Rad. V. G. Chlopin*, **7**, 114 (1956).

ponding to known levels in ^{9}Be. They concluded that the two neutrons of the (n, 2n) reactions are emitted in succession.

ANSEROVA *et al.* [2] investigated the respective directions of emission of the neutrons in the same reaction by the interaction of 14 MeV neutrons. By using Be-loaded photographic emulsions they determined the total linear impulsion of the two neutrons emitted, by measuring the energies and the relative angle of emission of the α-particle fork from the disintegration of ^{8}Be. The impulsion will be optimal for neutrons emitted in the same direction and with the same energy. This process is suggested by observation of pick-up reactions (n, d) and (p, d) and by the possible existence of a stable « di-neutron ». After examination of 84 forks they concluded that the two neutrons are not emitted in the same direction and with the same energy, but in different directions and with different energies.

A third possible mechanism of the (n, 2n) reaction would consist in simultaneous emission of the two neutrons by a compound nucleus, *i.e.* a three-body breakup. This process would be favored by simple nuclear structures such as magic neutron cores with one or two extra neutrons.

The relative importance of all three mechanisms considered can be classified by the relative probabilities of the existence of two intermediate quantum states, in the compound nucleus and in the residual nucleus (neutrons emitted in succession), of one intermediate quantum state, in the compound nucleus (simultaneous emission by the compound nucleus) and of no intermediate quantum state (pick-up reaction). This classification is related to the interpretation of inelastic scattering data from the interaction of 14 MeV neutrons in the aspects of the statistical model. GRAVES and ROSEN [3], STELSON and GOODMAN [4], and WHITEMORE and DENNIS [5], by using photographic emulsion techniques, measured the distribution in energy of the inelastically scattered neutrons from the interaction of 14 MeV neutrons with various elements. They assigned a parameter analogous to a temperature, T, at an excitation

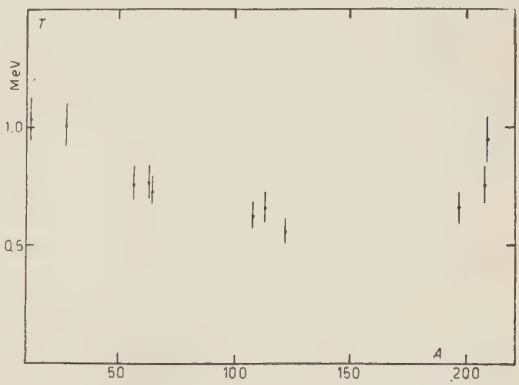

Fig. 1. – Nuclear temperature versus mass number of the target nucleus. Data taken from Ref. [3].

[3] E. GRAVES and L. ROSEN: *Phys. Rev.*, **89**, 343 (1953).
[4] P. H. STELSON and C. GOODMAN: *Phys. Rev.*, **82**, 69 (1950).
[5] B. G. WHITEMORE and G. E. DENNIS: *Phys. Rev.*, **84**, 296 (1951).

energy $E_0 = (10 \div 13)$ MeV of the residual nucleus, which is defined as

$$T = -\left[\mathrm{d} \ln \omega(E_0 - E_n)/\mathrm{d}E_n\right]^{-1} . \tag{1}$$

Fig. 1 shows a plot of their results versus A, the mass number of the residual nucleus; the temperature seems to be essentially independent of A. Whereas in the aspects of a statistical theory, based on the hypothesis of immediate formation of a compound nucleus and equal reduced widths for all channels, T would be proportional to $A^{-\frac{1}{2}}$.

The temperatures quoted are deduced from spectra composed of inelastically scattered neutrons and neutrons emitted in (n, 2n) reactions, if such reactions are energetically possible, the effect of the second contribution being not resolved in these experiments. Assuming successive emission of neutrons in (n, 2n) reactions, the correction of their effect on the spectra would increase by $(20 \div 30)\%$ for the heavier nuclei the temperature due to emission of the first neutron, increasing still more the deviations from the prediction of the statistical model. GRAVES and ROSEN [3] concluded, that their results would not support the hypothesis of simple sharing of the energy introduced into the nucleus by all nucleons.

This situation can be interpreted as well by a considerable contribution of simultaneously emitted neutrons, which would be favored by a partial sharing of the excitation energy. The maxima of their energy distributions would shift to higher energies with increasing A, due to the decreasing binding energy of neutrons. In this way the decrease of the temperature with increasing A would be compensated.

To investigate the principal mechanism of the (n, 2n) reaction from the interaction of 14 MeV neutrons and to decide the above mentioned alternative we used time-of-flight techniques to measure energy spectra of neutrons emitted by various elements.

2. – Experimental method.

2·1. *Time-of-flight technique.* – Two measurements on the neutrons must be made to establish the zero as well as the arrival time. The time zero has usually been established by using a pulsed neutron source [6]. This method is not recommended for high energy neutrons, because of the difficult background problems. Neutron pulses are delivered in 4π, giving rise to time-correlated background coincidences due to inelastic scattering in the surrounding objects.

---

[6] W. WEBER, C. W. JOHNSTONE and L. CRANBERG: *Rev. Sci. Inst.*, **26**, 526 (1956).

For the experiment described here, a time-of-flight technique in conjunction with the (d, t) reaction was chosen (7). A 100 keV deuteron beam bombarded a tritium-titan target. The reaction T(d, n)^{4}He yields a 14 MeV neutron associated with a 3 MeV recoil α-particle emitted at 180° with respect to the direction of the neutron. A plastic scintillator 0.1 mm thick and 5 mm in diameter within the target chamber of the accelerator detected recoil α-particles. The photomultiplier viewing the scintillator is protected against light coming from the target by a 0.5 μm thick aluminium foil. The α-signals thus supplied a time zero for associated 14.1 MeV neutrons in a conical beam, the width of which is defined by the solid angle of the α-particle detector. By establishing the time zero, a beam of monoenergetic neutrons having a known direction is obtained without the use of absorbers and collimators. The neutron beam did not meet, for a path of 10 meters, any material except the target chamber walls and the studied scatterer. Within this cone, at 20 cm of the neutron source, a scatterer, 5 cm long and 3 cm in diameter, was placed. It was faced by a neutron counter, containing a plastic scintillator, 5 cm thick and 5 cm in diameter, placed outside the time-correlated neutron beam at a distance of 50 cm from the scatterer, this distance representing the flight

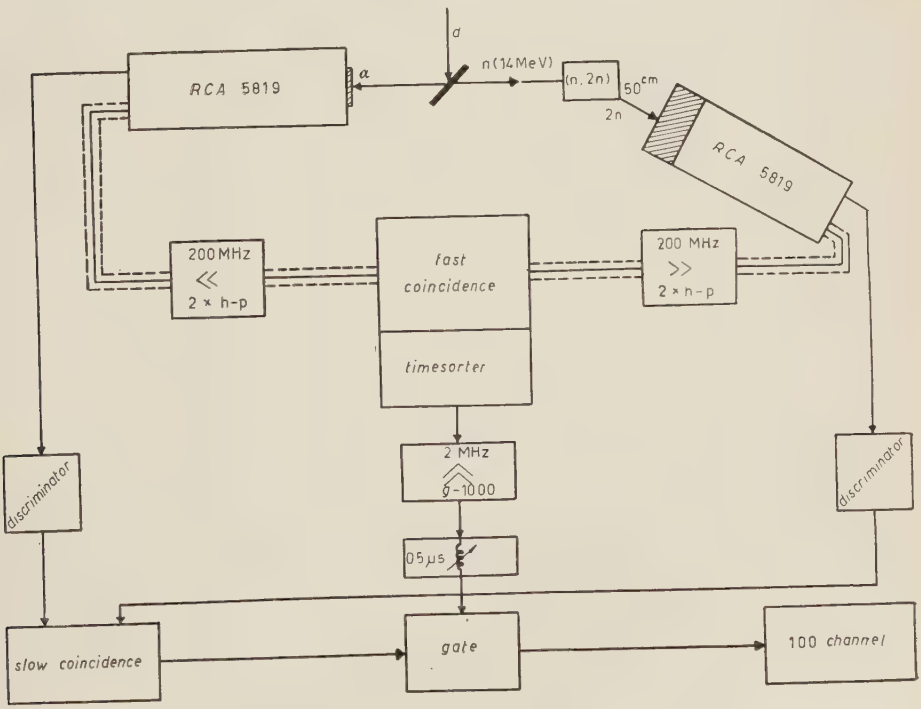

Fig. 2. – Block diagram of the electronic circuits.

(7) G. K. O'Neill: *Phys. Rev.*, **95**, 1235 (1954).

distance of neutrons emitted by the scatterer. The neutron signal thus supplied the arrival time.

Fig. 2 shows a block diagram of the electronic circuits. RCA 5819 photomultipliers with convex cathode having relatively small transit time fluctuations ([8]) were used. They were operated at 1250 V, with equal dynode-to-dynode voltages and doubled cathode-to-first-dynode voltage and subsequent distributed amplification.

The electronic circuits consist of a fast-slow coincidence circuit connected with a time-to-pulse-height converter. A complete description has been given elsewhere ([9]). The discriminators in the slow lines are adjusted in such a way that the slow coincidence output signal gates open the amplitude analyser only for signals analysed in the fast circuit which satisfied the required cut-off pulse height. The discriminator in the slow neutron line served as well to establish a well-defined minimum pulse height accepted by the electronics, a quantity needed in the calculation of the energy sensitivity of the neutron detector.

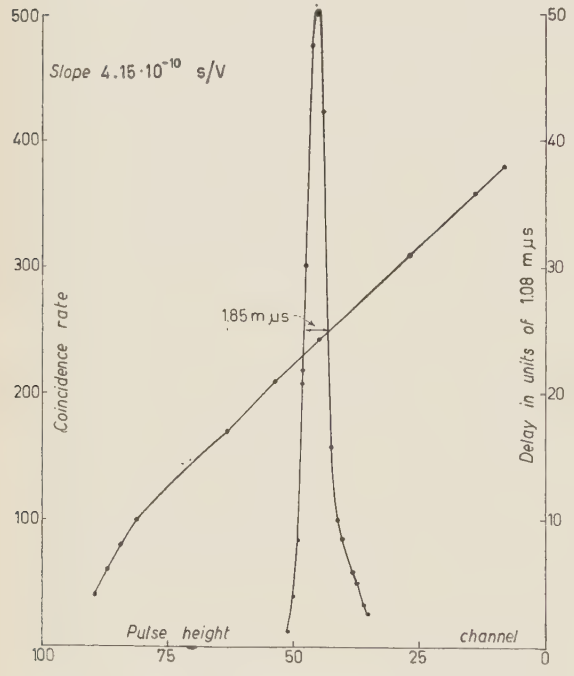

Fig. 3. – Calibration of the timesorter using ^{22}Na annihilation radiation. The response is linear from 8 to 43 ns. One of the resolution .....

The timesorter has been calibrated, using ^{22}Na annihilation radiation or (n-α) coincidences, by inserting known delays in one of the fast lines. The response of the time-sorter for a given delay was defined by the pulse height at the maximum of the corresponding resolution curve. Fig. 3 shows a calibration curve as well as one of the resolution curves. The response as a function of the delay was found to be linear in the region from 8 to 43 ns, representing flight times over 50 cm of neutrons of (10 ÷ 0.8) MeV. In this region the channel width of the am-

([8]) R. V. SMITH: *Westhinghouse Res. Lab.*, 60-94511-6-P6 (1956).
([9]) E. REMY and K. WINTER: *Journ. Phys. et Rad.*, **18**, 112A (1957).

2490

plitude analyser was $4 \cdot 10^{-10}$ s/V. Absolute calibration of the time scale with respect to the reaction to be studied was obtained by the known flight time of γ-rays accompanying (n, 2n) events as well as inelastic scattering in the studied scatterer.

2·2. *Background.* – The number of real time-of-flight events in our experiments was about

$$C_r = 8 \cdot 10^{-5} \cdot N_\alpha \,, \tag{2}$$

where N_α means the α counting rate per second. For the experiments described here the background was due to random coincidences and to time-correlated events due to inelastic scattering in the target chamber walls. The number of random coincidences is given by

$$C_f = 2\tau N_n \cdot N_\alpha = 2\tau \cdot N_\alpha^2 \cdot f \,, \tag{3}$$

where N_n means the counting rate of the neutron detector and f is a factor containing solid angles, sensitivity and possible attenuation of direct neutrons by a shield. The ratio of time-of-flight events to direct neutrons on the neutron detector being of the order of 10^{-5}, N_n can be taken as the counting rate of direct neutrons. τ, the effective resolution of the circuit, has been measured to be $1.01 \cdot 10^{-7}$ s, by counting singles and random coincidences of two independent γ-ray sources. In measuring it by (n-α)-singles and coincidences, without the scattering, we found $\tau = 2.00 \cdot 10^{-7}$ s, indicating time-correlated coincidences due to inelastic scattering events in the target chamber walls. By inserting a lead shield between neutron source and neutron detector, the direct neutron flux was attenuated by a factor of 10, and τ was found to be $1.02 \cdot 10^{-7}$ s, indicating the elimination of time-correlated coincidences. The ratio of real to random coincidences was found to be

$$\frac{C_r}{C_f} = 2.7 \cdot 10^{-4} \cdot N_\alpha^{-1} \,. \tag{4}$$

Admitting a ratio of 4, an α counting rate of $N = 6.7 \cdot 10^3$ c/s could be used yielding 0.5 real events per second.

The background spectrum was found to be uniform in the linear region of the timesorter (random coincidences) and showed a peak in the upper channels due to their increasing width in time. In order to establish the subtraction of this peak from a measured time-of-flight spectrum with the same statistic as that of the uniform part, we measured its form with very good statistics by using two independent sources of γ-rays. This spectrum has been normalized to the total background rate found in the experiments for a given neutron source strength and a given flux.

2·3. *Neutron detector sensitivity.* – The neutron detector energy sensitivity is defined by

$$S = C \cdot Y_i \cdot \left(\frac{E_n - E_r^{\min}}{E_n} \right), \tag{5}$$

Y_i meaning the interaction probability of neutrons of energy E_n in the volume of the scintillator and $E_r^{\min}$ the minimum recoil energy accepted by the slow neutron line. Y_i has been calculated up to neutron energies of 4.5 MeV, admitting only elastic neutron-proton interactions for detection, ^{12}C recoils not being accepted by the slow neutron line. $E_r^{\min}$ has been determined by comparing the respective pulse heights of proton recoils of 14.1 MeV and $E_r^{\min}$ with the known response curve of plastic scintillators. $E_r^{\min}$ has been (500 ± 50) keV in all experiments. The calculated sensitivity passed through a maximum at 2 MeV neutron energy, its total variation between 1 MeV and 4.5 MeV is 25%; the relative sensitivity is shown in Fig. 4.

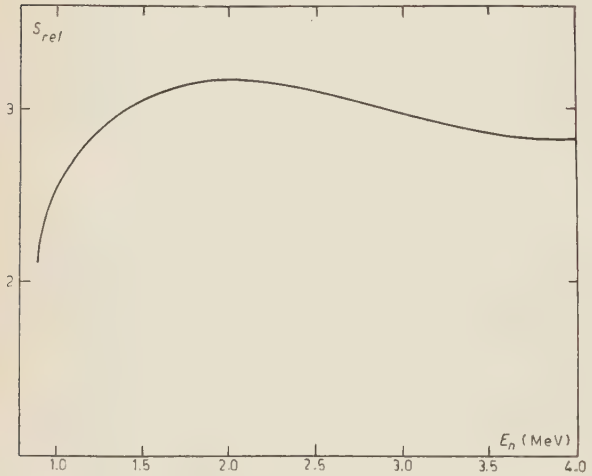

Fig. 4. – Neutron detector sensitivity calculated for a minimum recoil energy accepted by the slow neutron line $E_r^{\min} = (500 \pm 50)$ keV.

2·4. *Time and energy resolution.* – The total finite resolution of the time-of-flight measurement is determined by two groups of uncertainties; one which gives rise to constant relative errors $\Delta E/E \simeq 2\Delta t/t$, another which gives rise to energy dependent relative errors. In the first group there are: uncertainties due to:

1) the finite dimension of the scatterer in the direction of the flight path,

2) the finite dimension of the neutron detector;

in the second group there are all time uncertainties:

3) the finite resolution of the timesorter, mostly due to transit time fluctuations in the photomultipliers (~ 3 ns),

4) the transit time of 14 MeV neutrons through the scatterer, *i.e.* the uncertainty of the moment of the reaction (1 ns),

5) the uncertainty of the time zero, due to the target thickness and the α path geometry (0.5 ns).

Time-of-flight data have been taken at 90° with respect to incident neutrons, so uncertainties due to 1) and 4) can be considered to be approximately independent. Admitting a Gauss function for the different uncertainties, the time resolution for γ-rays has been computed to 3.2 ns in good agreement with the width at half height of observed γ lines. The total resolution for neutrons over 50 cm flight path varies from 10 to 20% for neutrons of (1÷5) MeV, *i.e.* neutron groups spaced by 200 keV in the region of 1 MeV can be separated.

3. – Results and discussion.

Time-of-flight spectra have been measured for $25 \cdot 10^6$ α-particles, or $2 \cdot 10^9$ neutrons in 4π, the total statistics varying from 2 500 to 4 000. Spectra obtained with ^{9}Be, ^{55}Mn, Fe, ^{127}I and ^{181}Ta are shown in Fig. 5-9, the time scale is linear, the corresponding neutron energies are indicated. Background has already been subtracted, but the spectra have not been corrected for the

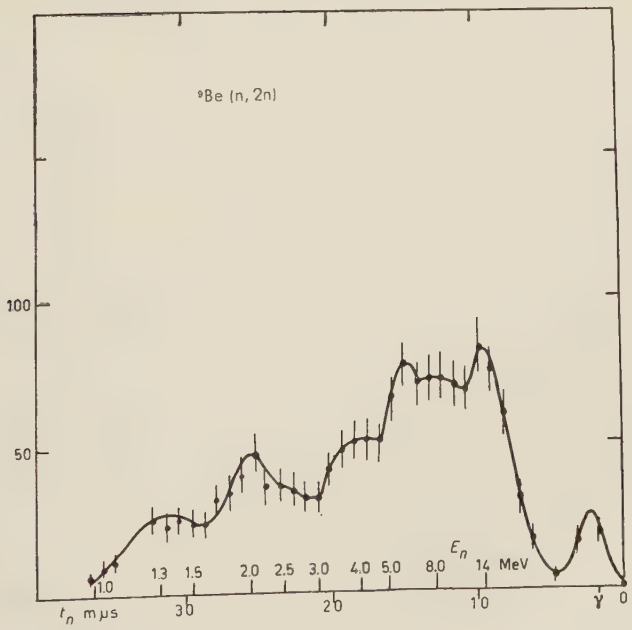

Fig. 5. – Neutron time-of-flight spectrum obtained with ^{9}Be.

energy sensitivity of the neutron detector. The peak marked γ at 1.7 ns of the time scale is due to γ-rays from the decay of the residual nucleus. The differential cross-section for elastic neutron scattering is small at 90° for heavy

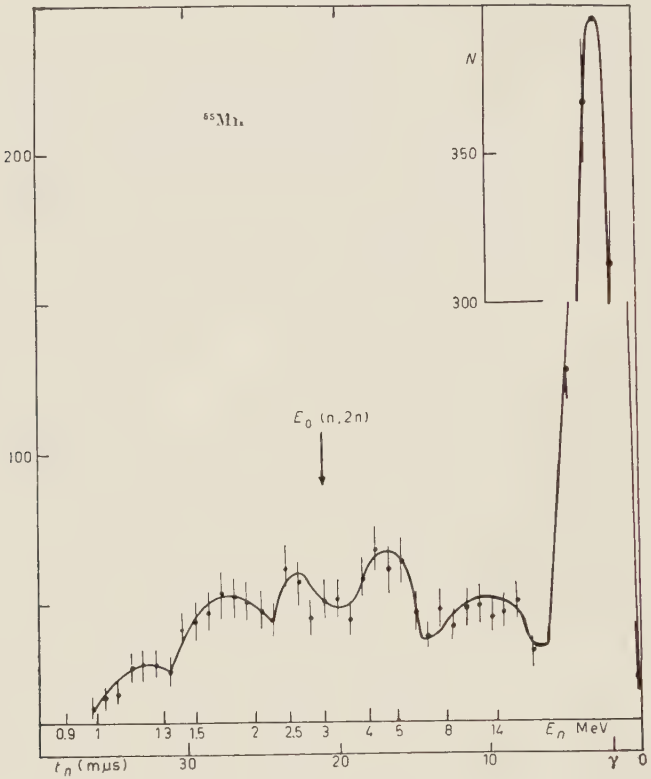

Fig. 6. – Neutron time-of-flight spectrum obtained with ^{55}Mn.

nuclei, as can be seen in the spectra. The spectra after correction for the energy sensitivity of the neutron detector are indicated in Fig. 10. They show neutron groups at low energies which are attributed to the subsequent emission of the second neutron in (n, 2n) reactions.

We will discuss here the case of ^{127}I with the help of Fig. 11, which shows a diagram of reactions in competition with the (n, 2n) reaction. The compound nucleus can decay by emission of a neutron or a proton, the latter branch leading to the (n, pn) reaction. Table I gives the threshold energies for (n, 2n) and (n, pn) reactions, values of the branching ratio, G_p/G_n, are given in column III, calculated for proton and neutron energies which permit the subsequent emission of a neutron of 1.3 MeV in contribution to the above mentioned low energy group. In the case of ^{127}I this ratio turns out to be $4 \cdot 10^{-3}$,

2494

TABLE I.

Element	Q(n, 2n) I	Q(n, pn) II	G_p/G_n III	$\frac{1}{2}$(14 MeV $- Q_b$) IV
^{55}Mn	— 11.0	— 7.2	$1.4 \cdot 10^{-1}$	1.5
^{54}Fe	—1 4.1	— 10.0	—	0
^{56}Fe	— 12.0	— 8.4	—	1.0
^{127}I	— 8.2	— 7.2	$4.2 \cdot 10^{-3}$	2.9
^{181}Ta	— 7.7	— 6.2	$2.1 \cdot 10^{-4}$	3.2

favoring the branch leading to the (n, 2n) reaction. We conclude that the low energy neutron group is not due to neutrons emitted in (n, pn) reactions.

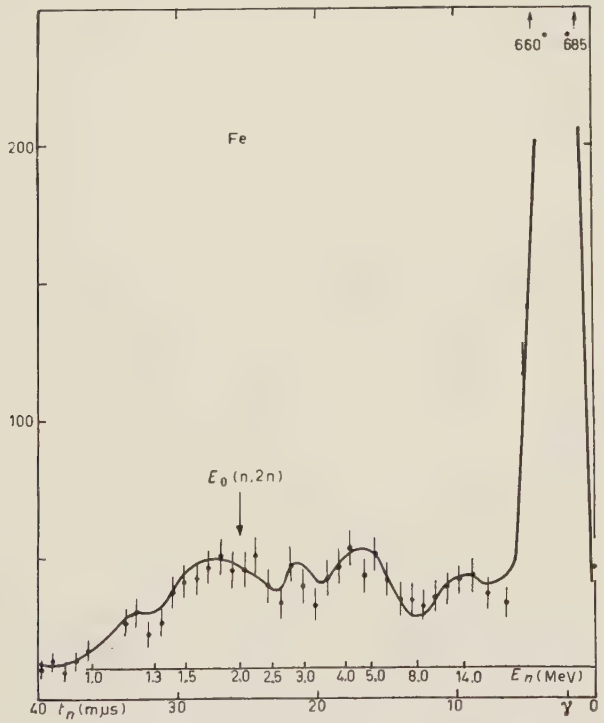

Fig. 7. – Neutron time-of-flight spectrun obtained with Fe.

Its interpretation as inelastic scattering of the first neutron would lead to a particular variation of the level density with excitation energy. Taking $f(E)/S_b \cdot E$ proportional to the level density, the latter would turn out to change suddenly its slope, a behavior which is not supported by other investigations [10].

[10] P. C. GUGELOT: *Phys. Rev.*, **93**, 425 (1954).

Furthermore, the shape of the spectrum is in qualitative agreement with calculations for successive emission on the basis of the statistical model, achieved by WEISSKOPF ([11]).

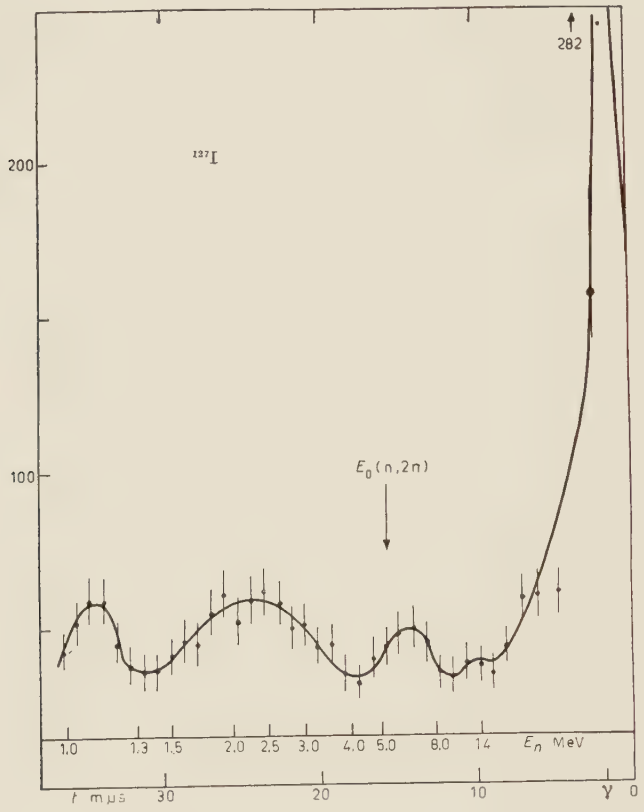

Fig. 8. – Neutron time-of-flight spectrum obtained with ^{127}I.

Simultaneous emission of the two neutrons of the (n, 2n) reaction has to be considered as a three-body breakup which would imply a continuous distribution of energy from zero to the maximum energy available. The maximum intensity would occur at $\frac{1}{2}(14\ \text{MeV} - Q_b)$, where Q_b means the binding energy of a neutron in the target nucleus. Values are listed in column IV of Table I.

In the case of ^{127}I no indication for simultaneous emission has been found (Fig. 8 and 10). The listed energy value for maximum intensity occurs on the slope of the continuum due to the emission of the first neutron. Simultaneous emission by the compound nucleus will be less probable for heavier nuclei

([11]) V. F. WEISSKOPF *et al.*: *NYO*, **636**, 153 (1951).

2496

(compare ^{181}Ta in Fig. 9 and 10), the reduced width for this process being smaller in the presence of a still greater number of nucleons in the compound nucleus.

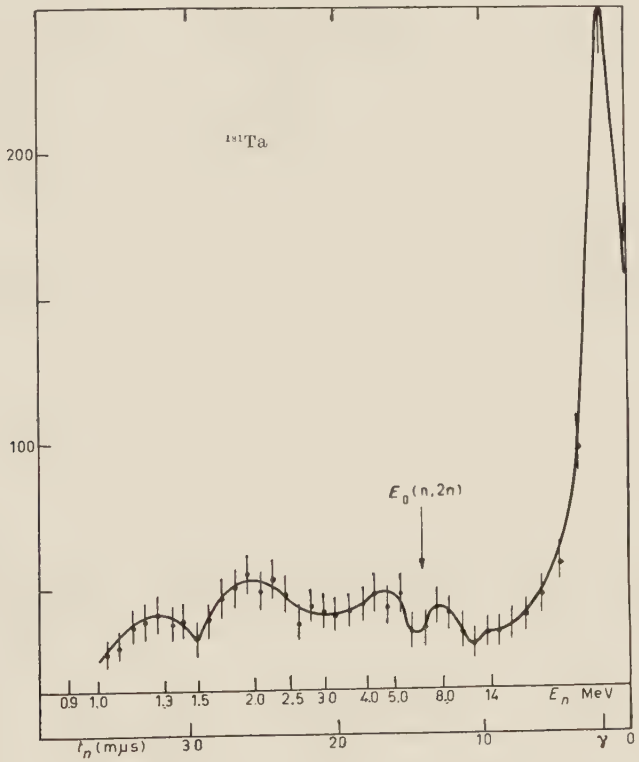

Fig. 9. – Neutron time-of-flight spectrum obtained with ^{181}Ta.

The neutron spectra observed for ^{55}Mn and Fe finally provide a quite sensitive test for simultaneous emission. The neutron configuration (magic+2) should favor the pick-up as well as simultaneous emission by the compound nucleus. Again, there is, in the limit of statistics, no indication for a three-body breakup. We conclude that this mechanism is very improbable for medium weight nuclei (and for incident neutrons of 14 MeV) in comparison with successive emission, even if the probability of a simultaneous distribution of energy on two neutrons in the presence of other nucleons is favored as in the cases of ^{55}Mn and ^{56}Fe.

It is concluded that the principal mechanism of the (n, 2n) reaction on medium weight and heavy nuclei induced by 14 MeV neutrons is successive emission. The consequences for the interpretation of inelastic scattering data will be discussed in Sect. **4**.

The pick-up mechanism in (n, 2n) reactions on ^{9}Be is favored by the simple structure of the target nucleus. HAEFNER ([12]) has shown that ^{9}Be can be considered as a system of a weakly bound neutron in the average potential of

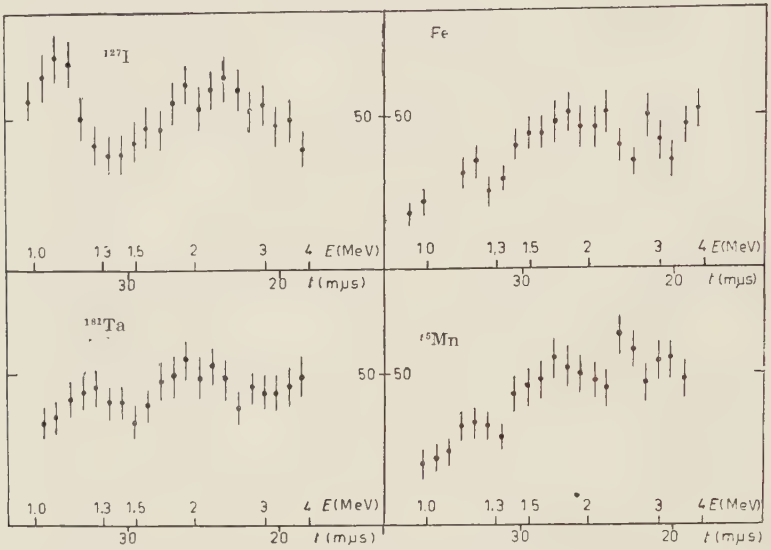

Fig. 10. – Neutron time-of-flight spectra corrected for the energy sensitivity of the neutron detector.

two preformed α-particles. This simple structure would favor as well a three-body breakup of the compound nucleus. The energy spectrum observed for ^{9}Be (Fig. 5) is simple because inelastic scattering is impossible or very improbable since the ground state energy of ^{8}Be is lower than the first excited state in ^{9}Be. So only elastic scattering and (n, 2n) reactions have to be considered. This simplification is supported by the small number of γ-rays observed, which are emitted in competition with the second neutron. We have listed neutron energies expected for successive emission to the levels of ^{9}Be and ^{8}Be in Table II,

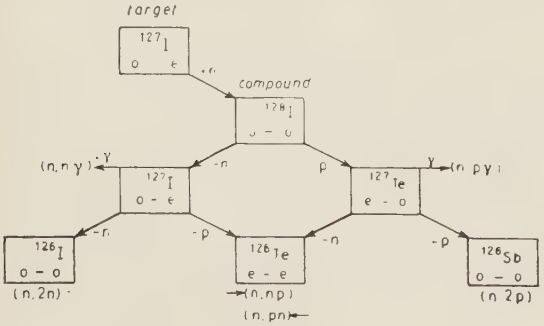

Fig. 11. – Competition diagram for the interaction of 14 MeV neutrons with ^{127}I.

([12]) P. R. HAEFNER: *Rev. Mod. Phys.*, **23**, 228 (1951).

TABLE II.

$n_1(^9\mathrm{Be})$	$n_2(^8\mathrm{Be})$				
14 MeV	—	—	—	—	—
12.2	—	—	—	—	—
11.5	0.8	—	—	—	—
10.9	1.4	—	—	—	—
9.2	3.1	—	—	—	—
7.2	5.1	2.2	0.9	—	—
6.1	6.2	3.3	2.0	0.8	—
2.7	9.6	6.7	5.4	4.2	1.95

calculated for all levels reported by AJZENBERG ([13]). Neutron groups at 1.3 MeV and 2 MeV are resolved, agreeing with calculated transition energies to levels of ^{8}Be. Neutron energies between 5 and 12 MeV are not resolved, containing either a great number of successive transitions (see Table II) or the maximum intensity for simultaneous emission or a mixture of both. In the spectrum observed there is no indication of the transition to the 11.3 MeV level in ^{9}Be which would yield 2.7 MeV neutrons. We cannot decide whether this level does not exist or whether this transition does not occur because the time between the emissions of the first and the second neutron at this excitation energy is very short, *e.g.* of the order of the transit time of nucleons over nuclear dimensions, so that there is no defined excited state between the two emissions.

A contribution of the pick-up mechanism could be identified by its angular correlation. Experiments on this question are in progress.

4. – Interpretation of inelastic scattering data.

The principal mechanism of the (n, 2n) reaction in medium weight and heavy nuclei is successive emission of the two neutrons. The compound nucleus and the residual nucleus have lifetimes which are long compared with the transit time of nucleons over nuclear dimensions: *e.g.* there are well defined intermediate quantum states between the emissions of the first and the second neutron. A partial distribution of the excitation energy, on a small fraction of the nucleons, would favor simultaneous emission.

The variation of the nuclear temperature versus A (Fig. 1) has consequently to be interpreted in the concepts of the compound nucleus. The correction for the effect of the subsequent emission of a second neutron, if energetically

([13]) F. AJZENBERG and T. LAURITSEN: *Rev. Mod. Phys.*, **27**, 77 (1955).

possible, increases the temperature due to the emission of the first neutron by (20÷30)% for the heavier nuclei, increasing still more the deviations from the predicted $A^{-\frac{1}{2}}$ behavior. The only hypothesis involved in this prediction which could have been violated is that of equal reduced widths for all levels. There is some evidence for a corrective transition factor, which favors certain transitions and forbids others. The importance of this factor would increase with increasing mass number. This suggestion is supported by the form of spectra observed in inelastic scattering of protons ([10]). LANE and WILKINSON ([14]) have interpreted this « selection rule » by the concept of fractional parentage. The energy spectrum of inelastically scattered neutrons would consequently not provide a direct measure of the level density of the residual nucleus.

* * *

We would like to express our gratitude to Professor FRANCIS PERRIN for his hospitality and for his continued encouragement.

We wish to acknowledge fellowships of the « Stifterverband für die Deutsche Wissenschaft » (E.R.) and of the « Commissariat à l'Energie Atomique » (K.W.).

([14]) LANE and WILKINSON: *Phys. Rev.*, **97**, 1199 (1955).

RIASSUNTO (*)

Si sono misurati gli spettri dei neutroni emessi da ^{9}Be, ^{55}Mn, Fe, ^{127}I e ^{181}Ta bombardati con neutroni di 14 MeV servendosi di tecniche basate sul tempo di volo. Si separano gli spettri continui dei primi dai gruppi di bassa energia dovuti ai neutroni incidenti. Nei nuclei di peso medio e pesanti è predominante l'emissione successiva. Non si può decidere sull'esistenza di un possibile contributo da parte di un'emissione simultanea dai nuclei leggeri. Si usano i risultati per interpretare i dati dello scattering anelastico derivante dall'interazione coi neutroni di 14 MeV.

(*) *Traduzione a cura della Redazione.*

2500

IL NUOVO CIMENTO Vol. IX, N. 4 16 Agosto 1958

A New Possible Theory of the μ-Meson.

I. Ulehla (*)

Joint Institute of Nuclear Research - Moscow

(ricevuto il 30 Aprile 1958)

Summary. — The paper presents a theory of the μ-meson as a particle with spin ½ described by anomalous equations differing from the Dirac equations. Calculation is carried out of the intrinsic magnetic moment of the μ-meson, the cross-section for Coulomb and Compton scattering, the self-energy and the electrodynamic correction to the magnetic moment of the μ-meson. An explanation is given of the similarity of the μ-meson and electron at low energies and their dissimilarity at very high energies in electromagnetic interaction. The difference in the masses of the electron and μ-meson is determined by means of the same electromagnetic cut-off for both particles.

Introduction.

It is known from experimental material that for electromagnetic interaction in the non-relativistic region the μ-meson negligibly differs from the electron. For example, its magnetic moment, measured by Lederman [1], is

$$m_\mu = 1.0024 \pm 0.0008 ,$$

while the magnetic moment of the electron has the value

$$m_e = 1.001167 \pm 0.000005 .$$

(*) Now: Institute of Nuclear Physics, Academy of Sciences, Prague.

(1) L. M. Lederman: *Proc. of the Internat. Conf. on Mesons and Recently Discovered Particles, Padua-Venice* (1957).

2501

Measurements of the cross-sections for μ-meson scattering in the relativistic region ([2]) and other such measurements point to the fact that at high energies the μ-meson does not behave like an electron. If these measurements are correct, the difference in the behaviour of the μ-meson and the electron in the relativistic region will have to be clarified.

Up to now the relatively large difference in the masses of the μ-meson and the electron have not been satisfactorily explained. As long as it was not definitely known that the meson has spin $\frac{1}{2}$ it was thought that this difference could be explained by means of the μ-meson as a particle with spin $\frac{3}{2}$ ([3]).

As will be seen, the effects mentioned can be explained by describing the μ-meson by anomalous equations which were found in paper ([4]). The existence of such equations for particles with spin $\frac{1}{2}$ seems at first debatable if we remember the proofs of WILD ([5]) and GEL'FAND and YAGLOM ([6]). These proofs are not however general, as is shown in paper ([4]).

Of all permissible anomalous equations we chose the simplest because it is the nearest to the Dirac equations from the structural point of view. These anomalous equations are characterised by the fact that they contain one free parameter called the parameter of anomality g. They are complicated and the calculations carried out were therefore not simple. In order to avoid mathematical difficulties we confined ourselves to the lowest approximations of the perturbation theory.

When working with anomalous equations the general method elaborated in quantum electrodynamics can be used without change except that the Dirac matrices γ_μ must be replaced by new matrices and the changes incurred by this substitution taken into consideration.

We shall first deal with the equations for a free μ-meson and will then show that the anomalous equations are compatible with «switching-on» of the electromagnetic field. We shall investigate the electromagnetic interaction of μ-mesons in detail and in conclusion will briefly mention other types of interaction.

1. – Free μ-meson.

The motion of a free μ-meson is described by the equation

$$(\beta^\mu \partial_\mu - i\varkappa)\varphi = 0\,, \tag{1}$$

([2]) J. LLOYD, A. W. WOLDENDALE: *Proc. Phys. Soc.*, A **68**, 1045 (1955).
([3]) J. MATHEWS: *Phys. Rev.*, **102**, 270 (1956).
([4]) I. ULEHLA: *Žu. Éksper. Teor. Fiz.*, **33**, 472 (1957).
([5]) E. WILD: *Proc. Roy. Soc.*, A **191**, 253 (1947).
([6]) M. GEL'FAND and M. YAGLOM: *Žu. Éksper. Teor. Fiz.*, **18**, 703 (1948).

2502

where the wave function φ has twenty components. The matrices β_μ are twenty-row irreducible matrices which satisfy the relations

$$\sum^P (\beta_\mu \beta_\nu \beta_\sigma \beta_\varrho - g_{\mu\nu}\beta_\sigma \beta_\varrho) = 0 , \tag{2}$$

where $\sum^P$ denotes summation over all permutations of the indices. The relations (2) are not the only ones satisfied by these matrices. There also exist certain relations of the fourth order such as

$$\beta_0\beta_1\beta_2\beta_0 + \beta_0\beta_2\beta_1\beta_0 = 0 ,$$

which are an analogue of the equations

$$\beta_0\beta_1\beta_2 = 0 ,$$

valid in the Duffin-Kemmer algebra for five-row representation, and which point to the fact that we are dealing with a special representation of some more general algebra. Relations of fifth and higher order in β_μ, not following from (2), also hold for the matrices β_μ. We shall deal with the algebra of the matrices β_μ in the appendix. The matrices β_μ contain one free parameter — the parameter of anomality g — whose value lies in the intervals $(-\infty, 0)$ and $(0, \frac{1}{3})$. For $g = 0$ wave equation (1) becomes the Dirac equation.

If we apply the operator $\beta^\nu \partial_\nu$ three times to Eq. (1) we obtain the Schrödinger-Gordon equation

$$(\Box + \varkappa^2)\varphi = 0 ,$$

from which it follows that the particle has a single mass $\varkappa$.

Since there exists a matrix $\Lambda = \Lambda^*$ satisfying the condition

$$\Lambda\beta_\mu = \beta_\mu^* \Lambda ,$$

we can derive wave equation (1) from the Lagrangian

$$L = i(\bar{\varphi}\beta^\mu \partial_\mu \varphi - i\varkappa\bar{\varphi}\varphi) , \tag{3}$$

where $\bar{\varphi} = \varphi^*\Lambda$. From this function we can derive the general momentum-energy tensor which is symmetrical and Hermitian

$$T_{\mu\nu} = i\,\bar{\varphi}\beta_\nu \partial_\mu \varphi + \frac{i}{2}\,\partial^\sigma\{\bar{\varphi}\,[\beta_\sigma I_{\nu\mu} + \beta_\nu I_{\mu\sigma} + \beta_\mu I_{\nu\sigma}]\varphi\} , \tag{4}$$

where $I_{\mu\nu}$ are generators of infinitesimally small rotations. We can also derive

from (3) the current density

$$j_\mu = -e\overline{\varphi}\beta_\mu\varphi\,. \tag{5}$$

We shall now show that wave equations (1) contain 16 subsidiary conditions by which the superfluous components are eliminated and that equations (1) describe particles with spin $\frac{1}{2}$. The subsidiary conditions can be derived the quickest in the spin-tensor notation of wave equations (1), in which these equations have the form

$$(2\partial^\mu + \gamma^\nu\gamma^\mu\partial_\nu)(r_1\chi^{(1)} + r_2\chi^{(2)}) = i\varkappa B^\mu\,, \tag{6a}$$

$$\tfrac{1}{2}s_1\partial_\mu B^\mu + k_1\gamma^\mu\partial_\mu\chi^{(1)} = i\varkappa\chi^{(1)}\,, \tag{6b}$$

$$\tfrac{1}{2}s_2\partial_\mu B^\mu + k_2\gamma^\mu\partial_\mu\chi^{(2)} = i\varkappa\chi^{(2)}\,, \tag{6c}$$

where

$$r_1s_1 = \frac{2}{3}k_1^2\frac{k_2}{k_1-k_2}\,, \qquad r_2s_2 = \frac{2}{3}k_2^2\frac{k_1}{k_2-k_1}\,,$$

$$s_1 = \varepsilon_1 r_1\,, \quad s_2 = \varepsilon_2 r_2\,, \quad k_1+k_2 = \lambda\,, \quad k_1 > k_2\,, \quad k_1 > 0\,.$$

$\lambda = 1$, $\varepsilon_1 = -\varepsilon_2 = 1$ for $g = \frac{4}{3}k_1k_2 > 0$, and $\lambda = -1$, $\varepsilon_1 = \varepsilon_2 = -1$ for $g < 0$. The twenty components of the wave function φ are formed by two Dirac spinors $\chi^{(1)}$ and $\chi^{(2)}$ and 12 independent components of the spin-vector B^μ, for which the following condition is valid

$$\gamma^\mu B_\mu = 0\,. \tag{7}$$

Condition (7) also follows directly from Eq. (6a) if it is multiplied by the operator γ_μ.

From Eqs. (6b) and (6c) we easily obtain the equation

$$\gamma^\mu\partial_\mu(r_1\chi^{(1)} + r_2\chi^{(2)}) = i\varkappa\left(\frac{r_1}{k_1}\,\chi^{(1)} + \frac{r_2}{k_2}\,\chi^{(2)}\right), \tag{8}$$

by means of which (6a) can be rearranged to

$$4\partial^\mu(r_1\chi^{(1)} + r_2\chi^{(2)}) - i\varkappa\gamma^\mu\left(\frac{r_1}{k_1}\,\chi^{(1)} + \frac{r_2}{k_2}\,\chi^{(2)}\right) = i\varkappa B^\mu\,. \tag{9a}$$

In Eqs. (9a) we have 12 subsidiary conditions (for $\mu = 1, 2, 3$) not containing time derivatives.

2504

The four remaining subsidiary conditions are obtained by applying the operator ∂_μ to Eq. (6*a*) and the operator $\gamma^\nu \partial_\nu$ to Eq. (8). The second derivatives are eliminated by combining these two equations. By means of Eqs. (6*b*, *c*) we eliminate the expressions $\gamma^\mu \partial_\mu \chi^{(1)}$ and $\gamma^\mu \partial_\mu \chi^{(2)}$ from the resultant equation and finally obtain

$$3i\varkappa \left(\frac{r_1}{k_1^2} \chi^{(1)} + \frac{r_2}{k_2^2} \chi^{(2)} \right) - \left(\frac{3}{2} \frac{r_1 s_1}{k_1^2} + \frac{3}{2} \frac{r_2 s_2}{k_2^2} + 1 \right) \partial_\mu B^\mu = 0 .$$

Since the expression in the brackets at $\partial_\mu B^\mu$ is zero, the last four subsidiary conditions read

$$\frac{r_1}{k_1^2} \chi^{(1)} + \frac{r_2}{k_2^2} \chi^{(2)} = 0 . \tag{9b}$$

If we consider the spinor $\chi^{(1)}$ independent, we obtain for it from Eq. (8) by means of (9*b*)

$$\left(\gamma^\mu \partial_\mu - i \frac{\varkappa}{\lambda} \right) \chi^{(1)} = 0 , \tag{10}$$

which is the Dirac equation. If we know its solution — *i.e.* the spinor $\chi^{(1)}$ — we determine the spinor $\chi^{(2)}$ from conditions (9*b*) and the spinvector B_μ from conditions (9*a*) and from Eq. (7).

That we obtained the Dirac equation for the spinor $\chi^{(1)}$ was only to be expected. This result shows that we are actually dealing with a particle having spin $\frac{1}{2}$. It cannot be inferred from this however that the μ-meson described by anomalous equations is identical with an electron, for the energy-momentum tensor (4) and current density (5) cannot be reduced by means of the subsidiary conditions to the energy-momentum tensor or current density for an electron.

2. – Electromagnetic interaction of the μ–meson.

If the problem can be formulated so that the wave equations for the μ-meson can be derived from the Lagrangian, then the « switching-on » of the electromagnetic field leads to no difficulties. The interaction term can be defined in the « classical » way as

$$L_{\text{int}} = j_\mu A^\mu , \tag{11}$$

i.e. the electromagnetic interaction of the μ-meson can be assumed normal. Although the algebra of matrices β_μ permits the construction of a number

of different and independent vectors such as

$$\beta_\mu, \quad \beta^\nu\beta_\mu\beta^\mu, \quad \beta_\mu\beta_\nu\beta^\mu, \quad \beta^\mu\beta_\mu\beta_\nu, \ldots,$$

we choose for the interaction term only that vector the divergence of which is zero — the vector of the current density (5).

For the case of electromagnetic interaction the number of subsidiary conditions does not change but their form differs from (9). After « switching-on » the electromagnetic field we write $D_\mu = \partial_\mu - ieA_\mu$ instead of ∂_μ in Eqs. (1) and (6). Proceeding in the same way as when deriving the subsidiary conditions in part I, we derive the following equations instead of Eqs. (9*a*)

$$4D^\mu(r_1\chi^{(1)} + r_2\chi^{(2)}) - i\varkappa\gamma^\mu\left(\frac{r_1}{k_1}\chi^{(1)} + \frac{r_2}{k_2}\chi^{(2)}\right) = i\varkappa B^\mu, \tag{12a}$$

and instead of (9*b*)

$$\varkappa^2\left(\frac{r_1}{k_1}k_2\chi^{(1)} + \frac{r_2}{k_2}k_1\chi^{(2)}\right) = iegI^{\mu\nu}\left(\frac{1}{2}\right)F_{\mu\nu}(r_1\chi^{(1)} + r_2\chi^{(2)}), \tag{12b}$$

where $I^{\mu\nu}(\frac{1}{2}) = \frac{1}{4}(\gamma^\mu\gamma^\nu - \gamma^\nu\gamma^\mu)$. When deriving Eqs. (12*b*) we used the relations

$$[D_\mu D_\nu] = -ieF_{\mu\nu}, \qquad \gamma^\mu\gamma^\nu D_\mu D_\nu = -ieI^{\mu\nu}(\tfrac{1}{2})F_{\mu\nu} + D^\mu D_\mu.$$

Equations (12) again contain 16 subsidiary conditions and always have a solution; the introduction of electromagnetic interaction does not therefore lead to any incompatibility.

The equations for the μ-meson have a certain relation to the Pauli equations for a particle with anomalous electromagnetic interaction. If we introduce a new spinor ψ defined by

$$\psi = r_1\chi^{(1)} + r_2\chi^{(2)},$$

then by means of conditions (12*b*) we can easily derive for it

$$\gamma^\mu\partial_\mu\psi + \frac{e}{\varkappa\lambda^{-1}}gI^{\mu\nu}\left(\frac{1}{2}\right)F_{\mu\nu}\psi = i\frac{\varkappa}{\lambda}\psi, \tag{13}$$

which is known as the Pauli equation. At first glance it would seem that the remaining components of the wave function φ can be forgotten and only the Pauli equation used. However the transition from equations for the μ-meson to Eq. (13) in the sense implied does not mean only a transition from one field to another, as we have already mentioned, but also a transition from a

particle with normal interaction to a particle with anomalous interaction. A particle described by Eq. (1) (with $\partial_\mu \to D_\mu$) cannot therefore be considered equivalent to a particle described by Eq. (13). As will be seen below, the results of the calculations differ in both cases.

2·1. *Intrinsic magnetic moment of the μ-meson.* – In a non-relativistic approximation the intrinsic magnetic moment of an anomalous particle — of the μ-meson — is easily determined. Its value, measured in Bohr magnetons, is

$$m = 1 - 2g , \tag{14}$$

and it is seen to be anomalous. If $g > 0$ then

$$\tfrac{1}{3} < m_\mu < 1 ,$$

while for $g < 0$

$$1 < m_\mu < \infty .$$

The magnetic moment of the μ-meson was measured very accurately by LEDERMAN [1], who obtained the value

$$m_\mu = 1.002\,4 \pm 0.000\,8 .$$

This can serve as a basis for estimating the magnitude of the parameter of anomality g. The parameter of anomality cannot be too large since it can hardly be expected that the electrodynamic correction to the value of the magnetic moment of a μ-meson would be much bigger than corrections in the electron theory. Thus g will have a value of the order

$$|g| \lesssim 10^{-3} . \tag{15}$$

2·2. *Coulomb scattering.* – When calculating Coulomb scattering of a μ-meson on a fixed centre we shall confine ourselves to the first approximation of the perturbation theory. The vertex of Feynman's diagram is represented by the operator $e\beta_\mu$ and the amplitude of the transition is therefore given simply by the expression

$$\bar{u}_2 \beta_0 u_1 .$$

The cross-section is determined, as is known, from the expression

$$\mathrm{d}\sigma = \left(\frac{e^2 Z}{\varkappa}\right)^2 \frac{\varkappa^2 E^2}{p^4 (1 - \cos\vartheta)^2} \frac{1}{2} \operatorname{Sp} P_2^+ \beta_0 P_1^+ \beta_0 \mathrm{d}\omega , \tag{16}$$

where $E=\sqrt{p^2+\varkappa^2}$ and $p_{1,2}^{+}$ are projection operators which, with respect to relations (2), have the form

$$P=\frac{\varkappa}{2p_0}\frac{(\beta p)^2}{\varkappa^2}\left[1+\frac{(\beta p)}{\varkappa}\right]; \qquad P^{+}=P_{p_0=E}.$$

The scalar product $\beta^{\mu}p_{\mu}$ is denoted by (βp).

If we calculate the trace in (16) we obtain the cross-section for the scattering of the μ-meson

$$(17)\quad \mathrm{d}\sigma=\pi\left(\frac{e^2Z}{\varkappa}\right)^2\frac{\varkappa^2}{p^2}\frac{\sin\vartheta\,\mathrm{d}\vartheta}{(1-\cos\vartheta)^2}\left[\frac{2\varkappa^2}{p^2}+1+\cos\vartheta+4g\left(1+g\frac{p^2}{\varkappa^2}\right)(1-\cos\vartheta)\right].$$

If we put $g=0$ in this expression we obtain the cross-section for scattering of the electron. The $\mathrm{d}\sigma$ obtained differs from the cross-section for Coulomb scattering of a particle described by the Pauli equation (13) as is seen in paper [7].

In the non-relativistic approximation $\mathrm{d}\sigma$ is the same for the electron and μ-meson since g is small. In the extreme relativistic case, however, $\mathrm{d}\sigma$ for a μ-meson is independent of its energy

$$(18)\qquad \mathrm{d}\sigma_{\mathrm{rel}}=4\pi\left(\frac{e^2Z}{\varkappa}\right)^2 g^2\frac{\sin\vartheta\,\mathrm{d}\vartheta}{1-\cos\vartheta},$$

and its angular dependence differs from the angular dependence for an electron. Both deviations obtained agree with those discovered by J. Lloyd and A. W. Wolfendale [2] when investigating the scattering of high energy μ-mesons in cosmic radiation. The region of energies $\gtrsim 10^6$ MeV, in which the deviations were observed, is also in agreement with expression (17) if we put $|g|\lesssim 10^{-3}$.

2·3. *Compton scattering.* – In calculating the scattering of a γ quantum on μ-mesons we again confine ourselves to the first approximation for the sake of greater mathematical simplicity. For Compton scattering the transition amplitude will have the known form

$$M=\bar{u}_2(\beta e_2)[(\beta,\, p_1+k_1)-\varkappa]^{-1}(\beta e_1)u_1+\bar{u}_2(\beta e_1)[(\beta,\, p_1-k_2)-\varkappa]^{-1}(\beta e_2)u_1,$$

where p_{μ} is the momentum of the μ-meson, k_{μ} the momentum of the γ quantum and e_{μ} the polarization.

The inverse operator must be known in order to calculate the traces. This

[7] H. C. Corben and J. Schwinger: *Phys. Rev.*, **58**, 953 (1940).

is easily found if we start from Eqs. (2)

$$[(\beta q)-\varkappa]^{-1}=\frac{1}{\varkappa^2}\frac{[\varkappa^2-(qq)+(\beta q)^2][\varkappa+(\beta q)]}{(qq)-\varkappa^2}.$$

We determined the exact values of the cross-sections $d\sigma_{\parallel}$ and $d\sigma_{\perp}$ for light polarized after scattering parallel and perpendicular to the plane of polarization of the incident light:

$$(19)\quad \begin{cases} d\sigma_{\parallel} = \frac{1}{4}\frac{e^4}{\varkappa^2}\frac{k_2^2}{k_1^2}\left\{2(1+\cos^2\vartheta)+[1-8g^2(1-g)^2]\eta+16g^2(1-g)^2\frac{k_1-k_2}{\varkappa}\right\}d\omega_1, \\ d\sigma_{-} = \frac{1}{4}\frac{e^4}{\varkappa^2}\frac{k_2^2}{k_1^2}\left\{(1-2g)(1-6g)\eta+16g^2(1-2g)\frac{k_1-k_2}{\varkappa}+16g^4\frac{k_1k_2}{\varkappa^2}\right\}d\omega, \end{cases}$$

where $\eta=k_1/k_2+k_2/k_1-2$.

In the general case the cross-section is given by the sum

$$d\sigma = d\sigma_{\parallel}+d\sigma_{\perp}.$$

For $g=0$ both cross-sections become the corresponding expressions known from the theory of the electron and for $g\neq 0$ differ from the cross-sections for a particle described by the Pauli equation (13), as can be seen from paper [8].

By integrating expressions (19) we obtain the total cross-section. Here, however, we only give their values in the non-relativistic and extreme relativistic approximations. For an energy of the incident quantum $k_1\ll\varkappa$ up to to the linear term in k_1

$$(20)\qquad \sigma_{\text{non-rel.}}=\frac{8\pi}{3}\frac{e^4}{\varkappa^2}\left(1-\frac{2k_1}{\varkappa}\right),$$

from which it follows that $\sigma_{\text{non-rel.}}$ for an electron and μ-meson are identical. For $k_1\gg\varkappa$ however

$$(21)\qquad \sigma_{\text{rel.}}=4\pi g^4\frac{e^4}{\varkappa^2}\frac{k_1}{\varkappa}.$$

In this case the cross-section increases linearly with the energy. The origin of the linear growth lies very high ($\gg 10^6$ MeV) due to the factor g^4 in expression (21).

---

[8] S. B. Batdorf and R. Thomas: *Phys. Rev.*, **59**, 621 (1941).

2·4. *Self-energy of the μ-meson.* – The self-energy of the μ-meson is determined by starting from the integral

$$\frac{e^2}{4\pi^3 i}\,\bar{u}\left\{\int \beta_\mu[(\beta, p-k)-\varkappa]^{-1}(kk)^{-1}\beta^\mu\,\mathrm{d}^4k\right\}u\,.$$

Calculation is carried out by the method of Pauli and Willars (9), by which we use one auxiliary mass $M=\lambda\varkappa$ only.

We get

$$E^{(2)}_{\mathrm{self}}=\frac{e^2\varkappa}{2\pi}\left\{\frac{3}{2}\lambda^2\left(2g-\frac{7}{4}g^2\right)+\right.$$
$$\left.+(3-6g+5g^2)\ln\lambda-\frac{1}{2}\left(1-2g+\frac{7}{4}g^2\right)\right\}\bar{u}u\ (*)\,. \tag{22}$$

For $g=0$ we have

$$E^{(2)}_{\mathrm{self}}=\frac{e^2\varkappa}{2\pi}\left(3\ln\lambda-\frac{1}{2}\right),$$

which is an expression well known from the theory of the electron.

It is seen from expression (22) that the self-energy of the μ-meson is quadratically divergent. If we consider the parameter λ as the parameter of cut-off we can explain the difference between the mass of the μ-meson and that of the electron. If we choose the value $\lambda\sim 8\cdot 10^3$ for $|g|=10^{-3}$ and the value of the parameter $\lambda\sim 2.5\cdot 10^4$ for $|g|=10^{-4}$ we get the ratio of the masses of the μ-meson and electron

$$\frac{\varkappa_\mu}{\varkappa_e}\sim 210\,.$$

2·5. *Electromagnetic correction to the magnetic moment.* – In calculating corrections to the value of the magnetic moment we limit ourselves for mathematical reasons to the correction of the second order. This means that we must determine the correction to the vertex part of the Feynman diagram. As is known, this is given by the integral

$$B_\nu=\frac{e^2}{4\pi^3 i}\int[(p-q, p-q)]^{-1}\beta_\mu[(\beta, q+k)-\varkappa]^{-1}\beta_\nu[(\beta q)-\varkappa]^{-1}\beta^\mu\,\mathrm{d}^4q\,, \tag{23}$$

(*) A numerical error is contained in the expression for the self-energy in the pre-print called *Electromagnetic Interaction of Anomalous Particles with Spin* ½.

(9) W. Pauli and F. Willars: *Rev. Mod. Phys.*, **21**, 434 (1949).

where the meaning of the individual quantities is seen from the diagram

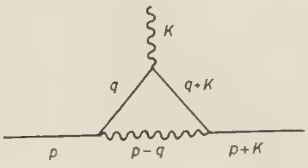

The calculation of integral (23) is carried out by the same method as was used in calculating the self-energy. The correction (23), in the same way as the self-energy, contains logarithmic and quadratic divergence but does not contain terms with divergences of higher order. In the non-relativistic approximation, which we obtain by multiplying expression (23) from the right and left by the projection operator

$$\tfrac{1}{2}\beta_0^2(1+\beta_0)\,,$$

all terms with quadratic divergence vanish for $\gamma = 1, 2, 3$. In this approximation, which is the only interesting one, we can therefore limit ourselves to terms of the zero-th and first order in g and first order in k.

If we then determine the value of the magnetic moment from the generalized interaction term

$$\bar{\varphi}(\beta_\mu + B_\mu)A^\mu\varphi\,,$$

we obtain, after subtracting expressions with infra-red catastrophe,

$$m_\mu = 1 - 2g + \frac{\alpha}{2\pi}\,[1 + g(a + b\ln\lambda)]\,,$$

where a and b are constants ~ 1; thus the magnetic moment of the μ-meson will be

$$m_\mu = 1 - 2g + \frac{\alpha}{2\pi}\,,$$

if we consider the values of λ from Sect. 2·4. The result we obtain confirms the correctness of the estimate (15) of the magnitude of the parameter of anomality g.

3. – Conclusion.

This new interpretation of the properties of the μ-meson is based on one assumption. We assume the μ-meson as a particle described by the simplest anomalous equations, which contain one parameter of anomality g. The small value of this parameter explains why the μ-meson, interacting with the electromagnetic field, does not differ from the electron at normal energies and shows that differences between the two particles can only be expected at high energies ($\sim 10^6$ MeV). It also permits a suitable explanation of the difference in mass of the μ-meson and the electron.

So far we have not dealt with questions of other types of meson interactions than electromagnetic interaction. This problem is complicated by the fact that several linearly independent Lagrangians can be constructed for the given type of interaction. For example, for scalar interaction we do not have only one scalar operator I, as in the Dirac algebra, but also other linearly independent scalars

$$(\beta\beta), \qquad (\beta\beta)^2, \qquad \beta_\mu\beta_\nu\beta^\mu\beta^\nu, \ldots .$$

The same is the case with vector interaction, tensor interaction etc. In general not all these operators are permissible, since some can lead to disruption in the number of subsidiary conditions and must therefore be eliminated. But even then we still have more coupling constants than in the Dirac theory.

Experimental data on μ-mesons are not yet so extensive that they could not be explained by a suitable choice of constants. We did not therefore think it of any great use to deal with other types of interaction except the decay $\pi \to \mu + \nu$.

If we describe the μ-meson by anomalous equations we can regard the electron as a limiting case of the μ-meson ($g \to 0$). As can be seen from expressions (17) and (19) the transition probability for an arbitrary process with a μ-meson will always be a polynomial in g.

$$W_\mu = a_0 + a_1 g + a_2 g^2 + \ldots + a_n g^n , \tag{24}$$

where the coefficients a_i depend on the momentum. If we put $g = 0$ in this expression we get the probability of transition for the electron

$$W_e = a_0 .$$

If we now consider the $\pi \to \mu + \nu$ decay as a direct process and choose the Lagrangian for it so that the coefficient a_0 in expression (24) is zero — this

can be done for arbitrary coupling for example by introducing the operator $(\beta\beta)$-4 into the interaction term — we get a finite probability W_μ for the $\pi \to \mu + \nu$ decay and the probability $W_e = 0$ for the decay $\pi \to e + \nu$. For the processes of the type $\mu^- + p \to n + \nu$ we must choose such Lagrangian (with S, T, V coupling only), which leads to non-zero coefficient a_0 in (24).

* * *

In conclusion the author would like to thank N. N. Bogoljubov and A. Salam for encouraging him in this work which is full of mathematical difficulties.

Appendix

We give here the algebraic relations necessary for the calculations in this paper. An important factor which greatly facilitates calculation of the traces is the possibility of writing the matrices β_μ in the form of a direct product

$$\beta_\mu = \gamma_\mu \times \alpha_\mu , \qquad \beta^\mu = \gamma^\mu \times \alpha_\mu . \qquad \text{(no summation).} \tag{A.1}$$

The matrices γ_μ are the well-known Dirac matrices, and the matrices α_μ form a certain algebra $\mathfrak{A}$ with which we shall deal in detail later.

If the matrix α_0 is known the matrices α_i $(i = 1, 2, 3)$ can be derived successively by means of the unitary transformations

$$\alpha_1 = (1 - w)\alpha_0(1 - w) ,$$

$$\alpha_2 = (1 - u)\alpha_1(1 - u) ,$$

$$\alpha_3 = (1 - v)\alpha_2(1 - v) .$$

The elements u, v, w are Hermitian operators satisfying the relations

$$\begin{cases} u^2 = 2u , \quad v^2 = 2v , \quad w = 2w , \\ uvu = u , \quad uwu = u , \quad vuv = v , \quad wuw = w , \\ vw = wv = 0 . \end{cases} \tag{A.2a}$$

The algebra $\mathfrak{A}$, which is formed by the elements α_0, u, v, w is determined on the one hand by the relations (A.2a), and on the other by the minimum condition for α_0

$$\alpha_0^3 = \lambda \alpha_0^2 , \qquad \text{where} \quad |\lambda| = 1 , \tag{A.2b}$$

and the relations between the element α_0 and the elements u, v, w:

$$\text{(A.2}c\text{)} \qquad \begin{cases} \alpha_0 u = u\alpha_0 = \alpha_0 v = v\alpha_0 = 0\,, \\ w\alpha_0 w = 0\,, \\ w\alpha_0^2 w = gw\,, \\ \alpha_0^2 w\alpha_0 + \alpha_0 w\alpha_0^2 = \lambda\alpha_0 w\alpha_0 + g\alpha_0\,. \end{cases}$$

From relations (A.2) it follows that the algebra $\mathfrak{A}$ has 26 linearly independent elements of the basis and two elements of the centre. It thus has two non-equivalent representations, one one-row, which is trivial, and one five-row:

$$\alpha_0 = \begin{vmatrix} . & . & . & . & . \\ . & . & . & r_1 & r_2 \\ . & . & . & -\sqrt{\tfrac{1}{2}}r_1 & -\sqrt{\tfrac{1}{2}}r_2 \\ . & s_1 & -\sqrt{\tfrac{1}{2}}s_1 & k_1 & . \\ . & s_2 & -\sqrt{\tfrac{1}{2}}s_2 & . & k_2 \end{vmatrix} \qquad u = \begin{vmatrix} \tfrac{1}{2} & \tfrac{1}{2} & \sqrt{\tfrac{1}{2}} & . & . \\ \tfrac{1}{2} & \tfrac{1}{2} & \sqrt{\tfrac{1}{2}} & . & . \\ \sqrt{\tfrac{1}{2}} & \sqrt{\tfrac{1}{2}} & 1 & . & . \\ . & . & . & . & . \\ . & . & . & . & . \end{vmatrix}$$

$$v = \operatorname{diag}|2, 0, 0, 0, 0|, \qquad w = \operatorname{diag}|0, 2, 0, 0, 0|,$$

where

$$r_1 s_1 = \frac{2}{3} k_1^2 \frac{k_2}{k_1 - k_2}\,, \qquad r_2 s_2 = \frac{2}{3} k_2^2 \frac{k_1}{k_2 - k_1}\,,$$

$$k_1 + k_2 = \lambda\,, \quad r_1 = \varepsilon_1 s_1\,, \quad r_2 = \varepsilon_2 s_2\,, \quad g = \tfrac{4}{3} k_1 k_2\,, \qquad k_1 > 0\,,\ k_1 > k_2\,.$$

$\varepsilon_1 = -\varepsilon_2 = 1$ for $\lambda = 1$ and $\varepsilon_1 = \varepsilon_2 = -1$ for $\lambda = -1$.

Of all the traces of linearly independent elements of the basis of the algebra $\mathfrak{A}$ the only non-zero ones are

$$\operatorname{Sp}\alpha_0 = \lambda\,, \qquad \operatorname{Sp} u = \operatorname{Sp} v = \operatorname{Sp} w = 2\,,$$

$$\operatorname{Sp}\alpha_0^2 = \operatorname{Sp} uv = \operatorname{Sp} uw = 1\,, \qquad \operatorname{Sp}\alpha_0^2 w = g\,.$$

The generators of the infinitesimal rotations are given by the expressions

$$I_{01} = \gamma_0\gamma_1 \times (\tfrac{1}{2} - w)\,, \qquad I_{12} = \gamma_1\gamma_2 \times (\tfrac{1}{2} - u)\,, \qquad I_{23} = \gamma_2\gamma_3 \times (\tfrac{1}{2} - v)\,.$$

The remaining $I_{\mu\nu}$ are determined from the above by means of the known relations for these operators. By means of a direct product we can also express

the matrix of spatial inversion as

$$J = \gamma_0 \times I ,$$

and the matrix, which we need for constructing $\overline{\varphi}$:

$$\Lambda = \gamma_0 \times \mathrm{diag}\,|1, 1, 1, \varepsilon_1, \varepsilon_2| .$$

RIASSUNTO (*)

Il lavoro presenta una teoria del mesone μ come particella di spin $\frac{1}{2}$ descritta da equazioni anomale differenti da quelle di Dirac. Si esegue il calcolo del momento magnetico intrinseco del mesone μ, della sezione d'urto per lo scattering coulombiano e Compton, della self-energia e della correzione elettrodinamica del momento magnetico del mesone μ. Si dà una spiegazione della similarità del mesone μ con l'elettrone alle basse energie e della loro dissimilarità alle altissime energie nell'interazione elettromagnetica. Si determina la differenza fra le masse dell'elettrone e del mesone μ per mezzo di un cut-off elettromagnetico uguale per le due particelle.

(*) *Traduzione a cura della Redazione.*

On the Determination of the Space-Group by the Statistical Method.

M. S. Farag

National Research Centre - Dokki, Cairo

(ricevuto il 6 Maggio 1958)

Summary. — Following A. J. C. Wilson and his collaborators, it is possible, by a study of the statistical distribution of X-ray intensities of Bragg reflections, to differentiate between centro- and non-centro-symmetric structures. This method was applied to a centred and a non-centred projection in the crystal structure of 1.3.5-triphenylbenzene. The results in both zones showed big discrepancies which could lead to an incorrect conclusion. These discrepancies are discussed in terms of the established structure which is of a layer type. The molecules are projected edgewise in the centred projection, and the electron density distribution appears in the other one, with some approximations, as if centred.

1. – Introduction.

One of the important early steps in X-ray crystal structure analysis is the determination of the space group symbol. From the systematically absent Bragg reflections, it is possible to deduce first the lattice type and then any screw axes or glide planes with their appropriate translations. The parts of the space group symbol which are then left to be found by methods other than X-rays are: rotation axes and mirror planes (1); the apparent presence of which in X-ray diffraction photographs is due to Friedel's law.

(1) N. F. M. Henry and K. Lonsdale: *International Tables for X-ray Crystallography*, Vol. **1** (1952).

2. – The statistical method.

Methods usually employed to find the complete space group symbol include studies of: crystal morphology, etch figures, optical activity, pyro- and piezo-electricity. However, a new method using X-ray data has been recently worked out by WILSON (2) and developed further by HOWELLS, PHILLIPS and ROGERS (3). According to these authors, if systematic absences and reflections having $\sin\theta \leqslant \lambda/a$, (where a is the shortest axis in the unit cell) are ignored, then the ratio $\langle|F|\rangle^2/\langle I\rangle$ has the value 0.785 for a non-centro-symmetric and 0.637 for a centro-symmetric structure, where the brackets $\langle\ \rangle$ indicate the average value for a certain $\sin\theta$ group. Accordingly if each intensity is expressed as a fraction Z, ($Z = I/\langle I\rangle$ of the local average intensity) then the fractions $N(Z)$ of the reflections whose intensities are less than or equal to Z will be:

$N(Z) = 1 - \exp[-z]$ for non-centro-symmetric structures designated by (1),

and

$N(Z) = \mathrm{erf}\,(\frac{1}{2}z)^{\frac{1}{2}}$ » centro-symmetric structures designated by $(\bar{1})$,

where erf is the error function.

The assumptions underlying the validity of this theory are briefly:

(i) that there should be a large number of atoms all occupying general positions and such that none of them dominate the intensity distribution.

(ii) that a sufficiently large number of intensities should be used in calculating the averages.

3. – The case of 1.3.5-triphenylbenzene $(C_6H_3)(C_6H_5)_3$.

The statistical method has been successfully used in many cases (3), but the space group of 1.3.5-triphenylbenzene presents an interesting deviation from this method. The crystal was first examined by X-rays by LONSDALE and ORELKIN (4), who found the unit cell dimensions and space group. The latter could be then $Pna\,2_1$, or Pnam, but since the crystal showed a positive pyro-electric effect, *i.e.* the crystal is polar, it was then unequivocally settled as the non-centrosymmetric one *i.e.* $Pna\,2_1$. The crystal structure was fully

(2) A. J. C. WILSON: *Acta Cryst.*, **2**, 318 (1949).
(3) E. R. HOWELLS, D. C. PHILLIPS and D. ROGERS: *Acta Cryst.*, **3**, 210 (1950).
(4) K. LONSDALE and B. ORELKIN: *Proc. Roy. Soc.*, A **144**, 630 (1934).

elucidated by the author ([5]). The unit cell which is orthorhombic has the following dimensions:

$$a = 7.47 \pm 0.02 A^0, \quad b = 19.66 \pm 0.05 A^0, \quad c = 11.19 \pm 0.03 A^0,$$

with four molecules per unit cell. The c-projection is the only one with a centre of symmetry. The number of independent reflections observed and expected theoretically for each zone are given in the following table:

(hkl)	Number of reflections observed	Number of reflections expected
okl	114	155
hol	49	61
hko	130	195

The probability distribution of X-ray intensities was studied for the (okl) and (hko) reflections; the (hol) type were ignored on account of their limited number. The intensities used were corrected for the Lorentz and polarization factors. Overlapping sin θ groups were found useful.

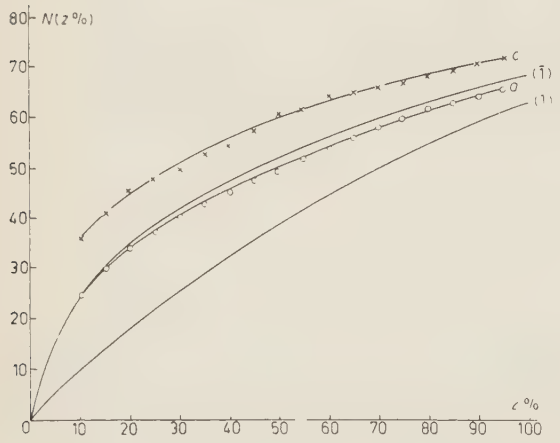

Fig. 1.

The experimental results for the 2 zones are shown in Fig. 1 together with the theoretical statistical distributions for centro- and non-centro-symmetric structures. Fig. 1 shows the following details:

1) The (hko) reflections: The intensity distribution for these reflections appears as a hyper-centro-symmetric one, *i.e.* as if the molecule had a centre of symmetry in a centro-symmetric projection. Such examples have been shown by Lipson and Woolfson ([6]) in the case of pyrene and 1:1:6:6 tetra-phenyl-hexapentaene. In the

([5]) M. S. Farag: *Acta Cryst.*, **7**, 117, 380 (1954).
([6]) H. Lipson and M. M. Woolfson: *Acta Cryst.*, **5**, 680 (1952).

present case the deviation may be due to the fact that the separate parts (phenyl groups) of the molecule are centro-symmetric, besides a violation of the first condition of the requirements necessary for the application of the theory. As has been shown by the author ([5]), the structure is of a layer type where the molecules are seen edgewise in the *c*-projection.

2) The (okl) reflections: The intensity distribution for these reflections shows that the *a*-projection is centro-symmetric rather than non-centro-symmetric; a conclusion which is simply incorrect. The discrepancy between the curves (a^-) and (1) in Fig. 1 may have the following explanation.

The *a*-projection, Fig. 2, has the two dimensional space group symbol cm 1, and the elements of symmetry are shown in the key diagram of the same figure. Although cm 1 is not a centro-symmetric space group yet the molecules are

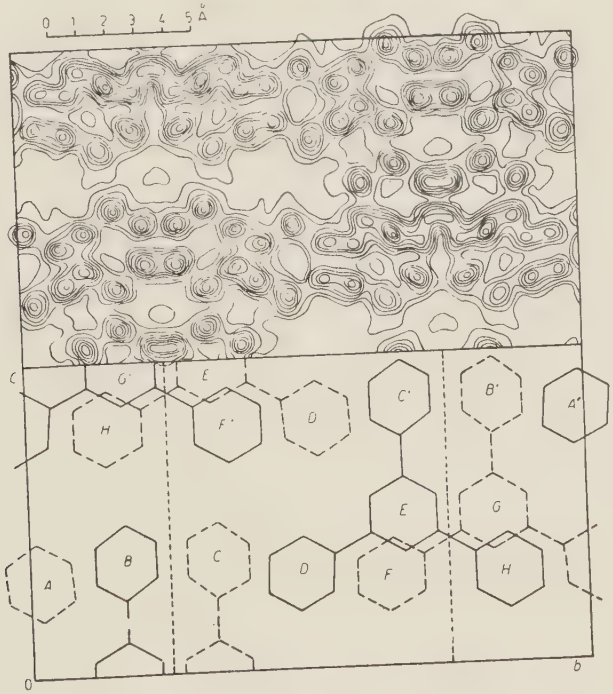

Fig. 2.

arranged in such a manner that, to a first approximation, the benzene rings A, B, C, ... etc. are apparently related to A', B', C', ... etc. by a centre of symmetry. This reason, of course, may be considered as a violation of the first condition for the requirements of the application of the theory, but unfortunately such an explanation could only be given at a late stage in the analysis of the structure.

4. – Conclusion.

From this example, and in the opinion of the author, a centre of symmetry may safely be detected by the statistical method if hyper-centro-symmetry is observed, otherwise physical tests are to be used. Such tests usually are powerful enough to place the crystal either in the hemihedral or in the holohedral class.

* * *

The author wishes to record his deepest thanks to Prof. K. Lonsdale, F.R.S., D.B.E. under whose supervision the determination of the crystal structure was carried out.

RIASSUNTO (*)

Secondo A. J. C. Wilson e coll. è possibile, per mezzo di uno studio della distribuzione statistica delle intensità dei raggi X delle riflessioni di Bragg, distinguere le strutture centro-simmetriche dalle non-centro-simmetriche. Questo metodo è stato applicato a una proiezione centrata e a una non centrata della struttura cristallina dell'1.3.5-trifenilbenzene. I risultati mostrarono nelle due zone gravi discrepanze che potrebbero portare a conclusioni errate. Si discutono tali discrepanze in termini della struttura accertata che è del tipo a strati. Le molecole si proiettano di taglio nella proiezione centrata e la distribuzione della densità elettronica appare nell'altra proiezione, con qualche approssimazione, come centrata.

(*) *Traduzione a cura della Redazione.*

Investigation of the Decay of Polonium-210.

Brat Pal Singh (*), H. S. Hans and P. S. Gill

Department of Physics, Muslim University - Aligarh (India)

(ricevuto l'8 Maggio 1958)

Summary. — Conversion coefficient of 800 keV γ-rays from the decay of Polonium-210 has been measured using scintillation method to be 0.039 ± 0.01. The value of conversion coefficient has also been obtained by the measurement of conversion electrons with an end window type G.M. counter. The absorption curve for electrons is given and its shape has been interpreted in the light of the results of Alphonse Lagasse and Jacqueline Doyeb (*Compt. Rend.*, **239**, (11), 670 (1954)). The value of conversion coefficient obtained in this way is 0.014 ± 0.005. The discrepancy between the two values has been explained as due to K and L shell ionization by α-particles. No coincidences were found between the different parts of γ-ray spectrum.

1. – Introduction.

Many workers (Grace *et al.* [1], Zajac *et al.* [2], Siegbahn and Slätis [3], etc.) have investigated the radiations from ^{210}Po. The following facts have been established:

1) Ground level of ^{210}Po decays predominantly through an α of 5.3 MeV to the ground state of ^{206}Pb.

2) A small fraction ($\sim 10^{-3}\,\%$) of the ground state of ^{210}Po decays through an α of 4.5 MeV to the excited level of ^{206}Pb followed by a γ-ray of 800 keV (Grace *et al.* [1], De Benedetti and Minton [4]).

3) A soft radiation of about 80 keV has also been observed.

(*) Research Scholar of Ministry of Education, Government of India.

(1) M. A. Grace *et al.*: *Proc. Phys. Soc.*, A **64**, 493 (1951).

(2) B. Zajac *et al.*: *Proc. Phys. Soc.*, **60**, 501 (1948).

(3) K. Siegbahn and H. Slätis: *Nature*, **159**, 471 (1947).

(4) S. De Benedetti and G. H. Minton: *Phys. Rev.*, **85**, 944 (1952).

2521

ZAJAC *et al.* [2] concluded by the critical absorption method that the soft radiation was of nuclear origin. GRACE *et al.* [1], on the other hand, considered the soft radiation to be X-rays of ^{206}Pb, by the same critical absorption method. These X-rays were interpreted by them as due to the conversion of 800 keV γ-rays. Conversion coefficient obtained from their measurements of X-rays and conversion electrons was found to be 6.7%. GRACE *et al.* [1] suggested that 800 keV γ-rays should be due to M_2 transition. DE BENEDETTI and MINTON [4] measured the angular distribution between 800 keV γ-rays and 4.5 MeV α-rays from which they concluded that 800 keV γ-rays were due to E_2 transition, for which the K conversion coefficient should be 0.009. This latter conclusion also fits better with the theoretical considerations of the decay of ^{210}Po (GOLDHABER and SUNYAR [5]). BARBER and HELM [6], who measured the total conversion coefficient to be 14%, suggested that a fraction of X-rays may be due to the K-shell ionization of α's passing through the source. PRINGLE *et al.* [7] estimated the conversion coefficient to be 20 to 30%. The difference in the values of conversion coefficient with GRACE *et al.* [1] was explained as due to the K-shell ionization due to α's. ALBURGER and FRIEDLANDER [8] measured the conversion electrons with a β-ray Spectrograph and found the conversion coefficient to be 1 to 5%.

In view of these controversial results about 80 keV radiation, a further study of the radiations from ^{210}Po was undertaken.

2. – Measurements by scintillation spectrometer.

^{210}Po, procured from Atomic Energy Commission Canada, was prepared by bombarding Bi_2O_3 with slow neutrons from the reaction ^{209}Bi(n, γ)^{210}Bi $\xrightarrow{5\ \text{days}}$ ^{210}Po. Its activity at the time of measurement was 0.05 micro curie/milligram. A source of 0.184 gm/cm^2 was prepared on a perspex disc. The spectrum of the radiations was taken with a scintillation spectrometer using NaI(TL) crystal by placing the source right over the crystal. The spectrometer was calibrated for different energies with γ-rays of ^{137}Cs, ^{203}Hg and ^{103}Ru. Enough absorber (perspex and aluminium) was placed between the source and crystal to absorb the α's and conversion electrons. The NaI(TL) crystal was one inch in diameter and half inch in thickness. The differential spectrum thus obtained is given in Fig. 1 (after subtracting the background) which clearly indicates the presence of two radiations, one at 76 keV and the other at

(5) M. GOLDHABER and A. W. SUNYAR: *Phys. Rev.*, **83**, 906 (1951).
(6) W. C. BARBER and R. H. HELM: *Phys. Rev.*, **86**, 275 (1952).
(7) R. PRINGLE *et al.*: *Phys. Rev.*, **87**, 384 (1952).
(8) D. ALBURGER and G. FRIEDLANDER: *Phys. Rev.*, **81**, 523 (1951).

2522

800 keV. No other γ-ray was noted between 20 to 150 keV. The small humps at about 0.27 and 0.40 MeV are due to back scattering, which was confirmed by their relative reduction for very thin source. The measurements of relative intensities of 76 keV and 800 keV radiations were carried out as follows. The detection efficiency of the crystal for the two radiations was taken to be $(1 - \exp[-\mu d])$ where μ is the total absorption coefficient for the particular radiation and « d » is the effective path length of the radiation through the crystal. The value of « d » was obtained by actually drawing various paths in the crystal and taking their averages. The value of μ was obtained from the graph of absorption coefficient of the γ-rays (K. SIEGBAHN [9]).

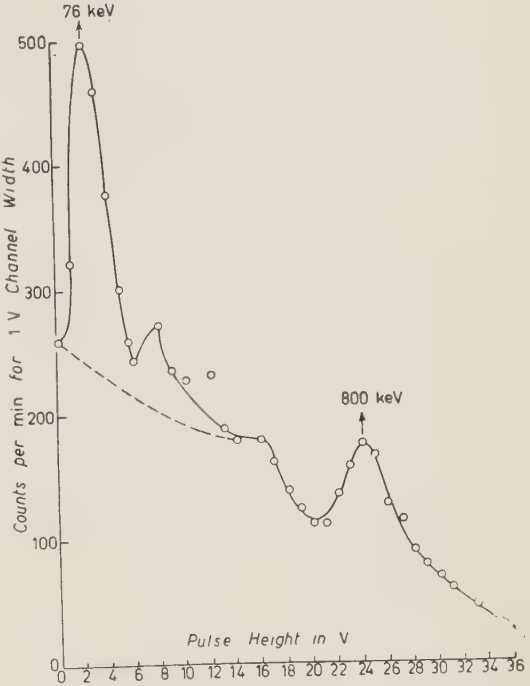

Fig. 1. – The differential pulse spectrum of the γ-rays and X-rays from Polonium-210.

For determining the total counts of 800 keV γ-rays, their Compton distribution was drawn as shown in Fig. 1 by the dotted line. Knowing the resolution of the spectrometer at 800 keV, it is possible to get the resolution at 76 keV. From this the base of 76 keV γ-ray was determined. Compton distribution of 800 keV γ-ray can then be drawn by smoothly joining the base to the Compton edge.

Total counts for 76 keV can, of course, be determined directly by the area under the peak.

Finally the absorption of these radiations in the aluminium covering and the source were also taken into account. Escape peak correction was not required because in both cases their contribution has been added to the total counts.

Apart from statistics, various sources of error are: (*a*) uncertainty due to the numerical integration used in determining « d ». The maximum error estimated was about 10%. (*b*) The uncertainty in drawing the total differential spectrum for the two radiations. After careful consideration the max-

(9) K. SIEGBAHN: *Beta-Gamma Ray Spectroscopy* (1955).

imum error in conversion coefficient due to this uncertainty was estimated to be 10%, the final value of conversion coefficient, thus obtained, was 0.039 ± 0.01.

3. – Measurement of conversion electrons.

A source of 6 mg/cm² was prepared on 8 mg/cm² cellulose tape. The source was put right over the window of an end window type G.M. counter, with the tape between the source and the window. The thickness of the window was about 3 mg/cm². In this way 11 mg/cm² absorber is inserted between the source and the counter which is enough to check α-particles. Counts, then, were taken for various thicknesses of aluminium inserted between the tape and the window. An absorption curve was drawn which is shown in Fig. 2, curve *B*. The thicknesses shown in the curve include half the thickness of the source, the thickness of the tape and window and the thickness of aluminium.

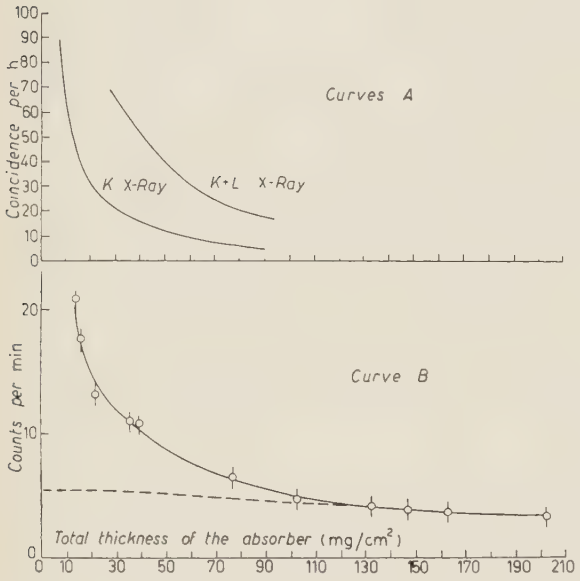

Fig. 2. – Curve *A*, shows the coincidences between the *K* and *L* X-rays and electrons for various thicknesses of absorber between the source and the electron detector as reported by LAGASSE and DOYEN (1954). Curve *B*, shows the number of electrons for various thicknesses of absorber between the source and the detector as observed by the authors.

Apparently, the graph can be divided into two parts; the first one extending up to about 100 mg/cm² and the other extending beyond that. The first portion can be interpreted as due to the electrons from *K*, *L*, shell ionization by α's and the second portion due to the genuine *K* and *L* conversion electrons. This interpretation is based on the following reasoning.

After Migdal's theoretical work on the *K*, *L*, shell ionization by α's (MIGDAL [10]), it was considered probable that α's of ^{210}Po contribute to the

[10] A. MIGDAL: *Journ. Phys.* (*U.S.S.R.*), **4**, 449 (1941).

X-rays and electrons through K and L ionization (BARBER and HELM [6], PRINGLE *et al.* [7], LAGASSE and DOYEN [11], ROY and GOES [12]). LAGASSE and DOYEN [11] measured the coincidences between the K X-rays and the electrons and also between the K and L X-rays and electrons, for various thicknesses of aluminium for selecting various energies of electrons. Their curves for the number of coincidences versus energy of electrons, give a continuous spectrum (Fig. 2, curve A), resembling very much the first portion of our curve (Fig. 2, curve B). Like our curve they also have a steep portion near about 80 keV followed by a lesser steep curve extending up to 300 keV. These coincidences are not due to conversion electrons because, in that case, coincidences should follow the curve of MARSHALL and WARD [13]. These coincidences have, therefore, been interpreted by them as between the K, L X-rays and electrons emitted by the process of K and L ionization due to α's. Similar reasoning can also be applied to the first portion of our curve. The second portion of the curve, when extended back, is similar to the one expected of monoenergetic electrons of 712 keV. The number of counts at zero thickness from this extrapolated curve has been, therefore, taken as due to the net conversion electrons. In the measurement of conversion electrons, the back scattering effect for electrons, which is only due to the finite thickness of the source, was considered very carefully. It was estimated to be much less than one percent in our case. This number includes K as well as L conversion electrons. No detectable counts were obtained after introducing 400 mg/cm^2 of aluminium between the counter and the source. This ensured that there was negligible contribution to the counts due to γ-rays.

The over-all efficiency of the G.M. counter was determined by the calibrated β sources of ^{234}Pa and ^{204}Tl obtained from Atomic Instrument Co., U.S.A. It was further checked by calculating the solid angle subtended by the source on the effective volume of the counter (BURTT [14]). The efficiency obtained from both these methods was 0.083 ± 0.009. The total number of γ-rays of this source were obtained by the same scintillation spectrometer as used previously. The source was placed right over the crystal and the pulses of all sizes were counted. It was ensured, however, that no α's or β's were counted. The geometrical and detection efficiency of the crystal was calculated as before. The contribution due to 76 keV radiation to the total counts and the corrections due to absorption were also taken into account.

The chief errors in the measurements of the conversion coefficient with the

---

(11) A. LAGASSE and J. DOYEN: *Compt. Rend.*, **239** (11), 670 (1953).
(12) R. R. ROY and M. L. GOES: *Compt. Rend.*, **237**, 1515 (1953).
(13) J. MARSHALL and A. G. WARD: *Can. Journ. Research*, A **15**, 39 (1937).
(14) B. P. BURTT: *Nucleonics*, **5**, 29 (1949).

above method were due to the uncertainty in the estimation of the over-all efficiency of the β counter and in the extrapolation in Fig. 2, curve B.

The final value of the total conversion coefficient thus obtained was 0.014 ± 0.005.

4. – Coincidence measurements.

It was also attempted to detect coincidences between the various portions of the γ-rays spectrum. For this two scintillation spectrometers in coincidence were used. The resolving time of the coincidence circuit was $2 \cdot 10^{-7}$ s. No genuine coincidences were observed between 800 keV and 76 keV radiations. Also there were no coincidences between 76 keV and the rest of the spectrum. Similarly no self coincidences were observed for 800 keV γ-rays.

5. – Discussion.

Within the experimental error the value of 0.014 ± 0.005 for the total conversion coefficient obtained by the measurements of conversion electrons is same as expected for E_2 transition (Rose tables [9]). This is in agreement with the angular distribution results of De Benedetti and Minton [4]. Comparing this result with the value of 0.067 obtained by the conversion electron measurements by Grace *et al.* [1], the discrepancy seems to be due to the fact that they also measured the electrons due to K and L shell ionization by α's as discussed in the measurements of conversion electrons.

On the other hand our value of 0.039 ± 0.01 for the conversion coefficient obtained from X-ray measurements is nearly the same (within the experimental error), as that of Grace *et al.* [1]. The reason for this higher value compared to 0.014 ± 0.005 seems to be due to the contribution of X-rays from the ionization by α's, which comes out to be 60% of the total intensity of X-rays. This is in qualitative agreement with the calculations of Roy and Goes [12] based on Migdal's theory.

The above results help to remove the ambiguity about the exact value of the conversion coefficient of 800 keV γ-rays as well as about the reason for the discrepancy in the measurements as reported in the literature.

RIASSUNTO (*)

Col metodo della scintillazione si è misurato il coefficiente di conversione dei raggi γ da 800 keV del decadimento del ^{210}Po, ottenendo 0.039 ± 0.01. Il valore del coefficiente di conversione è stato anche ottenuto misurando gli elettroni di conversione con un contatore G.M. a finestra terminale. Si dà la curva di assorbimento degli elettroni e la sua forma è stata interpretata al lume dei risultati di Alhonse Lagasse e Jacqueline Doyeb (*Compt. Rend.*, **239**, (11), 670 (1954)). Il valore del coefficiente di conversione così ottenuto è 0.014 ± 0.005. La diversità tra i due valori è stata attribuita alla ionizzazione degli strati K ed L dovuta alle particelle α. Non si sono trovate coincidenze tra le varie parti dello spettro dei γ.

(*) *Traduzione a cura della Redazione.*

On the Methods of Ionization Measurement in G-5 and K-5 Emulsions.

G. Cortini

Istituto di Fisica dell'Università - Catania
Centro Siciliano di Fisica Nucleare - Catania

G. Luzzatto and G. Tomasini

Istituto di Fisica dell'Università - Genova
Istituto Nazionale di Fisica Nucleare - Sezione di Genova

A. Manfredini

Istituto di Fisica dell'Università - Roma
Istituto Nazionale di Fisica Nucleare - Sezione di Roma

(ricevuto l'8 Maggio 1958)

Summary. — The results of measurements of ionization made in Ilford G-5 and K-5 photoemulsions by means of a semiautomatic apparatus are reported. The experimental fluctuations are in good agreement with values derived by simple formulae of practical use. While all the models proposed as yet for the mechanism of track formation appear to be oversimplified, an assumption is proposed to explain the results. The different methods of measurement are compared and some suggestion is given.

1. – Introduction.

The measurement of ionization in nuclear emulsions is a very important tool for the interpretation of the events, as it allows us to determine the velocities of the involved particles.

A number of papers have been published on the subject ([1-27]) in recent years and several of them ([13-21]) have described some semiautomatic apparatus intended to speed up the measurements.

The attempts to outline a model for the formation of the tracks ([21-27]) may appear to be less important. However, as we shall see, the solution of this problem is of relevance both for the adoption of a correct method of measurement, and for the calculation of fluctuations.

In the present paper we give further experimental results on the measurement of ionization (Sect. 2) and on the fluctuations, which fit rather well

([1]) L. Voyvodic: *Bristol Conf.* (1951), p. 16.

([2]) A. H. Morris: *Phil. Mag.*, **43**, 533 (1952); *Phys. Rev.*, **41**, 423 (1953).

([3]) R. R. Daniel and D. H. Perkins: *Proc. Roy. Soc.*, A **221**, 351 (1954); see also *Congr. Bagnères* (1953), p. 159.

([4]) M. G. K. Menon and C. O'Ceallaigh: *Proc. Roy. Soc.*, A **221**, 292 (1954).

([5]) G. Kayas: *Compt. Rend.*, **238**, 2153 (1954); *Journ. Phys. et Rad.*, **15**, 34 (1954).

([6]) A. Orkin-Lecourtois, G. Kayas and T. F. Hoang: *Suppl. Nuovo Cimento*, **12**, 398 (1954); **1**, 200 (1955).

([7]) P. H. Fowler and D. H. Perkins: *Suppl. Nuovo Cimento*, **12**, 236 (1954).

([8]) P. E. Hodgson: *Phil. Mag.*, **41**, 725 (1950).

([9]) C. O'Ceallaigh: *Phil. Mag.*, **42**, 1032 (1951).

([10]) C. O'Ceallaigh: *Bagnères Conf.*, (1953), p. 73.

([11]) T. F. Hoang: *Compt. Rend.*, **238**, 1790 (1954); *Suppl. Nuovo Cimento*, **1**, 186 (1955).

([12]) C. Castagnoli, C. Cortini and A. Manfredini: *Nuovo Cimento*, **2**, 301 (1955).

([13]) D. M. Ritson: *Phys. Rev.*, **91**, 1572 (1953).

([14]) G. Baroni and C. Castagnoli: *Suppl. Nuovo Cimento*, **12**, 364 (1954).

([15]) M. Della Corte: *Nuovo Cimento*, **12**, 28 (1954).

([16]) J. E. Hopper and M. Scharff: *CERN Secr. St. Measur.*, No. 12 (1954).

([17]) M. Renardier and Y. Avignon: *Compt. Rend.*, **233**, 393 (1951).

([18]) H. M. Mayer: *CERN Secr. St. Measur.*, No. 20 (1955).

([19]) M. V. Klein: *Rev. Sci. Instr.*, **28**, 964 (1597).

([20]) A. De Marco, R. Sanna, G. Tomasini: in the press. See also, G. Cortini, A. Manfredini, A. De Marco, R. Sanna, G. Tomasini: *Reports on Padua-Venice-Conference*, September 1957.

([21]) C. O'Ceallaigh: *CERN Secr. St. Measur.*, No. 11 (1954); see also, R. H. W. Johnston and C. O'Ceallaigh: *Phil. Mag.*, **45**, 424 (1954); *Nuovo Cimento*, **4**, 468 (1955).

([22]) M. Della Corte, M. Ramat and L. Ronchi jr.: *Nuovo Cimento*, **10**, 509 (1953); *Nuovo Cimento*, **10**, 1958 (1953).

([23]) A. J. Herz and G. Davis: *Australian Journ. Phys.*, **8**, 129 (1955).

([24]) W. W. Happ, T. E. Hull and A. H. Morrish: *Canad. Journ. Phys.*, **30**, 699 (1952).

([25]) G. Lovera: *Nuovo Cimento*, **12**, 154 (1954); I. Iori and A. Roveri: *Nuovo Cimento*, **2**, 165 (1955).

([26]) J. M. Blatt: *Austral. Journ. Phys.*, **8**, 248 (1955). For fluctuations see also: *Corrigendum*, in *Austral. Journ. Phys.*, **8**, 573 (1955).

([27]) P. H. Fowler and D. H. Perkins: *Phil. Mag.*, **46**, 587 (1955).

with the fluctuation formulae easily calculated by means of the Blatt method (Sect. 3). A short survey is made of the models of track formation proposed by different authors: all of them appear to be oversimplified, but a simple assumption on the growing of grains seems to fit well with the experimental results (Sect. 4). Finally, we compare the most important proposed methods of measurement and give some suggestion on these (Sect. 5). The most important results are summarized in Sect. 6.

2. – Experimental results: measurement of ionization.

We will use the term « r-gaps » for indicating a gap of length $> r$. The experimental quantities are:

(1) $H(r) =$ number of r-gaps per unit length,

(2) $B = H(0)$,

(3) $l(r) =$ total length of r-gaps per unit length,

(4) $w(r) = l(r)/H(r)$.

As we shall see at once, according to our results, $H(r)$ is an exponential decreasing function for r larger than a value r_0 of the order of $(0.2 \div 0.4)$ μm.

Therefore, we can add to the already defined quantities this other:

(5) $g =$ absolute value of the slope of the straight line which gives $\log [H(r)]$ as a function of r, for $r > r_0$.

The bulk of the measurements were made in a Ilford G-5 stack, exposed to 140 MeV protons. Some measurements will also be reported made on slow protons in K-5 Ilford emulsions and on one heavy track in a G-5 plate exposed to cosmic radiation. All the measurements were performed by means of a semiautomatic apparatus which is described elsewhere ([20]). It gives, at the same time B, $H(r)$ for 5 different values of r; and $l(0)$; it allows to deduce $w(0)$ from the ratio $l(0)/B$ as well as g, from the distribution of $H(r)$.

The « quantum » of measured lengths is 0.04 μm. The cell length is $t = 40$ μm The velocity of work is 1.2 mm per hour, included dead times. The stability of measurements was tested in various ways ([20]). Measurements were made by 3 different observers. While the generale results were completely coherent, some detectable, though rather small, differences between their results were observed; in order to avoid the use of 3 different calibration curves, at last only the measurements made by the most skilled observer were considered.

The general results are exhibited in Fig. 1.

The curves show the variation with the proton residual range R of $l(0)$, B, $H(0.2)$, $H(0.4)$ and $W(0)$ (all figures in μm). They support the general results already obtained by other authors ([12,27]).

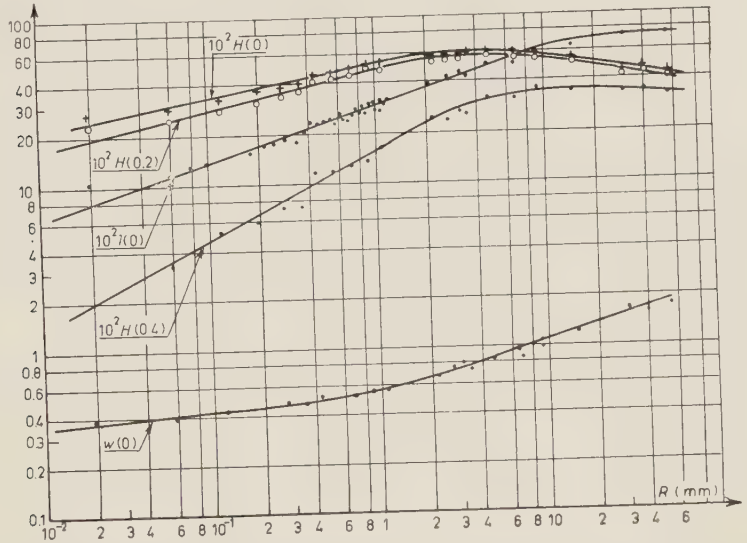

Fig. 1. Measurement of ionization parameters in underdeveloped G-5 emulsions. Abscissae: proton residual range. Ordinates: number of gaps or gap length in μm, on the same scale. All values reported for a cell $t = 100$ μm.

The known flat maximum of B begins at about 2 mm while in the FOWLER and PERKINS ([27]) work, it begins at about 4 mm and in the Rome work ([12]) it starts from ~ 10 mm. The Rome plates were very heavily developed, while those of the present work were rather underdeveloped, in order to discriminate between slow deuterons and protons.

Fig. 2 gives a selection of the measured $H(r)$ curves for 5 different values of the proton range R, that is of the ionizing power. Fig. 3 gives similar results for K-5 emulsions,

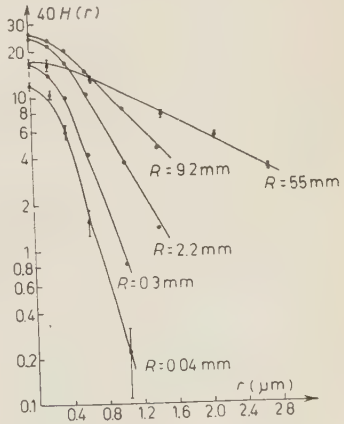

Fig. 2. – Integral gap length distribution for protons at various residual ranges. The values reported are for a cell $t = 40$ μm. Measurements on underveloped G-5 emulsions.

while Fig. 4 refers to a heavy track (assumed to be a boron or carbon minimum track) in G-5 emulsions.

As it is seen in the G-5 emulsion, all $H(r)$ curves turn out to be exponential only for $r > r_0 = (0.3 \div 0.4)$ μm. For $r < r_0$ the curves are always bent toward the r axis and are similar to each other.

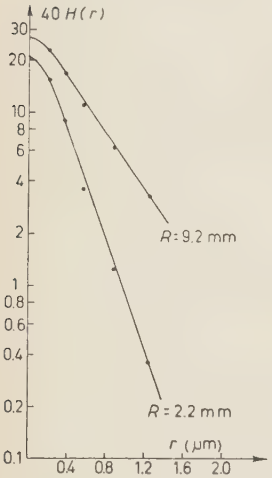

Fig. 3. – As Fig. 2. Measurement on K-5 emulsion.

As this result does not agree with those by other authors ([27]), we tested it in order to ascertain that it could not be due to systematic errors introduced by our measuring apparatus. Three different methods were used:

(i) Direct measurement by means of a standard eyepiece scale. The results seemed to be very subjective, and dependent on the microscope magnification.

(ii) Manual measurement by means of a filar micrometer.

(iii) Manual measurement by means of a filar micrometer arranged with a set of spider webs spaced in geometrical progression as proposed by O'CEALLAIGH ([28]). All these measurements were made on proton tracks with residual range $R = 3.2$ mm. The results of (ii) and (iii) are reported in Fig. 5, together

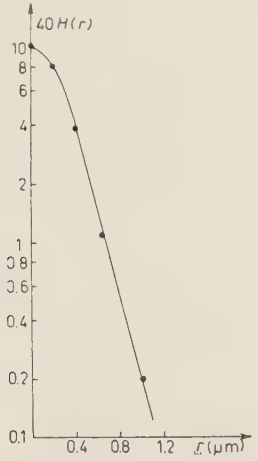

Fig. 4. – Integral gap length distribution for a heavy track. Measurement on G-5 emulsion strongly developed.

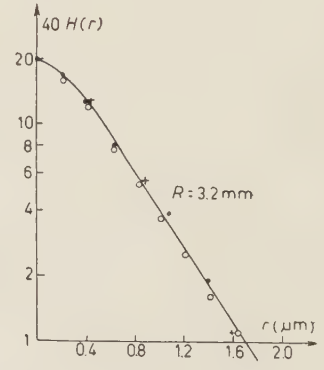

Fig. 5. – Gap length measured with different methods: + filar micrometer displaced by hand; ○ O'Ceallaigh method; ● our apparatus.

([28]) See ref. ([21]). Our grateful thanks are due to Dr. O'CEALLAIGH for having supplied to us a filar micrometric eyepiece.

with results obtained by means of our apparatus. The agreement between these measurements makes us confident that they are reliable. The different experimental methods can probably explain the difference between our results and F.P. ones.

An interesting connection has been found between two of the measured parameters; for every value of R, we found the equation:

$$B \equiv H(0) = g \exp [-2\gamma g] , \tag{6}$$

fitted well, as already found by various authors (see [34] eq. (2) and [26] eq. (3.1 *a*)).

Here 2γ is the diameter of the developed grain. Table I gives the 2γ values deduced from (6), by measurements at different proton ranges in G-5 and in K-5 emulsion. The values obtained by direct measurement and by the heavy track results are also reported.

TABLE I. – *Value of* 2γ (μm).

	G-5	K-5
Protons		
From eq. (6)		
Residual range mm		
0.16	0.605	—
0.48	0.615	—
0.84	0.618	—
2.2	0.597	0.524
3.2	0.618	—
4.7	0.634	0.543
6.7	0.639	—
9.2	0.633	—
13.4	—	0.583
Mean	0.620	0.553
Direct measurement	0.63	0.52
Heavy track		
From eq. (6)	0.605	—
Direct measurement	0.65	—

Note that eq. (6) would be an obvious consequence of a pure exponential $H(r)$ distribution (see below eq. (18A)) while it cannot be deduced in any simple way from our bent $H(r)$ curves.

25333

3. – Experimental results: fluctuations.

The important problem of the fluctuations of the measured parameters was recently investigated by LOVERA [29] and by O'BRIEN [30]. According to O'BRIEN's definitions, one must consider separately subjective (S) and emulsion processing (E) fluctuations, in order to determine the true track (T) fluctuations, that is the pure effects of the statistical process of track formation. E and S effects largely depend upon experimental conditions. If these are good, T effects are the most important ones.

We have calculated the fluctuations as follows. In each track a number of groups of cells has been selected. The number m of cells in each group was so small ($m = 4 \div 10$) that within it the ionization was practically constant. For each group we measured, besides other, the number $n = Bt$ of gaps per cell and the integral gap length $x = lt$, and we evaluated

$$(7) \qquad \bar{n} = \frac{1}{m} \sum_1^m n_i \,, \qquad \bar{x} = \frac{1}{m} \sum_1^m x_i \,,$$

as well as the Blatt fluctuation parameters:

$$(8) \qquad \mu_B^2 = \frac{1}{m-1} \frac{1}{\bar{n}} \sum (n_i - \bar{n})^2 \,,$$

$$\mu_l^2 = \frac{1}{m-1} \frac{1}{\bar{x}} \sum (x_i - \bar{x})^2 \,.$$

By putting $m - 1$ instead of m in the denominators, we take account of the fact that the deviations were taken with respect to the mean values (7) calculated for each particular group. Finally, the values (8) obtained from the particular tracks were combined with each other by calculating the quadratical mean, in order to obtain our best values of μ_B^2 and μ_l^2 at any given value of the range R.

With this procedure, we compare measurements made on the same track and in immediate succession so that we minimize the E and S effects. We think that the obtained values of the Blatt fluctuation parameters (8) correspond correctly to the pure T effects. If one calculates them directly from the general mean values, μ_B and μ_l are increased by some 10%:

In his work [30] O'BRIEN compares the experimental values of μ_B and μ_l with the Blatt predictions based on the model by Herz and Davis, and finds a good fit. As we shall see, it is reasonable to use, instead, the Blatt formulae derived from the O'Ceallaigh model. These give about the same results (with

[29] G. LOVERA: *Nuovo Cimento*, **4**, 1476 (1956).
[30] B. J. O'BRIEN: *Nuovo Cimento*, **7**, 314 (1958).

differences of a few units per cent—see also Appendix—) and are much less involved, so that they can be of practical use. In the particular but important case $r = 0$ (the one investigated by O'BRIEN and by us) they are:

$$\mu_B^2 = 1 - 4\gamma B \tag{9}$$

$$\mu_l^2 = \frac{2}{g}\left\{1 - \left(2\gamma + \frac{1}{g}\right) B\right\}. \tag{10}$$

The grain diameter 2γ, as well as the total blob number B are easily measured, while g (if not actually measured) can be derived from eq. (6). From (9) and (10) one immediately obtains the standard fluctuations δB and δl:

$$\frac{\delta B}{B} = \frac{\mu_B}{\sqrt{N}}, \qquad \frac{\delta l}{l} = \frac{\mu_l}{\sqrt{X}}, \tag{11}$$

where N is the total number of counted blobs and X the total measured gap length.

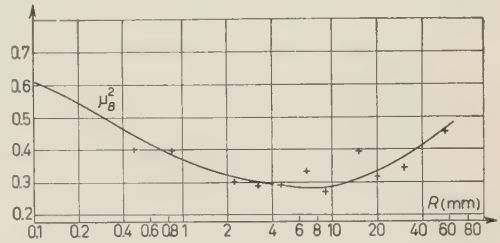

Fig. 6. – Experimental fluctuations of B compared with equation (8).

The Fig. 6 and 7 show the experimental values of parameters (8) in comparison with eqs. (9) and (10). For μ_B there is good agreement, while for μ_l we note a small but almost constant difference.

We shall see in Sect. **5** a possible reason for this difference.

In any case we think it useful to stress that (9) and (10) give fluctuations considerably smaller than pure Poisson distributions, so that their use is definitely advantageous for the correct evaluation of experimental errors.

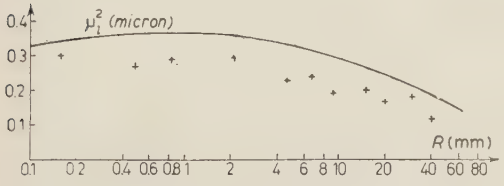

Fig. 7. – Experimental fluctuations of $l(0)$ compared with equation (10).

4. – Model of track formation.

Referring to the paper by BLATT ([26]), we put:

$Q(t)$ = « survival probability », that is the probability that the distance between the centre points of adjacent activated AgBr crystals along a track exceeds t;

$G(\gamma)\,\mathrm{d}\gamma$ = the distribution of the final grain radii, after focussing.

Two extreme models have been investigated in detail by various authors. In both of them $G(\gamma)$ is a δ-function; that is the radius γ is kept constant. For $Q(t)$ we have:

Model « A »:

$$Q(t) = \exp[-gt], \qquad (12)$$

(g = constant for a given ionization power of the particle).

Model « B »:

$$\begin{cases} Q(t) = 1, & 0 < t < \beta; \\ \quad = 1 - p, & \beta < t < 2\beta; \\ \quad = (1-p)^2, & 2\beta < t < 3\beta. \end{cases} \qquad (13)$$

(β = constant crystal distance along the track; p = constant for a given ionization power).

The model « *B* », proposed by HERTZ and DAVIS, is derived from the assumption that the crystals are arrayed along the path of the particle in a regular lattice of definite lattice spacing. This assumption is exaggerated, because in the emulsion there cannot be any long-range order. On the other hand, model « *A* » completely ignores the « graininess » of the emulsion before the processing. A more realistic attempt to take into account the real situation is a modification of model « *A* », that is:

Model « C »:

$$\begin{cases} Q(t) = 1, & 0 < t < \alpha, \\ \quad = \exp[-g(t-\alpha)] & t > \alpha. \end{cases} \qquad (14)$$

The models described include most of the assumptions made by different workers. The work by O'CEALLAIGH [21] can be reduced to model « *C* », with minor modifications. The same is true for the work by FOWLER and PERKINS (see the integral curve *b* in Fig. 5 of their paper) who deduce the exponential character of $Q(t)$ by considering in a very detailed way the mechanism of track formation.

The model by HAPP, HULL and MORRISH [24] is similar to model « *A* » but these authors assume a bell distribution function for $G(\gamma)$. The model by DELLA CORTE *et al.* [22] is similar to model « *B* », with the particular assumption $2\gamma = \beta$ and the same is true for the fluctuation results by LOVERA. *et al.* [25].

By means of his general method, BLATT gets from the different assumptions on $Q(t)$ and $G(\gamma)$ the corresponding distribution formulae for the relevant experimental quantities (1) to (3).

To avoid confusion, it should be recalled that the symbols used by BLATT

in his paper are:

$$t = \text{cell length}$$

$$n_r(t) = tH(r)\,, \tag{15}$$

$$x_r(t) = tl(r) - rn(t)\,, \tag{16}$$

$$w^B(r) = x_r/n_r = w(r) - r\,. \tag{17}$$

In eq. (17) the index B in w^B has been put in order to distinguish the different meaning of the symbol w in the BLATT paper and in eq. (4). The parameter x means the total length per cell of r-gaps, computing for each gap only the length *in excess of* r. For $r=0$, $x=lt$. The symbols n and x have already been used by us in eqs. (7) and (8), with the meaning of $n(0)$ and $x(0)$.

In the limit $t \gg 2\gamma + r$; $t \gg 1/g$, that is for suitable cell length, the Blatt results are as follows:

Model « A »:

$$H(r) = g \exp\left[-g(2\gamma + r)\right] = B \exp\left[-gr\right], \tag{18A}$$

$$w(r) = \frac{1}{g} + r\,, \qquad \text{that is} \qquad w^B(r) = \frac{1}{g}\,. \tag{19A}$$

The ionizing power is related to the value of g.

Model « B »:

$$H(r) = \frac{1}{\beta}\, p(l-p)^{\Gamma}\,, \tag{18B}$$

$$w(r) = \beta\left(\Gamma + \frac{1}{p}\right) - 2\gamma\,, \tag{19B}$$

with Γ integer part of $(2\gamma + r)/\beta$.

The ionizing power is related to the value of p.

Model « C »:

$$H(r) = \exp\left[g\alpha\right]\left[1 + g\alpha\right]^{-1} g \exp\left[-g(2\gamma + r)\right], \tag{18C}$$

$$w(r) = \frac{1}{g} + r\,. \tag{19C}$$

All the results (18*A*) to (19*C*) can be directly deduced from elementary considerations. The Blatt method allows one to derive the same parameters under more complicated assumptions, and to deduce in a simple way the fluctuation formulae (see Sect. **5**).

2537

An extensive comparison of the models « A » and « B » with experimental results was performed by CASTAGNOLI, CORTINI and MANFREDINI ([12]) and by FOWLER and PERKINS ([27]).

CASTAGNOLI *et al.* studied in the first place $H(0)$ and $w(0)$.

Their results could not be fitted with eqs. (18A) and (19A). A good fit was possible with (18B) and (19B), by adjusting the two parameters β and γ which are relevant in model B (while in model « A » the only parameter at disposal is γ).

On the other hand, FOWLER and PERKINS, studied the gap length distribution, that is the function $H(r)$ for variable r. They found an exponential curve for the whole r range of interest and for any value of g. Besides this, they found empirically the equation (6).

A general prediction of models « A » and « C » is that the limit w^0 of $w(0)$ for increasing ionization is zero. This is contradicted by the results of experiment. FOWLER and PERKINS made the assumption that the experimental minimum value w^0 of w corresponds to the exponential distribution of the gaps between crystals, before processing, along the path of the charged particles. This picture is completely coherent.

However, we are now facing the difficulty of explaining the initial bend of the H curves shown in Fig. 3, 4 and 5. This bend cannot be explained by any one of the models considered as yet.

Models « A » and « C » give a pure exponential curve. One can try to fit it with the model « B », by considering that the « graininess » effect will be important only on the short distances: the fluctuation in crystal locations and in γ are expected to round off the discontinuities of equation (18B) as soon as $\Gamma > 3 \div 4$, so giving a continuous exponential curve. For smaller Γ we can expect some type of bending.

However, the calculations made by F.P. for fluctuating distances of crystals as well as those made by us for fluctuating γ (see Blatt « modified Herz-Davis model ») show that this is not the case. The growing of crystals during processing is so large that no detectable effect is expected with reasonable values of the crystal distance β and of the grain radius γ, as soon as the fluctuation is supposed appreciable. Besides, the small calculated bend can be made to go towards the r axis as well as in the opposite direction as a consequence of small variations of the chosen parameters.

All in all, the detailed calculations on any known model necessarily forces us to admit that the experimental distribution ought to be purely exponential.

The only way out of these difficulties is to admit that all the models are oversimplified, and that some new effect must be considered.

The first attempt one can make is to consider some short-distance effect which involves only the short gaps. However, such an effect would not explain the very good fit that we find with eq. (6) as shown by Table I, for all our

2538

measurements in G-5 as well as in K-5 emulsions [note that eq. (6) is a particular case of eq. (18*A*)].

This result shows that the bend cannot be due to the *disappearance* of short gaps. Otherwise, we would expect for $H(r)$ $(r > r_0)$ much smaller values than those experimentally found, or we should be obliged to take for G-5 emulsions $2\gamma \sim 0.4$ μm, which is unacceptably small.

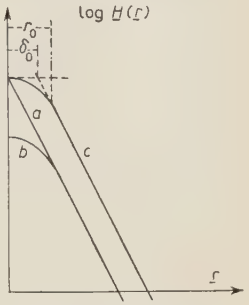

Fig. 8. – Explaining the meaning of r_0 and δ_0.

In other words, the experimental curves cannot be deduced from the pure exponential function (see curve *a*, Fig. 8) by bending it near the origin (curve *b*), but by a long range effect which gives a curve like *c*.

Adoption of model « *C* » gives no practical advantage because the constant factor $\exp[\alpha g]/(1+\alpha g)$ in eq. (18*C*) turns out to be not much larger than unity and almost irrelevant for practical purposes for all reasonable values of α.

So, we go back to model « *A* », and propose the following tentative explanation. *It is by no means true that the centres of developed grains necessarily coincide with the crystal centres.* During processing, we have considerable mechanical displacements. The growing in the direction of unaffected compact AgBr crystals is more difficult than the interpenetration of adjacent sponge-like developed grains. This effect tends to reduce the blob lengths and to increase the gap lengths (see Fig. 9), while it does not alter appreciably either $H(0)$ or g.

Fig. 9. – A very schematic picture of the growing of grains under the assumptions specified in the text.

So, eq. (6) is still valid, while (18*A*) must be substituted with

$$H = B \exp[-g\{r - \delta(r)\}] = g \exp[-g\{[2\gamma - \delta(r)] + r\}], \tag{20}$$

where $\delta(r)$ is an increasing function of r, which becomes a constant, δ_0 say, for $r > r_0$ (see Fig. 8)

$$\begin{cases} \delta(r) = 0 & r = 0, \\ \delta(r) = \delta_0 & r > r_0. \end{cases} \tag{21}$$

Eq. (19*A*) is now valid only for $r > r_0$.

The r_0 value is $(0.3 \div 0.4)$ μm for G-5 plates and $(0.2 \div 0.3)$ μm for K-5 plates. Eqs. (18*A*) and (20) fit with all our results, as well as with those by CASTAGNOLI *et al.* and with the Herz results reported by BLATT (see [26], page 266).

All the quoted results give $\delta_0 \sim 0.20$ μm in reasonable agreement with our present value, $\delta_0 = 0.24$ μm, for G-5 plates.

For K-5 plates we have $\delta_0 \sim 0.10$ μm, which shows that δ_0 is strongly dependent on the crystal diameter. Of course, the processing can produce some variation of δ_0.

The preceding considerations make it reasonable to use—at least as a first approximation—the Blatt fluctuation formulae for pure exponential distributions.

These are (9) and (10) for measurements made with $r=0$. For the more general case $r \neq 0$, we have

$$\mu_H^2 = 1 - 2(2\gamma + r)g \exp\left[-g(2\gamma + r)\right], \tag{22}$$

$$\mu_x^2 = \frac{2}{g}\left\{1 - \left[1 - g(2\gamma + r)\right] \exp\left[-g(2\gamma + r)\right]\right\}. \tag{23}$$

Here μ_x is the fluctuation parameter for the variable $x_r(t)$ (or $t^{-1}x_r(t)$) so that $\mu_x \to \mu_l$ for $r \to 0$.

The fact that the experimental values of μ_l are somewhat smaller than given by eq. (10) is in qualitative agreement with the initial bend of the $H(r)$ curves.

While in general the preceding formulae are only approximate, *in the case* $r > r_0$ exact expressions of μ_H^2 and μ_x^2 can be immediately derived from (22) and (23), by substituting 2γ with $2\gamma - \delta_0$:

$$\mu_H^2 = 1 - 2[(2\gamma - \delta_0) + r]g \exp\left[-g\{(2\gamma - \delta_0) + r\}\right], \tag{22'}$$

$$\mu_x^2 = \frac{2}{g}\left\{1 - \left[1 - g\{(2\gamma - \delta_0) + r\}\right] \exp\left[-g\{(2\gamma + \delta_0) + r\}\right]\right\}. \tag{23'}$$

5. – Methods of measurement.

On the basis of their results which give pure exponential $H(r)$ curves, FOWLER and PERKINS proposed a method of measurement based on eqs. (6) and (18*A*). For thin tracks they measure only B and deduce g by means of (6). For thicker tracks the value of B becomes insensitive to variations of ionization. Then the authors measure B and $H(r)$ for a single selected value of r, and deduce g by means of (18*A*). The deduced values of g, if normalized to the value g^* assumed by g for plateau relativistic particles, turn out to be independent on the processing of the plate ([27]).

The method does not require any special apparatus. For thin tracks (protons with R of the order of some cm) it is very simple and, as our results confirm the validity of eq. (6), in this case the method is not put in question. On the other hand, the method for thicker tracks seems to be subject to some dependence on the experimental counting technique.

If a measuring machine is available, the choice of the method must be made from a balancing of the following factors:

(i) Time of measurement and involved calculations.

(ii) Sensitivity of measured parameters on the ratio R/M of range to mass.

(iii) Fluctuations of the considered parameter.

(iv) Stability of results with variation of processing conditions and with location in the emulsion volume.

All these factors must be studied in any particular case, following the concrete experimental situation, and the aim of any given research (*e.g.*, measurement of mass or discrimination between particles of known masses, etc.). For the particular case of our plates, we decided between the parameters directly measured, to use $l(0)$ for $R < 10$ mm and $w(0)$ for $R > 10$ mm.

However, the exposed results show the convenience of completely eliminating the short gaps ($r < r_0$) from the computations, and to consider for each r-gap only the length in excess of r. This means to measure the variables $H(r_0)$ and $x_{r_0}(t)$ (see eq. (16)), and $w^B(r_0)$ (see eq. (17)).

Indeed, for $r > r_0$ we have a pure exponential curve, so that we can make direct measurements of $g = [w^B(r_0)]^{-1}$ without any difficulty or complication. Besides, just as a consequence of the bent curves $H(r)$, the difference between B and $H(r_0)$ is very small, so that the loss of information is negligible.

These conclusions are particularly true for the new emulsions Ilford K-5, where the bend is very small.

A minor modification of our apparatus can allow one to measure $x_r(t)$. This modification has already been made, and we plan to exploit it for further work.

6. – Conclusions.

Summarizing, our most important conclusions are as follows:

1) The gap length distribution $H(r)$ is exponential for $r > r_0$, with $r_0 = (0.3 \div 0.4)$ μm in G-5 emulsions and $r_0 = (0.2 \div 0.3)$ μm for K-5 emulsions. For $r < r_0$ the curves show a strong bend toward the r axis.

2) The simple Fowler-Perkins equation (6) is confirmed (see Table I).

3) None of the models proposed as yet for the track formation process is satisfactory. However, the pure exponential model supplemented by a simple assumption on mechanical displacements of grains (see page 717) gives account for all our results.

4) The statistical errors of measurement can be easily calculated using eqs. (11), by means of the first approximation Blatt-O'Ceallaigh formulae (9) and (10) for $r = 0$ and (22) and (23) in the general case. For $r > r_0$ eqs. (22′)

and (23′) give exact expressions of the fluctuations. Caution must be used in taking account of other effects (O'Brien E- and S-effects see page 712).

5) Among the parameters as yet measured, in our processing conditions the best ones are: $l(0)$ for residual range $R < 10$ mm; $w(0)$ for $10 \text{ mm} < R < 50$ mm. For larger R the Fowler-Perkins method would probabily be the simplest and the most convenient one.

6) For future work, we propose to use $x_{r_0}(t)$ and $w^B(r_0) = g^{-1}$.

* * *

Our thanks are due to Prof. E. Pancini for many useful discussions, to Ing R. Sanna for constant help in handling the measuring apparatus, to Miss Basiglio, and to Dr. L. Ciuffolotti for having performed the measurements and a part of calculations.

Appendix

On the fluctuation formulae.

Eq. (22), with its particular case for $r = 0$ [eq. (9)], holds for pure exponential $H(r)$ distribution, and, also, holds approximately for any known model ([29]). For instance, the Blatt-Herz-Davis formula reduces at once to (22) for $(2\gamma + r)/\beta = \Gamma + \frac{1}{2}$.

Eq. (23), with is particular case (10), seems also to be valid for any model. For instance, the Blatt-Herz-Davis formula can be put, with some algebra, in the form:

$$\mu_x^2 = \frac{2}{g}\left\{1 - \left[1 - g(2\gamma + r)\right] \exp\left[-g(2\gamma + r)\right]\right\} + \\ + \frac{2}{g}\left\{\exp\left[-g(2\gamma + r)\right] - \tfrac{1}{2}\right\} \operatorname{tgh}^2 \frac{g\beta}{2} .$$

The second term difference from eq. (23) is rather small: not more than $\sim 10\%$ of the first one.

RIASSUNTO

Si riferiscono i risultati di misure di ionizzazione eseguite in lastre Ilford G-5 e K-5 mediante un apparecchio semiautomatico. Le fluttuazioni sperimentali risultano in buon accordo con i valori desunti da semplici formule, di facile uso pratico. Mentre tutti i modelli proposti finora circa il meccanismo di formazione delle tracce appaiono semplicistici, se ne propone una modifica che spiega i risultati. Si discutono i metodi di misura e si danno in proposito alcuni suggerimenti.

The Coefficients of Friction and Wear.

P. Sen

National Physical Laboratory - New Delhi, India

(ricevuto il 12 Maggio 1958)

Summary. — The combination of the Savage surface energy and the Bowden and Tabor junction formation mechanisms of production of frictional energy is suggested. The physical description of the experiments is sufficiently simplified and represented by a stable state which envelopes the whole field of friction. This leads to a qualitative and satisfactory agreement with the observed results for the values of coefficients of friction between solid surfaces, between solid surfaces with thin liquid or solid soft metal films, for wear, and for the correlation between friction and wear. The coefficient of wear is defined analogously to the coefficient of friction.

1. – Introduction.

While an explanation, from which a semiquantitative agreement is available, can be found for a restricted set of experiments in the field of friction, no comprehensive theory which covers the whole field seems to exist, and there are to be found mutual contradictions between the explanations that are offered for the different sets of experiments. The most widely accepted theory of Bowden and Tabor [1] according to which friction is due to welded junctions is substantiated by the experiments of Bowden and Hughes [2] and Finch [3] in which such junctions are found to occur in high vacuum or by the joining of freshly cleaved surfaces respectively. But Finch [3] also pointed out that such a process would lead to much higher rate of wear than

(1) F. P. Bowden and D. Tabor: *The Friction and Lubrication of Solids* (Oxford, 1950).

(2) F. P. Bowden and T. P. Hughes: *Proc. Roy. Soc.*, A **172**, 263 (1939).

(3) G. I. Finch: *Proc. Phys. Soc.*, B **63**, 465 (1950).

the observed one and ARCHARD and HIRST [4] have shown that this discrepancy is of the order of 10^2 for soft metals and 10^4 for hard metals.

Then SAVAGE [5] showed that for thin liquid films of molecular dimensions between two sliding surfaces, under loads for which the Amonton's law is obeyed, the frictional energy can be derived from the surface energy of the liquid film and the experiments of GORODETSKAJA and KABONOV [1] on the variation of the coefficient of friction for an electrolytic liquid film due to the interfacial potential confirm his conclusions. But no attempt seems to have been made to extend this mechanism to the friction from metallic films whose significance in the reduction of wear was pointed out by FINCH [3].

The experiments on wear, for instance by BURWELL and STRANG [6], ARCHARD [7], ARCHARD and HIRST [4], and KERRIDGE and LANCASTER [8] indicate that while light wear follows Amonton's law and is essentially a surface phenomenon, no specific trends are found for heavy wear, although welded junctions, reminiscent of the Bowden and Tabor theory of friction, are observed and perhaps an appreciable layer of the sliding surface partakes in its occurrence.

In order to obtain a connected description of the above mentioned sets of experiments we shall follow the general principles of FINCH [3] and consider the surface energy and the welded junction mechanisms of friction together by combining the SAVAGE [5] and BOWDEN and TABOR [1] processes of production of frictional energy. Then we can allow the former process, which produces little wear, to account for the major part of the frictional energy and reserve the Bowden and Tabor mechanism to account for wear, for higher than expected coefficients of friction, and for the experiments of BOWDEN and TABOR [1] where the frictional shear is found to be equal to the shear strength of metals at room temperature. This combination of surface and junction mechanisms of friction is made by postulating that the temperature of the contacting surfaces in the steady state of uniform motion against one another is in the neighbourhood of the melting point of the more fusible surface. Then the area of contact becomes much larger than that obtained by BOWDEN and TABOR [1,9,10] from measurements of electrical conductivity across the contacting surfaces at rest and at room temperature. We note that

[4] J. F. ARCHARD and W. HIRST: *Proc. Roy. Soc.*, A **236**, 397 (1956).
[5] R. H. SAVAGE: *Journ. Appl. Phys.*, **19**, 1 (1948).
[6] J. T. BURWELL and C. D. STRANG: *Journ. Appl. Phys.*, **23**, 18 (1952).
[7] J. F. ARCHARD: *Journ. Appl. Phys.*, **24**, 981 (1953).
[8] M. KERRIDGE and J. K. LANCASTER: *Proc. Roy. Soc.*, A **236**, 250 (1956). Other references also are given here.
[9] F. P. BOWDEN and D. TABOR: *Proc. Roy. Soc.*, A **169**, 391 (1939).
[10] R. HOLM: *Electrical Contacts* (Uppsala, 1946).

2544

a larger area of contact has been obtained by ARCHARD [11] in the direct measurements of the true area of contact between surfaces in motion with respect to each other, but an alternate explanation, which is in agreement with the Bowden and Tabor hypothesis is also possible in this case and has been given by him. This increase in the area of contact makes possible a corresponding decrease in the strength of the forces that cause friction and therefore surface tension replaces welding and becomes the principal mechanism for production of friction.

2. – The surface energy mechanism of friction.

To obtain the frictional energy consider a hollow cylinder which may consist of several separate components, whose inner surface σ_1 is in contact with the outer surface σ_2 of a rotating solid cylinder 2 and let their smoothed sliding surfaces be formed on the average of minute hemispherical asperities. Due to their small curvature even a small load will deform the contacting asperities plastically until the area of contact between the surfaces is sufficiently enlarged to reduce the body stress to its yield point value. When the inner cylinder revolves the area of contact will change and the plastic deformation shall reoccur until, in the stable state, the area of contact becomes constant and supports the yield stress. Due to the continuous supply of frictional energy the contacting surfaces will be heated and we shall assume that their temperature is in the neighbourhood of the melting point of the more fusible surface, say σ_1. Then the area of true contact is given by [1]

$$\sigma(1\,|\,2) = G/Y(1, L)\,, \tag{1}$$

where G is the load applied at the sliding surfaces and $Y(1, L_1)$ is the yield stress of the substance 1 in the neighbourhood of its melting point L_1 °C. Since the shear stress $s_\sigma(1, L_1)$ is equal to the surface energy $\gamma(1, L_1)$ in the plastic state and under the yield pressure, using von Mise's plasticity criterion [1]

$$3s_\sigma^2(1, T) + s_\tau^2(1, T) = Y^2(1, T)\,, \tag{2}$$

where $s_\sigma(1, T)$, $s_\tau(1, T)$ and $Y(1, T)$ are the shear, body, and yield stresses respectively at the temperature T °C, we obtain the minimum value of

[11] J. F. ARCHARD: *Proc. Roy. Soc.*, A **243**, 190 (1958).

$Y(1, L_1)$ to be

$$Y(1, L_1) \approx 2\gamma(1, L_1) . \tag{3}$$

A surface may be considered to be a regular array of molecules a few angstroms apart and as the surfaces in true contact over a small region slide over one another the interactions between their molecules will be broken and reestablished periodically. By supplying the binding energy the surfaces will be separated from their ground state to their excited states which in turn, when they come in contact again, will fall back to their ground state and release the binding energy, which will be carried away in the form of heat energy. The energy needed for these operations is supplied by the force that produces the sliding and is a part of the total frictional energy supplied to the system.

To obtain its estimate we note that the excited states can be either the « vapourized » states where the molten surface is separated from the solid surface and is independent of it or the « transferred » states where a monolayer of the molten surface σ_1 is torn from its bulk surface and sticks to the surface σ_2. The energies necessary for forming these states are

$$E_v(1\,|\,2) = \gamma(1, L_1)(1 + \cos\vartheta(1\,|\,2))\,\sigma(1\,|\,2) , \tag{4}$$

$$E_t(1\,|\,2) = 2\gamma(1, L_1)\sigma(1\,|\,2) , \tag{5}$$

respectively, where the equation (4) is the Dupré relation (Adams ([12])) and $\vartheta(1\,|\,2)$ is the angle of contact between the surfaces σ_1 and σ_2 at L_1 °C. A statistical estimate of the ratio η of the probability of the formation of the transferred states and the probability of the formation of the vapourized states is

$$\eta \approx \exp\left[(E_v(1\,|\,2) - E_t(1\,|\,2))/E_t(1\,|\,2)\right] \approx E_v(1\,|\,2)/E_t(1\,|\,2) , \tag{6}$$

and is in accord with Kerridge and Lancasters' ([8]) observed magnitude of less than unity.

Then, in the equilibrium state, the frictional energy is

$$\left\{\begin{aligned} F_\sigma(1\,|\,2) &= E_v(1\,|\,2)/(1 + \eta) + E_t(1\,|\,2)\eta/(1 + \eta) , \\ &= 4\sigma(1\,|\,2)\gamma(1, L_1)(1 + \cos\vartheta(1\,|\,2))(3 + \cos\vartheta(1\,|\,2))^{-1} , \end{aligned}\right. \tag{7}$$

([12]) N. K. Adams: *The Physics and Chemistry of Surfaces* (Oxford, 1941).

and the surface coefficient of friction $\mu_\sigma(1\,|\,2)$ is, by definition,

$$\mu_\sigma(1\,|\,2) = F_\sigma(1\,|\,2)/G \approx 2(1 + \cos\vartheta(1\,|\,2))(3 + \cos\vartheta(1\,|\,2))^{-1}. \tag{8}$$

It will have the maximum value of 1 when the angle of contact is zero or there is complete wetting and will have the minimum value 0 for $\vartheta = \pi$ which however is not found. We note that perhaps one of the physical modifications that occur when the Beilby layer is formed or when the hardness of the sliding surfaces is increased is the reduction of the wetting. The observed values of $\mu(1\,|\,2)$ are generally of the order unity for metals with oxide layers, of the order 20 for pure soft metals, and of the order 5 for pure hard metals. Thus while we find qualitative agreement for metals with oxide layers, we shall explain the higher values in Sect. **4** by showing that then there is an appreciable probability for the formation of junctions.

Now in accordance with the observations of KERRIDGE and LANCASTER [8] that light wear of surface σ_1 occurs after it has been transferred to the surface σ_2 we note that the transferred surface may also form a drop and detach itself and cause wear. Let $K(1)$ be the probability of the formation of the drop. Then the number of molecules of wear per unit sliding distance is given by

$$W_\sigma(1\,|\,2) = N(1)K(1)\eta\sigma(1\,|\,2) = GN(1)K(1)\eta/Y(1, L_1)\,, \tag{9}$$

where $N(1)$ is the molecular density of the surface σ_1. Defining the coefficient of wear $\omega_\sigma(1\,|\,2)$ analogously to the coefficient of friction as the wear per unit load we obtain

$$\omega_\sigma(1\,|\,2) = N(1)K(1)\eta/Y(1, L_1)\,. \tag{10}$$

KERRIDGE and LANCASTER [8] have estimated that the wear particles correspond to about six transferred layers and in that case $K(1) \approx \eta^6$, which is perhaps not an unreasonable estimate.

3. – Thin films.

The mechanism of friction when there exists a thin liquid film, a few molecules thick, between two sliding surfaces has been given by SAVAGE [5] and indeed the mechanism described in Sect. **2** for friction between two solid sliding surfaces corresponds to it. But now while the true area of contact remains the same as before, to produce sliding, work must now be done to separate the solid and the liquid film surfaces. Let $\mu_\sigma(1\,|\,3\,|\,2)$ denote the

coefficient of friction between the surfaces σ_1 and σ_2 in the presence of a thin film σ_3. Then we expect

$$(11) \qquad \frac{\mu_\sigma(1\,|\,3\,|\,2)}{\mu_\sigma(1\,|\,2)} = \frac{\gamma(3,L_1)\,(1+\cos\vartheta(3\,|\,2))(3+\cos\vartheta(1\,|\,2))}{\gamma(1,L_1)(1+\cos\vartheta(1\,|\,2))(3+\cos\vartheta(3\,|\,2))} \approx \frac{\gamma(3,L_1)}{\gamma(1,L_1)},$$

where $\vartheta(3/2)$ is the angle of contact between the surfaces σ_3 and σ_2 and the surface energy of the film σ_3 is to be taken at the temperature L_1 °C and yield pressure $Y(1, L_1)$. Furthermore

$$(12) \qquad \mu_\sigma(1\,|\,3\,|\,2)/\mu_\sigma(1\,|\,4\,|\,2) \approx \gamma(3, L_1)/\gamma(4, L_1)\,.$$

and these ratios are in general agreement with the observed ratios.

We can now extend the same mechanism to thin soft metal films between two hard sliding surfaces and we note that under loads at which Amonton's law is obeyed

$$(13) \qquad \frac{\mu_\sigma(\mathrm{Cu}\,|\,\mathrm{Pb}\,|\,\mathrm{steel})}{\mu_\sigma(\mathrm{Cu}\,|\,\mathrm{steel})} \approx \frac{\gamma(\mathrm{Pb}, L_{\mathrm{Cu}})}{\gamma(\mathrm{Cu}, L_{\mathrm{Cu}})} \approx \frac{350}{1100} \approx .3\,,$$

while the observed values are

$$(14) \qquad \frac{\mu_\sigma(\mathrm{Cu}\,|\,\mathrm{Pb}\,|\,\mathrm{steel})}{\mu_\sigma(\mathrm{Cu}\,|\,\mathrm{steel})} \approx \frac{.2}{.8} = .25\,.$$

Again since $\mu(\mathrm{steel}\,|\,\mathrm{In}\,|\,\mathrm{steel})$ is .04 and $\mu(\mathrm{steel}\,|\,\mathrm{steel})$ is .4 the expected value of $\gamma(\mathrm{In}\,|\,L_{\mathrm{steel}})$ is 150 dynes/cm at L_{steel} and $Y(\mathrm{steel}, L_{\mathrm{steel}})$.

4. – Junction formations.

Besides the surface excitation the formation and rupture of welded junctions contributes to frictional energy and wear. Junctions can be formed due to adhesion of freshly cleaved surfaces or to permanent plastic deformation due to excessive loading or to adhesion of pure metals in high vacuum, and we note that such junctions are found in every frictional process. A rupture of a junction will generally occur for the softer substance and require a yield shear at a temperature much below the temperature of the sliding surfaces and which may be approximately put equal to the room temperature and is denoted here by R °C. Although the thickness of a few molecular layers only is involved here, we may call it the « body » mechanism of friction in comparison with the surface mechanism described earlier and we can attribute the major portion of wear to it.

2548

Let us consider the junctions formed by adhesion at low loads and let $\xi_s(1\,|\,2)$ be the probability of an area of contact to be an area of adhesion. Then the total frictional energy and the total wear per unit sliding distance are

$$(15)\quad \begin{cases} F(1\,|\,2) = F_\sigma(1\,|\,2) + F_\tau(1\,|\,2) \\ \qquad = \sigma(1\,|\,2)\,[4\gamma(1, L_1)(1 + \cos\vartheta(1\,|\,2))\cdot \\ \qquad\qquad \cdot(3 + \cos\vartheta)1\,|\,2))^{-1}(1 - \xi_s(1\,|\,2)) + s_\sigma(1, R)\xi_s(1\,|\,2)]\,, \end{cases}$$

and

$$(16)\quad W(1\,|\,2) = W_\sigma(1\,|\,2) + W_\tau(1\,|\,2) = \\ = N(1)\,\sigma(1\,|\,2)\,[K(1)\eta(1 - \xi_s(1\,|\,2)) + J(1)\xi_s(1\,|\,2)]\,,$$

respectively. Here $J(1)$ are the number of molecules which are detached per molecular contact, and we have assumed that the area of tear and the area of adhesion are the same. Furthermore if the adhesive areas are assumed to follow the laws of plasticity and Amonton's law holds, we obtain

$$(17)\quad \mu(1\,|\,2) = 2^{-1}\,[4(1 + \cos\vartheta(1\,|\,2))(3 + \cos\vartheta(1\,|\,2))^{-1}(1 - \xi_s(1\,|\,2)) + \\ + s_\sigma(1, R)\xi_s(1\,|\,2)/\gamma(1, L_1)]\,,$$

$$(18)\quad \omega(1\,|\,2) = N(1)/Y(1, L_1)\,[K(1)\eta(1 - \xi_s(1\,|\,2) + J(1)\xi_s(1\,|\,2)]\,.$$

We note that for $s_\sigma(1, R)/\gamma(1, L_1) \approx 10^3$, $2\cdot10^4$ and $\mu(1\,|\,2) \approx 20$, 5 respectively we should have $\xi_s(1\,|\,2) \approx 4\cdot10^{-2}$, $4\cdot10^{-4}$, which is in qualitative agreement with the observations of ARCHARD (7) and ARCHARD and HIRST (4).

Adhesion can be considered to be due to the penetration of a rectangular potential barrier, whose width is a and height is equal to the yield stress $Y(2, R)$ of the body at the room temperature R °C, by the molecules of the molten surface σ_1 whose energy is represented by the stress $s_\tau(1, L_1)$. Then $\xi_s(1\,|\,2)$ is the probability of the penetration of the potential barrier and we find (13)

$$(19)\quad \xi_s(1\,|\,2) = 16\,\frac{s_\tau(1, L_1)}{Y(2, R)}\exp\,[-\beta a Y^{\frac{1}{2}}(2,R)]\,,$$

where β is a constant. The quantities $K(1)$, $J(1)$ and a that occur in the relations (17) and (18) depend on the physical and chemical structure of the surfaces and to determine their nature we need more experimental results.

(13) L. I. SCHIFF: *Quantum Mechanics* (New York, 1949).

Generally since there is little surface wear we may expect $K(1)$ to be small and we expect $J(1)$ to be of the order unity. Then to explain the variation of $\xi_s(1\,|\,2)$ from 10^{-2} to 10^{-4} for soft and hard metals we expect the width and height of the potential barrier to increase with the hardness of the surface.

We note that a chemisorbed oxide layer is generally found on the surfaces of most metals. While the surface friction and wear are not appreciably affected by it the probability for the formation of junctions is found to be much less and this may be attributed to the increase in the height and width of the repulsive potential barrier which must be penetrated for intermetallic contacts to occur. Thus under these conditions the coefficients of friction are of the order of unity or less and furthermore, as pointed out by FINCH [3], since the oxide layer which is rubbed away by the surface wear is immediately reformed due to the presence of oxygen in the atmosphere, a stable state where the friction is of the order unity and the wear is low, exists for the metals that are used in bearing engineering.

By applying high loads BOWDEN and HUGHES [2] have obtained values of $\xi_s(1\,|\,2)$ of the order of unity and we shall now determine the coefficient of friction under these conditions. Let Σ_1 be the total area of surface σ_1 and let G_0 be the load such that

$$\Sigma_1 Y(1, L_1) = G_0 \,. \tag{20}$$

Then

$$s_\tau(1, L) = \begin{cases} Y(1, L_1) & \text{for } G < G_0 \,, \\ G Y(1, L_1)/G_0 & \text{for } G > G_0 \,. \end{cases} \tag{21}$$

From (19) and (21) we note that while $\xi_s(1\,|\,2)$ remains constant for $G < G_0$ it is proportional to G for $G > G_0$ and we may write

$$\xi_s(1\,|\,2) = \begin{cases} \xi_Y(1\,|\,2) & \text{for } G < G_0 \,, \\ G\xi_Y(1\,|\,2)/G_0 & \text{for } G > G_0 \,. \end{cases} \tag{22}$$

Then for $G > G_0$

$$\mu(1\,|\,2) = G_0/(2G)\,[4(1 + \cos\vartheta(1\,|\,2))(3 + \cos\vartheta(1\,|\,2))^{-1}(1 - G\xi_Y(1\,|\,2)/G_0) + \\ + G s_\sigma(1, R)\xi_Y(1\,|\,2)/(G_0\gamma(1, L_1))] \,, \tag{23}$$

and

$$\omega(1\,|\,2) = G_0 N(1)/(G Y(1, L_1))\,[K(1)\eta(1 - G\xi_Y(1\,|\,2)/G_0) + J_1(1) G\xi_Y(1\,|\,2)/G_0] \,, \tag{24}$$

and we note that under these simple assumptions while the contributions of the surface term become negligible the contributions of the body term remain the same as for (17) and (18) and Amonton's law is followed.

5. – Conclusion.

To determine the nature of the mechanism which produces frictional energy the physical description of the experiments is much simplified and is formulated in terms of a stable state that envelopes the whole field of friction. Then the surface process of SAVAGE ([5]) and the junction process of BOWDEN and TABOR ([1]) for the production of frictional energy are combined by postulating that the areas of true contact are in a plastic and almost molten state under an yield stress and at a temperature in the neighbourhood of the melting point of the more fusible surface. We then find that a qualitative and satisfactory agreement is obtained with the observed results for the values of the coefficients of friction between solid surfaces, between solid surfaces with thin liquid or solid soft metal films, and for the correlation between the coefficients of friction and wear.

To obtain more quantitative results some of the approximations made in order to get a simple statement of the problem will have to be discarded and we should like to enumerate the assumptions that have been made here. Frictional energy is generally accompanied by wear and therefore the area of contact of the sliding surfaces is constantly changing, specially when there is heavy wear, but we have assumed a constant area of contact. Then all the physical, structural and chemical properties of the sliding surfaces and of their interaction with each other have been collected together in their surface and intersurface energies. The physical and chemical reactions at the surface such as the formation of Beilby layer and oxide layer have not been fully treated although it is known that they influence much the coefficients of friction and wear. Then it is assumed that the temperature at the sliding surface is the melting point of the more fusible surface L_1 °C, but perhaps a lower temperature is found which can influence the results appreciably. The conductivity of the substances and the rate of supply of the thermal energy, which will determine the body and surface temperatures and the shear stresses, have also been neglected. Then the wear parameters $K(1)$ and specially $J(1)$ are not fully defined and to do so a more explicit distinction between the body and surface layers in our model seems necessary.

* * *

This work was done at the National Chemical Laboratory, Poona, and the author is grateful to Professor G. I. FINCH for kind hospitality, for suggesting the problem and for helpful discussions.

RIASSUNTO (*)

Si propone la combinazione dell'energia di superficie di Savage col meccanismo di Bowden e Tabor della formazione di giunti per la produzione dell'energia di attrito. La descrizione fisica degli esperimenti risulta sufficientemente semplificata e rappresentata da uno stato stabile che avviluppa l'intero campo di attrito. Ciò porta ad un soddisfacente accordo qualitativo coi valori osservati dei valori dei coefficienti di attrito tra superficie solide e tra superficie solide con interposte sottili pellicole di liquidi o di metalli teneri, per quanto riguarda l'usura e la correlazione fra attrito e usura. Si definisce il coefficiente di usura in analogia al coefficiente d'attrito.

(*) *Traduzione a cura della Redazione.*

On Convergence to the Møller Wave Operators (*).

M. N. Hack

Argonne National Laboratory - Lemont, Illinois

(Ricevuto il 23 Maggio 1958)

It has been recognized by physicists for some time that the proper formulation of time-dependent scattering theory is in terms of *wave packets*, *i.e.*, normalizable state vectors. Recently it was shown by J. M. Cook [1], by means of rigorous methods of the theory of linear operators in Hilbert space, that for potentials of integrable square

$$\int_{\infty}^{\infty}\int_{-\infty}^{\infty}\int_{-\infty}^{\infty} V(\boldsymbol{r})^2\,\mathrm{d}x\,\mathrm{d}y\,\mathrm{d}z < \infty \tag{1}$$

the limits of the $U(0,t)$ operators as $t \to \pm\infty$ exist strongly and are in general, *i.e.*, when the total Hamiltonian has bound states, properly isometric (defined everywhere and norm-preserving, but non-unitary) [2].

From the standpoint of the stationary-state formulation of scattering theory it is expected, and it will be proved here, that the results of Cook remain valid for potentials which fall off at large r faster than $1/r$, and which are required to be square integrable only in the finite domain. That is, we impose the following conditions on the potential:

$$\int_{|\boldsymbol{r}|\leq R} V(\boldsymbol{r})^2\,\mathrm{d}\boldsymbol{r} < \infty \qquad \text{for all finite } R \tag{2}$$

and

$$V(\boldsymbol{r}) = O(r^{-\alpha}) \qquad \text{as } r \to \infty, \text{ for some } \alpha > 1, \tag{3}$$

uniformly in direction of $\boldsymbol{r}$.

(*) Work performed under the auspices of the U. S. Atomic Energy Commission.

(1) J. M. Cook: *Journ. Math and Phys.*, **36**, 82 (1957).

(2) M. Rosenblum: *Pacific Journ. Math.*, **7**, 997 (1957) has proved the following theorem. Let A and B be self-adjoint operators with weakly absolutely continuous spectral measures and let the « potential » $P = B - A$ be a completely continuous operator such that the trace of $|P|$ is finite. Then the limits as $t \to \pm\infty$ of $U(0,t) = \exp[iBt]\exp[-iAt]$ exist strongly and unitarily transform A into B.

For φ in a certain subset $\mathfrak{G}$ of the Hilbert space $\mathfrak{H}$ of all square integrable functions of $\boldsymbol{r}=(x, y, z)$ it is shown in reference (1) that

$$U(s,t)\varphi = \varphi + i \exp[iKs] \int_s^t \mathrm{d}\tau \exp[-iH(s-\tau)] V \exp[-iK\tau]\varphi \tag{4}$$

and that the linear manifold $\mathfrak{M}$ spanned by $\mathfrak{G}$ is dense in $\mathfrak{H}$. Here K is the closure of $-\nabla^2$, *i.e.*, it is the kinetic energy operator in suitable units, $H=K+V$, and

$$U(s,t) = \exp[iKs] \exp[-iH(s-t)] \exp[-iKt] .$$

The set $\mathfrak{G}$ consists of those elements φ of $\mathfrak{H}$ whose Fourier transforms are functions of the form $\varphi(\boldsymbol{p}) = \exp[-a^2(\boldsymbol{p}-\boldsymbol{p}_0)^2]$ with $a^2 > 0$.

From the convergence of the integral

$$\int_{-\infty}^{\infty} \| V \exp[-iK\tau]\varphi \| \mathrm{d}\tau < \infty \tag{5}$$

it follows (1) for arbitrary $\varepsilon > 0$ that

$$\| U(0,t)\varphi - U(0,s)\varphi \| = \| U(s,t)\varphi - \varphi \| =$$
$$= \| \int_s^t \exp[-iH(s-\tau)] V \exp[-iK\tau]\varphi \, \mathrm{d}\tau \| \leqslant \int_s^t \| V \exp[-iK\tau]\varphi \| \mathrm{d}\tau < \varepsilon ,$$

for s and t sufficiently large, positively or negatively. Consequently the strong limits of $U(0,t)\varphi$ as $t \to \pm\infty$ exist by virtue of the completeness of $\mathfrak{H}$, first of all for φ in $\mathfrak{G}$ and then by the density of $\mathfrak{M}$ for all φ in $\mathfrak{H}$. The isometry of the limit operators follows from the strong convergence and the unitarity of $U(0,t)$.

In this note, Equation (5) is established for potentials satisfying conditions (2) and (3). The existence of the strong limits and their proper isometry then follows from the argument of Cook (3). From the relation (4)

$$|\exp[iKt]\varphi(\boldsymbol{r})|^2 = (4(a^4+t^2))^{-\frac{3}{2}} \exp[-c(\boldsymbol{r}-\boldsymbol{b})^2] ,$$

where φ is in $\mathfrak{G}$ and

$$\boldsymbol{b} = 2t\boldsymbol{p}_0 , \qquad c = \frac{1}{2}\frac{a^2}{a^4+t^2} ,$$

we have

$$\| V \exp[iKt]\varphi \|^2 = \int V(\boldsymbol{r})^2 |\exp[iKt]\varphi(\boldsymbol{r})|^2 \mathrm{d}\boldsymbol{r} = (4(a^4+t^2))^{-\frac{3}{2}} I ,$$

(3) We remark that the strong continuity of $V \exp[-iKt]\varphi$ as a function of t which is used in the proof of Eq. (4) holds, for φ in $\mathfrak{G}$, for potentials satisfying (2) and (3) by dominated convergence. We note also that H is self-adjoint in the present case, since potentials satisfying (2) and (3) fulfil the conditions of Kato: *Trans. Amer. Math. Soc.*, **70**, 195 (1951).

(4) An inconsequential omission of a factor of 2 in ref. (1) has been taken into account in the formula for c.

2551

where

$$I = \int \exp\left[-c(\boldsymbol{r}-\boldsymbol{b})^2\right] V(\boldsymbol{r})^2 \, \mathrm{d}\boldsymbol{r}$$

and the integrations are extended over all space. By (3) there exists an $R_1 > 0$ such that

$$V(\boldsymbol{r}) \leq \frac{M}{r^\alpha} \qquad \text{for } r \geqslant R_1 .$$

Without loss of generality we can assume $\alpha < \frac{3}{2}$. For $r \geqslant 2b$,

$$(\boldsymbol{r}-\boldsymbol{b})^2 \geqslant (r-b)^2 \geqslant \tfrac{1}{4} r^2 .$$

Therefore, letting $R = \max\{2b, R_1\}$,

$$I \leqslant \int_{r \leqslant R} V(\boldsymbol{r})^2 \, \mathrm{d}\boldsymbol{r} + \int_{r \geqslant R} \exp\left[-\tfrac{1}{4} c r^2\right] \frac{M^2}{r^{2\alpha}} \, \mathrm{d}\boldsymbol{r} \leqslant J + \gamma c^{\frac{1}{2}(2\alpha-3)} ,$$

where γ is a constant independent of t and

$$J = \int_{r \leqslant R} V(\boldsymbol{r})^2 \, \mathrm{d}\boldsymbol{r} .$$

Suppose now that $2b > R_1$ and set

$$J_1 = \int_{r \leqslant R_1} V(\boldsymbol{r})^2 \, \mathrm{d}\boldsymbol{r} .$$

Then

$$J = \int_{r \leqslant R_1} V(\boldsymbol{r})^2 \, \mathrm{d}\boldsymbol{r} + \int_{R_1 \leqslant r < 2b} V(\boldsymbol{r})^2 \, \mathrm{d}\boldsymbol{r} \leqslant J_1 + \int_{r \leqslant 2b} \frac{M^2}{r^{2\alpha}} \, \mathrm{d}\boldsymbol{r} = J_1 + \mu b^{3-2\alpha} .$$

This inequality holds also when $2b \leqslant R_1$, since then $J = J_1$. Thus

$$\| V \exp\left[iKt\right]\varphi \|^2 \leqslant \left(4(a^4 + t^2)\right)^{-\frac{3}{2}} \left(J_1 + \mu b^{3-2\alpha} + \gamma c^{\frac{1}{2}(2\alpha-3)}\right) .$$

Recalling the expressions for b and c in terms of t, we see that

$$\| V \exp\left[iKt\right]\varphi \| = 0\left(\frac{1}{|t|^\alpha}\right) \qquad \text{as } |t| \to \infty .$$

Therefore

$$V \exp\left[iKt\right]\varphi \to 0 \qquad \text{as } t \to \pm\infty$$

and

$$\int_{-\infty}^{\infty} \| V \exp\left[-iK\tau\right]\varphi \| \, \mathrm{d}\tau < \infty .$$

Branching Ratio of ThC (^{212}Bi).

D. Prosperi

C.N.R.N., Laboratorio Fisico della Divisone Geomineraria - Roma

S. Sciuti

Istituto Nazionale di Fisica Nucleare - Sezione di Roma

(ricevuto il 27 Giugno 1958)

A knowledge of the branching ratio of ThC is of considerable interest both for the nuclear spectroscopy of heavy elements and for applicative questions concerning the Thorium radioactive family.

The first reliable measurements of the branching ratio are due to Kovarik and Adams [1] who determined it by examining the α activities of ThC and ThC'

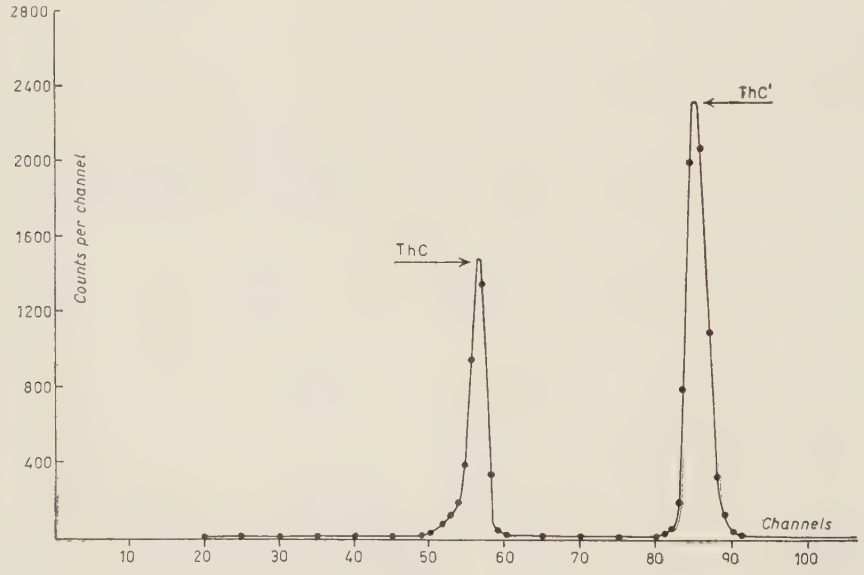

Fig. 1.

[1] A. Kovarik and N. Adams: *Phys. Rev.*, **34**, 413 (1938).

2556

using a plane ionization chamber and layers of old Thorium oxide.

Recently, SENFTLE, FARLEY and LAZAR ([2]) have carried out new measurements using a proportional counter and very thin layers of ThB in equilibrium with ThC and ThC'. The results obtained by these authors are not in complete agreement with those obtained by KOVARIK and ADAMS.

For this reason we have undertaken a precise redetermination of the branching ratio of ThC.

A 2π gridded ionization chamber ([3]) connected to a 100 channel pulse height analyzer was used in the work. The technique used for preparing the source was analogous to that described by SENFTLE and coworkers.

Nickel discs of 10 cm diameter were suspended over about 500 g of aged Thorium nitrate contained in a metal vessel. The Thoron decay products deposited themselves spontaneously upon the discs which were kept at — 150 V with respect to the vessel. The time required for the deposition was about 20-hours. Each disc was then placed in the chamber which permitted the measurements of the α activities of ThC and ThC' .

A typical pulse-height spectrum is given in the figure; the width of two α lines is about 2% at half height. In the table are given the final results of the above mentioned authors and our value which was obtained by taking the average of nine independent determinations.

Authors	branching ratio $\frac{\alpha}{\alpha+\beta}$
KOVARIK and ADAMS	0.337 ± 0.009
SENFTLE and coworkers	0.362 ± 0.006
Present work	0.352 ± 0.003

As one can see from the table we obtained for the branching ratio a value which lies between those previously found. The expected over-all uncertainty is less than 0.9%.

([2]) F. E. SENFTLE, T. A. FARLEY and N. LAZAR: *Phys. Rev.*, **104**, 1629 (1956).

([3]) D. PROSPERI and S. SCIUTI: *Precise Radiometric determination of Uranium and Thorium contents in Ores.* Communication presented at Geneve Conference, September 1958.

Photoneutrons from Au.

S. Cavallaro, V. Emma, C. Milone and A. Rubbino

Istituto di Fisica dell'Università - Catania
Centro Siciliano di Fisica Nucleare - Catania

(ricevuto il 30 Giugno 1958)

In order to extend the experimental knowledge on the photonuclear interaction, the energy spectrum of the photoneutrons from Au has been studied with the experimental method described in a previous paper [1].

A 60 g Au target was irradiated by a collimated 30 MeV bremsstrahlung beam from the B.B.C. Turin betatron. The photoneutrons emitted at angles of 90° with the photon beam were detected by means of the proton recoil tracks in Ilford C2 200 μm thick emulsions. The plates were screened against the neutrons coming directly from the betatron and from the low energy photons coming from the target.

Normally the plates were scanned with 55× oil immersion Koristka objectives and 8× eyepieces: (« slow scanning »). Only for very short tracks the length was measured with a 100× objective. Following the conventional method [1-2], only the recoil tracks were considered which come to rest inside the emulsion and had an original direction into a « square piramid » of 15° semiaperture centred in the neutron beam direction.

An additional « fast scanning » — see [1] — was made with a 30× objective in order to improve the sta-

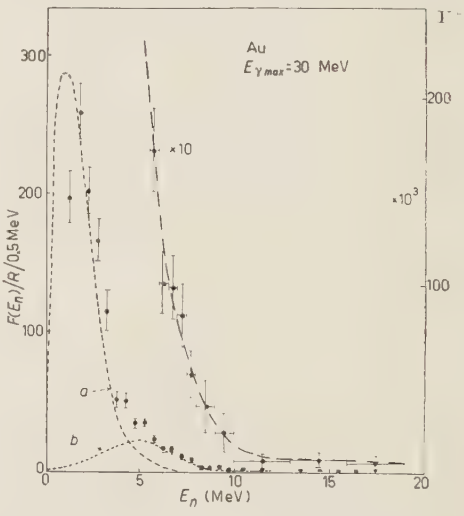

Fig. 1. – Energy spectrum of the photoneutrons from Au emitted at ~90° with the γ-ray beam. ⊕ = Experimental figures. For the high energy tail figures are multiplied by 10. The curve (*a*) is the evaporation spectrum calculated under the assumption indicated in the text. Curve (*b*) is a spectrum calculated for direct emission under the hypothesis that the residual nucleus after the neutron emission is left in the ground state. Y^+ = neutrons/R/0.5 MeV/mole/$\Delta\Omega$.

(1) G. Cortini, C. Milone, A. Rubbino and F. Ferrero: *Nuovo Cimento* (1958) in press.

(2) L. Rosen: *Nucleonics*, **11**, 7, 32; **11**, 8, 38 (1953).

2558

tistics over 3.5 MeV neutron energy: the track lenght measurements were made with a 55× objective.

Exposure and scanning data are summarized in Table I.

TABLE I.

Element	$^{197}_{79}$Au
Weight (g)	60
(γ, n) threshold (MeV)	7.9
$E_{\gamma max}$ (MeV)	30
Dose (Roentgen)	2647
Slow scanning ($\varphi < 15°$)	
Scanned volume	54 mm³
Number of tracks $E_n \leqslant 5$ MeV	774
Number of tracks $E_n > 5$ MeV	45
Supplementary scanning with 100× for low energy	16 mm³
Number of tracks $E_n \leqslant 4$ MeV	186
Fast scanning	
Scanned volume	210 mm³
Number of tracks ($\varphi \leqslant 15°$)	
3.5 MeV $< E_n < 5$ MeV	62
$E_n > 5$ MeV	145
Number of tracks ($15° < \varphi \leqslant 30°$)	
$E_n > 5$ MeV	135

Taking into account the appropriate factors [1], from the experimental proton spectrum the Au neutron spectrum shown in Fig. 1 is obtained. The background was 3%.

The energy distribution may be compared in the conventional way with the evaporation theory [3]. The expected differential neutron energy spectrum $F(E_n)$ is (*):

$$F(E_n) = K E_n \sigma(E_n) \cdot \int_{B_0+E_n}^{E_\beta} \omega(E_R)\, \sigma_{\gamma n}(E_\gamma) I(E_\gamma, E_\beta)\, dE_\gamma \Big/ \int_0^{E_\gamma - B_n} E_n \sigma(E_n) \omega(E_R)\, dE_n$$

where:

E_n = neutron energy;

$\sigma(E_n)$ = reaction cross section for neutrons of energy E_n on residual nucleus [4];

B_0 = binding energy

$\omega(E_R)$ = energy level density in residual nucleus with excitation energy $E_R = E_\gamma - B_0 - E_n$;

$\sigma(\gamma, n)$ = cross section for the (γ, n) process [5];

$I(E_\gamma, E_\beta)$ = bremsstrahlung spectrum with maximum energy E_β [6,7].

Assuming for $\omega(E_R)$ the form

$$\omega(E_R) = C \exp \sqrt{\alpha E_R},$$

curve (a) is obtained for $\alpha = 1{,}6(A-40)^{\frac{1}{2}}$ [8].

The experimental spectrum shows two points of disagreement with respect to the calculated one.

First, we note a high energy tail

(*) As Prof. G. CORTINI pointed out to us, the integral in the denominator of this formula cannot be ignored as was mistakenly done in a preceeding paper [1]. Therefore the evaporation curves of fig. 2 and 3 of the quoted paper correspond to density level distributions rather lower than indicated there (3.1). This gives no changement in the conclusions of paper [1].

(3) V. F. WEISSKOPF and D. H. EWING: *Phys. Rev.*, **57**, 472 (1940).

(4) H. FESHBACH and V. F. WEISSKOPF: *Phys. Rev.*, **76**, 1550 (1949).

(5) R. MONTALBETTI, L. KATZ and J. GOLDEMBERG: *Phys. Rev.*, **91**, 659 (1953).

(6) L. KATZ and A. G. W. CAMERON: *Can. Journ. Phys.*, **39**, 437 (1957).

(7) C. MILONE, S. MILONE-TAMBURINO, R. RINZIVILLO, A. RUBBINO and C. TRIBUNO: *Nuovo Cimento*, **7**, 729 (1958).

(8) B. C. DIVEN and G. M. ALMAY: *Phys. Rev.*, **80**, 407 (1950).

already observed in other elements by various authors ([9-11]), which must be interpreted, as is usual with a direct emission process, the Au tail is somewhat smaller than observed by us ([1]) in Cr and Ta (Fig. 2). In order to get a rough

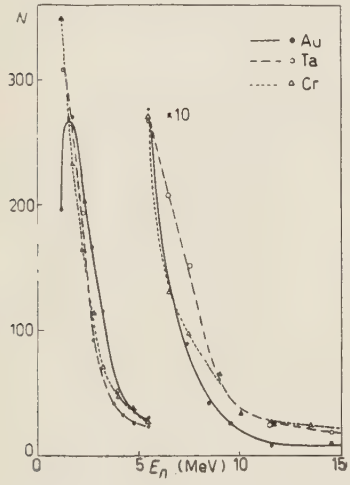

Fig. 2. – Photoneutrons spectra from Au, Cr and Ta for $E_n > 1$ MeV. N = number of photoneutrons per 0.5 MeV interval. Arbitrary units. Figures are normalized to the same total number of neutrons.

idea of the relative importance of the direct process we considered the very schematic assumptions that $\sim 15\%$ of the photoneutrons are emitted through direct processes and that the residual nucleus is left in its ground state.

Under these assumptions and taking the experimental photonuclear cross section ([5]), we get the curve (b) in Fig. 1.

The experimental points for $E_n > 2$ MeV agree well with curves $(a)+(b)$.

We point out that under the same assumptions the theoretical spectrum from Pb agrees well with the experimental one obtained by Toms and Stephens ([11]).

([9]) P. R. Byerly jr. and W. E. Stephens: *Phys. Rev.*, **81**, 473 (1951).

([10]) G. A. Price: *Phys. Rev.*, **93**, 1279 (1954).

([11]) M. E. Toms and W. E. Stephens: *Phys. Rev.*, **108**, 77 (1957).

Turning now to the low energy part of the spectrum, we find that the low energy peak in the Au spectrum is obtained for neutron energy higher than that expected according to the evaporation theory.

The position of the calculated maximum may suffer some shift according to the assumed nuclear level density distribution but, for a coincidence of the calculated with the experimental maximum one obtains a much higher disagreement in the other region of the spectrum.

The resolution of the nuclear emulsions in the low energy region ($1 \div 2$ MeV) is rather poor. Besides the discrimination of the tracks according the dip angle becomes very critical in the same region. Therefore the experimental figures in this interval may have experimental errors much higher than the statistical ones. Therefore we do not attribute any special significance to the small disagreement between theoretical

Fig. 3. – Experimental energy spectra from Cu ([9]), Pb ([11]) and Au, and theoretical curves calculated for evaporation.

and experimental position of low energy maximum. However we point out that a similar displacement may be observed in the photoneutron spectrum from Pb ([11]) by TOMS and STEPHENS (Fig. 3).

On the contrary an agreement on the position of the maximum is found for the photoneutrons from Cu ([9]).

* * *

We thank prof. R. RICAMO and Prof. G. WATAGHIN who put at our disposal the means for making the present work, and prof. G. CORTINI for constant help and many useful discussions.

We thank also all the colleagues of the laboratories of Catania and Turin for their friendly help.

We are particularly indebted to Dr. F. FERRERO for the exposure of the plates.

A Search for Particles of 550 m_e.

M. Conversi, E. Fiorini, S. Ratti, C. Rubbia, C. Succi and G. Torelli

Istituti di Fisica delle Università di Milano e di Pisa
Istituto Nazionale di Fisica Nucleare - Sezioni di Milano e di Pisa

(ricevuto il 14 Luglio 1958)

At an altitude of 2550 m a.s.l., a search is being carried out for the particles of ~ 550 electronic masses reported by Alyhanian *et al.* [1]. In about one year of measurements performed at an altitude of 3200 m a.s.l. these authors reported 11 examples of such a particle, at a rate of $\sim 1/200$ that of cosmic-ray muons stopping in the same range interval (average range ~ 60 g/cm^2 of copper).

Recently Orear *et al.* [2] did not find any 550-mass particle in a sample of 550 muons stopped in an emulsion stack exposed to cosmic rays. An indication for the existence of 550-mass particles would appear, nevertheless, from more recent results of Keuffel and coworkers [3] in their mass spectrum of cosmic ray particles under 15 cm of lead (*).

In the present experiment mass determinations are essentially based on measurements of energy loss and range. A fairly large solid angle of acceptance (10.5 ster cm^2) should make it possible to detect some 550-mass particles in a comparatively short time, if they exist in the abundance reported by the Soviet Group [1].

The apparatus is shown in Fig. 1. The large bottom chamber [4] (C.R.) contains 17 plates of plexiglass each 0.3 cm thick and is used for range and scattering measurements. The change of the ionization in the various « gaps » of C.R. can be used to obtain further information. The top chamber (C.I.) is used essentially to recognize, from lack of alignment of the tracks in C.I. and C.R., possible interactions occurring between C.R. and the pro-

[1] A. I. Alihanian *et al.*: *International Conference on High Energy Physics* (Moscow, May 1956); A. I. Alihanian, N. V. Šostakovič, A. T. Dadaian, V. N. Fedorov and B. N. Deriagin: *Žurn. Éxp. Theor. Phyz.*, **4**, 817 (1957), also for previous references.

[2] J. Orear, E. Bierman and S. Rosendarff: Postdeadline paper for the 1958 New York Meeting of the *Am. Phys. Soc.*

[3] J. W. Keuffel, R. L. Call and W. H. Sandmann: *Bull. Am. Phys. Soc.*, **3**, 162 (1958).

(*) A few days ago other results have been reported, together with those contained in this letter, at the C.E.R.N. Conference (Geneva, July 1958), in the general report on strange particles by J. Steinberger.

[4] E. Fiorini, R. Giacconi and C. Succi: *Nuovo Cimento*, **6**, 943 (1957).

portional liquid scintillator D. The pulses of this counter, which allows measurements of energy loss of about

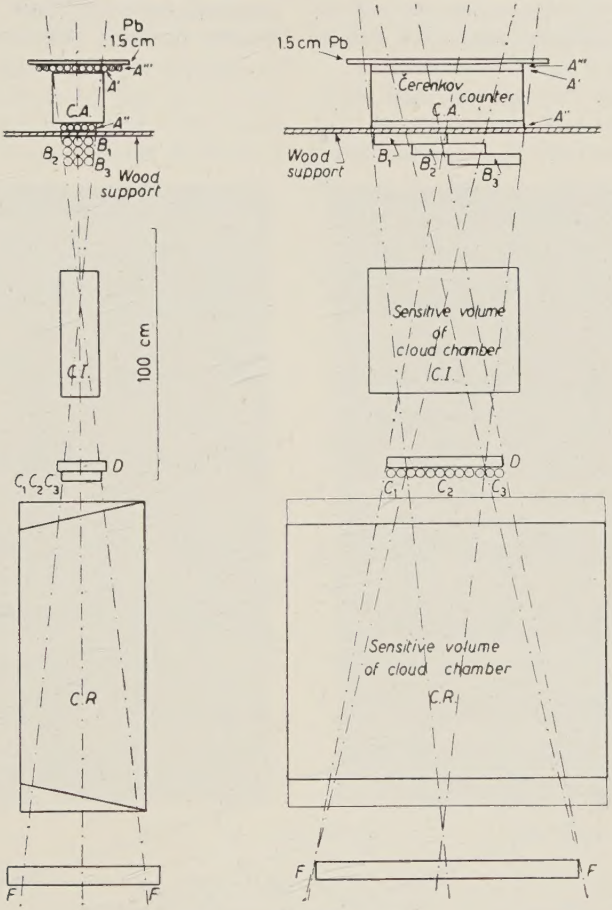

Fig. 1.

15% accuracy, are displayed (after a convenient amplification of linearity better than 5% and gain stable within $\pm 2\%$) on the sweep of a « 515 Tektronics » oscilloscope, whenever a triggering pulse occurs.

Triggering pulses are produced by ionizing particles that:

a) cross the solid angle defined by the Geiger counters A', A'', B, C and the scintillator D;

b) do not cross either the Geiger counters A''', or the large liquid scintillator F;

c) do not produce light crossing the Čerenkov counter C_A (efficiency $> 99.9\%$ for relativistic particles).

The cloud chambers are expanded by the triggering pulses and stereoscopic pictures are taken, simultaneously with the picture of the oscillogram giving the pulse height of the counter D.

Mixed coincidences between counter B_1 and C_1, B_2 and C_2, B_3 and C_3, ensure that the solid angle of acceptance is

2563

entirely covered by the large scintillator F, used in anticoincidence. The top lead thickness, the anticoincidence counters A''' and the anticoincidence Čerenkov counter C_A, reduce to a small value the triggering background due to the electrophotonic component of the cosmic radiation.

The anticoincidence counter C_A is such that electrons, muons and pions crossing counter D are all eliminated. On the contrary, 550-mass particles cer-

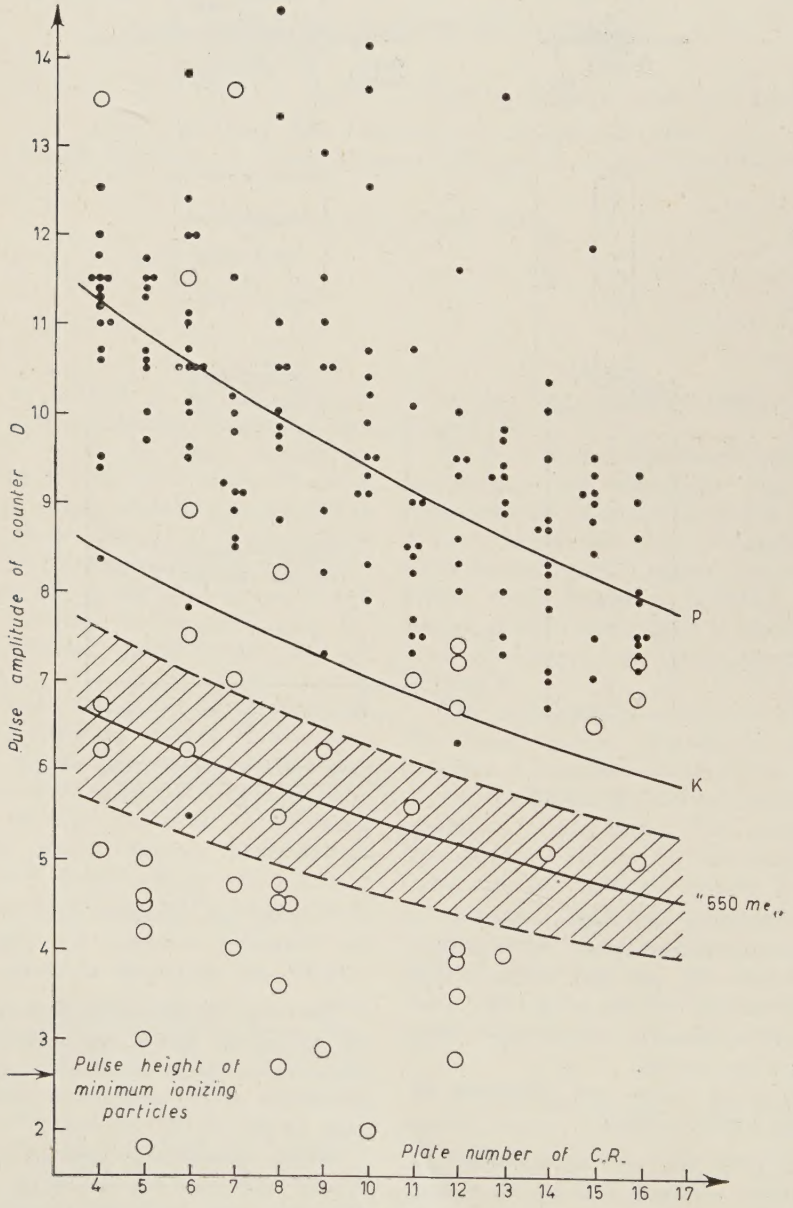

Fig. 2.

2564

tainly do not produce light in C_A, if they are not accompanied by fast ionizing particles and lose energy only by ionization before stopping in the plates of C.R.

Up to date 1556 pictures have been collected in the nearly 610 h of measurement. This time must be reduced to ~ 430 h on account of the dead time (~ 7 min) of the chambers. We have analysed only those pictures showing a particle which, after entering the apparatus, stops (with or without interaction) between the 3th and the 16th plate of C.R. The rate of muons stopping in this same range interval after crossing the solid angle of the apparatus, is estimated to be about 3 per hour (the Čerenkov counter prevents light mesons from being actually recorded). This rate is derived from the well known sea level intensity ([5,6]) and altitude dependence ([6,7]) of slow cosmic-ray muons. Hence, if 550-mass particles exist in the abound-ance reported ([1]) we should have recorded 6 of them.

Each event analysed is represented in Fig. 2 by a dot or by a small circle.

A dot corresponds to a particle which stops after having lost energy in C.R. only by ionization. On account of the small thickness of the plates of C.R., these events can be recognized unambiguously by visual estimate of their change in ionization along the track. A small circle corresponds to a stopping particle which clearly interacts in C.R.

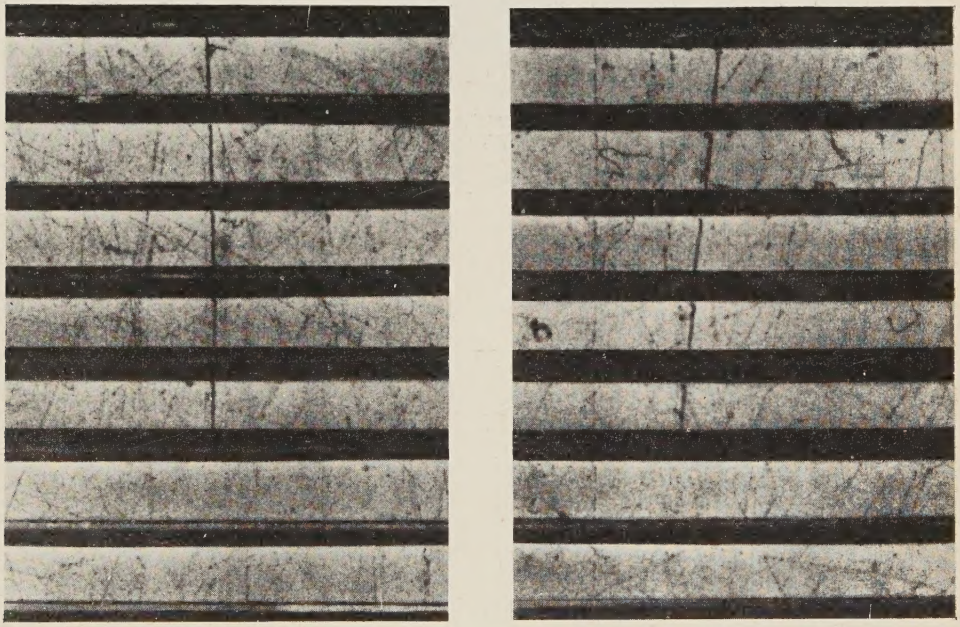

b *a*

Fig. 3.

The shaded region of Fig. 2 is that in which 550-mass particles should fall (if they lose energy only by ionization) with a probability of $\sim 90\%$. This can be seen directly from the distribution of the identified protons around the corresponding curve of Fig. 2.

All but one of the 9 events inside the shaded region of Fig. 2 correspond to protons (or K-particles) clearly interacting in one of the plates of C.R. In

([5]) B. Rossi: *Rev. Mod. Phys.*, **20**, 537 (1948).

([6]) M. Conversi: *Phys. Rev.*, **79**, 749 (1950).

([7]) B. Rossi, M. Sands and R. Sard: *Phys. Rev.*, **72**, 120 (1948).

each of these 8 events the track of the triggering particle is characterized by lack of appreciable scattering and change in ionization in the gaps before the plate in which it ends.

In Fig. 3*a* is reproduced the picture (taken while C.I. was unfortunately not operating) of the event corresponding to the only dot falling in the shaded region of Fig. 2. For purpose of comparison the picture of an identified proton stopping in the same plate of C.R. is reproduced in Fig. 3*b*. The absence of an appreciable scattering through the plates and the small change of ionization in the gaps of C.R., as well as the similarity of the track of Fig. 3*a* to that of Fig. 3*b*, strongly suggests that the only dot falling in the shaded region of Fig. 2 corresponds to a proton which lose part of its energy interacting in the material between counter *D* and C.R.

If this interpretation is correct we must conclude that no 550-mass particles have been recorded in a time interval in which we expected 6 of them, on the basis of their reported abundance [1].

* * *

It is a pleasure for us to aknowledge the contribution given to this work by Drs. G. M. DE' MUNARI, A. EGIDI and M. TOLLER.

PROPRIETÀ LETTERARIA RISERVATA

Direttore responsabile: G. POLVANI

Tipografia Compositori - Bologna

Questo Fascicolo è stato licenziato dai torchi il 30-VIII-1958

2566